A Study of Diamonds with Syngenetic Inclusions

Martin C. Wilding

Doctor of Philosophy

University of Edinburgh

1990

I declare that the work described in this thesis is my own, except where otherwise stated.

Martin C. Wilding

".....every element says something to someone (something different to each) like the mountain valleys or beaches visited in youth. One must perhaps make an exception for carbon because it says everything to everyone, that is, it is not specific, in the same way that Adam is not a specific ancestor - unless one discovers today (why not ?) the chemistylite who has dedicated his life to graphite or the diamond. And yet it is to carbon that I have an old debt, contracted during what were for me decisive days. To carbon, the element of life, my first literary dream was termed, insistently dreamed in an hour and a place when my life was not worth much: yes I wanted to tell the story of an atom of carbon."

Primo Levi (1919-1987), The Periodic Table.

Abstract

This thesis has investigated the chemical and physical conditions of natural diamond formation by integrated studies of the geochemistry of mineral inclusions in diamond, the nitrogen aggregation state and the carbon isotopic compositions of diamonds themselves. The diamonds studied were selected from two different sources, namely Bultfontein (Kimberley, South Africa) and Sao Luiz (North East Brazil).

Diamonds from the Bultfontein mine occur in a Cretaceous kimberlite pipe intruded into the Archean Kaapvaal craton. The diamonds are dominated by peridotite paragenesis inclusions, of which chromites are the most numerous. Equilibrium temperatures, indicated by these inclusions, are 930 and 955^{o}C. The high abundance of chromites is interpreted as indicating a relatively shallow depth of origin. Bultfontein diamonds therefore probably formed in a thickened part of the craton where the geothermal gradient was low.

Infra-red studies of the Bultfontein diamonds show a low degree of nitrogen aggregation. There are two populations of diamonds, one population showing high nitrogen content but low aggregation state, the other having a lower nitrogen concentration but more aggregated nitrogen. The geochemical environment of formation for the two populations appears to be the same. The two different populations indicate either two separate formational events separated by a long time period, or, more favoured, two separate environments of formation one with high nitrogen the other with low nitrogen.

The carbon isotope studies of the Bultfontein diamonds show a mean $\delta\ ^{13}C$ value of -4.66 $^{o}/_{oo}$. The isotope compositions are skewed towards heavier values and this is probably a result of isotope fractionation processes which occurred between diamonds and a C-O-H vapour. The skewness of the carbon isotope values for the Bultfontein diamonds probably results from the precipitation of diamond by CH_4 oxidation reactions. The Bultfontein diamonds probably formed by the introduction of oxidising fluids into a reduced area of the lithosphere.

Cathodoluminescence studies of large diamonds and the study of the variation of $\delta\ ^{13}C$ across a diamond by ion microprobe suggest that some of the diamonds formed under conditions of fluctuating oxygen fugacity. This has resulted in the formation of cuboid cores in large diamonds and a variation in $\delta\ ^{13}C$ of 4 $^{o}/_{oo}$ across a single diamond.

Diamonds from the Sao Luiz alluvial mine are believed to be derived from a series of diamondiferous kimberlites intruded into a Proterozoic fold belt in North East Brazil. The diamonds show two principle groups of inclusions, both of which suggest a very deep origin for these diamonds. One group is dominated by garnet, and may be termed eclogitic, the other group is dominated by magnesiowustites.

Garnetiferous inclusions from Sao Luiz are divided into two groups. Group I garnets have normal silica contents and originate at depths shallower than 200km. Group II have high silica contents than normal garnets with silicon atoms apparently occupying octahedral sites in the garnet structure. The Group II garnets are believed to represent solid solutions of garnet and pyroxene formed at high pressure and probably originated over a range of depths from 200 to 450km. Some of the inclusions are composite and consist of clinopyroxene and garnet phases. In these bimineralic inclusions a range of temperatures of equilibrium from 1297 to 1616^{o}C have been calculated, consistent with estimated geotherms for the asthenosphere. The garnet and pyroxene phases in the bimineralic inclusions are believed to have been separate before incorporation into the diamonds and are not the result of the decomposition of a single high pressure phase. In some of the Group II inclusions the high-silica phases have undergone a limited decomposition which has produced a series of complicated textures that consist of normal garnet and the high-silica phase.

Oxide and other silicate inclusions from the Sao Luiz diamonds suggest an even deeper origin. Magnesiowustites (MgO-FeO) inclusions are probably derived from depths greater than 650km. These inclusions have high Fe/Fe+Mg ratios and thus do not appear to be average products of the perovskite structured (high pressure) mantle. The silicate phases include $CaSiO_3$ composition phases that indicate a depth

of origin below 450km. Olivine, diopside and pure silica phases are also present. Two silicon carbide inclusions were also recovered.

A limited study of the carbon isotope compositions and the infra red characteristics of these diamonds has been completed. The garnet-bearing diamonds show a range of $\delta\ ^{13}C$ values from -6.70 to -12.57 $^{o}/_{oo}$, values much lighter than the assumed mantle composition. These diamonds may have formed by CO_2 reduction reactions but it is more likely that a number of finite carbon reservoirs of different isotopic composition exist in the asthenosphere. The diamonds which contain the deeper inclusions have $\delta\ ^{13}C$ values of -5 $^{o}/_{oo}$. The deep diamonds are mostly Type II, that is they contain no nitrogen that is detectable by infra red. The Type I diamonds have high IaB contents and can be shown to indicate rapid aggregation of nitrogen. It is possible that the nitrogen in the deep diamonds aggregated rapidly to form defects that are invisible to infra red as a result of the high temperatures of formation.

The precipitation of diamonds at Sao Luiz that contain garnet inclusions probably occurred at the interface of oxidised areas at the top of the asthenosphere with more reduced areas. The other, deeper diamonds formed under more reduced conditions as shown by the presence of two inclusion of silicon carbide. The deep diamonds probably precipitated from a CH_4-H_2 vapour by H_2 loss, as such the deep Sao Luiz diamonds may have been in redox equilibrium with the earths core.

Acknowledgements.

It would not have been possible to complete this thesis without the help of my three supervisors; Jeff Harris, Ben Harte and Tony Fallick, who have improved earlier versions of the text and have provided much guidance and encouragement over the last three years.

Barry Hawthorne and Roger Clement of Anglo-American have shown a keen interest in this project and have made samples available for study. They also provided funds to enable me to visit South Africa in 1987 and the U.S.A in 1989. Dr. J. E. Field is thanked for inviting me to three of the De Beers Diamond Conferences.

The Diamond Trading Company (DTC) has provided invaluable help over the past three years. In particular Geoff Wollet and Steve Roth of the DTC polishing laboratory in London produced sawn and polished diamond sections that enable a detailed study of the infra red and cathodoluminescence characteristics to be made. Infra red and cathodoluminescence studies were carried out at the DTC Research and Development Laboratory in Maidenhead under the supervision of Martin Cooper and Chris Welbourn. Mike Gaukroger (also of DTC Maidenhead) provided a section of diamond, sawn from a synthetic diamond, for use as an ion microprobe standard.

At Edinburgh University Pete Hill, Stuart Kearns and John Craven are thanked for their assistance while I was using the electron microprobe facilities. Richard Hinton and John Craven provided much help during ion microprobe analysis. Jim Smith, of the workshop at Edinburgh University made the steel crusher used to break the diamonds for inclusion extraction.

The isotope facilities at the Scottish University Research and Reactor Centre (East Kilbride) were used under the supervision of Tony Fallick and Terry Donelly. Some infra-red measurements were made at King's College, London, with the help of Alan Collins.

Peter Deines, of the Pennsylvania State University is thanked for taking the time to discuss the finer points of isotope fractionation processes with me, whilst I was visiting the U.S.A. Both Peter, and his wife Melissa, are thanked for their hospitality during my visit. Tony Carrington, of De Beers, is thanked for the information that he provided concerning the locality and the geological setting of the Sao Luiz mine in Brazil.

During the past three years I have had the opportunity to discuss many aspects of my thesis with many people who have researched in similar fields, in particular John Gurney, Steve Richardson and Rory Moore, Linton Jaques, John Valley, Nick Odling, Guy Cooper, Stuart Boyd, Simon Lawson and many others.

I am also grateful to Mike Matthews, Hugh Nicholson and John Valley who have all patiently proof read sections of this thesis.

Finally I would like to thank all my fellow postgraduate students at Edinburgh who have made the past three years so enjoyable and also my family for their continued support.

Contents

Chapter 4

Nitrogen and Carbon Characteristics of Bultfontein Diamonds.

Chapter 5

Origin of Bultfontein Diamonds

Chapter 6

Garnet-Rich Inclusions from Sao Luiz.

Chapter 7

Non-Garnetiferous Inclusions from Sao Luiz

Chapter 8

Origin of Sao Luiz Diamonds

References

Appendices

List of Figures

List of Tables

Chapter 1

Introduction to Diamonds.

1.1 Introduction.

Diamond has been a natural gemstone for thousands of years because it possesses the three important properties which make a good gem; namely: beauty, rarity and durability. Initially, because of its extreme hardness, few attempts were made to alter its natural shape and diamond was less valuable than gems such as ruby, which were more easily shaped. Indian lapidaries discovered that diamond could be polished with diamond powder, but early polishing was usually just to remove frosted surface coats or to disguise crystal flaws rather than to produce faceted gems. Many of the famous gems which have been known since the times of the Mogul Emperors (1000 A.D.), such as the Koh-i-Nor diamond, were of this type (Smith, 1912). During the mid sixteenth century, faceting of diamonds was developed, principally in Venice. The brilliant cut diamond was developed by Vincentti Peruzzi from the natural octahedron shape of diamond. The brilliant cut (Fig.1.1) is probably the best way of appreciating the properties of dispersion, lustre and refractive index which makes diamond such a distinctive mineral, and since the development of this cut, in the sixteenth century diamond has become one of the most highly prized natural substances on Earth.

Diamond is the hardest known natural mineral. It is forty times harder than it's nearest neighbour on the Moh's hardness scale. Because of it's hardness, non gem quality diamond is in demand as an abrasive. Natural diamond is used in cutting blades as sintered powders, as single crystals, and in the manufacture of polishing pastes. Further uses of diamond result from it's thermal and electrical properties and include use as heat sinks, radiation detectors and a possible future use of diamonds as semiconductors (See Field, 1979).

Table Cut

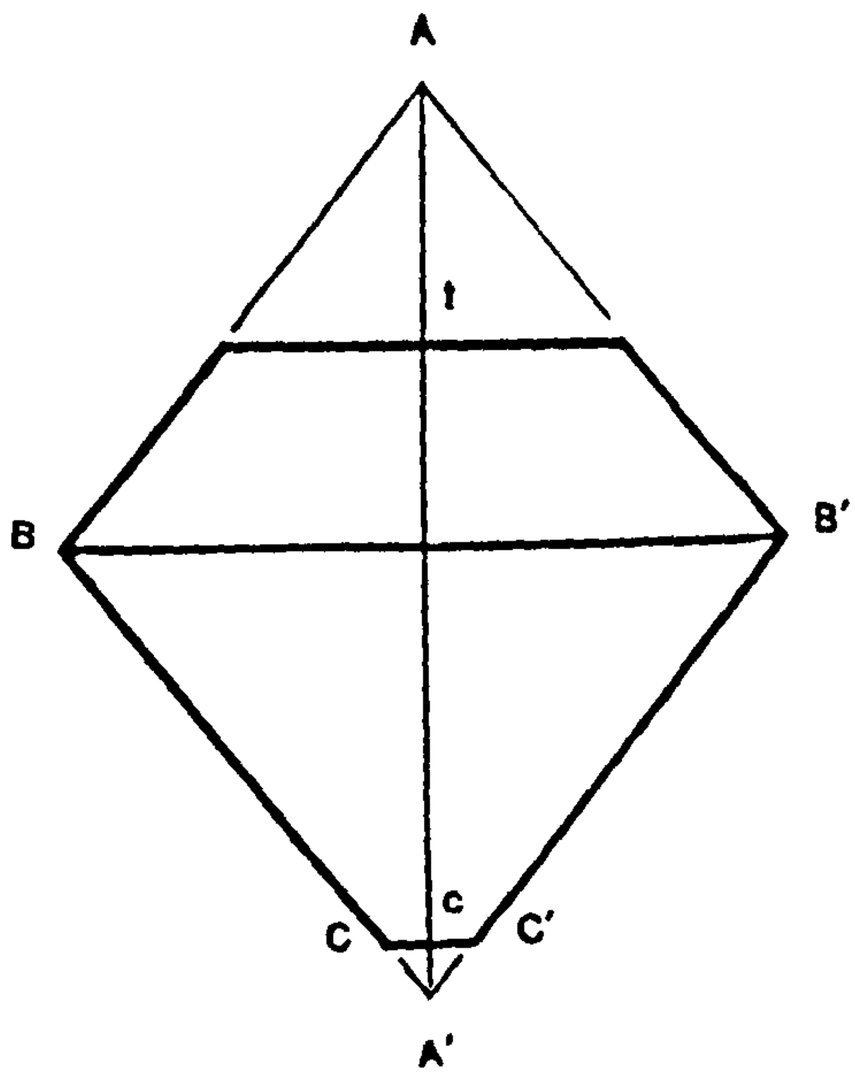

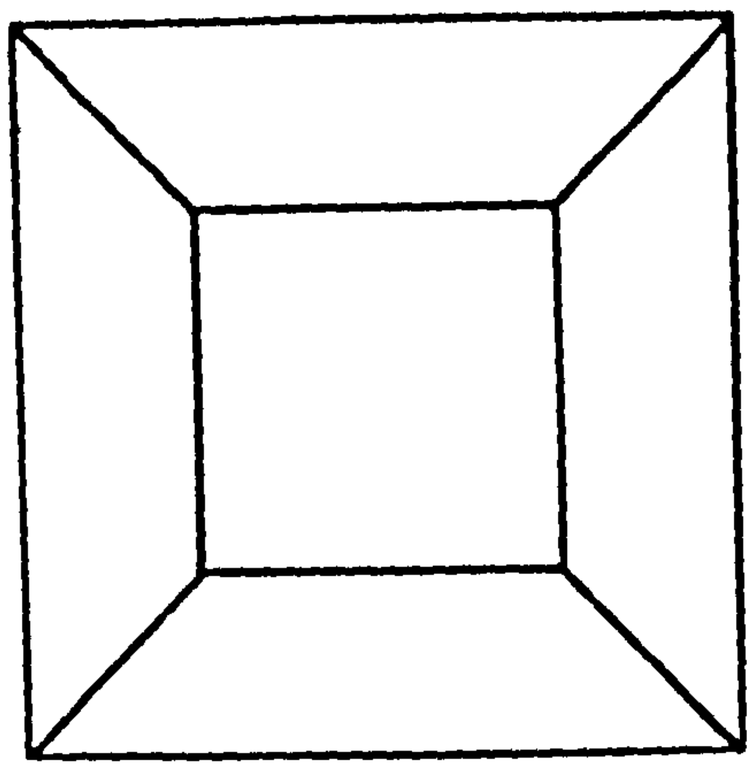

Brilliant Cut

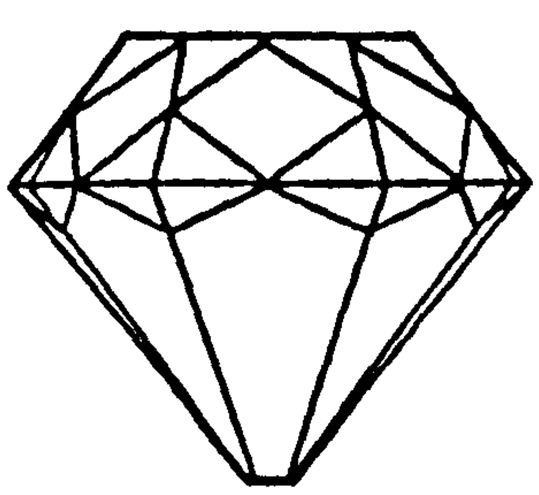

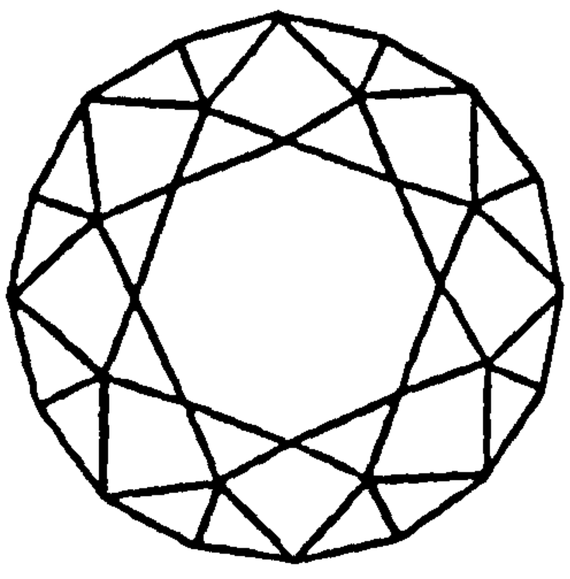

Crown

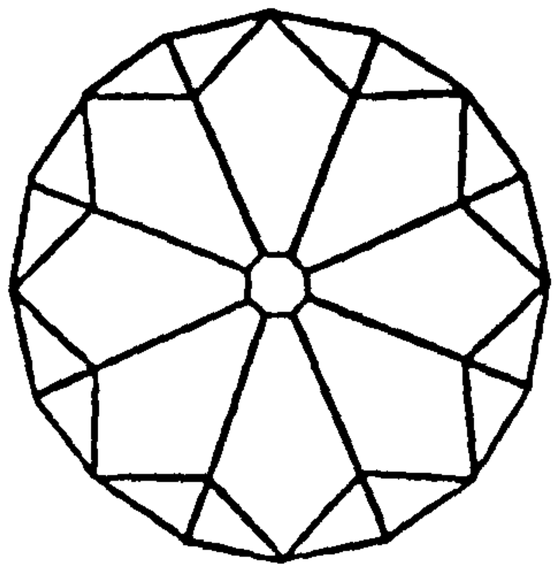

Pavillion

Fig. 1.1

Brilliant Cut Diamond.

The brilliant cut is the most common cut of gem quality diamonds and was developed from the table cut diamond which is a modification of the octahedron shape of natural diamond. The dispersion of light or "fire" of the diamond is enhanced by total internal reflections within the brilliant cut. The table cut dimensions are such that the distance At is typically 5/18 of the distance AA' and Ac is 1/18 of AA'. The brilliant has 58 facets, 25 on the top or crown of the stone and 33 on the base or pavillion, the pavillion and crown are separated by a girdle which should be as thin as practical. Because the brilliant is developed from octahedral diamonds an important economic factor of any mine is the abundance of large octahedra and diamonds that can be easily cleaved into octahedra.

In 1953 diamond was synthesized by scientists working at the ASEA laboratory in Stockholm, and in 1955 by General Electric in the U.S.A.. Both teams used a carbon/solvent catalyst to overcome the considerable kinetic barrier that prevents direct conversion of graphite to diamond. Following this early success diamonds have been synthesized by De Beers at the Diamond Research Laboratory in Johannesburg and it is now possible to grow diamonds with specific shapes and physical properties (Wedlake, 1979).

The value of diamond, as an industrial mineral and a natural gem, has made it one of the most studied minerals in the world. Geological research into diamonds is summarised by Harris (1987) and includes studies of the physical characteristics of diamond, their colour, growth history, age and studies of the mineral inclusions in diamond and substitutional impurities that are found in the diamond lattice.

1.2 Natural Diamond Occurrence.

India was the most important source of natural diamond during historical time. Diamonds were found in sandstones, conglomerates and alluvial deposits surrounding Golconda near Hyderabad. Following discovery of diamonds in Brazil, again in alluvial deposits, these two major diamond producing countries were in competition with each other until the 1860's. In 1867 the discovery of diamonds in South Africa led to rapid development of diamond fields, initially in alluvial gravels associated with The Orange and Vaal rivers. Further deposits to the south and east of the Vaal river on the farms of Bultfontein, Dortsfontein and De Beers were initially thought to be dry river gravels from abandoned tributaries. Particularly rich in diamond were the diggings at Colesburg Kopje, later to become the Kimberley Mine and the associated mining settlement was the basis of the present city of Kimberley.

It became evident during the exploitation of these "dry" diggings that they were different from alluvial gravels and sands. The mined material was soft and friable with abundant mica flakes, garnets, diopsides, ilmenites, and occasional large rounded nodules.

This unusual, ultrabasic rock was termed kimberlite by Lewis (1887). Kimberlite is defined as a hybrid igneous rock that contains fragments of different rock types in a matrix of ultrabasic minerals. The kimberlite matrix consists of olivine, orthopyroxene and phlogophite with carbonate and serpentine minerals (Smith, 1983, Mitchell, 1986). The kimberlite matrix shows variable amounts of K_2O(0.98-2.10 wt.%), CaO(7.6-10.6wt.%), Al_2O_3(4.4-4.9wt.%), TiO_2(2.03-2.32wt.%), P_2O_5(0.66-0.76wt.%) and CO_2 (7.4-3.3wt.%). Kimberlite is also enriched in rare earth elements relative to chondrites (Dawson, 1980, 1984). Kimberlite is assumed to have a mantle origin because it contains xenoliths of mantle rocks (including lherzolite, harzburgite, dunnite and eclogite). The kimberlite was shown to consist of an oxidized upper part called "yellow ground" and a deeper, unoxidised part, known as "blue ground". The marked change in texture led many miners to believe that the base of the "yellow ground" was the base of a supposed alluvial deposit.

Subsequent to the work of Lewis, major studies of South African kimberlites were completed by Wagner (1914) and Williams (1932) with a comprehensive study of Siberian kimberlites by Bobrievich *et al.* (1959). Since then scientific interest has been considerably expanded through the International Kimberlite Conferences, first started in 1973.

In addition to kimberlite diamonds have also been found in economic quantities in one lamproite intrusion in Australia. Lamproites are ultrapotassic, magnesian rocks consisting of olivine, orthopyroxene, clinopyroxene and sanidine. Low concentrations of diamonds have been reported in ultramafic bodies in fold mountain belts and in island arcs (Dawson, 1979). Haggerty and Nagieb (1989) have found diamonds in high sodium volcaniclasite breccias near the

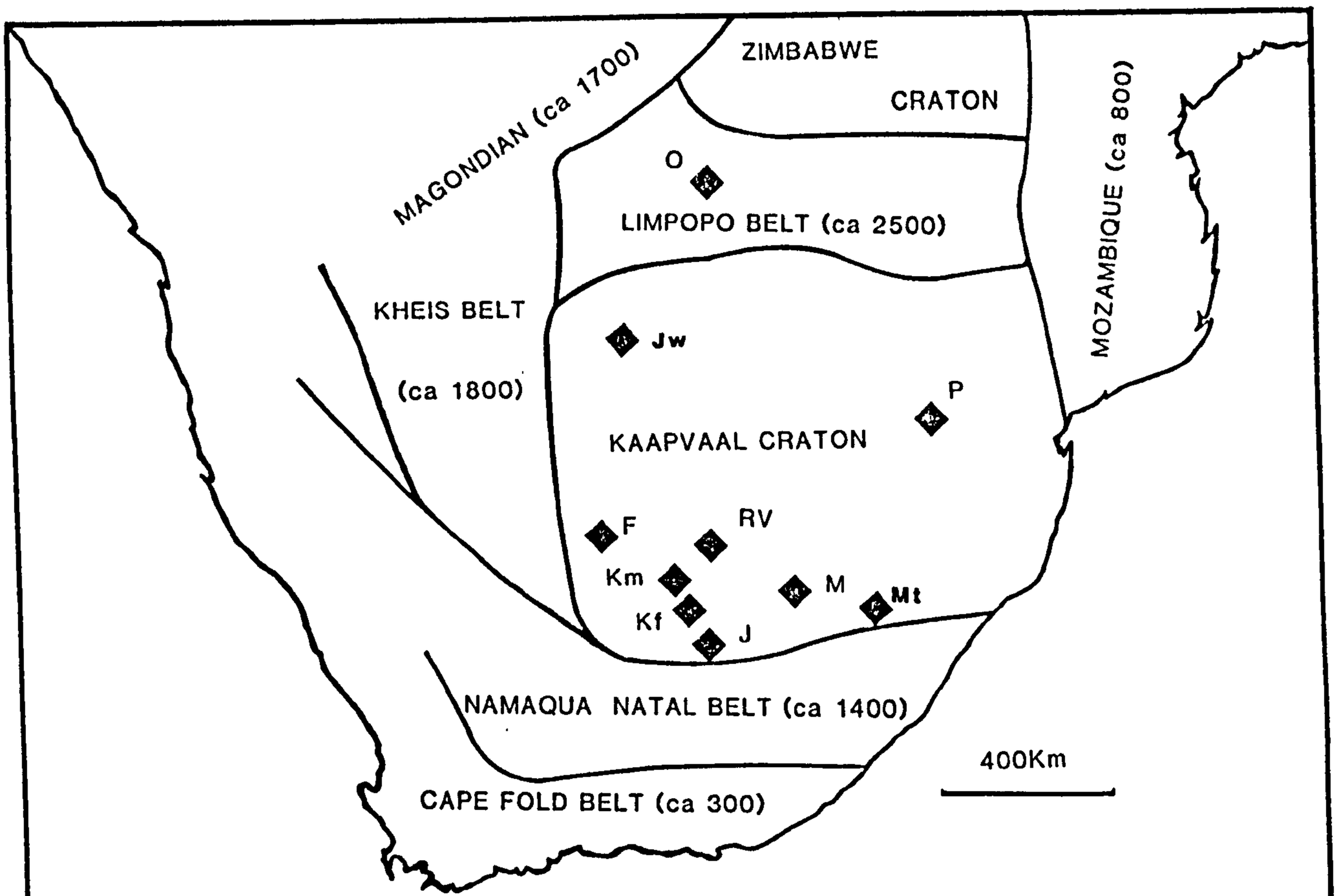

TECTONIC FEATURES OF SOUTHERN AFRICA

Fig. 1.2
Tectonic Features of Southern Africa.

Diamondiferous Kimberlites are restricted to the Kaapvaal Craton, the Zimbabwean Craton and the Limpopo Belt, although the latter is believed to be a former Archean Mobile Belt (Coward & Fairhead, 1980). Important diamondiferous kimberlites include Finsch (F), Roberts Victor (RV), Monastery (M), Premier (P), Jagersfontein (J), Koffiefontein (Kf) and Orapa (O). The mines at Kimberley (KM) are the De beers Pool Mines. Jwaneng in Botswana is shown as Jw and the Mothae Mine in Lesotho is shown as Mt (see for example Dawson, 1984).

Syrian Graben. A hexagonal polymorph of diamond, lonsdaleite, occurs in meteorites probably as a result of the high temperatures and pressures developed during meteorite impact.

Diamond occurs in kimberlite and lamproite as a trace mineral. In kimberlites a grade of 100 carats of diamonds per 100 tonnes is considered to be very economic. Only one lamproite is at present being mined, at Argyle, in Australia and this has a grade of 200-300 carats per 100 tonnes.

Generally, diamondiferous kimberlites are restricted to cratons, where the basement is formed of moderate to weakly deformed rocks of low to medium metamorphic grade, and where metamorphism is no later than 2400ma. As can be seen in figure 1.2 the diamondiferous kimberlites of Southern Africa are restricted to the Kaapvaal Craton and the Archean Limpopo Belt. Cratons act as rigid blocks and are thus surrounded by younger fold belts, in figure 1.2 the fold belts that surround the craton are devoid of diamondiferous kimberlites. Cratons posses a thick, keel-shaped lithosphere that is of sufficiently low temperature to have diamonds present as a stable phase.

Diamonds are resistant to chemical attack and posses great mechanical strength. As a consequence when kimberlites are eroded, diamonds can be transported by river systems away from their primary source. Diamonds can become concentrated in river gravels and if the concentrations are high enough the alluvial deposits can be exploited. In addition, diamonds can be concentrated in beach sediments by sedimentary processes and the deposits of Namibia that are currently being mined are of this type.

1.3 Aims and Objectives.

It was concluded in the early part of this century that kimberlites were derived from great depths (Wagner, 1914 & Williams, 1932). A study of the graphite to diamond transition, (see figure 1.3) by Kennedy and Kennedy (1976) and Bundy (1980), has shown that natural diamond originates at pressures

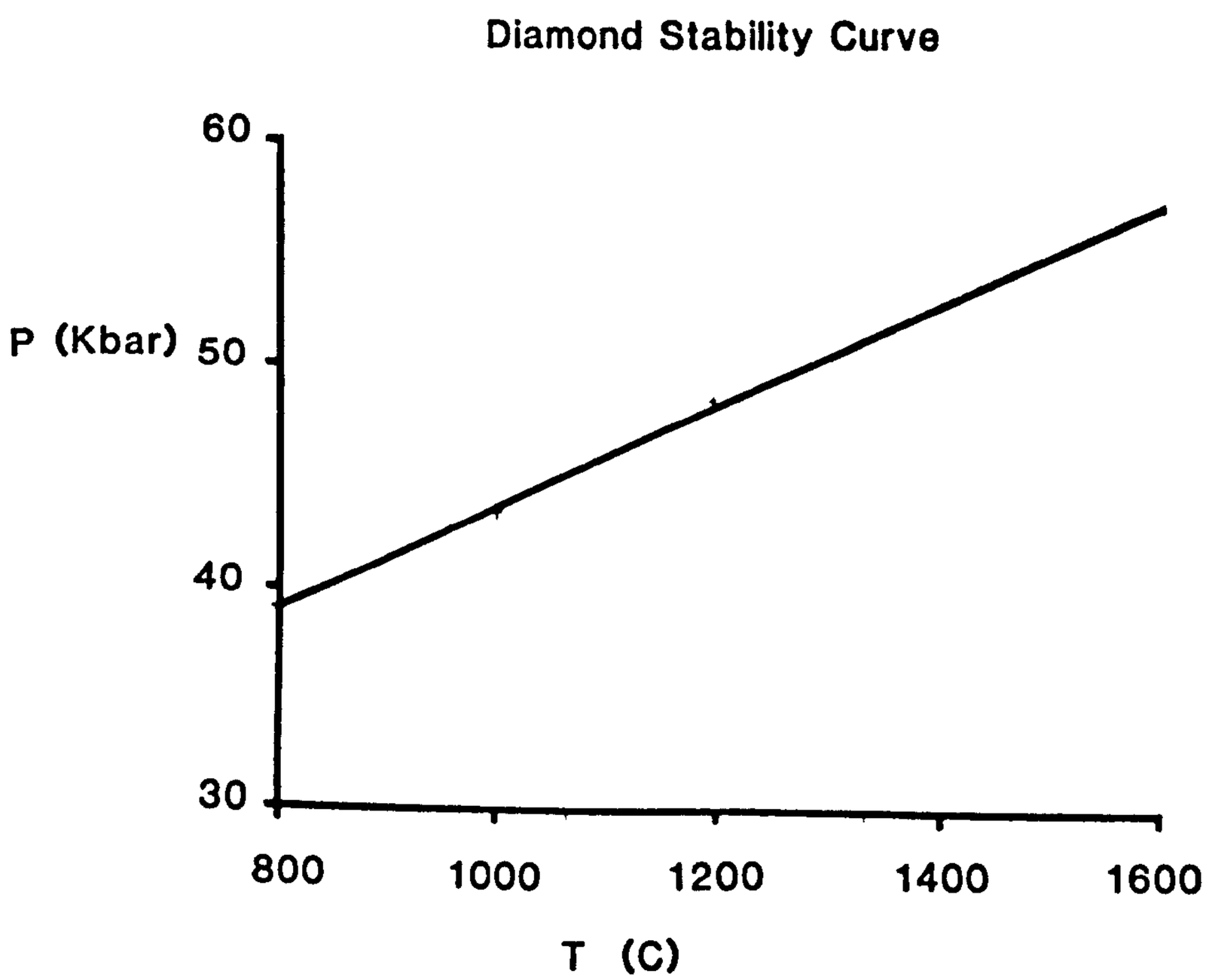
Diamond Stability Curve
60
P (Kbar)
50
40
30
800
1000
1200
1400
1600
T (C)

Fig 1.3.

Diamond Stability Curve.

The experimental results of Kennedy and Kennedy (1976) have determined the transition of diamond to graphite defined by the equation P(kbar) = 19.4 + $T^{o}C$/40kbar. This equation is consistent with pressure and temperature estimates from syngenetic diamond inclusions and conditions of growth for synthetic diamonds.

and temperatures corresponding to depths in excess of 120km. Although kimberlites contain diamonds and both kimberlites and diamonds are mantle derived, until recently the genetic relationship between the two was uncertain. A problem for example was whether diamonds were phenocrysts in a kimberlite magma, or xenocrysts as a consequence of the fragmentation of diamond-bearing mantle rocks.

Diamonds preserve geochemical information from the upper mantle in the form of syngenetic mineral inclusions and as substitutional impurities in the diamond lattice. A study of these characteristics will reveal details of the chemistry and processes which occur in the upper mantle.

The general aim of diamond studies is to establish the inter-relationship between diamond and kimberlite, and the chemistry, thermal structure, and redox conditions of the mantle. To investigate these features, three broad lines of inquiry are used: the study of mineral inclusions, the study of nitrogen impurities, and the study of carbon isotopes. Within these general objectives this thesis will examine the characteristics of diamonds from two distinct localities.

The two mines studied are the Bultfontein mine at Kimberley, South Africa and the Sao Luiz alluvial mine in Brazil. The Bultfontein mine consists of a Cretaceous kimberlite pipe intruded into the Archean, Kaapvaal Craton while the diamonds from Sao Luiz are believed to have been derived from Cretaceous kimberlites within a Proterozoic fold belt of the north east Mato Grosso area of Brazil. Bultfontein data enables a comparison to be made with diamonds from other mines on the Kaapvaal Craton and in particular, investigates the variations of the three characteristics referred to above within a cratonic environment. The diamonds at Sao Luiz are used to investigate the processes of diamond formation beneath a Proterozoic fold belt. Particular attention is paid to the depth of origin of these diamonds through study of the chemistry of inclusions, because the kimberlites originate in lithosphere that is thinner than that in cratons.

More than one source of diamond may be sampled by an individual kimberlite. Diamond characteristics within these single sources are therefore examined in order to assess any such variations.

This thesis will also examine the mineral inclusions in diamonds from the two mines. The composition of such minerals is directly related to the chemistry of the diamond growth environment and provides information on the temperature, pressure and redox conditions of diamond growth. Infra red techniques were used to reveal the nature of nitrogen aggregation in diamond and provide some kinetic evidence for the environment of diamond growth. In addition an infra red technique was used to establish the variation in nitrogen characteristics across diamonds.

Carbon isotope studies were used to look for different carbon growth environments with respect to paragenesis, and to assess how the d ^{13}C composition is influenced by fractionation processes. During the course of this study a non-destructive technique to measure the carbon isotope composition of small areas of diamond by ion microprobe was developed. In consequence the micro-variation of carbon isotopes across a diamond can now be determined.

The basic characteristics of diamonds and the techniques used to study them are presented in chapter 2. The characteristics of Bultfontein diamonds and their inclusion compositions are presented in chapter 3. In chapter 4 the nitrogen and carbon characteristics of Bultfontein diamonds are documented. In chapter 5 the implications for mantle composition and evolution of the Bultfontein diamonds are discussed. The characteristics of Sao Luiz diamonds and their inclusions are outlined in chapters 6 and 7 and in chapter 8 their relationship to mantle composition and their depth of origin is discussed.

Chapter 2.

Kimberlites, Diamonds and Inclusions.

This chapter will outline the characteristics of kimberlite and will discuss the composition of the mantle. The chemistry of diamond inclusions is then detailed because diamonds are chemically related to kimberlites and mantle compositions. Other characteristics of diamond are then discussed, including diamond morphology, carbon isotope composition and nitrogen aggregation state. In the final section of this chapter the techniques used to study diamonds are outlined.

2.1 Kimberlite Characteristics.

Kimberlite occurs as dykes and sills and conical intrusions of variable width, termed diatremes or pipes. The extensive mining of kimberlite in Southern Africa, has enabled Hawthorne (1975) to produce three dimensional models of these kimberlite diatremes. Figure 2.1 shows that three main zones of diatreme are defined: At relatively deep levels there is a feeder dyke zone, which consists of discrete columns of kimberlite which have thermal aureoles in the wall rock and in which localized brecciation has occurred. A middle or diatreme zone grades from the feeder zone, and represents breakthrough of the kimberlite into higher levels of country rock. The accompanying decompression of gas results in further brecciation and incorporation of large fragments of wall rock as "floating reefs". The upper crater zone consists of bedded tuffs, wall rock breccias and kimberlite breccias which represent the pyroclastic deposits from the explosive breaching of the ground surface by kimberlite.

Smith (1983) divided kimberlites from Southern Africa into two groups on the basis of emplacement age, mineralogy, geochemical and isotopic character. These two groups are shown in Table 2.1. Group I kimberlites have emplacement

Model of Kimberlite Pipe

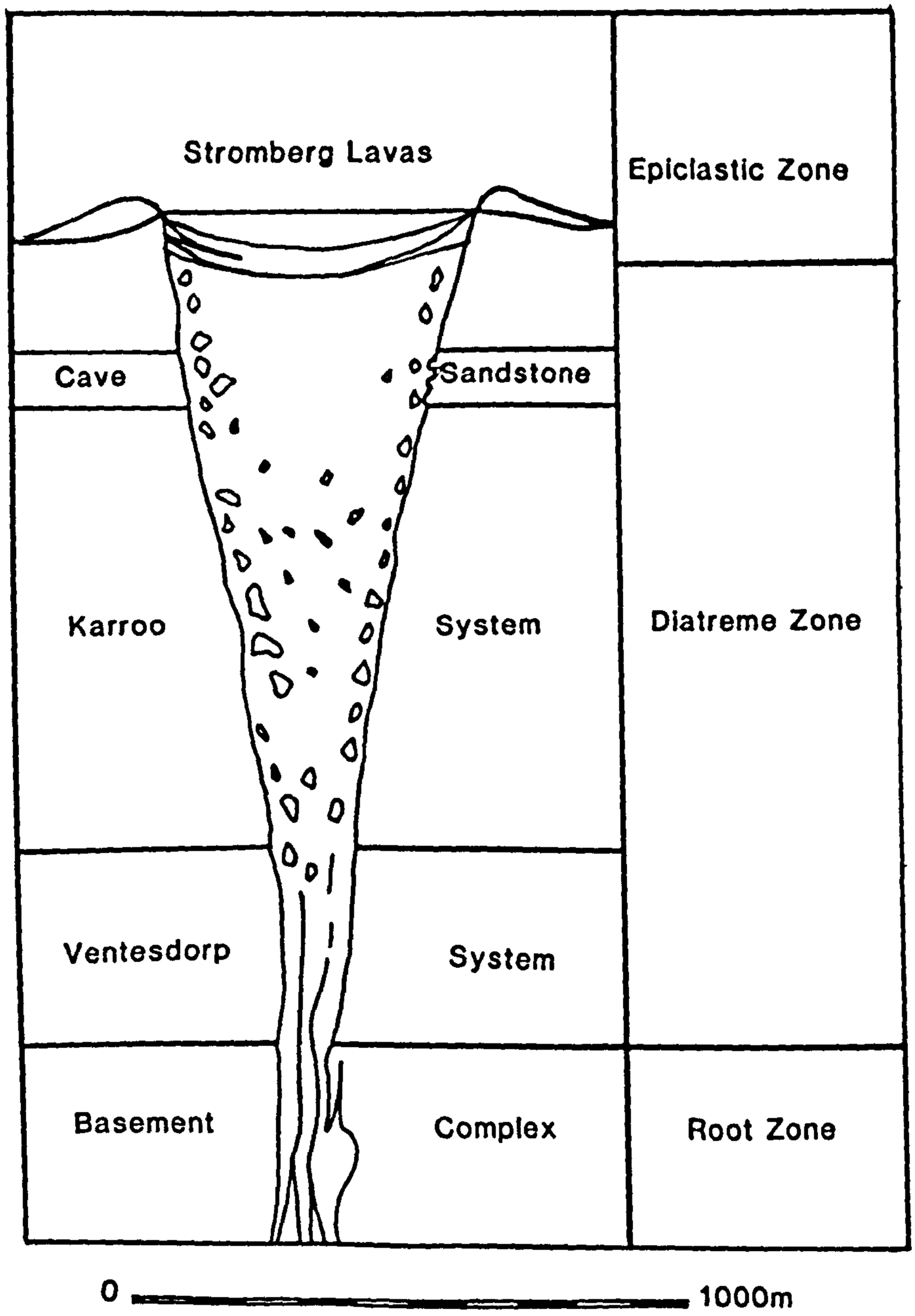

Fig 2.1.

Model of a Kimberlite Pipe.

The kimberlite pipe model of Hawthorne (1975) is based on the field relations of the numerous kimberlite pipes in South Africa and their different degrees of erosion. The kimberlite pipe is divided into three. The top epiclastic zone comprises kimberlitic tuffs and breccias which may show a stratification, a result of washing of tuff into crater lakes and subsequent deposition as a sediment, this zone is characteristic of kimberlites which have undergone little erosion such as the kimberlites of Orapa, Botswana and Mwadui, Tanzania. the diatreme zone comprises primary kimberlite and inclusions of wall rock material and is characteristic of the more deeply eroded kimberlites such as those in the Kimberley area of South Africa. The root zone consists of dykes of kimberlite magma which sometimes culminate in "blind" kimberlite channels with no diatreme or epiclastic expression, the root zones are typical of the deep levels currently being mined at Kimberley, the kimberlite emplacement is largely controlled by jointing in the country rock and joint bounded contacts are common. The development of a kimberlite pipe is envisaged as an upward migration of embryonic kimberlite magmas followed by explosive breaching of the surface to form an early epiclastic or crater zone, diatreme development results from the post breakthrough modification of crater zones by vapour-solid fluidised systems which result from magma degassing and develop downwards to depths of up to approximately 1000m below surface level (Dawson, 1984).

Table 2.1

Kimberlite Groups

	Group I	GroupII
Age	86-114ma	114-150ma
$^{87}Rb/^{86}Sr$	0.04-1.52	0.14-0.78
$^{87}Sr/^{86}/Sr$	0.7033-0.7044	0.7074-0.7109
$^{147}Sm/^{144}Nd$	0.085-0.096	0.062-0.087
$^{143}Nd/^{144}Nd$	0.51271-0.51277	0.51208-0.51227
$^{238}U/^{204}Pb$	17.2-61.3	8.36-19.0
$^{206}Pb/^{204}Pb$	18.86-19.04	17.21-17.63
$^{207}Pb/^{204}Pb$	15.52-15.69	15.47-15.62

From Smith (1983)

ages of 80 to 114ma (Allsop & Barrett, 1975) and are mica-poor with only minor amounts of phlogopite present. Group II kimberlites have much older emplacement ages of 114 to 140ma and have phlogopite as a dominant groundmass mineral.

The significant variations in Sr, Pb and Nd characteristics also correlate with the two major divisions. Group I kimberlites have low initial strontium isotope values of 0.7033 to 0.7044 compared to 0.7074 to 0.7109 in Group II. Group I kimberlites have Pb values which indicate a higher amount of radiogenic lead than in Group II, for example $^{206}Pb/^{204}Pb$ ratios of 18.86 to 19.04 for Group II compare with 17.21 to 17.63 for Group I. U/Pb ratios in Group II are higher as a result of the lower Pb content. According to Kramers (1977) the differences in isotopic compositions represent differences in the chemistry of the mantle source. the low $^{143}Nd/^{144}Nd$ ratios for Group II kimberlites and their high initial $^{87}Sr/^{86}Sr$ and high $^{87}Rb/^{86}Sr$ ratios indicate a Sm and Rb enriched source (Kramers *et al.*, 1981). Group I kimberlites originate in an ordinary, undifferentiated or slightly depleted source (Kramers *et al.*, 1979 and Richardson *et al.*, 1985).

Of the kimberlites from the Kaapvaal Craton, shown in figure 1.2, Kimberley, Monastery and Jagersfontein are all Group I , while Roberts Victor and Finsch are Group II.

2.2 Mantle Composition.

Examination of mantle material is mainly through the study of xenoliths in ultrabasic, basic and alkali igneous rocks.

A classification of the texture, mineralogy and chemistry of mantle xenoliths has been proposed by Harte (1987 and 1983) and in kimberlites four main groups of such rocks are recognised (e.g. Harte, 1983):

1) Megacrysts: These are large, single crystals. Most commonly these are garnet, diopside and ilmenite but may also be olivine and orthopyroxene.

2) Peridotites: These are rocks of dominantly olivine and orthopyroxene but often contain small amounts of garnet and clinopyroxene.

3) Eclogites: Eclogites consist mainly of clinopyroxene and garnet with occasional kyanite, corrundum and spinel. Clinopyroxene and garnet compositions are relatively calcium and iron rich in comparison to equivalent minerals in peridotites.

4) Glimmerites and MARID suite rocks: These distinctive rocks consist of phlogopite only (Glimmerite) or an assemblage of phlogopite (Mica), Amphibole, Rutile, Ilmenite and Diopside (MARID). These phases are rich in Mg, Fe, Ti, K, Ba and trace incompatibles and are similar to phases found in veins in metasomatised peridotites. MARID suite rocks may originate as incompatible enriched melts introduced along stress induced pathways in peridotites (Dawson, 1987).

The most common nodules in kimberlites are peridotites. These consist of harzburgites (olivine and orthopyroxene) and lherzolites (olivine, orthopyroxene and clinopyroxene). Olivine and orthopyroxene comprise more than 80% of these rocks consists. In addition garnet and sometimes chrome spinel maybe present. Olivine poor rocks such as garnet websterite are rare, as are complete olivine rocks (dunite).

The texture and geochemistry of peridotite xenoliths are very diverse. Harte and Gurney (1980) and Harte (1983) have divided these xenoliths into three textural groups:

A. Coarse xenoliths; Characterised by equant mineral grains of 2 to 10mm in size.

B. Deformed xenoliths; Which show porphyroclastic and mosaic textures,

C. Modally metamorphosed xenoliths; These show evidence of fluid infiltration in the form of phlogopite, ilmenite, richterite, oxides and sulphides.

On the basis of the chemistry the peridotites are divided into two groups; fertile and depleted. Fertile peridotites are those which are enriched in basaltic

components such as CaO and Al_2O_3 (greater than 2.0 wt.%), and TiO_2, Na_2O and K_2O (usually greater than 0.2 wt.%). Fertile peridotites also have a low Mg/Mg+Fe ratio (0.90 to 0.91). Geothermobarometry studies distinguish "Hot" and "Cold" peridotites. Hot peridotites have equilibrium temperatures greater than 1100°C while cold peridotites have equilibrium temperatures of 900 to 1100°C.

The relatively fertile nature of hot xenoliths and the depleted character of cold xenoliths has been attributed to a derivation from the asthenosphere and the lithosphere respectively (Boyd, 1973, Boyd & Finnety, 1980). Harte & Gurney, (1980) consider that the Fe-Ti enrichment in hot deformed xenoliths may represent the migration of Fe, Ti, Ca, Na, Al and LREE between wall rock peridotite and intrusive, asthenosphere derived magma bodies. In addition the mantle can be altered by infiltrating metasomatic fluids (Bailey, 1984, Harte, 1987 and Wyllie, 1987).

2.3 Inclusions in diamond.

Diamonds contain inclusions which may be either, syngenetic, that is formed during diamond growth, or epigenetic, formed subsequent to diamond growth as defined by Harris (1968a and b). Table 2.2 lists the minerals that occur as inclusions in diamonds. Syngenetic inclusions are usually discrete crystals of up to 200mm in size, but may also be irresolvable clouds. Syngenetic inclusions are those which have stability fields that overlap those of diamond formation. They often have a cubo-octahedral morphology and are frequently aligned parallel to the diamond (100) and (111) crystal directions. Harris and Gurney (1979) have suggested that this is a result of the mutual growth of diamond and the inclusion, the diamond morphology imposing onto the inclusion because of it's higher form energy.

Epigenetic minerals are invariably red or brown and occur rarely as discrete crystals, but more often as mineral powders located in obvious surface fractures

Table 2.2

Inclusions in Diamond.

Syngenetic		Epigenetic
Periodotite	**Eclogite**	
Garnet (purple)	Garnet (orange)	Goehtite
Olivine	Clinopyroxene	Quartz
Orthopyroxene	Kyanite	Muscovite
Chromite	Coesite	Graphite
Clinopyroxene	Rutile	Sulphide
Mg-ilmenite	Ilmenite	Mn-ilmenite
Sulphide	Sulphide	Haematite
Zircon	MgO/FeO	Kaolinite
Coesite	Moissanite	Sellaite
Native iron	Corrundum	Xenotome
Clouds	Clouds	Acmite
Diamond	Diamond	Richterite
		Perovskite

in diamond. Epigenetic inclusions have stabilities that preclude a primary association with diamond.

Meyer and Boyd (1972) subdivided syngenetic inclusions into two groups: The peridotite (or ultramafic) paragenesis and the eclogite paragenesis. Both inclusion types occur in the same diamond mine but the abundance of each inclusion type varies with locality.

2.3.1 Peridotite suite inclusions.

Olivines: These are generally colourless inclusions which have a cubo-octahedral morphology. Olivine inclusions have a restricted range in magnesium composition from Mg/Mg+Fe values of 0.91 to 0.95. The chrome contents of these olivines (over 0.4 wt.%) is much higher than the chrome content of olivines of similar magnesium content such as olivines from komatiites. However some olivines, such as those from Finsch have no detectable chrome. Meyer and Boyd (1972) and Meyer (1975) have suggested that some of the olivine chrome may be in the divalent form (Cr^{2+}). Hervig *et al* (1980) have reported minor amounts of Na (~90ppm) and Ca (~280ppm) with trace amounts of Li, Sc and Ti, which increase with iron content.

Orthopyroxenes: These are usually colourless cubo-octahedra that have a similar appearance to olivine. The orthopyroxene are generally very magnesian with Mg/Mg+Fe values of 0.91 to 0.95. Some orthopyroxenes are relatively iron rich with values of Mg/Mg+Fe of 0.77 to 0.91. Most of these iron rich orthopyroxenes have been recorded at Orapa by Gurney *et al* (1984). Calcium contents of orthopyroxene inclusions are very low, usually less than 0.5 wt.%.

Garnets: Garnet inclusions of peridotite paragenesis have a distinct purple to deep red colour that is a result of high chrome contents, usually greater than 6.0wt.%. The garnets are very pyrope rich and have Mg/R^{2+} values of 0.77 to 0.65. Calcium contents are low (less than 5.0wt.%) and the garnets are usually referred to as sub- or low-calcic garnets.

Clinopyroxenes: These are very rare and have a deep emerald green colour which is a function of chrome contents of up to 1.0wt.%. Mg/Mg+Fe values range from 0.93 to 0.94. The calcium contents range from Ca/Mg+Ca values of 0.46 to 0.37. The sodium contents are high (1.0 to 2.0wt.%) and Sobolev (1977) has termed these compositions chrome-omphacites.

Chromites: Chromite or chrome spinel inclusions have high chrome contents with up to 66.0wt.% Cr_2O_3. The magnesium contents are variable and Mg/Mg+Fe ratios range from values of 0.30 to 0.60. The chromites are usually solid solutions between $FeCr_2O_4$ and $MgCr_2O_4$, with only a limited amount of spinel solid solution (up to 13% of $(Fe,Mg)Al_2O_4$).

Peridotite suite inclusions have different compositions to equivalent minerals found in mantle xenoliths. Olivines and orthopyroxenes have higher magnesium contents (Mg/Mg+Fe 0.93 compared to 0.90 to 0.91). Peridotite paragenesis garnet inclusions have lower calcium contents than garnets in lherzolites. Chromite inclusions have up to 20wt.% more chrome than chromites in lherzolite nodules. Peridotite paragenesis clinopyroxenes are rare even though there may be up to 10 modal % of clinopyroxene in lherzolites.

Studies by Richardson *et al* (1984) have shown that peridotite suite garnet inclusions in diamonds have an age of 3.3 Ga $\pm$ 0.1. This work has also showed that garnet inclusions have high $^{87}Sr/^{86}Sr$ and high $^{144}Nd/^{143}Nd$ ratios and suggest an enrichment in Rb and Sm of the diamond source prior to diamond formation. Peridotite suite inclusions have similar magnesian contents to olivines and orthopyroxenes in komatiites (Arndt & Nisbet, 1982). There is also a similarity between eruption ages of komatiites, 3.54Ga, (Viljoen *et al*, 1982) and peridotite suite diamonds. Gurney (1984) has suggested that diamonds may originate in a harzburgite layer that is a remnant from komatiite volcanism.

2.3.2 Eclogite suite inclusions.

The minerals which comprise eclogite paragenesis inclusions are also shown in table 2.2. The most abundant eclogite inclusions are clinopyroxene and garnet.

Clinopyroxenes: These have calcium, magnesium and iron contents that are close to augite compositions. The Mg/Mg+Fe ratios range from 0.68 to 0.88. Sodium contents divide clinopyroxenes into two groups (Meyer, 1987). Low sodium clinopyroxenes have less than 2.0 wt.% Na_2O and have been termed calc-silicate group by Sobolev *et al.* (1984). Clinopyroxenes with high concentrations of sodium (2.0 to 8.0 wt.%) are termed omphacite. Both types of clinopyroxenes have low chrome contents, less than 0.1 wt.%, and have lower Mg/Mg+Fe ratios (~0.7) than peridotite suite clinopyroxenes.

Garnets: Eclogite suite garnet inclusions have an orange to red colour and have a lower chrome content than peridotite paragenesis garnets (usually less than 0.1 wt % Cr_2O_3). The garnets have pyrope-almandine compositions with a range in Mg/Mg+Fe contents of 0.59 to 0.72. Calcium contents show a range of Ca/R^{2+} values of 0.18 to 0.27. In addition there may be up to 1.0 wt.% of titanium and sodium.

Other eclogite suite inclusions include coesite, a high pressure polymorph of quartz which occurs as colourless cubo-octahedra.

Also recorded as eclogite suite inclusions in diamonds are kyanite, rutile, moissanite and corrundum (ruby).

Richardson (1986) determined the ages for eclogite paragenesis garnets and clinopyroxenes. Burgess *et al.*, (1989) and Philips *et al.* (1989) have determined the ages of eclogite paragenesis clinopyroxenes. For four mines the inclusions have a range in ages of 990 to 1580ma (see Richardson, 1989). Eclogite paragenesis inclusions are considerably younger than peridotite paragenesis garnets.

2.3.3 Sulphide inclusions.

Sulphides are the most common inclusion in diamond according to Harris and Gurney (1979) and may occur as thin smears on internal diamond cleavage surfaces, and as coats associated with discrete crystals. The most common sulphides belong to the system Fe-Ni-Cu-S and are pyrrhotite, pentlandite, chalcopyrite and pyrite. In addition haezlewoodite, cubanite and native iron occur as sulphide inclusions.

From phase studies sulphides in the mantle exist as a single phase, monosulphide solid solution (M_{ss}). Sulphide inclusions generally show exsolution textures with exsolutions of chalcopyrite and then pentlandite exsolved from M_{ss} to leave a pyrrhotite host. These features probably represent the exsolution of excess nickel and copper during the breakdown of monosulphide solid solution.

Sulphides can coexist with inclusions of both peridotite and eclogite paragenesis. Yefimova *et al* (1983) have shown that subsolidus (M_{ss}) peridotite paragenesis sulphides have a high nickel contents (from 16.5 to 29.8 % Ni). Eclogite paragenesis sulphides have low nickel values of 0.5 to 8.2 % Ni (see Gurney, 1989).

2.4 Diamond characteristics.

Diamonds crystallise as single crystals and polycrystalline aggregates (bort and carbonado). Ten groups of diamond have been classified by Orlov (1973), five of which are single crystals. The two most common single crystal forms are the octahedron (Group I) and cube (Group II). Modifications of the basic octahedral or cubic shape result from dissolution of the diamond. There is a complete transition from octahedra to dodecahedra diamonds with rounding of four fold coigns until each octahedron face becomes triple faceted and a dodecahedron is produced as shown in figure 2.2 (Williams, 1932, Harris *et al*, 1975). Cubic diamonds show a similar modification and form hexatetrahedra.

Diamond Morphology

Octahedron

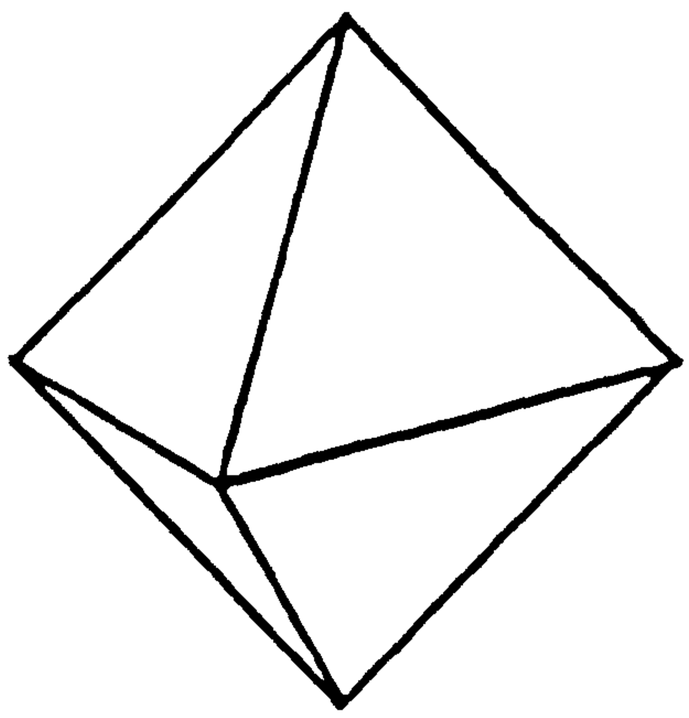

Dodecahedron surfaces on octahedron

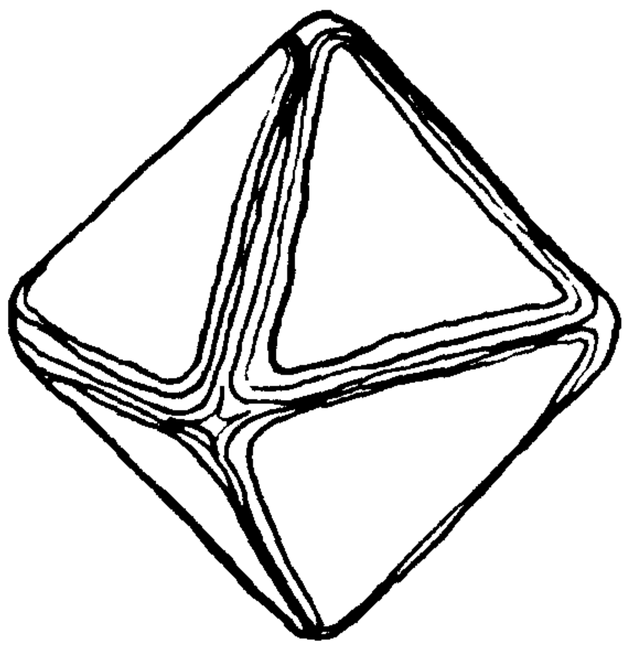

Rhombic dodecahedron

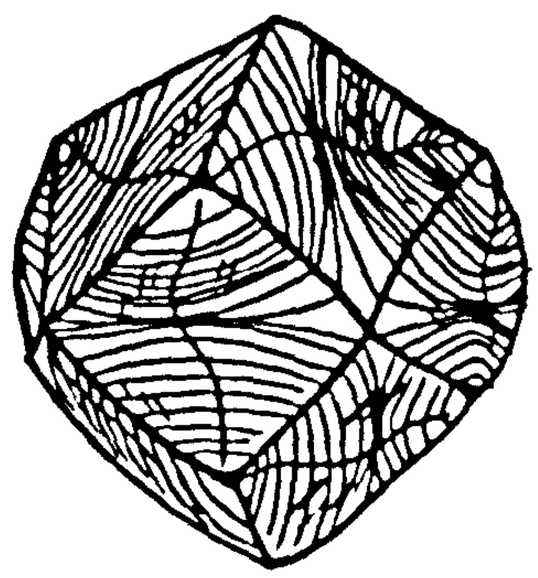

Fig 2.2

Diamond Morphology.

Most natural diamonds have a basic octahedral morphology which has variants in the form of macles (twins of octahedra) and aggregates of octahedra. An important modification of the octahedron is the development of dodecahedral diamonds which result from the dissolution of diamond by corrosive fluid along fourfold crystal directions. The development of the rhombic dodecahedral diamond shape is a progression through an octahedral diamond with dodecahedral faces developed on the edges of the (111) faces. In dodecahedron diamonds the surfaces are rounded and often show plastic deformation lines parallel to the (111) cleavage direction, striations on the dodecahedral faces represent individual growth increments. There is a sinuous medial line on the dodecahedral surfaces which represents the meeting of dissolution fronts from opposite four fold directions.

Group III diamonds show differences in colour between the core and rims and are termed coated stones. Group IV diamonds are also coated but have coats that are structurally different from the cores. Group V diamonds have a high concentration of graphite. The remaining five groups are different forms of polycrystalline aggregates. Diamonds are frequently twinned in the form of triangular crystals (macles) consisting of two octahedral (111) faces separated by a twin (macle) plane parallel to the (111) direction. Aggregated crystals are distinguished from macles by the fact that they show aggregation along an irregular, common surface, rather than the macle plane.

In table 2.3 the classifications of diamonds according to Harris *et al* (1975) are shown. Primary divisions are based on the crystal shape. Further divisions are made on the basis of transparency, colour, inclusion content and surface features.

Colourless, yellow and brown are the three main body colours for diamonds. In addition diamonds may have a blue body colour as a result of boron impurities. Transparent green coats can occur on diamonds and, Vance *et al*, (1973) have shown these to be a result of α particle bombardment. Green coated diamonds are most common in the weathered, upper levels of kimberlites where uranium rich ground waters can circulate.

Surface features of diamond are diverse. Commonly these included hillocks, striations, ruts, growth lamellae and etch pits. An example of the etch features present are the pyramidal shaped etch pits, termed trigons which are shown in figure 2.3. The edges of trigons are aligned parallel to the cleavage directions of diamonds and are referred to as being positive if they are aligned in the same orientation as the octahedral edges. Experiments by Harris and Vance, (1972) which etched diamonds by volatiles exsolved from kimberlite produced both positive and negative trigons, but experiments by Yamaoka *et al* (1980) showed that the orientation of trigons varies as a function of the partial pressure of oxygen. At low oxygen fugacities the trigons produced have a positive orientation while

Table 2.3

Diamond Characteristics.

Primary Divisions.

Crystal Forms.	Others.
Octahedra	Macles
Dodecahedra	Spheres
Cubes	Irregular
Tetrahedra	Crystal Aggregates

Secondary Divisions.

Transparency	Colour
Transparent	Colourless
Opaque	Yellow
	Brown
	Green
	Orange & Amber
	Pink & Mauve
	Blue
	Black
	Grey
	Smokey
Inclusion Content.	**Surface Features.**
	Transparent Coats
None	Graphite Coats
Few (1-3)	Opaque Coats
Many (>3)	Frosting

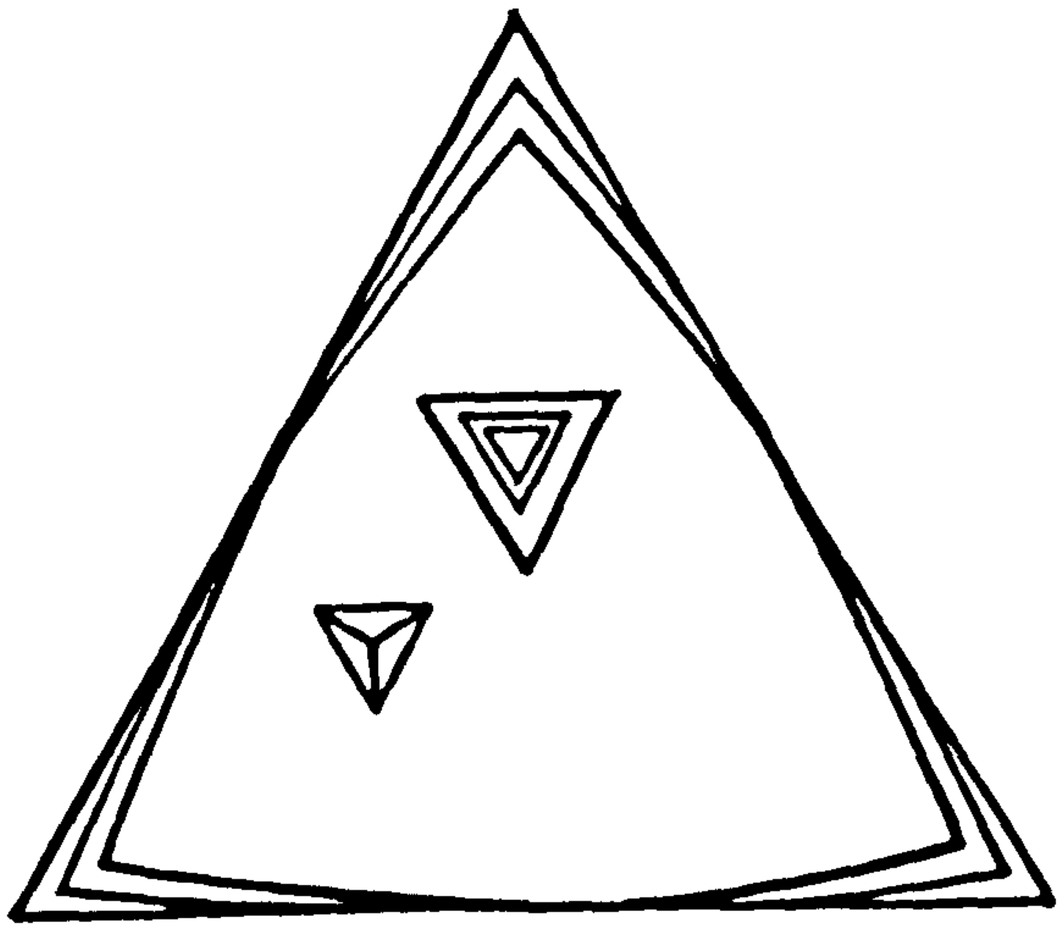

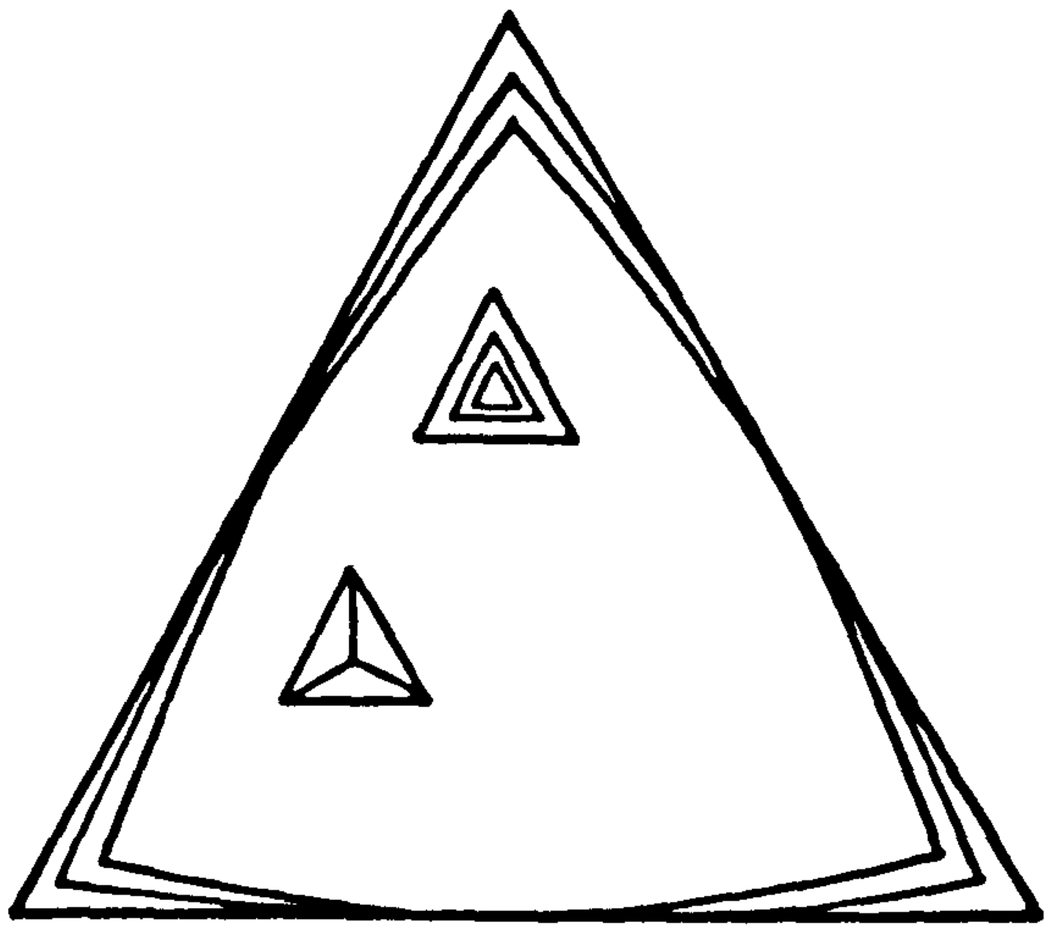

Diamond Surface features

Fig 2.3

Diamond Surface Features.

Two octahedral (111) faces are shown both of which show the development of trigons. In the upper diagram the trigons are negative, that is the orientation of the apicies of the trigons and the octahedron faces differ by 180^{o}. The lower diagram has positive trigons. Shallow trigons have a pyramidal shape while deeper trigons show stepped edges.

at relatively high oxygen fugacities negative trigons are developed. Such a result is consistent with the observation that positive trigons are rare.

Plastic deformation lines are another common etch feature, these probably result from deformation processes in the mantle. Plastic deformation lines are seen as closely spaced, multiple lines that are parallel to the diamond cleavage directions. Plastic deformation features are independent of diamond size and are assumed to have been produced following diamond formation. Harris *et al* (1983) have noted that there is a close correlation between plastic deformation features and brown diamonds.

2.5 Carbon isotope composition.

Studies of the stable carbon isotopes in diamond have shown that most diamonds have a $\delta\ ^{13}C$ value of between -4 and -9 $^{o}/_{oo}$ vs PDB (Deines, 1980). Much of the initial work suggested that there was an average mantle carbon isotope composition close to -5 $^{o}/_{oo}$. More detailed studies of diamonds from known mines, and of known paragenesis have shown that there is a wide range of carbon isotope values from as low as -34 $^{o}/_{oo}$ (Sobolev *et al.*, 1979) to as high as +5 $^{o}/_{oo}$ (Sobolev *et al.*, 1979; Sobolev, 1984). In consequence the distribution of carbon isotopes is skewed towards light carbon isotope values. Nevertheless, as shown by Harris (1987) in figure 2.4, the mode carbon isotope values from a large number of localities including Australia, Southern Africa and the Soviet Union are close to -5 $^{o}/_{oo}$. Deines (pers.comm.) believes that the effects of isotope fractionation in the upper mantle can only account for a range of 4 to 5 $^{o}/_{oo}$ which, if true, indicate that isotopic heterogeneities exist within the mantle.

The two diamond parageneses show different carbon isotope compositions. As shown by Deines *et al.* (1984) $\delta\ ^{13}C$ values for eclogitic diamonds values show a wide range from -34 to +2 $^{o}/_{oo}$, whilst peridotite suite diamonds have a generally more restricted range of heavier values between -9 and -2 $^{o}/_{oo}$.

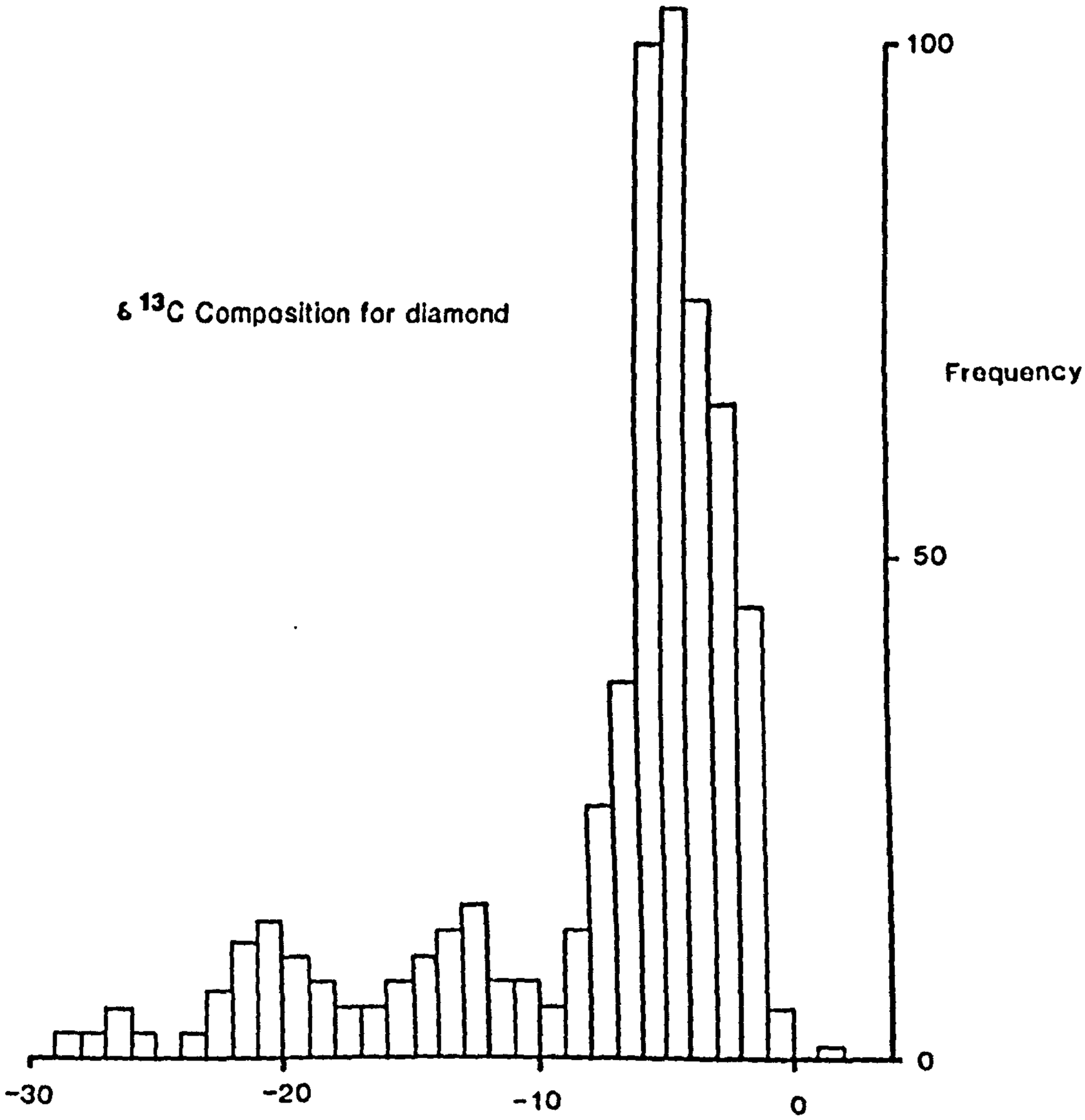
δ 13C Composition for diamond
100
50
0
Frequency
-30
-20
-10
0
13C

Fig 2.4

Carbon Isotope Composition.

Shown are values for $\delta\ ^{13}C$ for diamonds from a number of localities including Southern Africa and the U.S.S.R. (Deines, 1980). The mode of the $\delta\ ^{13}C$ values is between -6 and -5 $^{o}/_{oo}$. A significant feature is the fact that there is a wide range in carbon isotope values from +3 to -34 $^{o}/_{oo}$ and a positively skewed distribution. This distribution is similar to that of kimberlites and carbonatites.

2.6 Nitrogen Impurities in Diamond.

The most important substitutional impurity in diamond is nitrogen. Up to 0.55wt.% may be present although values normally range between zero and 2500ppm (Bibby, 1982). Substitution of nitrogen is determined by infra red spectroscopy, but there are other methods including ultraviolet spectroscopy, mass spectrometry and neutron activation analysis. Using infra red spectroscopy two divisions of diamond can be made; Type I which contain nitrogen and represent 98% of natural diamond, and Type II which contain no nitrogen that is detectable by infra red absorption (Robertson *et al.*, 1934). These two types are shown in table 2.4.

Table 2.4 also shows that Type I diamonds can be further subdivided depending on whether the nitrogen occurs as single substitutional atoms (Type Ib) or whether it is aggregated (Type Ia). Type Ib diamond has a distinctive yellow/amber colour and is rare in nature, whereas all synthetic diamonds are Type Ib.

Type IaA aggregate comprises a pair of nitrogen atoms (Davies, 1976). The Type IaB aggregate is more complicated and contains four nitrogens and a vacancy. Usually there is a combination of IaA and IaB nitrogen and the relative amounts are determined by measuring the absorption coefficient at two wavenumbers shown in figure 2.5, 7.8mm for Type IaA and 8.3mm for IaB. In addition there is a further absorption line at 7.3mm, which is termed the platelet peak. Platelets are complicated aggregates of nitrogen and possibly carbon which are aligned along the (100) crystal direction and may be observed using electron microscopy and X-ray diffraction.

Table 2.4

Nitrogen Characteristics.

Type I	**Type II**
> 30ppm Nitrogen	< 30ppm Nitrogen
Type Ia	**Type IIa**
Aggregated nitrogen	No nitrogen or Boron
IaA (nitrogen pairs)	
IaB (4 nitrogens + vacancy)	
N3 (2 nitrogens + vacancy)	
Platelets	
Type Ib	**Type IIb**
Non-aggregated	> 30ppm Boron
nitrogen.	

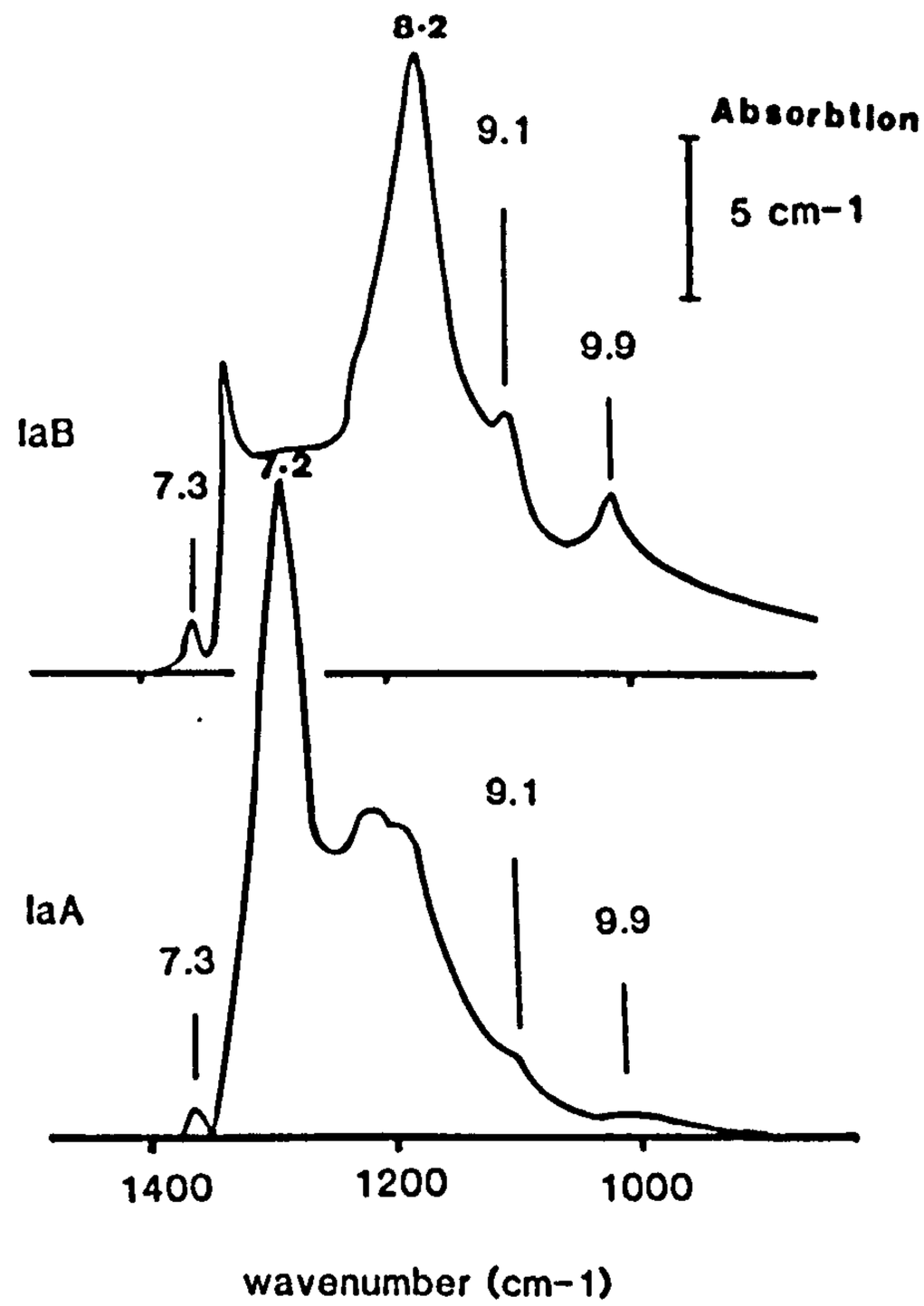

Infra Red Absorption Spectra for Type IaA and IaB Diamonds

Fig. 2.5.

Infra Red Absorption Spectra.

Most natural diamonds are Type Ia and contains nitrogen in an aggregated form as A or B centres. Infra red absorption spectra are used to determine the relative contribution of each of the aggregate.. IaA nitrogen has a strong absorption line at $1282cm^{-1}$ (7.8μm) and IaB has an absorption line at $1175cm^{-1}$ (8.2μm) in addition there is a further peak at 7.3μm which is the platelet peak. Natural diamond spectra are decomposed using the method of Davies (1981) to estimate the amounts of each aggregate.

From the evidence of nitrogen studies in synthetic diamonds nitrogen is believed to enter natural diamond as single substitutional atoms. Studies of the nitrogen aggregation process by Chrenko *et al.* (1977) and Evans and Qi (1982) have shown that single substitutional nitrogen aggregates to nitrogen pairs (Type IaA) and then to more complicated aggregates (IaB and platelets). The degree of aggregation is dependent on temperature and time. The aggregation rate of single nitrogen to pairs is faster than the IaA dissociation to higher aggregates and the process is believed to be irreversible (Evans & Qi, 1982).

In addition to nitrogen aggregation characteristics some data on the nitrogen isotopes of diamond is now available from the studies by Javoy *et al.* (1984) and Boyd *et al.* (1987). Values of $\delta\ ^{15}N$ for diamonds from Mbuji Mayi (Zaire) vary between -11 and +6 $^{o}/_{oo}$ corresponding to a limited range of carbon isotope values.

The second most important substituted ion in diamond is boron. Boron influences the diamond's electrical properties and in Type IIb diamond boron causes semiconductor behaviour. Type IIb diamonds are rare in nature but often have a distinctive, feint blue body colour.

In addition many non substitutional elements occur in diamonds and these are studied, primarily, by neutron activation analysis (Sellschop *et al.*, 1979, & Bibby, 1982)). Up to 57 elements have been documented in diamond including Mg, Si, Fe, Ca, volatile species, S, Ga, Ge, Br, Gd, Pt, Pb and U. It has been concluded that the non substitutional elements occur as sub-microscopic inclusions of quenched melt or equilibrated magma derived from melting of mantle material. Noble gases and alkali elements have been studied by Ozima *et al.*, (1984), and the noble gas isotope ratios of $^{40}Ar/^{36}Ar$ and $^{3}He/^{4}He$ range from values close to atmospheric to more primordial values similar to meteorites. Harris (1987) reviews recent studies of the argon and helium characteristics of diamonds.

2.7 Analytical techniques.

The investigations into the geochemical characteristics of inclusions and diamonds were pursued by determining inclusion chemistry and the infra red absorption spectra, cathodoluminescence pattern and carbon isotope compositions of diamonds.

Syngenetic mineral inclusions were liberated from the diamond by using a steel jawed crusher. The inclusions were picked from the resulting debris and mounted in epoxy resin in 5mm brass standard tubes and then polished for electron microprobe analysis using 6, 1 and 0.25mm diamond pastes. The inclusion chemistry was determined at The Edinburgh University Department of Geology and Geophysics on one of two instruments; a Cambridge Instruments Microscan Mk V using a beam current of 30nA and an accelerating voltage of 20KV and a Cameca Camebax instrument with a beam current of 20nA and 20KV accelerating voltage. Electron microprobe analyses were carried out using wavelength dispersive (WDS) X-ray analysis and the X-ray counts were measured relative to metal (Cr, Ni, Fe, Ti, Mn, Fe), oxide (MgO, Al_2O_3) and silicate ($CaSiO_3$,$NaAlSi_3O_8$, $KAlSi_3O_8$) standards. "On line" ZAF correction procedures were used. Back scattered electron images and stage driven line scans which are of particular importance to the Sao Luiz inclusions were obtained on the Camebax instrument.

The nitrogen aggregation state of the diamonds was determined by infra red absorption spectroscopy at two laboratories; King's College, Physics Department, London and the Diamond Trading Company (DTC) Research and Development Laboratory at Maidenhead. Parallel sided cleavage chips were used in order to minimise reflections from diamond surfaces, and for single diamond crystals the infra red spectra were taken across parallel octahedral surfaces. Diamonds were mounted in indium metal and placed into one of two instruments; a Perkin Elmer instrument at Kings College and a Digilab FTS-40 Fourier

Transform Infra Red Microscope at DTC. In addition large octahedral diamonds were sawn and polished at the DTC Polishing Laboratory in London. Infra red spectra were taken from these large diamonds on the Maidenhead instrument using a computer driven microsampling attachment which enabled the nitrogen abundance to be determined for areas of 50mm x 50mm at 100mm intervals.

Two methods of carbon isotope analysis were used. 1) Standard carbon combustion and CO_2 extraction techniques for measurement in a gas source mass spectrometer. 2) $^{13}C/^{12}C$ measurement by secondary ion mass spectrometry (SIMS) on the Cameca IMS 4F Ion Microprobe at Edinburgh.

The combustion of diamond fragments from which syngentic inclusions were removed was carried out at the Scottish University Research and Reactor Centre (S.U.R.R.C) at East Kilbride, the CO_2 extraction and purification line used is shown diagramatically in figure 2.6. Diamond fragments were sealed in evacuated quartz tubes with 2.0g of CuO and placed in a furnace at 900^oC for eight hours. The tubes were joined onto an extraction and purification line and broken. The gas from the tube was passed through a slush trap consisting of acetone and solid CO_2 to condense any H_2O present and then into a trap of liquid nitrogen (-196^oC) to condense CO_2. Non condensible gases (N_2 and excess O_2) were then pumped away. The gas sample was then trapped in a cold finger chilled with liquid nitrogen and the yield measured in a mercury manometer. Finally the sample was trapped in a sample tube and removed from the extraction line for mass spectrometer analysis using a standard reference gas. Graphite of known isotopic composition (NBS21) was also combusted and extracted through the same purification system to measure the fractionation effects of the extraction procedure and results the accuracy was found to be $\pm$ 0.15 $^o/_{oo}$.

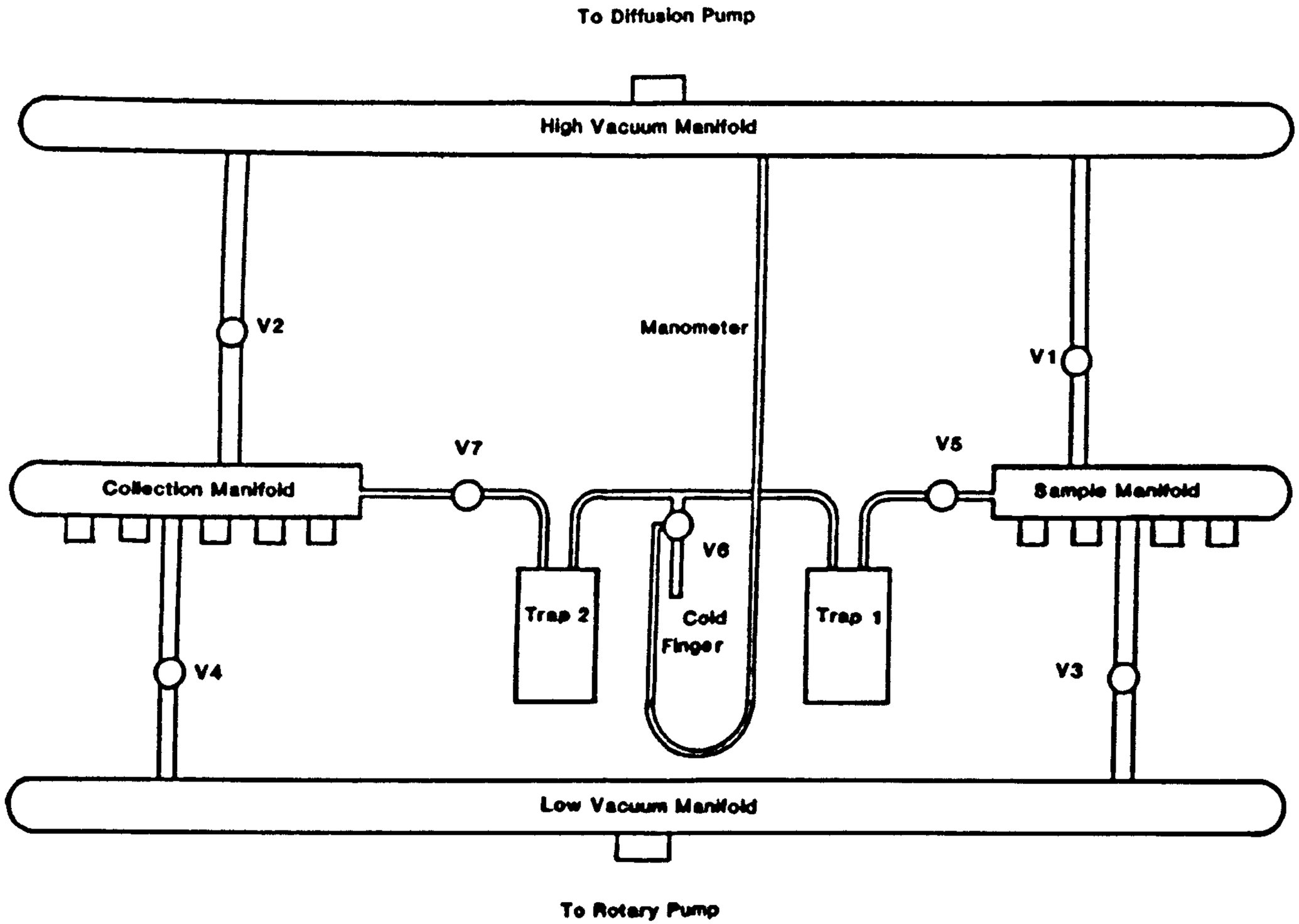

CO2 Extraction Line

Fig 2.6

CO_2 Extraction Line.

This apparatus is used to purify the products of diamond fragments combusted in sealed quartz tubes with copper oxide prior to mass spectrometer analysis. Sealed sample tubes are attached to the sample manifold which is evacuated by a rotary pump and mercury diffusion pump. the sample tube is then broken and the combustion products are allowed to pass through a "slush" trap (trap 1) comprising solid CO_2 and acetone to condense H_2O and then into a liquid nitrogen trap (trap 2) to condense CO_2. Remaining non condensible gases (N_2, H_2 and O_2) are pumped away. The purified CO_2 is then trapped by liquid nitrogen in a cold finger and the yield measured on a manometer. Following purification CO_2 is condensed in a collection tube and removed from the line for analysis in a separate mass spectrometer.

The second method of carbon isotope analysis employed was use secondary ion mass spectrometry (SIMS) (Reed,1989 and Whyte & Wood, 1987) using ion microprobe facilities at Edinburgh. The samples were sputtered by Cs+ ions which were accelerated over 10KV to produce a maximum primary beam current of between 200 and 300nA. The secondary negative ions were accelerated into the mass spectrometer and entrance and exit slits were constrained to resolve three peaks, the ^{12}C peak at mass 12.000, the ^{13}C peak at 13.0036 and the ^{12}CH peak at 13.0782. The ^{12}CH peak was found to decrease in height as vacuum conditions improved in the instrument. Preliminary analyses of diamonds from the Premier mine and Bultfontein mine were disappointing but the reproducibility of results was considerably improved by continued magnet calibration between analyses and by mounting the diamond in a conducting medium (indium metal).

A synthetic diamond was used as a standard for analyses and for instrument calibration. A large cubic synthetic diamond was polished to remove surface roughness, a cause of local charging effects. Because there are fractionation effects between different growth sectors a (100) growth sector (determined by cathodoluminescence) was removed by laser sawing. Carbon isotope analyses by ion microprobe for this (100) sector were found to be reproducible to within 1 $^{o}/_{oo}$ and this synthetic diamond was therefore used as a standard. A fragment of the standard showed a mean absolute isotope value of $\delta^{13}C$ -23.331 $\pm$ 0.1 $^{o}/_{oo}$ vs PDB which was determined by using the standard combustion techniques at S.U.R.R.C described above. Thus the absolute isotope ratio for natural stones could be determined and these are further discussed in chapter 4.

Chapter 3.

Morphology and Inclusion Chemistry for Bultfontein Diamonds

3.1 The Bultfontein mine.

Diamonds from Bultfontein have been mined since 1870 following their initial discovery by Cornellius Duplooy on 6th November 1869 (Janse, 1984). The realization that such occurrences represented a series of diamondiferous kimberlite pipes led to the establishment of Kimberley as a centre for diamond mining (Wagner, 1914). Four of these kimberlites are presently being mined by De Beers Consolidated Diamond Mines Ltd. This so called De Beers Pool comprises Bultfontein, Dutoitspan, Wesselton and De Beers. Other kimberlite pipes near to Kimberley include the famous Kimberley Mine or "Big Hole" which ceased production in 1914, several abandoned mines such as St. Augustine, sub economic kimberlites such as Kampfersdam and minor kimberlite intrusions worked by operators other than De Beers.

The Bultfontein and Dutoitspan mines are within a few hundred metres of each other and initially they were operated as two separate concerns. Under the present, single administration both mines are accessed by a single, centrally situated shaft, the Joint Shaft. The Bultfontein and Dutoitspan kimberlites are mined by the block cave underground mining system and are operated to depths of 750m and 798m respectively. The projected closure date of both mines is 1994.

As shown by Clement (1978) the Dutoitspan kimberlite body consists of at least eighteen discrete intrusions and has the most complex intrusive history of any of the kimberlites surrounding Kimberley. The Bultfontein kimberlite body is distinct in that there is no root zone (Hawthorne, 1975) and the diatreme flares direct from the feeder channel to form an ellipsoidal body which has a NNW elongation, a surface representation of the trend of the feeder dyke (Fig.3.1). The absence of a root zone has been attributed by Clement (1978) to vapour-solid fluidisation during diatreme formation which has extended downward to remove the root zone. Poor accessibility

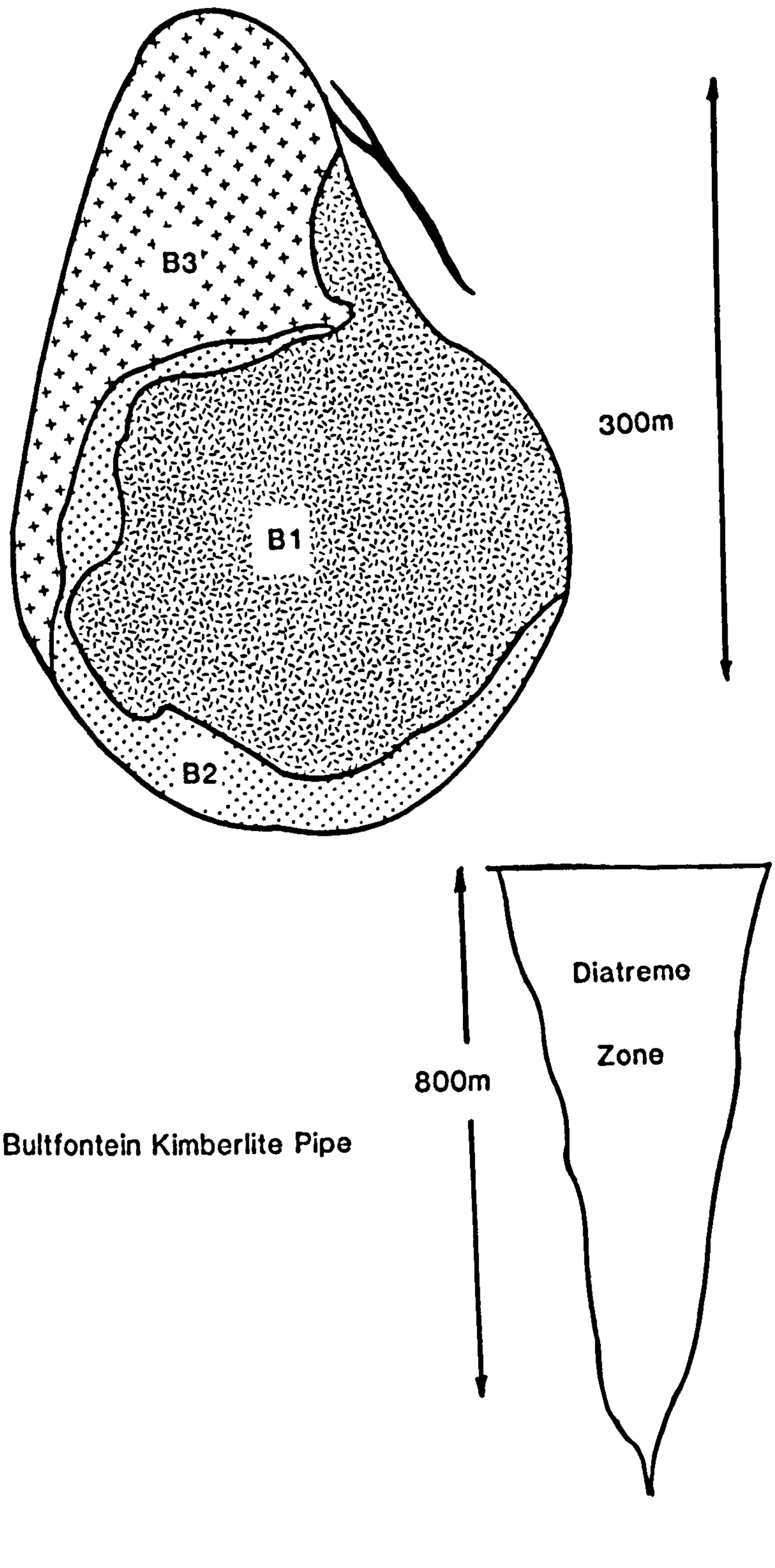
B3
B1
B2
300m
Diatreme
Zone
800m
Bultfontein Kimberlite Pipe

Fig. 3.1

The Bultfontein Kimberlite Pipe.

The kimberlite body at Bultfontein is eliptical with a NNW elongation which corresponds to the trend of a feeder channel. The body is approximately 300m in maximum dimension and flares directly from the feeder channel at depths of over 800m. There is no distinct root zone and this has been attributed to the downward extension of vapour-solid fluidisation processes. The earliest kimberlite is B3, which is restricted to the north-west part of the intrusion. The final kimberlite, B1, is enclosed within two earlier kimberlites.

made the accurate mapping of kimberlites in the Bultfontein body difficult but three discreet kimberlites have been established from old records, although additional bodies may not have been recognised (Clement, 1978). The earliest Bultfontein kimberlite (B3) occupies a NW extension of the pipe and is separated from the second kimberlite (B2) by a sharp contact. The final kimberlite (B1) is totally enclosed within B2. There are a number of precursor ultrabasic dykes controlled by joints in the country rock which surround the later intrusion. The distributions of different kimberlites at Bultfontein are shown in figure 3.1.

The Kimberley pipes and precursor dykes were intruded into the Archaen Kaapvaal Craton between the Late Jurassic and Mid Cretaceous (95 to 85ma) (Allsopp & Barrett, 1975). Other kimberlite groups of similar age occur at Koffiefontein and Jagersfontein. The diamond mine at Premier is currently the only Precambrian kimberlite mined for diamonds in Southern Africa.

Mantle xenoliths from the Bultfontein kimberlite consist mainly of peridotites with rarer eclogite and MARID suite nodules. Polymict xenoliths, which consist of clasts of both peridotite and eclogite minerals, were interpreted by Lawless *et al.* (1979) as disequilibrium assemblages of mantle minerals with no crustal component. Wyatt and Lawless, (1984) have also suggested that veins of ilmenite, sulphide and phlogopite that are prominent within the polymict xenoliths are disruptive intrusive melting events which occurred prior to the main kimberlite eruption .

3.2 Diamond morphology and inclusion abundance.

The inclusion bearing diamonds for this study were collected over a period of five years by sorting staff at Kimberley as part of a programme of research to determine physical characteristics of the diamonds for the four individual mines in the De Beers Pool.

In the present study morphology, colour and inclusion abundance have been determined using the classifications of Harris *et al.* (1975) and these results then

compared with the diamond characteristics for the total production of Bultfontein (Harris *et al.*, 1984).

Figure 3.2 shows that the total diamond production from Bultfontein is dominated by irregular shaped diamonds. The number of aggregates increases with diamond size. The number of macles and dodecahedral stones remains constant for each size category. Figure 3.2 also shows the shape characteristics for inclusion-bearing diamonds from Bultfontein. With these diamonds the dominant crystal form is the macle and the abundance of dodecahedral diamonds is low.

In terms of colour the total production for Bultfontein has a high abundance of yellow and colourless stones forming between 60% and 80% of the total. In contrast the inclusion bearing diamonds are mostly brown, 52%, with colourless diamonds forming the remainder.

Of the total Bultfontein production 14% show plastic deformation as closely spaced lines parallel to the (111) direction (Harris *et al.*, 1983). In contrast 80% of the inclusion-bearing diamonds show evidence of plastic deformation. In addition to the plastic deformation lines aggregated diamonds have highly strained boundaries between constituent crystals, shown by high polarisation colours and, as would be expected, these boundaries are often sites of preferential dissolution.

Other noticeable features of the inclusion-bearing diamonds are the presence of trigonal etch pits developed on the few (111) faces of the diamonds, examples of these features are shown in figure 3.3. These trigons sometimes coalesce to form hexagonal pits. As these pits are obviously crystallographically controlled, they are probably the result of a "static" etch occurring with volatiles exsolved from kimberlites (Harris & Vance, 1972).

Growth lamellae, such as those shown in figure 3.4 are seen on the (111) surfaces of octahedra, macles and in constituent crystals of aggregates. The edges of the (111) surfaces show evidence of resorption in the form of rounded surfaces that correspond to the (110) directions (Harris *et al.*, 1975).

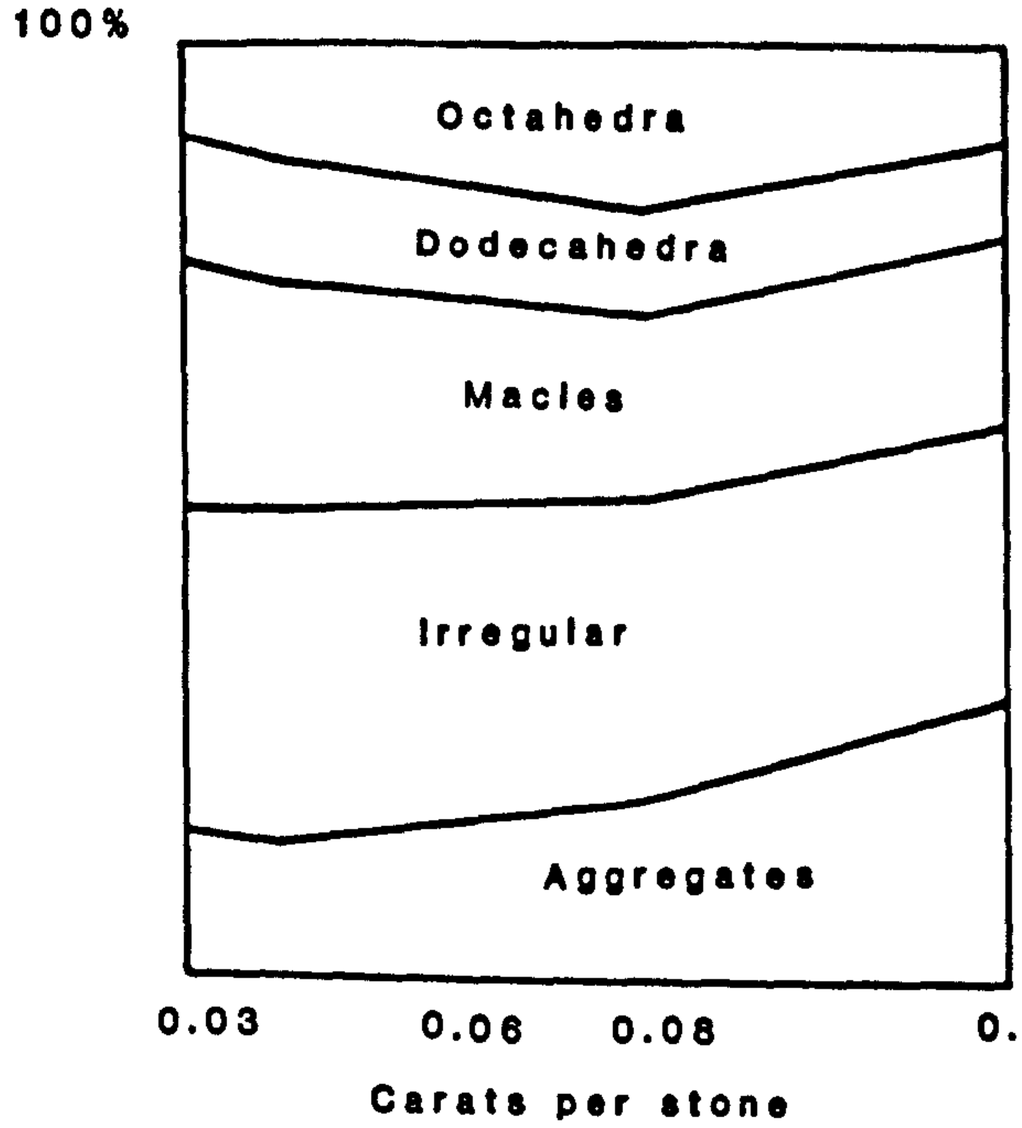

Characteristics of Bultfontein diamonds

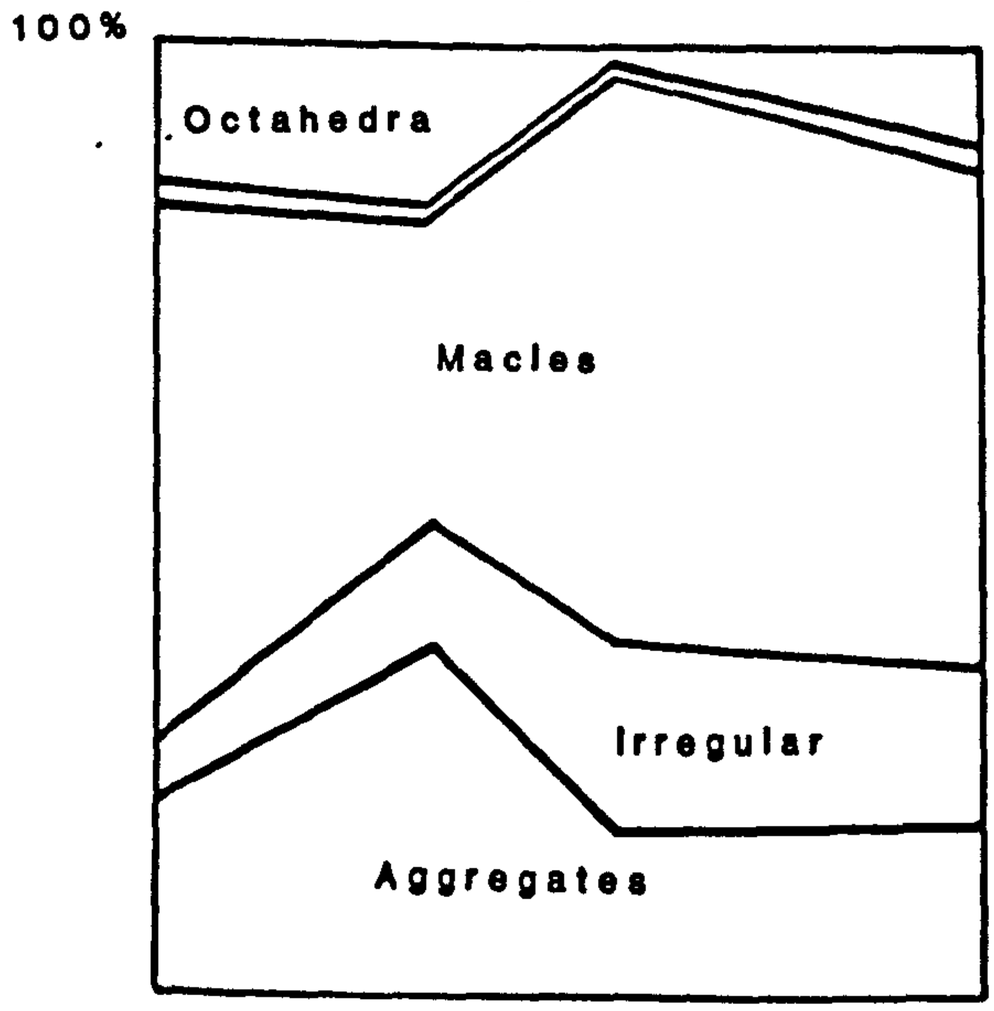

Characteristics of Bultfontein inclusion bearing diamonds

Fig. 3.2

Morphology of Bultfontein diamonds.

The total diamond production is characterised by irregular and aggregated stones (Harris *et al*, 1979). The inclusion bearing diamonds from Bultfontein principally consist of macles whilst octahedra are rare.

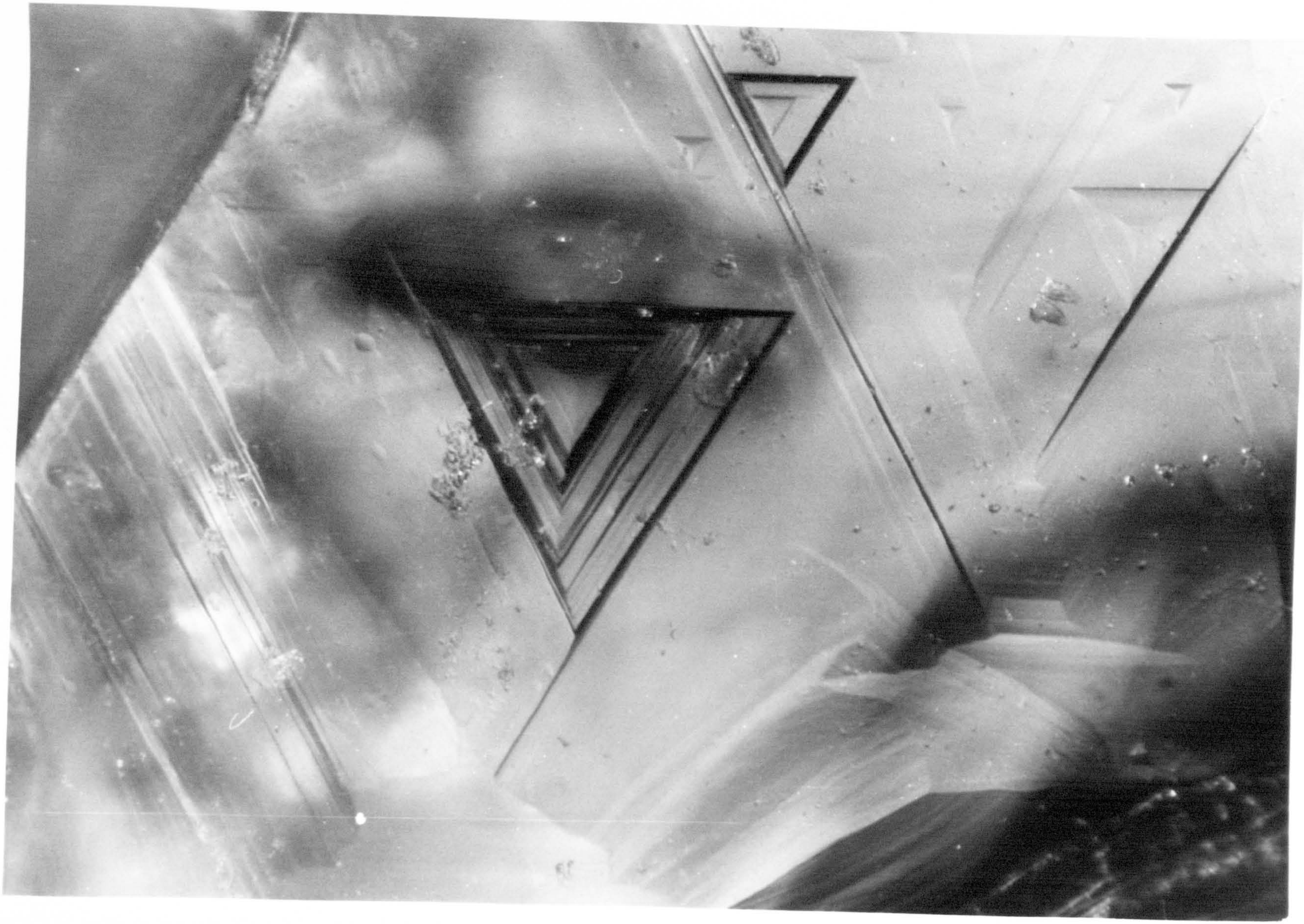

Fig. 3.3

Typical View of a (111) Surface.

In detail the surface of this diamond is irregular and shows trigons of different sizes from 10 to 100μm. shallow trigons are pyramidal in shape and larger trigons have stepped sides. The sizes of the trigons are related to the size of the dislocations that intersect the diamond surface. Prominent fractue lines parallel to the (111) direction can also be seen. The largest trigon has a size of 150μm.

Fig. 3.4.

Growth Lamellae in Bultfontein Diamond.

A fragment of an octahedral diamond shows shield lamellae on the (111) face. Each lamellae only partly covers the octahedron face. The edge of the octahedron shows rounded edges as a result of etching along the four fold crystal direction and it is in this area of etching that the growth lamellae are revealed. The diamond has a maximum dimension of 2mm.

Table 3.1 shows the inclusion abundances of diamonds from the De Beers Pool as shown by Harris et al, (1984). It can be seen that peridotite suite inclusions dominate at all three mines and the proportion of eclogite suite inclusions is less than 10%.

In Table 3.2 the abundances of inclusions from Bultfontein, using data from this study, are compared with data from three other mines on the Kaapvaal Craton. At Premier eclogite paragenesis inclusions are abundant. Although peridotite suite inclusions dominate at Roberts Victor and Koffiefontein the abundance of sulphide inclusions at these two mines is much greater than at Bultfontein. Bultfontein and the other three mines in the De Beers Pool are distinct because of their low eclogite and low sulphide abundances and also have a very high abundance of chromite inclusions.

Inclusion morphology and orientation shows a close relationship to that of the diamond. As shown in figure 3.5, colourless inclusions in particular have (111) faces of cubo-octahedra aligned parallel to the (111) faces of diamond and (100) faces aligned parallel to the cubic directions of diamond. Such a relationship suggests that the inclusion morphology is imposed by the diamond. Work by Harris and Gurney (1979) has shown that the imposition of diamond morphology occurs during mutual growth as a result of the higher form energy of the diamond.

3.3 Peridotite suite inclusion chemistry.

Diamonds were chosen from those that comprise Table 3.2 to reflect the high peridotite content of Bultfontein diamonds: Peridotite suite inclusions account for 78% of the inclusion population, eclogite bearing constitue only 8%. Sulphides (12%) and irresolvable clouds (2%) form the remainder.

3.3.1 Chromites.

Electron microprobe analyses show that the chromite inclusions from Bultfontein are individually homogeneous. Concentrations of chrome fall in a narrow range from 64 wt.% to 66 wt.% Cr_2O_3. This represents 87% of the chromite solid

Fig 3.5.

Imposed Morphology on Colourless Inclusions.

This colourless inclusion in diamond is aligned within the (111) plane of the diamond and has a morphology imposed on it by the diamond. The inclusion is a cubo octahedron with (111) faces parallel to the diamond (111) faces and (100) faces planar to the diamond four fold crystal direction.

Table 3.1

Syngenetic Inclusion Abundances for the De Beers Pool Mines.

	De Beers	Bultfontein	Dutoitspan	Wesselton
Peridotite Paragenesis (%)				
Chromite	31.5	41.1	30.0	6.5
Ol/Opx	33.7	34.7	32.5	37.9
Garnet	9.0	4.5	7.5	29.2
Cpx	-	-	1.3	1.4
Combinations	5.6	8.2	10.0	15.2
Eclogite Paragenesis (%)				
	7.8	5.4	9.9	5.8
Sulphides (%)				
	12.4	6.2	8.8	4.2

(All data from Harris *et al.*, 1983)

Table 3.2

Syngenetic Inclusion Abundances at Bultfontein Compared with Other Mines on the Kaapvaal Craton.

	1	2	3	4
Peridotite Paragenesis (%).				
Chromite	40	0	18	1
Olivine	11	13	34	13
Orthopyroxene	20	6	18	11
Garnet	6	2	11	10
Clinopyroxene	1	1	1	0
Eclogite Paragenesis (%)				
Garnet	2	13	2	3
Clinopyroxene	6	28	8	1
Sulphide(%)				
	12	36	9	61

Locality

1 Bultfontein

2 Premier (Gurney *et al*, 1985)

3 Roberts Victor (Gurney *et al*,1984)

4 Koffiefontein (Gurney *et al*, 1986)

solution component $(Fe,Mg)Cr_2O_4$ with an aluminium concentration (7.63 wt. % Al_2O_3) equivalent to a spinel ($(Fe,Mg)Al_2O_4$) component of 13%. The analyses are presented in Appendix 1.

As shown in figure 3.6, the Bultfontein chromites are more chrome and magnesium rich than chromite inclusions from Finsch, (Gurney *et al*, 1979) Jagersfontein, Koffiefontein, Premier, Roberts Victor and Orapa (Gurney *et al*, 1984) and from other localities such as Sierra Leone, Ghana and the Yakutia kimberlite in Siberia, USSR (Sobolev, 1977). The chromite compositions of the inclusions are also much more chrome and magnesium rich than those in kimberlites (Shee, 1984) and peridotite nodules (Sobolev, 1977) the latter having between 44 and 60 wt.% chrome.

Individual chromites from Bultfontein have variable FeO and MgO content, with a range of Fe/Fe+Mg ratio from 0.37 to 0.24. Aluminium content varies with the Fe/Fe+Mg ratio with high aluminium chromites being more iron rich. Such a relationship suggests a coupled substitution between $Mg^{2+}Cr^{3+}$ and $Fe^{2+}Al^{3+}$. Up to 0.43 wt.% TiO_2 and 0.12 wt.% NiO is present in the chromites. MnO was not determined because of the interference of Mn kα and Cr Kβ X-ray peaks.

It was noticed that the Fe/Fe+Mg ratio of the chromites, and to a limited extent the Cr and Ti content, varied with the position of the inclusions within the diamonds. Inclusions close to the centre of the diamond (including those on macle planes) were more Mg and Cr rich than those on diamond peripheries which were more Fe and Ti rich, this relationship is shown in figure 3.7. All of the iron in the chromites was calculated as FeO. Recalculation of the spinel formulae for Fe and Ti rich inclusions showed that up to 0.5 Fe^{3+} may be present per 24 cations, such values represent a very small magnetite fraction (less than 1%) in the spinel formula.

The iron and magnesium variations for chromites in different positions have been shown to correspond to coupled substitutions of $Fe^{2+}Al^{3+}$ for $Mg^{2+}Cr^{3+}$, $Fe^{2+}Ti^{4+}$ for $2Mg^{2+}$ and possibly limited $Fe^{2+}Fe^{3+}$ for $Mg^{2+}Cr^{3+}$. Such a substitution would seem to indicate that as the diamond grew the environment became more enriched in iron and titanium, and possibly even Fe^{3+}.

Compositions of chromites from selected localities

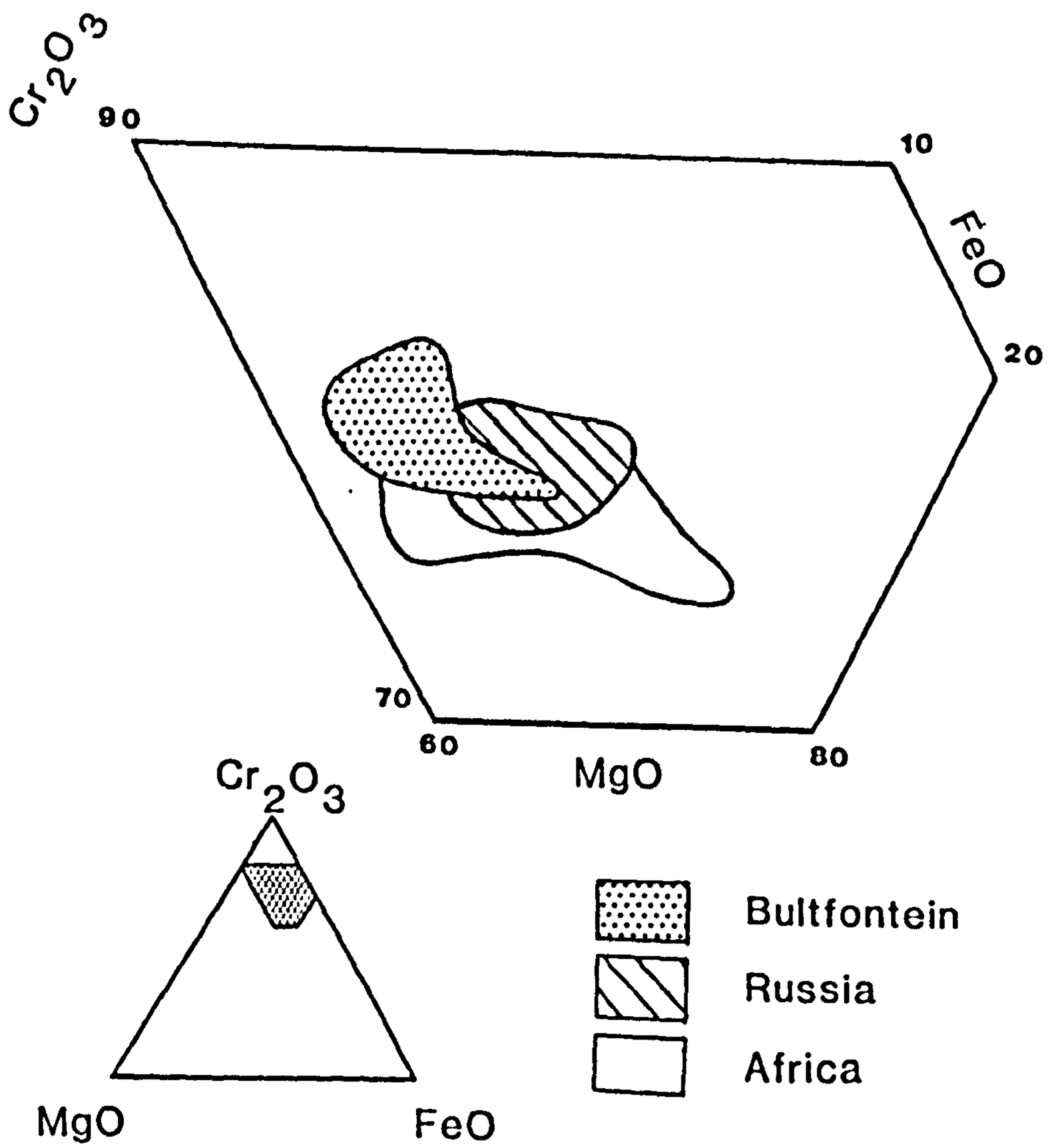

Fig.3.6.

Chromite compositions.

The chromites at Bultfontein are chrome and magnesium rich. The Bultfontein chromites have a range in composition, also seen at other localities such as Siberia, and in other African diamonds. There is a range from Al^{3+} and Fe^{2+} rich compositions to more Cr^{3+} and Mg^{2+} compositions, possibly indicating a change in environment. Bultfontein chromites are the most chrome and magnesium rich.

Chromite variation for Bultfontein

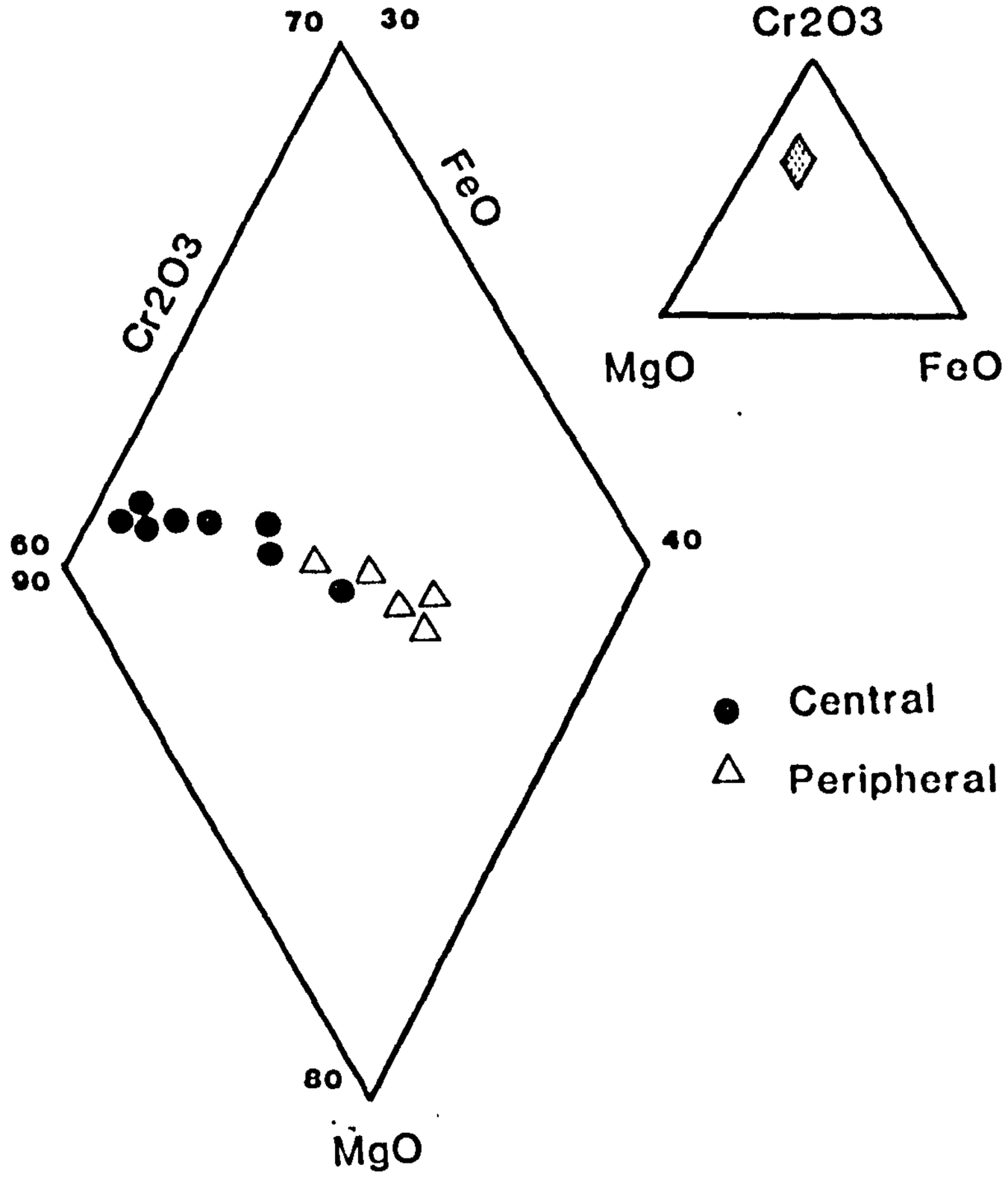

Fig. 3.7

Compositional change in chromites.

A range in chromite compositions occurs in the Bultfontein diamonds from high Mg^{2+} and Cr^{3+} to more Fe^{2+}, Al^{3+} and Ti^{4+} rich compositions. Chromites recovered from the diamond peripheries are more enriched in iron and titanium than those occurring near the diamond cores. The peripheral chromites were totally enclosed within the diamond and it is therefore, likely that the compositional changes represent a change in environmental conditions, and are not a consequence of alteration by the kimberlite.

Stable Spinels at 10^{-7} and 10^{-9} atm fO_2

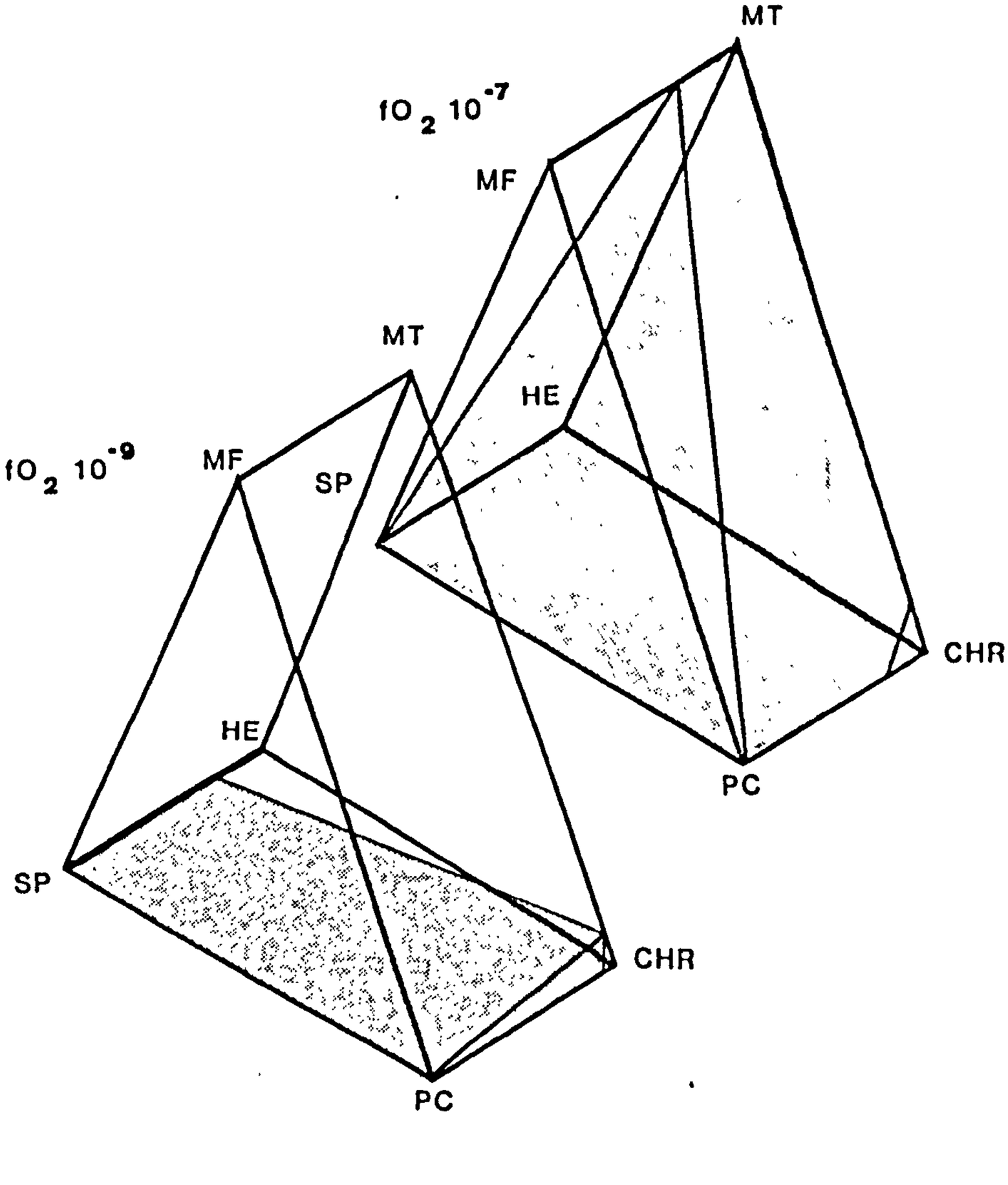

Fig. 3.8.

fO_2 Conditions for Spinels.

Two stablity fields are shown for spinels at different oxygen fugacities (Haggertey, 1979). At higher fO_2 the magnetite component of spinel is stable ($fO_2 = 10^{-7}$ atm). At low fO_2 (10^{-9} atm) only the spinel component is stable. Diamond inclusions show little magnetite and spinel components and are likely to be formed under reduced conditions.

Chromites and spinels recovered from kimberlites frequently show a change in composition from chromian and magnesian cores to rims of titanomagnetite (Shee, 1984). Also most kimberlite spinels show evolutionary trends towards more Fe and Ti rich compositions (Haggerty, 1976), including an increase in Fe^{3+} content. Spinels and ilmenites from kimberlites show an increase in Cr/Al content attributed to an increase in Cr^{2+}/Cr^{3+}. These changes are a result of either pressure increase or oxygen fugacity decrease (Haggerty, 1979). Since the most likely control on the composition of spinels in diamonds is oxygen fugacity, as the pressure of diamond formation is high, the chromites may indicate a specific oxygen fugacity or a range of oxygen fugacities during diamond growth. Figure 3.8, taken from Haggerty (1979) shows that the stability of magnesiochromites is influenced by oxygen fugacity. As can be seen from figure 3.8 the chrome spinels are likely to have formed under reduced conditions close to 10^{-9} atm and as a consequence there is only a small fraction of Fe^{3+} present. This low oxygen fugacity may also prevent Cr^{3+} partitioning into chrome pyropes.

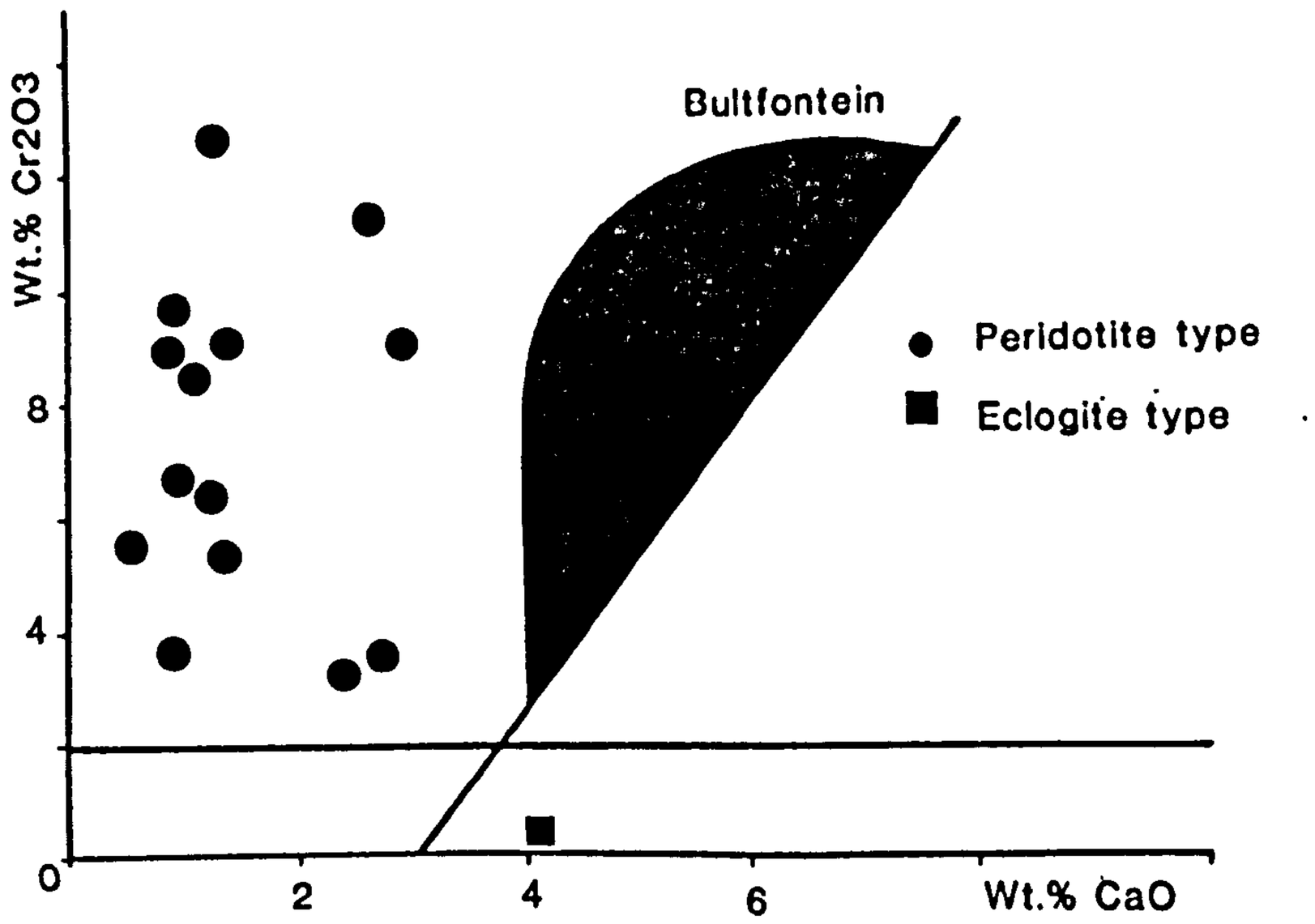
Wt.% Cr2O3
8
4
0
2
4
6
Wt.% CaO
Bultfontein
Peridotite type
Eclogite type

Fig. 3.9.

Bultfontein chrome pyrope compositions.

Garnet compositions from Bultfontein show sub-calcic compositions with a wide range in CaO and Cr_2O_3 contents. The shaded area represents lheerzolite garnets from heavy mineral concentrates (Boyd & Gurney, 1982), peridotite nodules and polymict xenoliths (Lawless, 1978) from the Bultfontein mine. The garnet inclusions in diamond range from calcium rich to calcium poor and overlaps with the field of other garnets. The whole garnet inclusion assemblage may represent a continuum from calcic compositions, in equilibrium with clinopyroxene, to more depleted sub-calcic compositions. A single eclogite garnet composition is shown, this has a very low chrome content and high calcium and no genetic relationship between the two parageneses is inferred. The line from 3.0wt.% CaO represents the lherzolite trend, the horizonteal line at 2.0 wt.% Cr_2O_3 represents the division between peridoite (above) and eclogite (below) paragenesis inclusions.

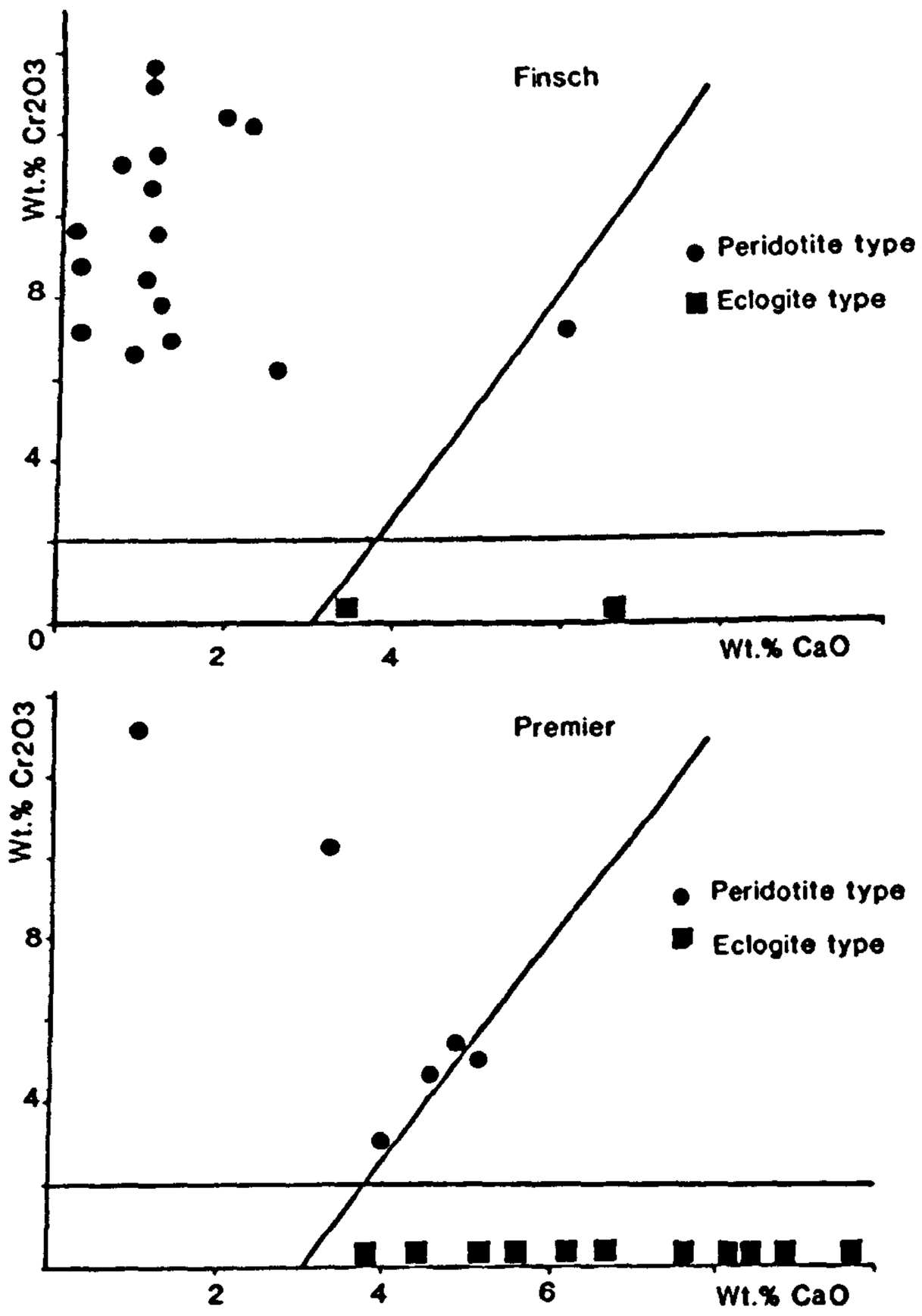
Finsch
Wt.% Cr2O3
Wt.% CaO
Peridotite type
Eclogite type
0
4
8
2
4

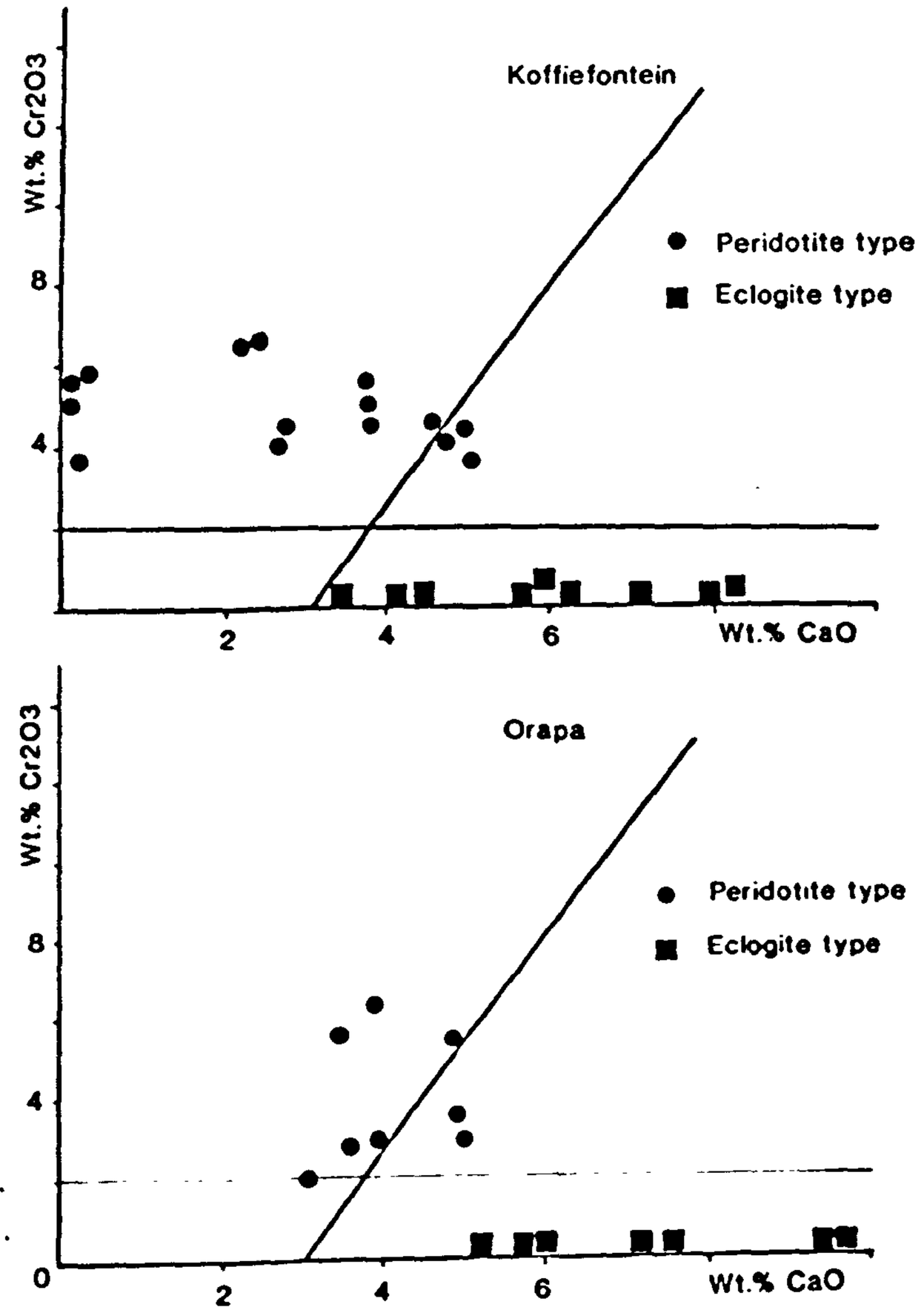
Koffiefontein
Wt.% Cr2O3
Wt.% CaO
Peridotite type
Eclogite type
4
8
2
4
6

Premier
Wt.% Cr2O3
Wt.% CaO
Peridotite type
Eclogite type
4
8
2
4
6

Orapa
Wt.% Cr2O3
Wt.% CaO
Peridotite type
Eclogite type
0
4
8
2
4
6

Fig. 3.10.

Chrome pyrope compositions from the Kaapvaal Craton.

A comparison with peridotite garnets from other localities on the Kaapvaal Craton shows that peridotite suite garnets from Orapa and Premier are more calcium rich and lie close to the calic trend. This means that they may be in equilibrium with peridotite paragenesis clinopyroxene. At Finsch and Roberts Victor compositions are chrome rich and indicate an absence of clinopyroxene. Eclogite suite inclusions are shown for completeness.

3.3.2 Chrome pyropes.

The electron microprobe analyses of purple garnet inclusions from Bultfontein diamonds show a restricted range of Mg/Mg+Fe values of 0.88 to 0.90. The calcium values range from 0.89 to 2.33 wt%. The garnets are very chrome rich with a range of Cr_2O_3 contents from 3.75 to 12.65 wt.%, this corresponding to a maximum knorringite ($(R^{2+})_3Cr_2Si_3O_{12}$) content of 47.9% (Ringwood, 1977). The remaining 52.1% is pyrope ($(R^{2+})_3Al_2Si_3O_{12}$). Up to 0.08 wt.% Na_2O is also present.

As can be seen in figure 3.9 the garnet inclusions are chrome rich and sub-calcic, and as such, they do not lie on the lherzolite trend. These compositions are matched by garnets from heavy mineral concentrates in the kimberlite. Garnets from peridotite nodules at Bultfontein (Lawless, 1978) and from polymict xenoliths (Lawless *et al*, 1979 and Wyatt & Lawless, 1984) show a range in calcium and chrome contents from sub-calcic to lherzolite compositions.

In figure 3.10 the composition of garnet from four other mines on the Kaapvaal Craton are shown. At Premier data from Gurney *et al* (1985) shows that there are two groups of garnet; one group has sub-calcic compositions whilst the other shows a lherzolite trend. At Orapa (Gurney *et al*, 1984) most garnet inclusions have compositions close to the lherzolite trend. Most of the garnet inclusions from Finsch (Gurney *et al*, 1979) and Koffiefontein (Gurney *et al*, 1984) are sub-calcic.

3.3.3 Colourless Inclusions.

Colourless inclusions are the most abundant silicates at Bultfontein. From microprobe analyses orthopyroxenes are the most numerous. Assuming that the parcel of diamonds is representative of the inclusion population the ratio of orthopyroxene to olivine is approximately 2:1.

Orthopyroxenes are highly magnesian with a narrow range between enstatite ($MgSiO_3$) contents of En_{93} and En_{92}. Up to 0.35 wt.% CaO is present in

orthopyroxenes where the iron content is lower. Nickel and chrome concentrations are between 784 to 1414ppm and 273 to 2463ppm respectively.

Orthopyroxenes from other mines on the Kaapvaal Craton show similar, restricted Mg/Mg+Fe rations. Chrome contents show values of 496ppm for Finsch (Gurney *et al*, 1979) and 1402ppm for Roberts Victor (Harris *et al*, 1984). No nickel data is available for these two mines.

Olivine compositions also show restriction in their MgO and FeO content and range between Fo_{93} and Fo_{90}. Significant amounts of Cr (34 to 273ppm) and Ni (1807 to 3064ppm) are also present. Calcium is not detectable as is common in high magnesian olivines (Jurewicz & Watson, 1988, a & b). The chrome contents at Roberts Victor are 58ppm, which is within the range of values seen at Bultfontein. At Finsch, however, the olivines have no detectable chrome. Nickel information has not been published for these two mines.

Olivines and orthopyroxenes from Bultfontein show significant variation in the nickel and chrome contents. Experimentally determined partition coefficients for nickel and chrome (see Irving, 1978 for review) and simple batch melting calculations (Cox *et al*, 1979) can be used to predict the behaviour of these elements in residues from partial melts of garnet lherzolites. Figure 3.11 shows the range of nickel contents in olivine and orthopyroxene that might be expected to result from partial melting of two model lherzolites. Olivines correspond to 10 to 50% partial melt, while the much higher chrome contents of orthopyroxene correspond to values as high as 70% partial melt, although two inclusions show values equivalent to 10% melting. If the assemblage produced in residues consists of both olivine and orthopyroxene then the diamonds inclusions would have formed as a result of approximately 50 to 70% partial melt, which is a values that lies between the compositions of olivines and orthopyroxenes.

Nickel partitioning is dependent on the MgO content of melts (Hart & Davis, 1978) and from the partitioning evidence a high MgO melt may have existed during diamond formation (Clark & O'Hara, 1979). The Mg/Mg+Fe ratio is constant in

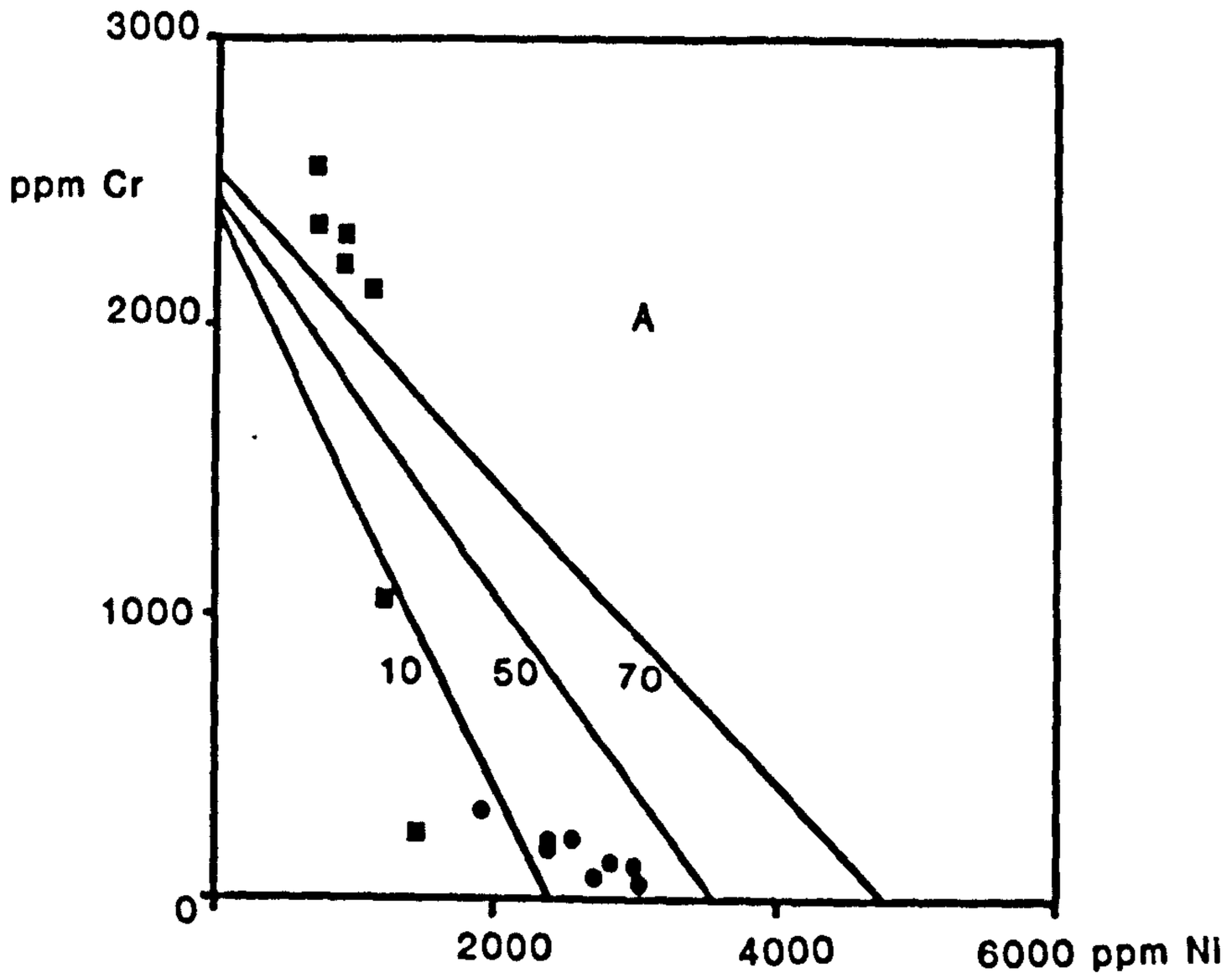
3000
ppm Cr
2000
1000
0
A
10
50
70
2000
4000
6000 ppm Ni

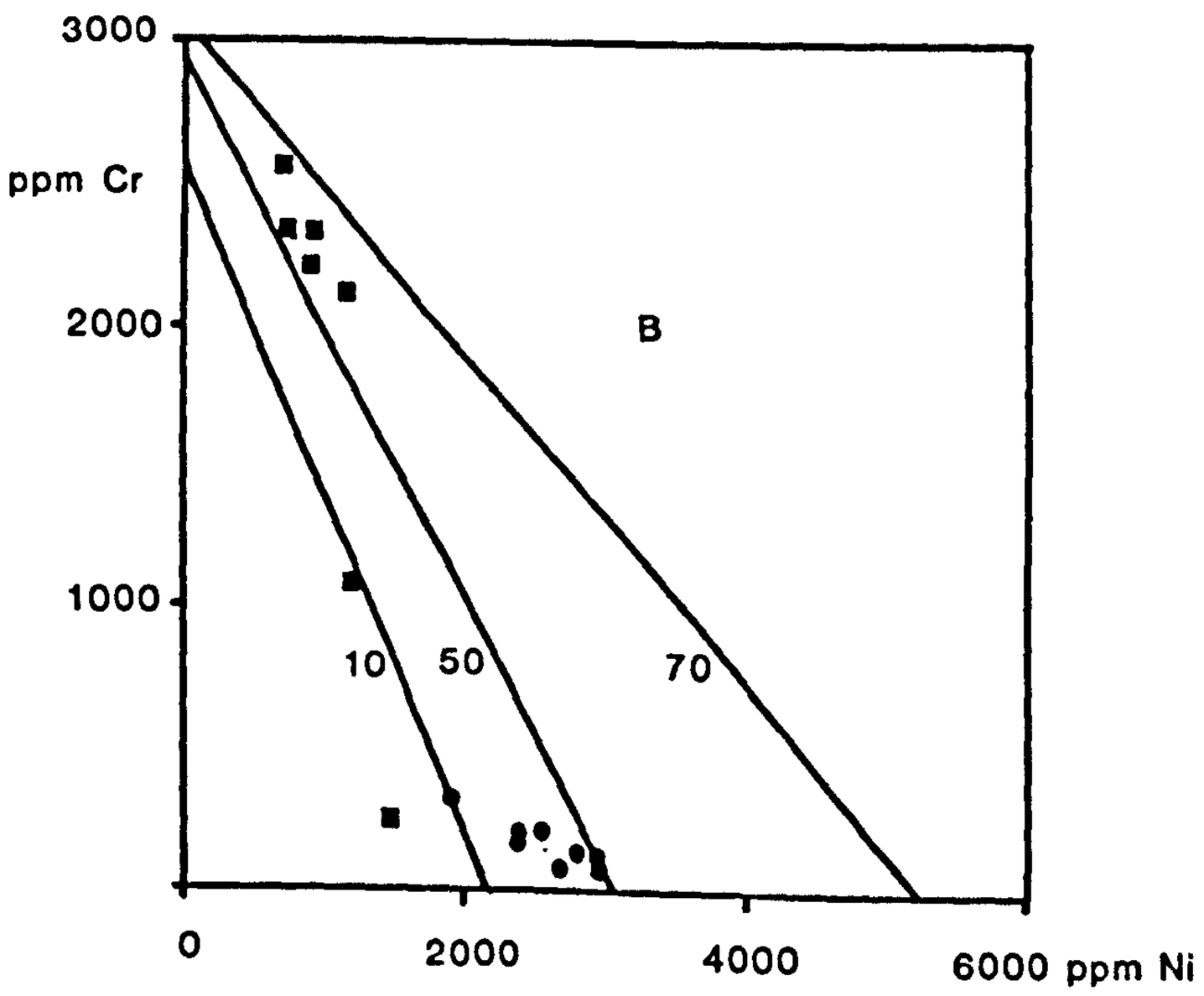
3000
ppm Cr
2000
1000
0
B
10
50
70
2000
4000
6000 ppm Ni

Fig. 3.11.

Ni and Cr contents of olivines and orthopyroxenes from Bultfontein.

Values for nickel and chrome for olivine (circles) and orthopyroxene (squares) inclusions in Bultfontein diamonds are shown. Also shown are Ni and Cr concentrations is residues from a 10, 50 an 70% partial melt of two model lherzolites. The upper diagram (A) has a starting composition of 70% olivine and 20% orthopyroxene, while in the lower diagram (B) the initial composition has 80% olivine and 10% orthopyroxene. In both cases high degrees of partial melt are necessary to produce the inclusion compositions.

olivines and orthopyroxenes. Despite this nickel and chrome show a wide range of values. No specific nickel or chrome content can be assigned for a MgO content of the inclusions at Bultfontein. It is noticeable that the nickel and chrome contents of komatiites, which are also regarded as high degree partial melts of primary mantle, are similar to the levels in the inclusions (Cawthorn & McIver, 1977; Bickle *et al*, 1977; Bickle, 1982). The amount of chromium in olivines does not relate to growth in the presence of chromite because olivines from chromite deposits are not enriched in Cr. Meyer and Boyd (1972) suggested that some chrome in olivine may be divalent. The major controlling factor on the Cr^{2+}/Cr^{3+} ratio is probably oxygen fugacity (Meyer, 1975) and high Cr contents in olivine may represent more reduced conditions.

In addition to the olivines and orthopyroxenes three other colourless inclusions were found, all of which are believed to be syngenetic. These are: a volatile bearing MgO phase, considered to be magnesite ($MgCO_3$), a potassium feldspar and two silica phases (99wt.% SiO_2), probably coesite.

The magnesite inclusion was a transparent cubo-octahedra which has had a morphology imposed by the enclosing diamond. There were no fractures in the diamond which connected the inclusion to the diamond surface and it is unlikely that the magnesite was a product of the alteration of silicate inclusions. The magnesite composition was pure end member magnesite with 46wt% MgO.

Potassium feldspar has been recognized as an inclusion of eclogitic paragenesis (Prinz *et al*,1975) and also may occur as exsolution lamellae in eclogitic clinopyroxenes. The potassium feldspar was the only inclusion in the diamond and so the paragenesis was uncertain.

The two silicate inclusions have SiO_2 contents of 99 to 100wt.%. Although the mineral structure is undetermined these inclusions are probably coesite, which has been recognised as an inclusion of eclogitic paragenesis. However, the two examples at Bultfontein coexist with inclusions of peridotite paragenesis, namely orthopyroxene and chrome pyrope garnet, and these inclusions do not differ significantly from the

compositions of other peridotite suite inclusions. Reaction between olivine and coesite to produce orthopyroxene would probably eliminate any minor silica phases present in the lithospheric mantle. It is possible that the high abundance of orthopyroxene inclusions at Bultfontein represents such a reaction.

3.3.4 Chrome diopsides.

Chrome diopside inclusions are very rare at Bultfontein. The four which have been analyzed show a range in composition. Mg/Mg+Fe ratios vary from 0.86 to 0.83 which is much more iron rich than the Mg/Mg+Fe ratios for olivine and orthopyroxene. For this reason it is unlikely that there was equilibrium between the clinopyroxene and the two other phases. Calcium contents show a range from 16.0 to 18.75 wt.%. High concentrations of Na_2O (1.64 to 6.35 wt.%) and Cr_2O_3 (1.48 to 3.47 wt.%) exist suggesting ureyite ($NaCrSi_2O_6$) substitution. Concentrations of aluminium are low and there is little evidence for aluminium in tetrahedral sites (Al^{IV}).

Clinopyroxenes of peridotite paragenesis are documented by Sobolev (1977) in diamonds from the U.S.S.R. They all have high chrome contents (up to 3.54wt.%) which distinguish them from eclogite paragenesis clinopyroxenes. Sodium contents are high (2.25 to 3.33 wt.%) and Sobolev has termed these compositions chrome omphacites. There is little evidence in the chrome diopsides for either jadeite substitution or aluminium in octahedral coordination. The Mg/Mg+Fe ratios of 0.95 for the Russian clinopyroxenes indicates that the iron content is lower than at Bultfontein.

3.4 Eclogite suite inclusion chemistry.

3.4.1 Garnets.

Two orange, eclogite paragenesis garnets were analysed from Bultfontein. These have a limited composition with an Mg/R^{2+} values of 0.5 (where R^{2+} ions are Mg, Fe, Ca and Mn). Chrome contents are low (0.06 wt.%) and there are minor amounts of Na_2O (0.18 wt.%) and TiO_2 (0.36 wt.%). Titanium is probably incorporated into the aluminium sites in the garnet structure. It is unlikely that the apparent concentration of P_2O_5 of 0.7 wt.% represents the true value of phosphorous because during microprobe analyses the first order P Kα peaks and the second order Ca Kβ peaks interfere.

Although there is only a small data base for the Bultfontein eclogite paragenesis garnets, the Mg/R^{2+} ratios at Bultfontein are within the range of values from Orapa (0.48 to 0.80) and Premier (0.40 to 0.60). In addition the latter two mines also show minor amounts of sodium (0.19 and 0.26 wt.% respectively) and titanium (0.29 and 0.89wt.%).

3.4.2 Clinopyroxenes.

The analysis of 6 eclogite suite clinopyroxene inclusions from Bultfontein show a range in Mg/Mg+Fe ratios of 0.45 to 0.49. Sodium contents are high (4.68 to 2.13 wt.%) and correlate with high aluminium contents (2.56 to 8.41 wt.%) probably representing jadeite substitution, as a function of high pressure. In addition aluminium apparently replaces silica indicating Tschermak substitution. At mines such as Premier, jadeite substitution is higher in eclogite suite clinopyroxenes. An ilmenite lamella is present in one inclusion. The ilmenite lamella is too small for a detailed chemical analysis but has an apparent content of 28.0 wt.% TiO_2 and 25 wt.% FeO, with the remaining 47% apparently formed from MgO, CaO and SiO_2. This probably represents the composition of the surrounding clinopyroxene. It is difficult to

determine the amount of ferric (Fe^{3+}) and ferrous (Fe^{2+}) iron in the ilmenite, which would indicate the amount of haematite (Fe_2O_3) present: If the ilmenite was a product of high fO_2 alteration fluids then the ferric component would probably be higher. In the absence of this information it is impossible to determine whether the ilmenite lamella is a product of alteration, or is a primary feature.

3.5 Sulphide inclusions.

Sulphide inclusions belong to the system Fe-Ni-S and at high temperatures monosulphide solid solution (Mss) is the dominant phase (Craig, 1974). Most sulphide inclusions in diamonds represent subsolidus re-equilibration of Mss. These relationships are shown in figure 3.12. Initially excess Cu is exsolved as chalcopyrite, folllowed by nickel, exsolved as pentlandite. The exsolution of pentlandite occurs at temperatures below 600^{o}C at atmospheric pressure. According to Yefimova and Sobolev (1983) and Tsai *et al.* (1979) sulphides of peridotite paragenesis have a high nickel content (16.5 to 29.8wt.%), whereas eclogite paragenesis sulphides have nickel contents of less than 10wt.%.

Of the ten sulphides analyses from Bultfontein eight showed exsolution textures. The sulphides consisted of pyrrhotite ($Fe_{1-x}S$) with flame-like exsolution lamallae 1 to 3mm wide of pentlandite ($(Fe,Ni)_8S_9$). On four of the sulphides chalcopyrite ($(Cu,Fe)_2S$) rims were visible, although these were two small for analysis. There was no pyrite (FeS_2) or cubanite ($CuFe_2S_3$) present. In the pyrrhotite there are significant amounts of Co (0.42wt.%) and Cr (0.7wt.%), which have higher concentrations (more than 0.9) in the exsolution lamellae.

From figure 3.12 the relationships between pentlandite and pyrrhotite relative to monosulphide solid solution (Mss) are shown. If the Mss has a nickel content of 10% then only small amounts of pentlandite will be exsolved during re-equilibration. The sulphides from Bultfontein were the only inclusions present in the diamonds and so the paragenesis is unknown. However, the amount of pentlandite exsolved is probably greater than 10 modal % and the sulphides probably have a peridotite

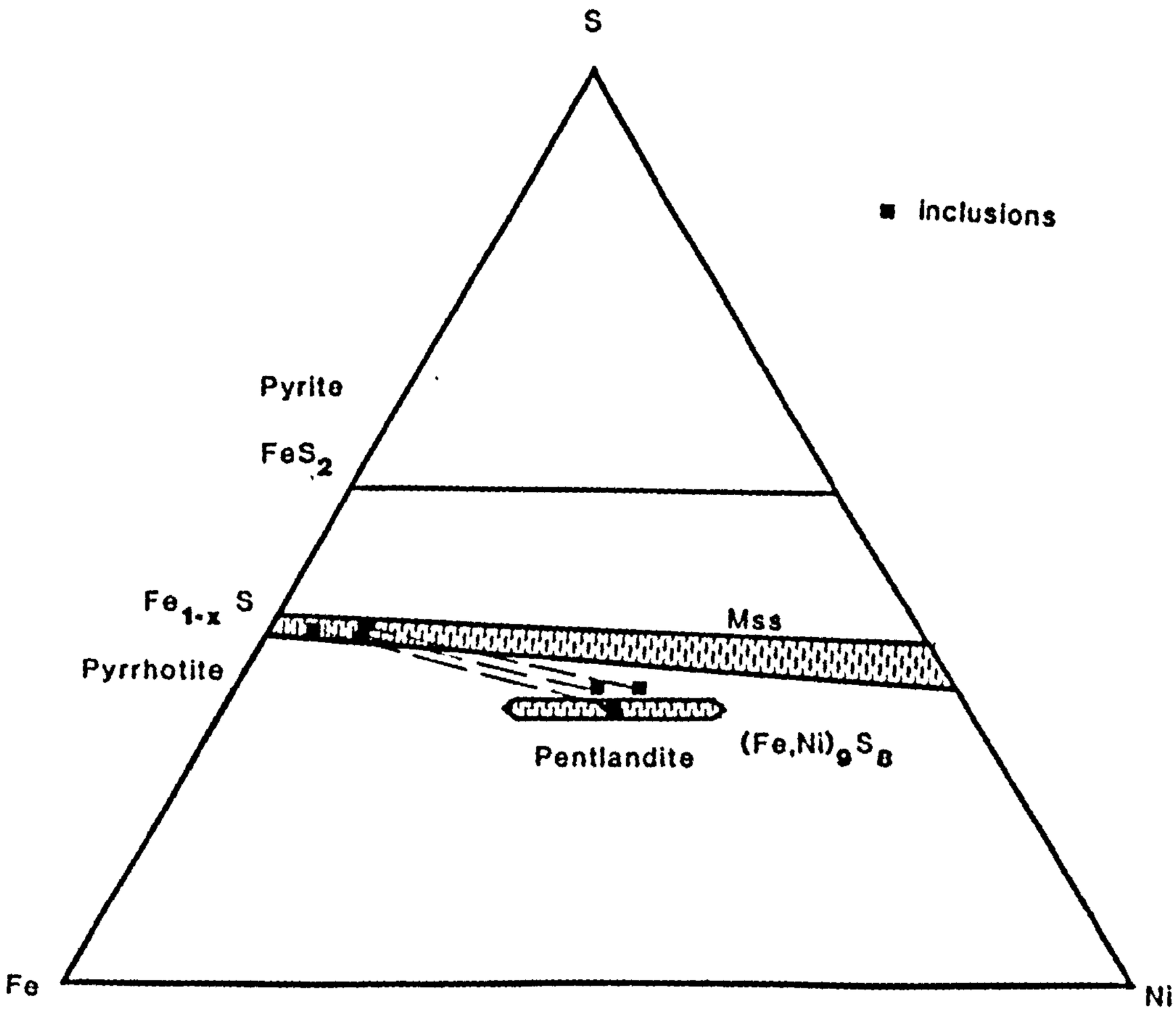
S
Inclusions
Pyrite
FeS_2
Fe_{1-x} S
Pyrrhotite
Mss
Pentlandite
$(Fe,Ni)_9S_8$
Fe
Ni

Fig 3.12.

Fe-Ni-S system.

High temperature monosulphide solid solution (M_{ss}) breaks down to form chalcopyrite and M_{ss} at lower temperature, then excess Ni is exsolved as pentlandite. The sulphide inclusions show exsolutions of pentlandite within pyrrhotite hosts indicating the presence of M_{ss} in the original growth environment. These data are from Craig (Craig, 1974) at are all for atmospheric pressure.

paragenesis. Further evidence for this conclusion was the presence of discrete sulphide flakes, too small for analysis, associated with rossette fractures surrounding peridotite paragenesis inclusions.

One sulphide was found to coexist with native iron. As this sulphide was heazlewoodite (Ni_3S_2), which is only stable at low temperatures, both minerals are considered to be epigenetic.

3.6 Equilibrium conditions at Bultfontein.

Pressure and temperature of Bultfontein diamond formation can be estimated by using established geothermometers and geobarometers. The only coexisting minerals were two peridotite pairs of orthopyroxene and garnet. Temperature estimates were made using the geothermometer of Harley (1984) based on Fe-Mg partitioning. The partitioning of aluminium between orthopyroxene and garnet (Wood & Banno, 1973, Wood, 1974 and MacGregor, 1974) can be used to estimate pressure. To obtain the pressure estimates the modification of this geobarometer by Nickel and Green (1979) were used since this best approximates to peridotite assemblages (Carswell & Gibb, 1985).

Another possible method of estimating temperature is based on the Cr^{3+} partitioning between olivine and orthopyroxene (Hervig & Smith, 1982). Unfortunately in this case the amounts of chrome in olivine and orthopyroxene are very close to electron microprobe detection limits and so this method was not used.

Temperature estimates using the two orthopyroxene-garnet pairs (Harley, 1984) gave temperatures of 930 and 955^{o}C and pressure estimates are determined as 41 to 43 Kbar and 50 to 55 Kbar respectively.

As can be seen in figure 3.13 the Bultfontein P-T estimates lie well within the diamond stability field, defined by the graphite-diamond boundary of Kennedy & Kennedy (1976). Pressure estimates and temperature estimates (at assumed pressures of 50Kbar) are compared with the Bultfontein values in figure 3.13. The Bultfontein diamonds show a lower temperature of origin than the other mines such as Finsch

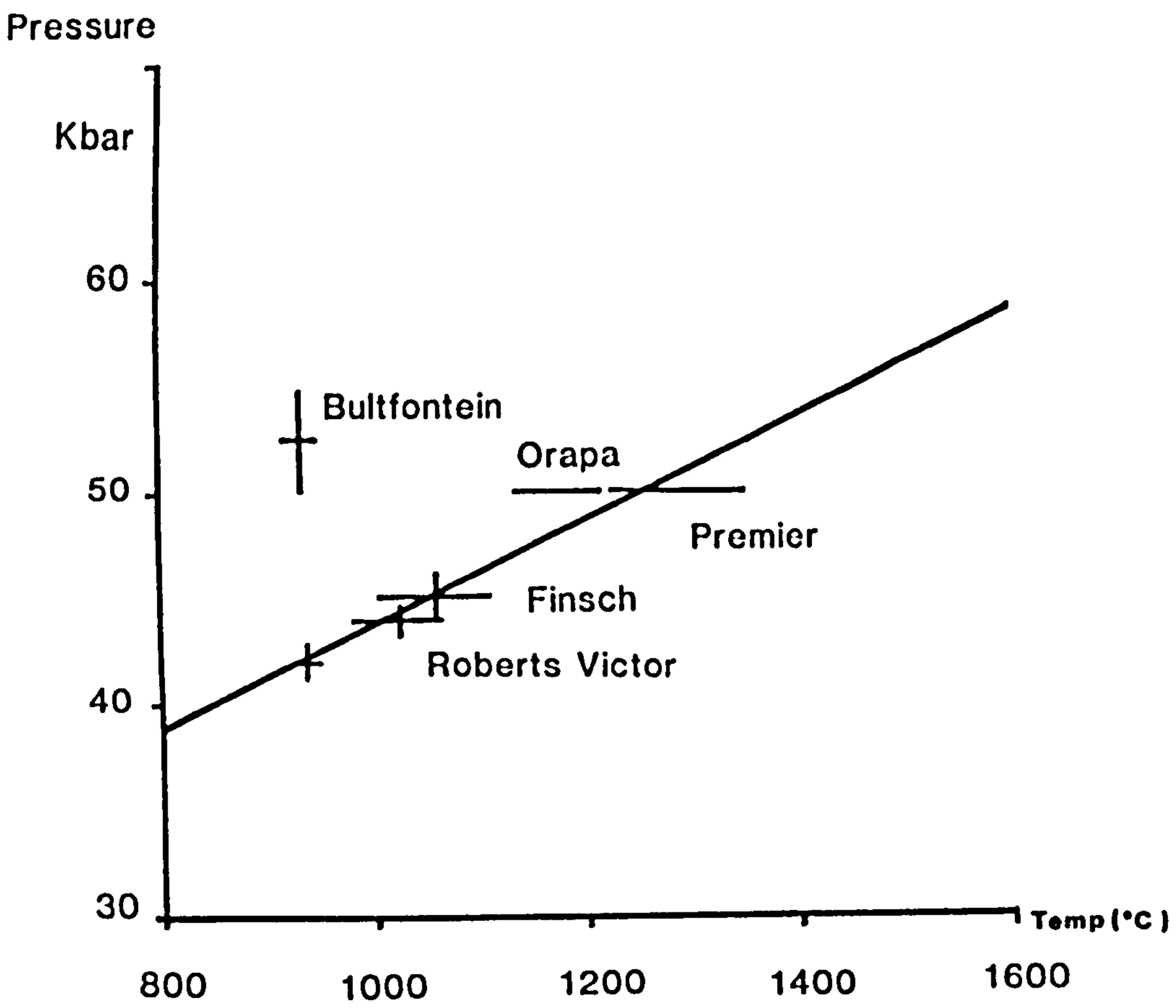

Pressure temperature estimates for Southern African Diamonds

Fig. 3.13

Pressure and temperature estimates for Bultfontein diamond inclusions.

Comparison of Bultfontein diamond inclusions with pressure and temperature estimates from other localities on the Kaapvaal Craton show that the diamonds at Bultfontein formed at lower temperatures and to a certain extent pressure than other mines, implying a shallower depth of origin.

(Harris *et al*, 1979), Orapa (Gurney *et al*, 1984) and Premier (Gurney *et al*, 1985). It is noteworthy that the mines which contain diamonds with higher equilibrium temperatures occur closer to the edges of the craton. Additional evidence for the possible great depth of origin for diamonds peripheral to the craton is seen at Monastery and Jagersfontein mines where inclusions of garnet-pyroxene solid solution occur (Moore & Gurney, 1985).

3.7 Conclusions.

From the morphological and geochemical studies of the inclusion-bearing diamonds the following conclusions are drawn:

1. There are differences in the morphological characteristics between the inclusion-bearing diamonds and the total production at Bultfontein. The inclusion-bearing diamonds are mostly macles, whilst in the total production irregular diamonds are more abundant. Macle growth occurs under conditions of super-saturation at high energies (Bishop, 1967) and inclusion-bearing diamonds might have grown under such conditions. Harris and Gurney (1979) have noted that at Finsch most inclusion-bearing diamonds are macles. The inclusion-bearing diamonds at Bultfontein show a high degree of plastic deformation which suggests that they resided in the mantle for a long period of time.

2. The Inclusion-bearing diamonds from Bultfontein are dominantly of peridotite paragenesis. Eclogite paragenesis and sulphide-bearing diamonds have a low abundance. The most abundant inclusion is chromite, which also dominates at the three other mines in the De Beers Pool. Other mines on the Kaapvaal Craton, such as Finsch and Koffiefontein, which are also dominated by peridotite suite inclusions, have lower chromite abundances. The high chromite content of the diamonds from the De Beers Pool is a feature shared with Russian diamonds.

3. There is evidence for a variation in chemistry of the growth environment. The Mg and Fe contents of chromites vary across the Bultfontein diamonds such that peripheral chromites are more enriched in Fe and Ti than chromites at the centre of the diamonds. Such an increase in Fe and Ti is compatible with the evolution of a mantle derived melt.

4. Peridotite paragenesis garnet inclusions are sub-calcic and indicate growth of garnet in the absence of clinopyroxene in a harzburgite assemblage. Peridotite suite clinopyroxenes are rare and also have a Mg/Mg+Fe ratio lower than olivine and orthopyroxene inclusions, which also favours a harzburgite environment for diamond growth.

5. The chemistry of the olivine and orthopyroxene inclusions from Bultfontein shows very magnesian compositions and also high nickel and chrome contents that favour a high degree of partial melting. These compositions are similar to orthopyroxenes and olivines in komatiites and Bultfontein diamonds may originate in a harzburgite layer that is a remnant from komatiite volcanism.

6. Sulphide inclusions have nickel contents that indicate a peridotite origin. The abundance of sulphides is, however, low in comparison to other mines on the Kaapvaal Craton.

7. Pressure and temperature estimates for the Bultfontein diamonds suggest a relatively low temperature and low pressure origin when compared to other South African localities.

Chapter 4

Nitrogen and carbon characteristics of Bultfontein Diamonds.

4.1 Nitrogen characteristics.

Ninety five inclusion-bearing diamonds were studied for their nitrogen aggregation state by using infra red absorption spectroscopy (outlined in chapter 2). The diamonds studied comprised 84 parallel sided cleavage chips, from which inclusions had been recovered, and 11 diamonds which had (100) surfaces polished onto them. Parallel sided fragments were used in order to reduce the reflections from diamond surfaces during infra red spectroscopy. Infra red spectra were decomposed using the methods of Davies (1981) and Collins (1980) to give nitrogen concentrations at the IaA peak (7.8μm, 1282cm^{-1}), the IaB peak (8.5μm, 1180cm^{-1}) and the platelet peak (7.3μm, 1370cm^{-1}). The nitrogen characteristics are summarised in Table 4.1 and Appendix 2.

In Table 4.1 it can be seen that 69 of the diamonds contain nitrogen in the IaA aggregate, that is the 1282/1180 ratio is greater than 1.0. None of the diamonds are IaB and 7 diamonds show IaA nitrogen only. 11 of the diamonds are Type II.

Figure 4.1 shows the nitrogen data for the inclusion-bearing diamonds from Bultfontein. The ratio 1282/1180 is a measure of the IaA and IaB nitrogen contents, a value of 0.36 indicates a IaB diamond, whereas a value of 2.0 indicates that all of the nitrogen is in the IaA aggregate. The total absorption at 1282 cm^{-1} is a measure of the total nitrogen present. From figure 4.1 it can be seen that Bultfontein diamonds are characterised by high IaA contents. The 1282/1180 ratio for all the inclusion-bearing diamonds ranges from 0.45 to 2.0. Between these values the peridotite suite diamonds range from 0.45 to 2.0. The few eclogite suite diamonds have a much more restricted range from 1.4 to 1.6. The total absorption measured at 1282cm^{-1} ranges from 2.2 to 48.8 which corresponds to nitrogen concentrations over the range of 109 to 1457ppm, with a mean of 479ppm.

Table 4.1

Bultfontein Nitrogen Characteristics.

	IaA	IaA-B	IaB	II
Peridotite				
Chromites	29	0	0	2
Ol/Opx	22	2	0	4
Garnets	6	0	0	1
Cpx	4	0	0	1
Eclogite				
	4	0	0	2
Sulphides				
	5	2	0	1

Table 4.2

Nitrogen Characteristics for Roberts Victor, Finsch and Premier.

	IaA	IaB	II
Roberts Victor			
Peridotite	40	5	16
Eclogite	5	0	7
Sulphides	19	0	1
Finsch			
Peridotite	57	2	23
Eclogite	11	0	0
Premier			
Peridotite	26	0	11
Eclogite	73	6	0

Bultfontein Inclusion-Bearing Diamonds

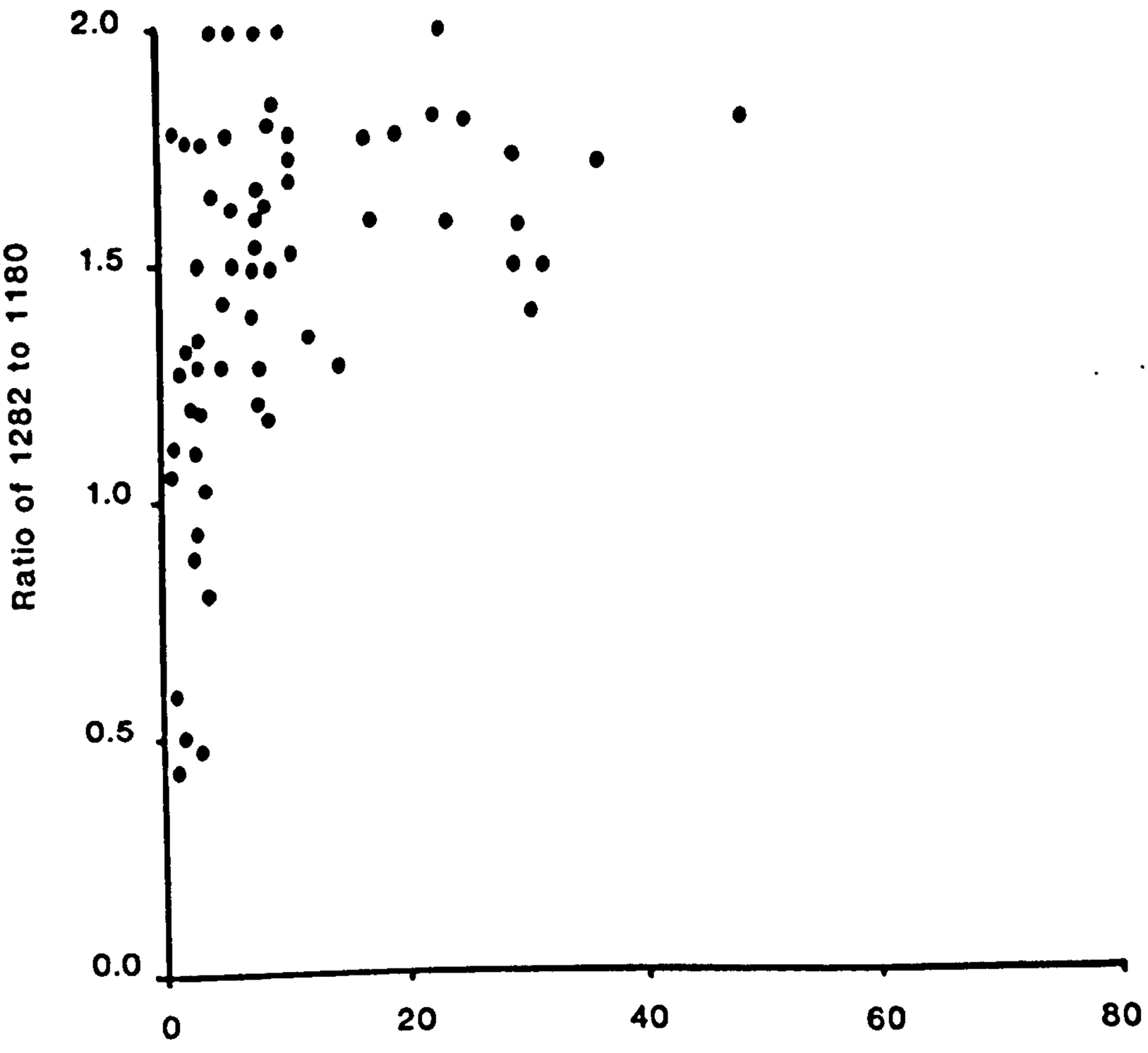

Fig. 4.1

Nitrogen Characteristics of Bultfontein Inclusion Bearing Diamonds.

The ratios of absorption at $1282cm^{-1}$ and $1180cm^{-1}$ show the relative amounts of IaA and IaB nitrogen in the inclusion-bearing diamonds. The total nitrogen content is shown by the total absorption at $1282cm^{-1}$. The Bultfontein inclusion bearing diamonds show high IaA contents and high total nitrogen values. A value of 0.36 on the ordinate indicates a Type IaB diamond.

The nitrogen characteristics for another inclusion-bearing suite of diamonds from the De Beers Pool (Bultfontein being one mine of this group) are shown in figure 4.2 (Davies and Harris, 1980). Both sets of data are characterised by high IaA contents and high total absorption at 1282cm^{-1}. The similarity of the nitrogen characteristics of the Bultfontein diamonds and diamonds from the De Beers Pool indicates that the diamonds studied in this project are not atypical.

The nitrogen characteristics of Bultfontein inclusion-bearing diamonds can be compared with inclusion-bearing diamonds from three other mines on the Kaapvaal Craton (Deines *et al.*, 1984, 1987 and unpubl). In Table 4.2 the data from Roberts Victor, Finsch and Premier mines are summarised. Among peridotite paragenesis diamonds all three mines show a greater abundance of Type II diamonds. The data however do not enable a direct comparison of the IaA and IaB contents between the mines. Diamonds from Premier mine have a high abundance of eclogite paragenesis inclusions and 6 show high Type IaB content and low absolute nitrogen concentrations (Deines *et al.*, 1984). Harris and Collins (1980) found a similar relationship in eclogite paragenesis diamonds from the Argyle mine in Australia.

Bultfontein, Roberts Victor and Finsch mines are all dominated by peridotite suite inclusions. There is a variation in the total nitrogen concentrations in peridotite suite diamonds at these three mines which is shown in figure 4.3. Bultfontein diamonds show high absolute nitrogen concentrations and the data are skewed towards higher values. Finsch mine has a notably low absolute nitrogen content, while the diamonds at Roberts Victor have intermediate values. Type II diamonds are not shown in this diagram (see, however, Table 4.2).

The nitrogen concentrations of inclusion-bearing diamonds at Bultfontein varies with inclusion type, as shown in Appendix 2 and summarised in Table 4.3.

The highest concentrations of nitrogen occur in sulphide-bearing diamonds which have a range of total nitrogen from 211 to 1467ppm (mean value

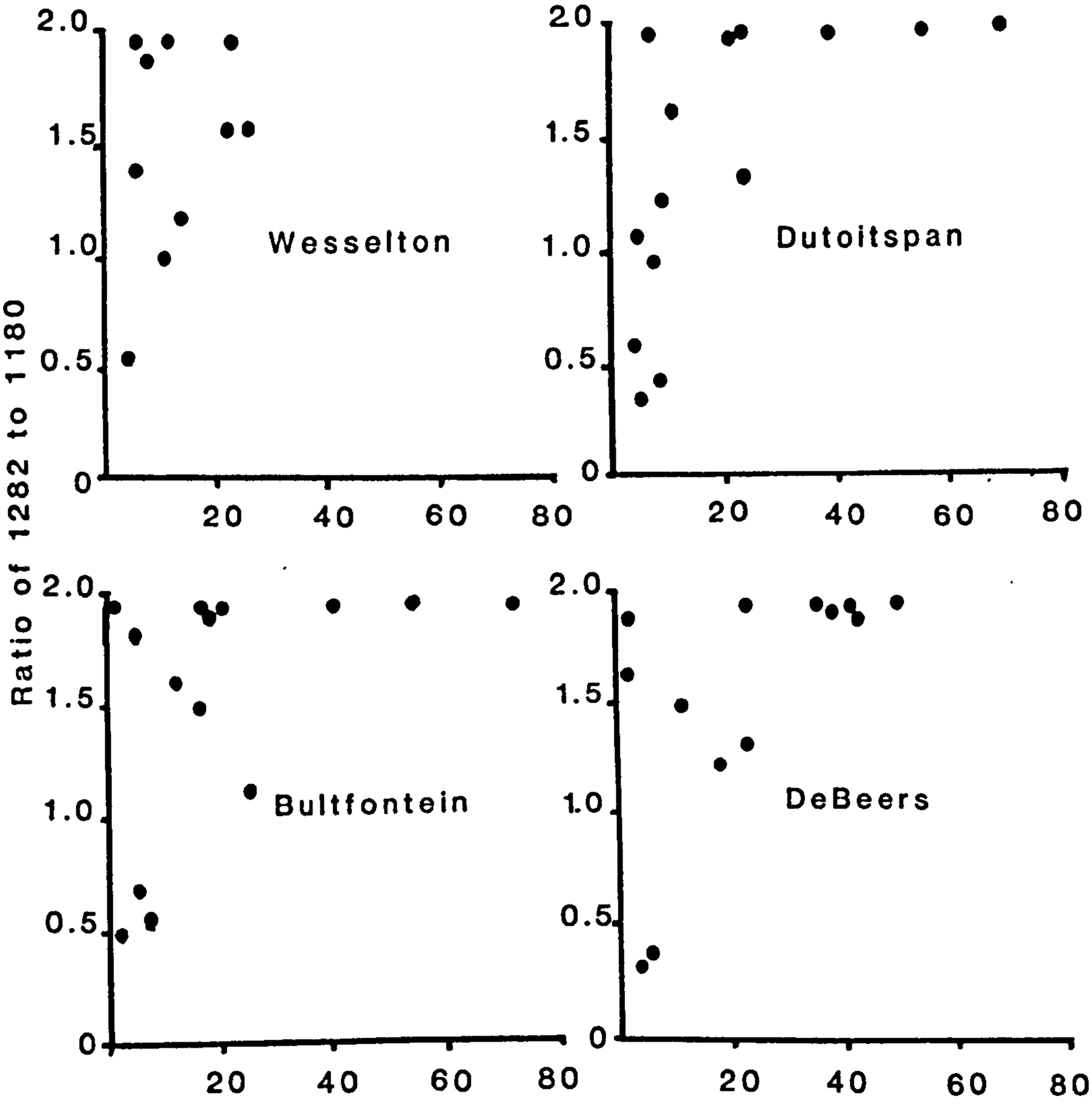
Wesselton
Dutoitspan
Bultfontein
DeBeers
Ratio of 1282 to 1180
0
0.5
1.0
1.5
2.0
20
40
60
80
Total Absorption at 1282 cm-1 in cm-1

Fig 4.2.

Nitrogen Characteristics of the De Beers Pool Mines.

From the ratio of absorption at $1282cm^{-1}$ to $1180cm^{-1}$ the level of IaA and IaB nitrogen can be determined. The total absorption at $1282cm^{-1}$ is a measure of the total nitrogen present. These data for the De Beers Pool are taken from Davies and Harris (1980) and show the nitrogen characteristics for the four mines in the Kimberley area. The plots show high concentrations of IaA nitrogen but a variation in total nitrogen concentration. Diamonds with more IaB nitrogen show a lower nitrogen content. On the ordinate of the graph a value of 2.0 indicates a IaA diamond, while a value of 0.36 indicates a Type IaB diamond.

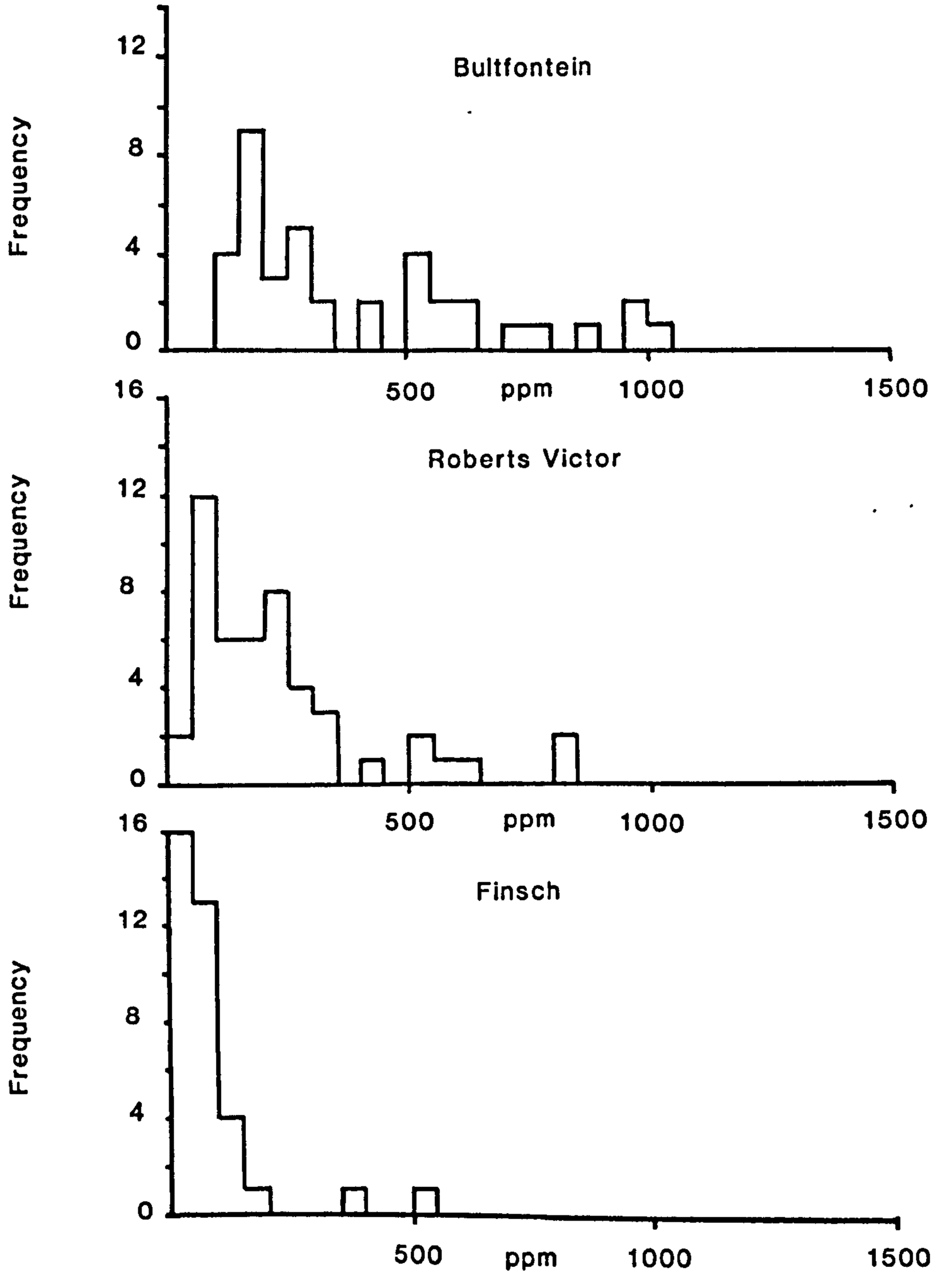
Bultfontein
Frequency
12
8
4
0
500
ppm
1000
1500
Roberts Victor
Frequency
16
12
8
4
0
500
ppm
1000
1500
Finsch
Frequency
16
12
8
4
0
500
ppm
1000
1500

Fig. 4.3

Nitrogen Contents for Peridotite Suite Diamonds from Bultfontein, Roberts Victor and Finsch.

The total nitrogen concentrations for peridotite suite diamonds from Bultfontein show higher values than Roberts Victor and Finsch. At Finsch the nitrogen concentrations are very low. In all three mines the data is skewed towards low nitrogen contents.

Table 4.3

Nitrogen Concentrations for Bultfontein Peridotite Suite Diamonds.

	Range of 1282/1180	Range of Total Nitrogen	Mean.
Chromite	1.1-2.0	48-1358	443
Ol/Opx	0.45-2.0	93-978	268
Garnet	1.2-1.9	153-303	240
Cpx	1.3-1.9	133-858	485
Sulphide	0.6-1.8	211-1467	824

824ppm). At Finsch and Roberts Victor diamonds which contain sulphides also show the highest nitrogen concentrations.

The relative concentrations of nitrogen and the aggregation states of nitrogen are useful as a potential indicator of temperatures of formation and possibly mantle residence time. Studies of synthetic diamonds by Chrenko *et al.*, (1977) have shown that single substitutional nitrogen when subject to high temperature will aggregate to Type Ia. The rate of aggregation can be expressed in terms of second order kinetics as follows:

$$Kt = 1/C - 1/C_o$$

Where K is the rate constant ($ppm^{-1}min^{-1}$), C_o is the initial concentration (ppm), C is final concentration and t is time. The activation energy can be expressed as:

$$K = Ae^{-E/kT}$$

where E is the activation energy and A and *k* are constants. At temperatures above 2000K (1727°C) values of K are 1.74×10^{-4} $ppm^{-1}min^{-1}$ and E 2.6*e*V.

Evans and Qi (1982) have determined the values of rate constants (K) for nitrogen aggregation from Ib to Ia over a range of temperatures and pressures appropriate to mantle depths. At low temperatures (900°C) the rate constant is; 2.9×10^{-9} ppm^{-1} min^{-1} for an initial concentration of 1140ppm (2×10^{26} m^{-3}) as can be seen from Table 4.4, a period of 5.7×10^{10} years would be required to transform all the Ib nitrogen into an aggregated form (Ia), a period obviously older than the age of the earth. Type Ib diamonds are rare in nature so the rate constants must have higher values in order to produce the common Type IaA diamonds. At higher temperature (1400°C) the rate constant for a nitrogen concentration of 2×10^{26} m^{-3} of nitrogen is such that a period of only 2.2×10^{4} years aggregates all the nitrogen as IaA (Table 4.4).

The aggregation process for Type IaB nitrogen is more complicated because IaA centres do not directly aggregate to IaB centres.

Table 4.4.

T^oC	$t_{99.999\%}$ Ia
900	5.7×10^{10}
1000	1.2×10^{9}
1100	4.3×10^{7}
1200	2.5×10^{6}
1300	2.0×10^{5}
1400	2.2×10^{4}

Time, in years, for 99.999% transition from Type Ib to Type Ia diamond with activation energy of 5*e*V (Evans & Qi, 1982).

Table 4.5.

T^oC	$t_{20\%}$	$t_{50\%}$
900	2.8×10^{15}	1.1×10^{16}
1000	7.6×10^{12}	3.0×10^{13}
1100	4.9×10^{10}	2.0×10^{11}
1200	6.4×10^{8}	2.9×10^{9}
1300	1.4×10^{7}	5.6×10^{7}
1400	4.9×10^{5}	2.0×10^{6}

Times, in years, to aggregate 20 and 50% IaB nitrogen from IaA nitrogen with an activation energy of 7.6*e*V (Evans & Qi, 1982).

Platelet development (Bursill & Glaisher, 1985) and N3 centre formation accompanies the IaA to IaB transition. Nevertheless Evans & Qi (1982) suggest that similar second order kinetics dominate the IaA to IaB transition. Activation energies of 7.6 *e*V give periods to aggregate 20% of IaB of 7.9 x 10^{12} years for 1000^{o}C. Lower temperatures and therefore activation energies, as shown in Table 4.5, would show more extended periods of aggregation. For example, at 900^{o}C a period of 2.8 x 10^{15} years would be required to nucleate 20% of the A aggregate to the B aggregate. Measurements of the activation energy and rate constants for IaA to IaB nitrogen are poorly known and are at present being refined.

The relative amounts of nitrogen in the IaA or IaB aggregate can be determined by plotting the ratio of absorption at 7.8μm produced by the IaA aggregate and the total absorption at the 7.8μm peak. Figure 4.4 shows this ratio plotted against the ratio of absorption at the peaks 7.3μm and 7.8μm, which is a measure of the amount of nitrogen in platelets. Platelet growth accompanies the regular transition from IaA to IaB nitrogen and it would be expected that as the $7.8_{A}/7.8_{Total}$ ratio decreases the ratio of 7.3/7.8 increases (Woods, 1986).

Figure 4.4 plots the 7.3/7.8 against $7.8_{A}/7.8_{Total}$ ratio for peridotite suite diamonds from Bultfontein. As can be seen the nitrogen characteristics vary with inclusion type. Chromite-bearing diamonds are Type IaA with a few of low IaB contents ($7.8_{A}/7.8_{Total}$ less than 1.0). Diamonds which contain olivine and orthopyroxene appear bimodal but follow quite closely a linear relationship between IaB content and platelet concentration. One group has relatively high platelet and IaB nitrogen while the other group has a relatively high IaA. Diamonds containing garnets also show two populations similar to those for olivine and orthopyroxene. Diamonds which contain clinopyroxenes of both peridotite and eclogite paragenesis and sulphide-bearing diamonds all show high IaA contents with virtually no IaB nitrogen.

The aggregation of nitrogen is controlled by temperature, time and the initial concentration of nitrogen. The nitrogen data from

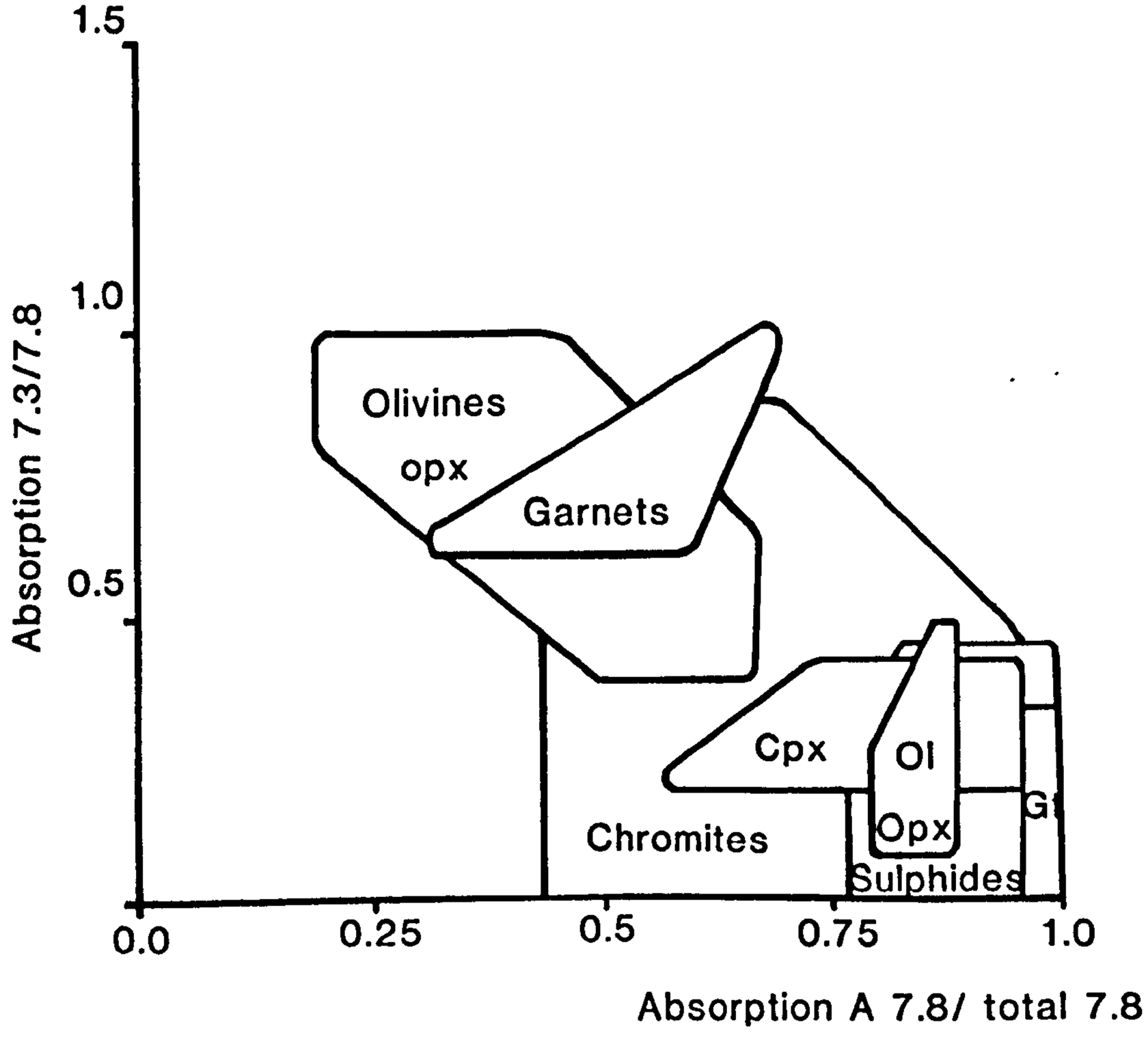

Nitrogen aggregation state for Bultfontein

Fig 4.4.

Platelet and IaB content at Bultfontein.

The ratio 7.8Λ/7.8Total is a measure of the contribution of IaB nitrogen to the absorption peak at 7.8μm, when the value is equal to 1, all the nitrogen is aggregated as the IaA aggregate. The diagram shows an inverse linear relationship with diamonds that show high platelet peaks containing more IaB nitrogen.

Diamonds with different inclusion types show different nitrogen characteristics. Diamonds with olivine and orthopyroxene inclusions show two groups. One group has high platelet and high IaB characteristics, the other group shows more IaA nitrogen and lower platelet content. Diamonds which contain garnets also show two similar groupings. In diamonds which contain chromites the concentrations of IaB nitrogen and the platelet contents are low.

Bultfontein highlights the possibility that there are two groups of diamonds, one group containing olivine, orthopyroxene and garnet and having a high IaB content. The other group containing most of the chromites but also some olivine, orthopyroxene and garnet. This second group is dominated by Type IaA nitrogen.

The average amount of nitrogen in the group with high IaB contents is 232ppm wuth a 1σ of 66. For the group with high IaA the mean concentration is are 520ppm, although the range is greater ($1\sigma = 428$).

The differences in the nitrogen aggregation states between the two groups may result from differences in the initial concentration of nitrogen with aggregation over the same time and under the same temperature conditions, as shown by the equations above. Microprobe analyses show that there are no chemical differences between the olivines and orthopyroxenes of the two groups. Inclusions in both groups therefore grew under identical geochemical conditions. Temperature estimates for garnet and orthopyroxene pairs from the high IaB group give values of 930 to 955^{o}C.

For the Bultfontein diamonds there are two possible explanations for the two groups of nitrogen characteristics: First that the differences in IaB content result from differences in the initial concentration of nitrogen. Second that two populations represent two phases of diamond growth that are separated by a long period of time. From the data shown in Table 4.5 the time taken to aggregate 20% of the nitrogen as IaB at 1000^{o}C is 3.8×10^{13} years for initial nitrogen concentrations of 232ppm. For initial concentrations of 520ppm the time taken to aggregate 20% IaB is 1.7×10^{13} years. At temperatures of 1200^{o}C the time required to aggregate 20% IaB for the two concentrations is 3.1×10^{9} and 1.4×10^{10} years respectively. For low nitrogen concentrations the time required to aggregate IaB nitrogen is less than for high initial nitrogen concentrations, for example the time taken to aggregate 20% of the nitrogen in diamonds with 232ppm of nitrogen would only aggregate 3% in diamonds with 520ppm nitrogen. Diamonds which contain olivine, garnet and orthopyroxene are mostly

macles, whereas chromite-bearing diamonds are mainly aggregates and irregular stones. Conditions of formation for diamonds which contain garnet, olivine and orthopyroxene were probably supersaturated in carbon, allowing macle formation. Chromite-bearing diamonds therefore formed under different conditions (not supersaturated in carbon). Whether one set of conditions gave rise to another with time or whether they represent isolated occurrences, with different initial nitrogen concentrations, remains unknown.

4.2 Carbon isotopic compositions.

The carbon isotope compositions for 95 chips of inclusion-bearing diamonds were determined using the method described in Chapter 2. These data are presented in Appendix 2. The analyses have a typical precision of 1σ 0.17 $^{o}/_{oo}$ and the accuracy of analyses, based on the comparision with the NBS21 standard, is $\pm$ 0.26 $^{o}/_{oo}$. The carbon isotope values were measured on diamond fragments different to those used for infra red studies.

The carbon isotope values for the Bultfontein peridotite and sulphide-bearing diamonds range from $\delta\ ^{13}C$ of -0.46 to -10.29 $^{o}/_{oo}$ (eclogite suite diamonds show a more limited range of $\delta\ ^{13}C$ from -6.6 to -4.6 $^{o}/_{oo}$). The mean carbon isotope value is $\delta\ ^{13}C$ -4.66 $^{o}/_{oo}$ vs PDB. The distribution of isotope values is not Gaussian and values for peridotite suite diamonds are skewed towards compositions enriched in ^{13}C.

Although the carbon isotope values for Bultfontein are limited, the mean δ values of isotopic composition varied with inclusion type as shown in figure 4.5. Diamonds with chromite inclusions are the most ^{13}C enriched with a mean $\delta\ ^{13}C$ value of -3.76 $^{o}/_{oo}$, with a distribution skewed towards heavier compositions (for 33 diamonds). The mean value for 26 olivine and orthopyroxene-bearing diamonds is -4.95 $^{o}/_{oo}$ and are similarly skewed towards heavier compositions. The carbon isotope ratio for the 11 diamonds which contain peridotite paragenesis

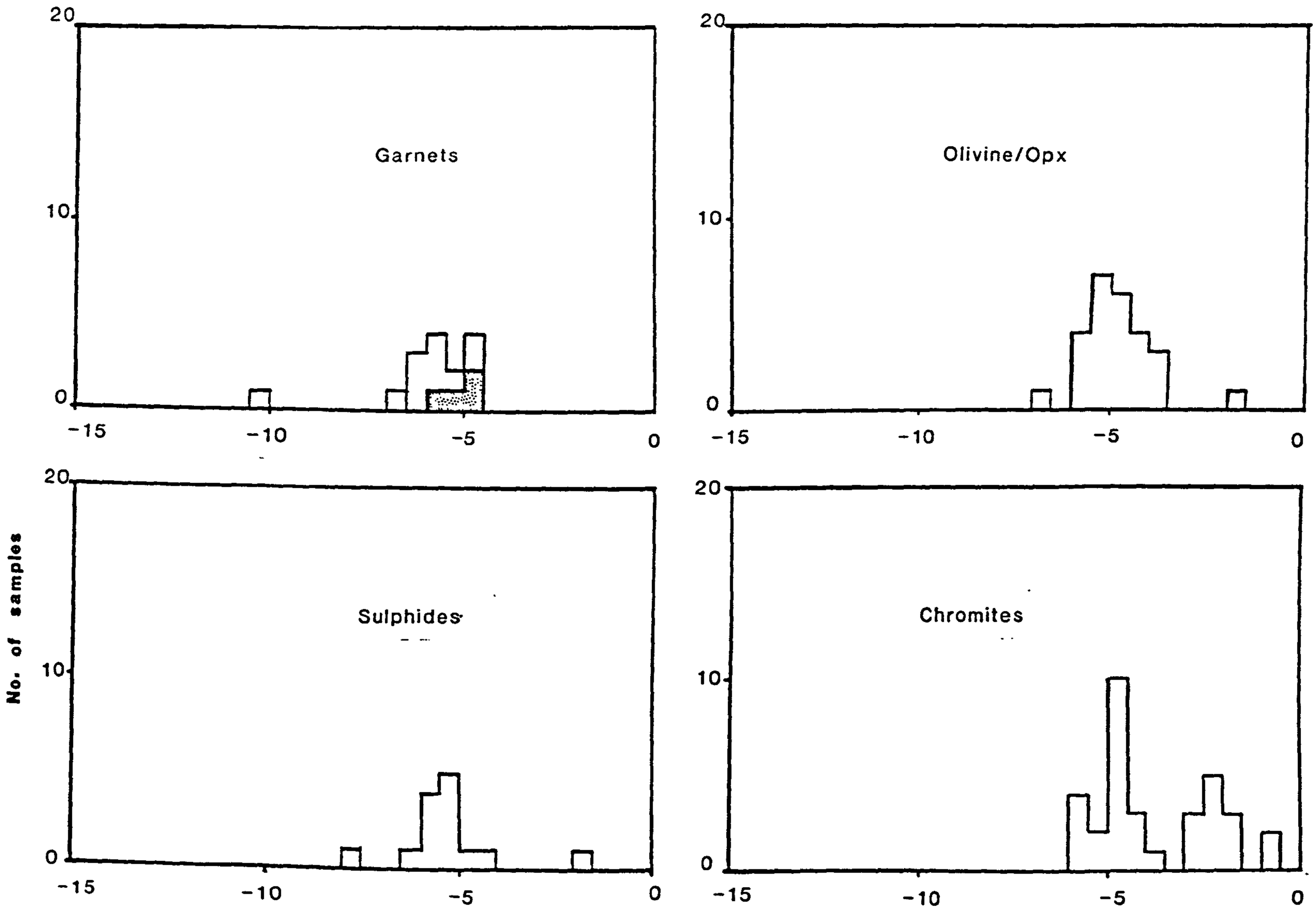

Isotope variation for Bultfontein diamonds

Fig 4.5.

Carbon Isotope Variation with Inclusion Type.

Differences in carbon isotope characteristics for garnet, olivine, orthopyroxene, sulphide and chromite-bearing diamonds are shown. Diamonds which contain garnet are isotopically light. Diamonds with olivine and orthopyroxene are skewed towards heavier values. Diamonds with the heaviest $\delta\ ^{13}C$ values contain chromites and compositions are skewed towards lighter values. The shaded area beneath the garnet histogram represent the $\delta\ ^{13}C$ values for eclogite paragenesis diamonds.

garnets has a mean $\delta\ ^{13}C$ value of -6.04 $^{o}/_{oo}$ and shows no skewness. In contrast the mean value for diamonds which contain eclogite suite garnets is -5.26 $^{o}/_{oo}$. Sulphide-bearing diamonds have a mean $\delta\ ^{13}C$ value of -5.25 $^{o}/_{oo}$.

In comparison to similar work from other sources on the Kaapvaal Craton by Deines *et al.* (1984 & 1987) the mean $\delta\ ^{13}C$ value for the Bultfontein diamonds is found to be relatively ^{13}C enriched, as shown in figure 4.6. At Finsch the mean $\delta\ ^{13}C$ value for 93 analyses is -5.98 ($1\sigma = 1.10$) $^{o}/_{oo}$ and at Premier the mean $\delta\ ^{13}C$ for 66 diamonds is -4.84 ($1\sigma = 1.82$) $^{o}/_{oo}$ (Deines *et al.*, 1984). At Roberts Victor the mean $\delta\ ^{13}C$ value is -6.40 ($1\sigma = 3.25$) $^{o}/_{oo}$ for 95 analyses (Deines *et al.*, 1987).

Statistical analyses of the data from the four mines (see Cheeney, 1983) show that Bultfontein, Premier and Roberts Victor diamonds were probably derived from a reservoir with the same isotopic composition (Student's t test to 95% confidence), since the predicted range of means from the source overlaps. An isotopically lighter source is favoured for Finsch. Further testing (Kolmogorov-Smirnov) confirms a separate origin for Finsch because there is a greater discrepancy in the cumulative frequency of isotope compositions between Finsch diamonds and the cumulative frequency of diamonds from Bultfontein, Premier and Roberts Victor.

A Gaussian (or normal) distribution would be expected from a single isotopic source if all the carbon present in a given reservoir is converted into diamond, or if the carbon reservoir is infinitely large. The distribution of data from Finsch, Premier and Bultfontein is not Gaussian. At Finsch and Bultfontein the values are skewed towards heavier isotope compositions while at Premier the data is slightly skewed towards lighter, ^{13}C depleted values. At Roberts Victor on the other hand the data define a normal distribution. Non Gaussian distributions of data at Finsch, Roberts Victor and Bultfontein may result from sampling of diamonds from different isotopic reservoirs which contradicts

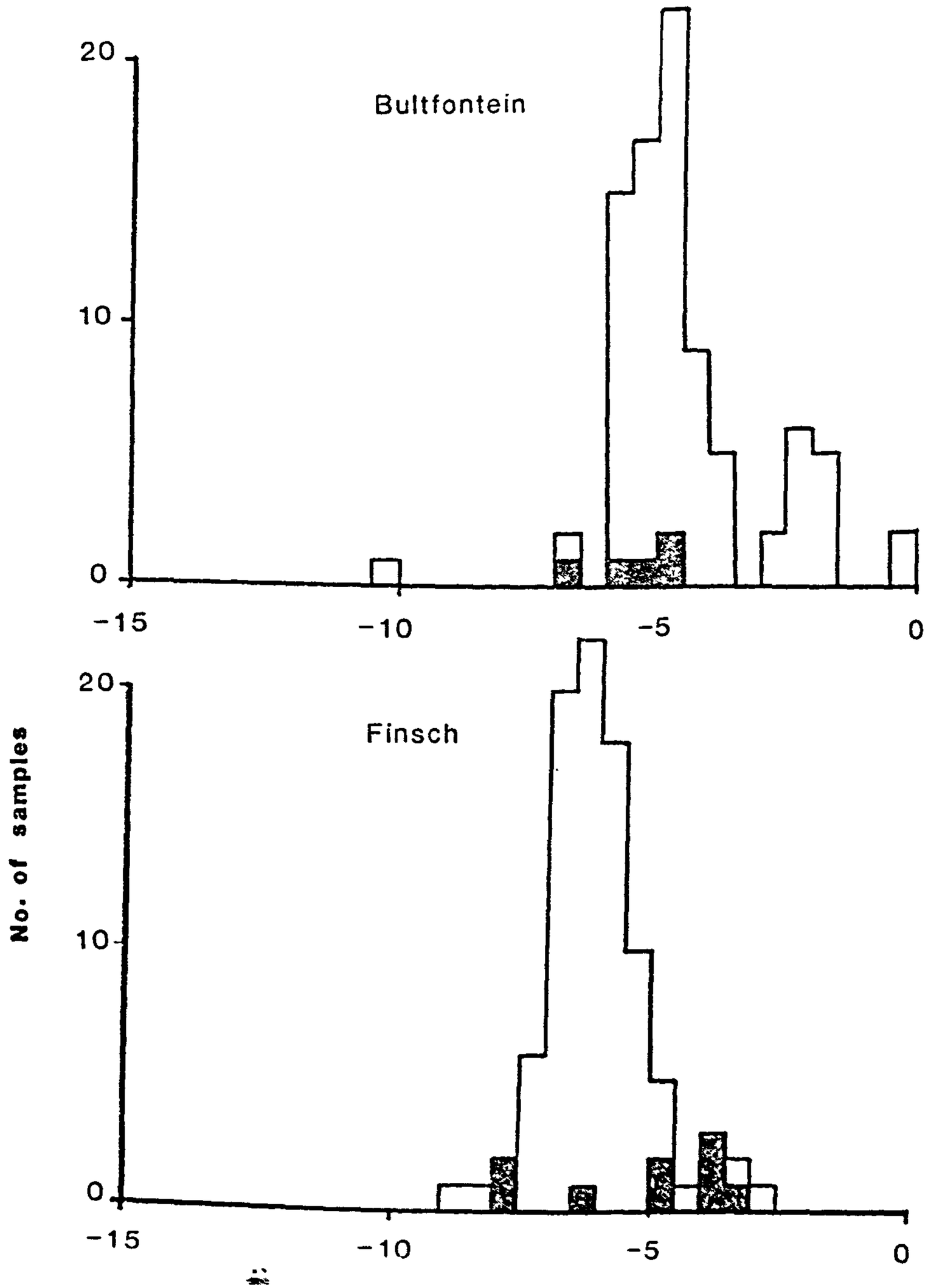
Bultfontein
20
10
0
-15
-10
-5
0

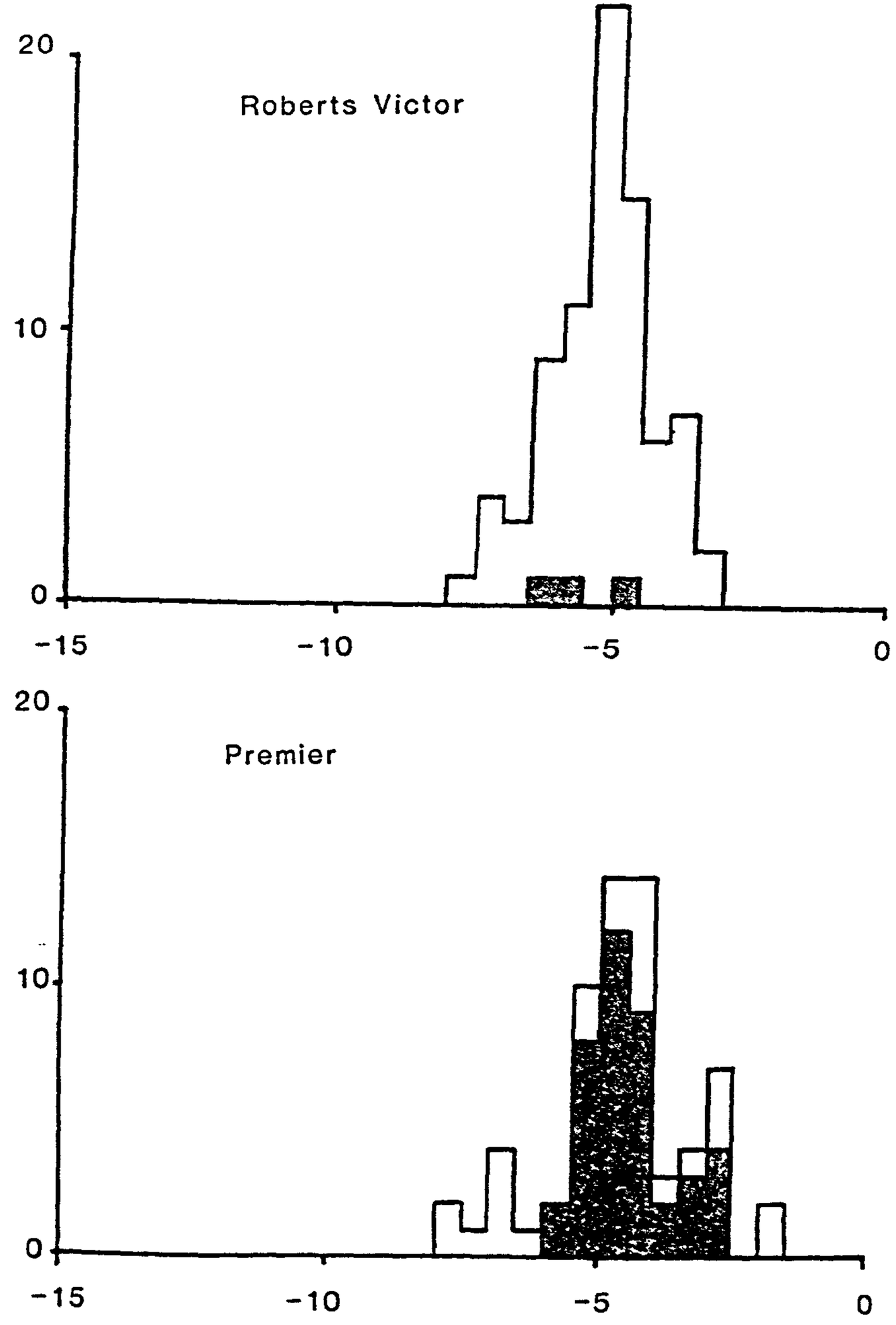
Roberts Victor
20
10
0
-15
-10
-5
0

Finsch
No. of samples
20
10
0
-15
-10
-5
0

Premier
20
10
0
-15
-10
-5
0

Fig 4.6.

Carbon Isotope Composition for Mines on the Kaapvaal Craton.

The data shown are for four mines, Premier, Finsch and Roberts Victor (Deines, 1982 & Deines *et al.*, unpubl.) and Bultfontein (this study). Shaded sections show eclogite suite diamonds and unshaded areas are peridotite diamonds. Bultfontein peridotite suite diamonds show a heavier mean carbon isotope composition, two populations and a skewness towards light $\delta\ ^{13}C$ values. Diamonds from Finsch mine, are isotopically lighter than Bultfontein diamonds and are probably derived from a different carbon reservoir. At Finsch the $\delta\ ^{13}C$ values are also skewed towards heavier values. Roberts Victor and Premier mines are skewed towards negative $\delta\ ^{13}C$.

the predicted mean reservoir compositions. A more favoured explanation is that the skewed distributions result from isotope fractionation processes which are discussed later.

For the Bultfontein inclusion-bearing diamonds there is no correlation between $\delta\ ^{13}C$ values and nitrogen characteristics. The change in carbon isotope composition with inclusion type shows olivine and orthopyroxene-bearing diamonds of the two groups have lighter isotope values than chromite-bearing diamonds.

The mean values for carbon isotopes for diamonds from Bultfontein (-4.66 $^{o}/_{oo}$) are close to the values ascribed to mantle derived rocks such as carbon as carbonate in carbonatites and kimberlites and carbon as graphite in meteorites (~-5 $^{o}/_{oo}$)(Deines & Wickman, 1973; 1975). The range of $\delta\ ^{13}C$ of -0.46 to -10.29 $^{o}/_{oo}$ and the non Gaussian distribution for Bultfontein would not be expected if there had been complete conversion of elemental mantle carbon to diamond, or precipitation of diamond from an infinite reservoir. It is also possible that the non Gaussian distributions in isotopic compositions at Bultfontein result from heterogeneities within the source reservoir, for example heterogeneties that result from primary earth accretion (Clayton, 1986) or from mantle mixing processes such as subduction (Kyser, 1986). Despite the range in isotope composition however it is clear that the mode of $\delta\ ^{13}C$ values at Bultfontein is close to the value of mantle carbon of ~ -5 $^{o}/_{oo}$.

If separate carbon reservoirs were sampled in the production at Bultfontein then the data would be expected to show a normal distribution around the mean $\delta\ ^{13}C$ value for each reservoir.

The data from Bultfontein shows small differences in carbon isotope composition with each inclusion type. As previously mentioned the olivine, orthopyroxene and garnet bearing diamonds show a skewness towards heavier isotopic compositions. The non Gaussian distribution (i.e. skewness) of the

Bultfontein diamonds is discussed in the next section in terms of limited carbon reservoirs and diamond precipitation processes.

4.3 Isotope Fractionation Processes.

If the total amount of carbon present in a given, restricted reservoir in the mantle is transformed into diamond and there is no isotopic communication with the surroundings then the diamond will have the same $\delta\ ^{13}C$ value as the reservoir. If only a specific amount of carbon in a reservoir is transformed into diamond the $\delta\ ^{13}C$ value of the diamond may differ from the reservoir as a result of isotope fractionation processes. The latter situation can be applied to the upper mantle. According to Deines (1980) the equilibrium conversion from graphite to diamond is free from isotope effects. Reactions between CO_2-rich melts and diamonds would only produce a small fractionation. The greatest isotope fractionation occurs when carbon is precipitated from interactions of C-O-H volatiles. In the upper mantle the volatile species present in a C-O,H free vapour phase will be H_2O, H_2, CO_2 , CO, CH_4 and O_2, in addition carbon (as graphite or diamond) will be stable if the oxygen fugacity is appropriate. The abundance of each species is controlled by the following equilibria:

$$2H_2 + O_2 = 2H_2O$$

$$2CO + O_2 = 2CO_2$$

$$CO + 3H_2 = CH_4 + H_2O$$

$$C + O_2 = CO_2$$

At any given temperature the vapour composition is dependent on oxygen fugacity and the stability of each species has been calculated by Deines (1980). These are shown in figure 4.7 for a pressure of 50kbar. With deposition from a vapour, most diamond will be either precipitated from CH_4 or CO_2 through reactions 1 to 4, shown below. Precipitation of carbon can occur at the interface between zones of contrasting oxygen fugacity (see figure 4.7). Haggerty

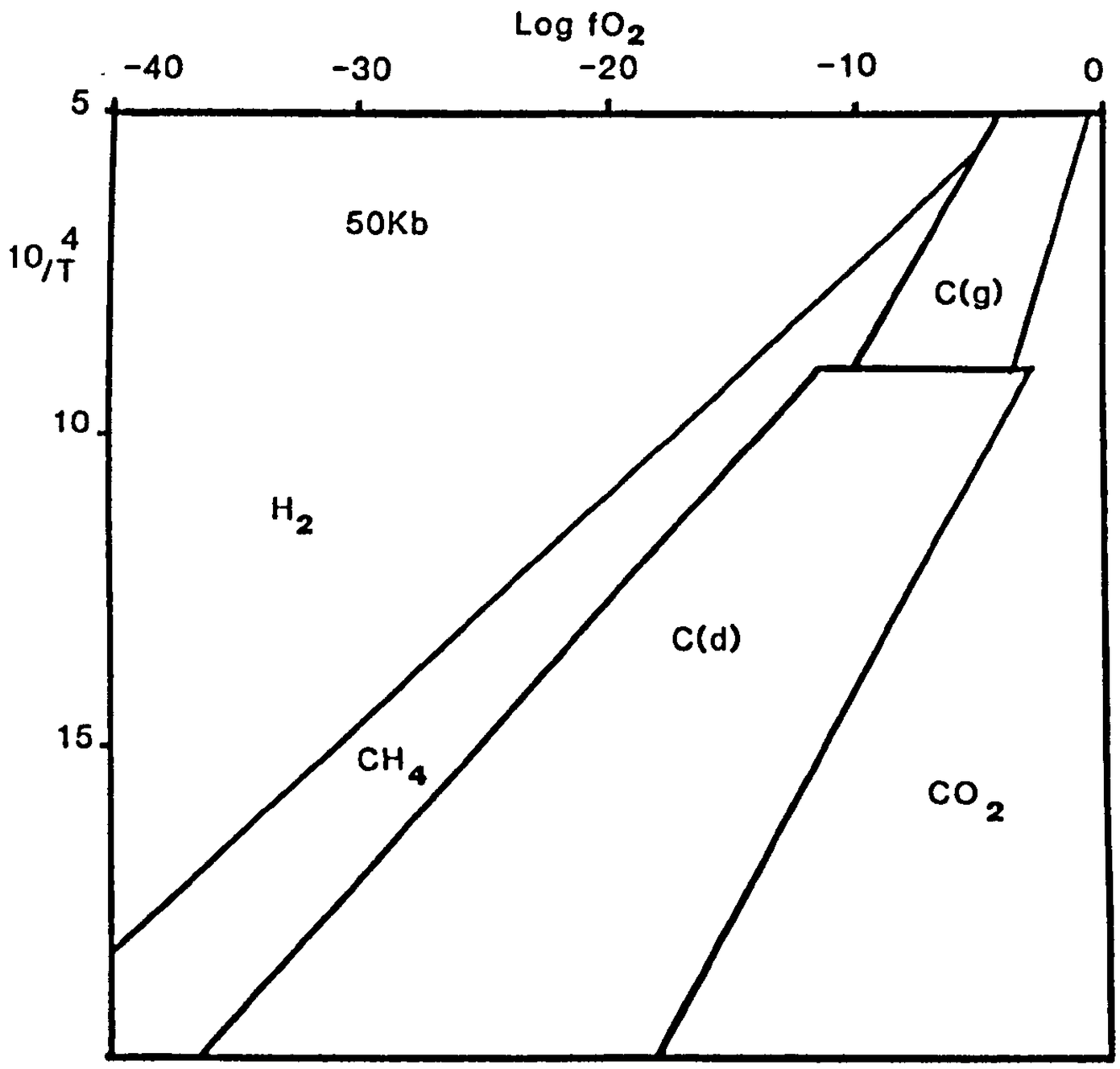
Log fO_2
-40
-30
-20
-10
0
5
10
15
$10/_T^4$
50Kb
H_2
CH_4
C(g)
C(d)
CO_2

Fig. 4.7.

Fields of carbon species as a Function of Pressure, Temperature and fO_2.

The stability fields for different carbon bearing species are shown as a function of temperature and oxygen fugacity for pressures of 50kbar. At low fO_2 carbon is stable as CH_4 and at high fO_2 carbon is stable as CO_2. CO is never a major carbon bearing species. Between the fields of CH_4 and CO_2 carbon is stable as graphite C(g) or diamond C(d) and H_2O is the dominant volatile. Carbon can be precipitated by CH_4 oxidation or CO_2 reduction (Deines, 1980).

(1986), for example, suggested precipitation can occur with the expected change in fO_2 conditions at the asthenosphere-lithosphere interface.

Precipitation of carbon occurs through the following reactions:

$$CO_2 = C + O_2 \qquad (1)$$

$$CH_4 = C + 2H_2 \qquad (2)$$

$$CO_2 + 2H_2 = C + 2H_2O \qquad (3)$$

$$CO_2 + CH_4 = 2C + 2H_2O \qquad (4)$$

CO reactions have been eliminated from consideration (see above).

The fractionation effects between different phases can be expressed as modifications of the fractionation factor $\alpha_{v\text{-}c}$, defined (Valley *et al.*, 1986) as:

$$\frac{^{13}C/^{12}C \text{ vapour}}{^{13}C/^{12}C \text{ solid}}$$

The value $\Delta\ 13C_{v\text{-}c}$, which is $\delta\ ^{13}C_v - \delta\ ^{13}C_c$, approximates to 1000ln $\alpha_{v\text{-}c}$ (the per mil fractionation). Deines (1980) has modelled the effects of changing oxygen fugacity on the precipitation of diamond from a vapour with a $\delta\ ^{13}C$ value of -5 $^{o}/_{oo}$. At low oxygen fugacity where CH_4 is the dominant species, fractionation factors tend towards $\Delta_{v\text{-}c} = \Delta_{CH4\text{-}c}$ (~-1) while at high oxygen conditions $\Delta_{v\text{-}c}$ is close to that of $\Delta_{CO2\text{-}c}$ (~+4). These relationships are shown in figure 4.8. There is a very narrow zone between the two fields where the value of $\Delta\ ^{13}C$ changes rapidly from CH_4 to CO_2 and this zone corresponds to the minimum carbon content in the vapour, whether the carbon is graphite or diamond. If, for example, there was an increase in oxygen fugacity from 10^{-14} to 10^{-12} at 950°C the $\Delta\ ^{13}C$ value would change from -1 to +3 and the $\delta\ ^{13}C$ value of the vapour would be 4 $^{o}/_{oo}$ heavier than the coexisting precipitated carbon.

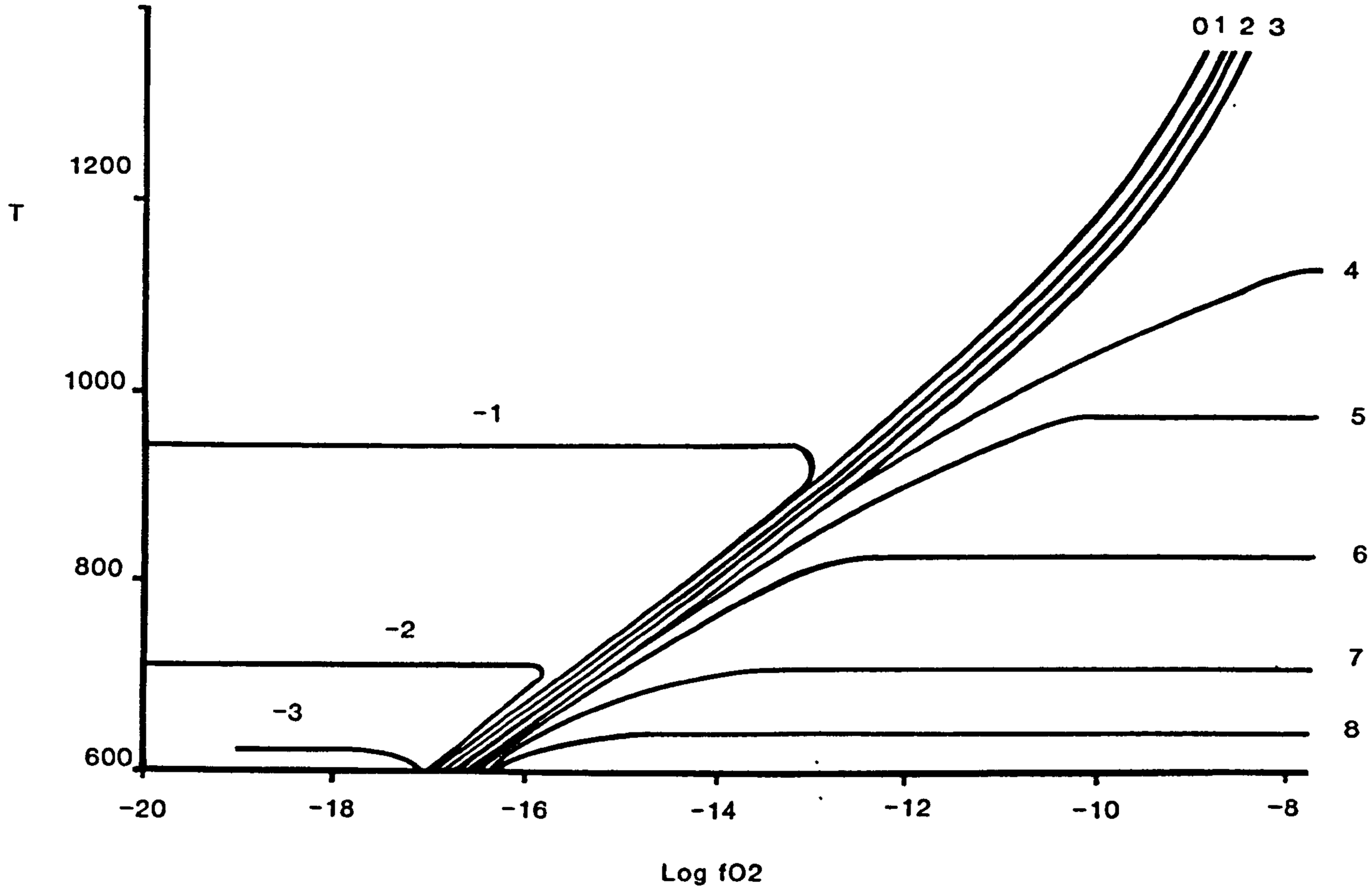
T
1200
1000
800
600
-1
-2
-3
0 1 2 3
4
5
6
7
8
-20
-18
-16
-14
-12
-10
-8
Log fO2

Fig. 4.8.

Isotope Fractionation Between Vapour and carbon.

Lines of equal $1000\ln\alpha_{v\text{-}c}$ are shown as a function of temperature and fO_2. The fractionation factor at low fO_2 approximates to $1000\ln\alpha_{CH4\text{-}c}$ and at high fO_2 to $1000\ln\alpha_{CO2\text{-}c}$. There is a transition between the two zones where the fractionation factor changes from one extreme to the other (Deines, 1980) and this corresponds to the minimum carbon content of the vapour, where diamond is most stable. The change in fractionation factor is such that at high oxygen fugacity where CO_2 is the dominant carbon-bearing species fractionation between diamond and vapour will mean the isotopic composition of diamond is $4\ ^{o}/_{oo}$ lighter.

If volatile reservoirs are relatively limited in extent then removal of carbon as diamond or graphite alters the bulk isotopic composition of the remaining vapour. Deines (1980) has predicted the sampling frequency of $\delta\ ^{13}C$ values for the two probable diamond forming reactions (1 and 2) for a mean vapour with a $\delta\ ^{13}C$ value of -5 $^{o}/_{oo}$. In reaction 1, which precipitates carbon by CO_2 reduction, the initial fractionation factors are close to $\Delta_{CO2\text{-}c}$, which has a value of 4. In consequence the diamond that is precipitated would have a $\delta\ ^{13}C$ value of -9 $^{o}/_{oo}$ if the mean vapour composition was -5 $^{o}/_{oo}$. If only a small volume of the carbon present in the limited reservoir is precipitated then the $\delta\ ^{13}C$ values will still be normally distributed around a mode close to -9 $^{o}/_{oo}$. When large amounts of carbon are precipitated from limited reservoirs the $\delta\ ^{13}C$ values become positively skewed because the reservoir becomes more ^{13}C enriched as carbon is precipitated.

For reaction 2, which is a CH_4 oxidation reaction, the initial fractionation factors are close to $\Delta_{CH4\text{-}c}$ (to -1) and $\delta\ ^{13}C$ values of precipitating carbon will be close to -4. The mode of the $\delta\ ^{13}C$ values will also be close to -4 $^{o}/_{oo}$. If there is a large amount of carbon precipitated from a limited reservoir then the reservoir becomes depleted in ^{13}C and the $\delta\ ^{13}C$ values become skewed towards lighter values.

If there is open system behaviour (Cole & Ohmoto, 1986), so that effectively the reservoir is infinite in extent, then the diamond carbon isotopic compositions for both cases outlined will show a normal distribution.

The distribution of $\delta\ ^{13}C$ values for Bultfontein peridotite paragenesis diamonds shows that there is a mode close to -5 $^{o}/_{oo}$ and the values are skewed towards heavier compositions. There are three possible explanations for this. The first is that diamond was precipitated from separate reservoirs, each of which had its own isotopic composition that was normally distributed about a mode. For this to occur each reservoir needs to be infinite in size, and this is unlikely in view of

the total carbon in the mantle. The second possibility is that diamond was precipitated by CO_2 reduction. As outlined earlier, in this situation the fractionation factors would be close to 4 and in order to produce a mode of $\delta\ ^{13}C$ values close to -5 $^{o}/_{oo}$ the CO_2 -bearing vapour would have a $\delta\ ^{13}C$ value of -1 $^{o}/_{oo}$.

The third possibility is that the carbon was precipitated by CH_4 oxidation and that the fractionation of carbon isotopes changed continually with changing redox conditions. For diamond precipitation by such a continually re-equilibrating vapour there are two possible cases. For CO_2 reduction the initial fractionation factors being close to 4 require that the first diamonds precipitated from a mean carbon vapour of -5 to have a value close to -9 $^{o}/_{oo}$. With continued precipitation, and therefore change in oxygen fugacity the fractionation factors decrease and diamonds with a $\delta\ ^{13}C$ close to -5 will be formed. In this case the distribution of $\delta\ ^{13}C$ would have a mode close to the mean of the vapour (-5$^{o}/_{oo}$), data would be skewed to lighter values. If the precipitation is by CH_4 oxidation then the skewness will be towards heavier values, with a mode at -5$^{o}/_{oo}$. The effects due to CH_4 oxidation cannot explain the magnitude of the skewness seen in Bultfontein diamonds.

The third possibility with carbon precipiated by CH_4 oxidation is favoured above the other two alternatives for the following reasons. Because the isotopic compositions of peridotite paragenesis diamonds from Bultfontein, Roberts Victor and Premier all suggest a single origin with a mean composition close to -5 $^{o}/_{oo}$ a series of infinite reservoirs of different compositions is therefore unlikely. The precipitation of carbon by CO_2 reduction is also unlikely because any CO_2 present in the mantle may occur as carbonate (CO_3^{2-}) in carbonatite melts (Green & Wallace, 1986), rather than CO_2 vapour. In addition to produce the distributions seen at Bultfontein by CO_2 reduction reactions the mean $\delta\ ^{13}C$ for the mantle must have a value close to zero which contradicts the evidence from

In spite of this lack of correlation between the predicted carbon isotopic compositions and the observed data, CH_4 oxidation is probably the best way of explaining the $\delta\ ^{13}C$ values of Bultfontein diamonds. It is possible that the large skewness results from $\Delta_{CH4\text{-}c}$ values that are greater than predicted.

At other dominantly peridotitic mines such as Finsch, the distribution of carbon isotopes is also skewed towards heavier isotope values and again implies precipitation of carbon by a continually equilibrating diamond precipitated by CH_4 oxidation. Although the source reservoir at Finsch is isotopically distinct from that at Bultfontein the reservoir at Finsch may have undergone some initial fractionation leaving a residue of slightly different isotopic composition.

At Roberts Victor mine the distribution of carbon isotopes in peridotite paragenesis diamonds is normal and this implies carbon precipitation from an infinite reservoir with no fractionation effects or during the initial stages of precipitation during CH_4 oxidation reactions ($\Delta_{v\text{-}c} \sim 0$ to 1).

Sulphide and eclogite suite diamonds from Bultfontein have a normal distribution of $\delta\ ^{13}C$ values about -5.25 $^{o}/_{oo}$, which also favours equilibrium precipitation of carbon but this time from an infinite mantle reservoir or by CH_4 oxidation such as was shown in reaction 3 from a reservoir in which a small amount of carbon was precipitated. The nickel content of the sulphide inclusions suggests that the sulphides have a peridotite origin, even though the nitrogen and carbon isotope data suggests a separate origin for peridotite suite diamonds and sulphide-bearing diamonds. At Premier, the $\delta\ ^{13}C$ values for eclogite paragenesis diamonds are skewed towards lighter isotopic compositions and at this mine it is concluded that some diamond precipitation was by CH_4 oxidation. Alternatively with continued equilibrium it is possible that some of the diamond was precipitated by CO_2 reduction. The interaction of CO_2 with sulphide could precipitate diamond through the following reaction (Haggerty, 1986):

$$2FeS + CO_2 = 2FeO + S_2 + C$$

Haggerty (1986) has suggested that eclogite- and sulphide-bearing diamonds may form under different redox conditions than peridotite-bearing diamonds.

4.4 Studies on larger diamonds.

Inclusion-bearing diamonds only represent a small fraction of the total diamond population at any locality. From the data for inclusion-bearing diamonds shown above it is apparent that there are changes in the nitrogen and carbon characteristics which can be related to diamond growth. It is important to note that the large diamonds do not contain any diagnostic inclusions and so the nitrogen and carbon data cannot be compared with the earlier work. Studies of larger diamonds have been made to determine how the environment of diamond formation changed during diamond growth and also to investigate the relationship between inclusion-bearing diamonds and the total diamond production. Up to now, equilibrium crystallisation with isotopic equilibrium has been considered. Studies of the larger diamonds will show that there is a clear disequilibrium growth for many diamonds.

30 diamonds ranging in size from -9 + 7 to -21 + 19 (weight range 0.10 to 1.55 m.c.) were polished parallel to the {001} direction for cathodoluminescence study and of these 11 were made into thin polished plates to enable detailed infra red studies.

4.4.1 Cathodoluminescence Patterns.

Cathodoluminescence is the luminescence emitted within a short time of the diamond being excited by a stream of electrons. In diamond the cathodoluminescence can result from crystal defects, such as nitrogen impurities, or radiation damage centres.

Cathodoluminescence shows the growth history of diamond through minor changes in colour and intensity of luminescence and changes in crystallographic orientation of growth increments (see figure 4.9 for example).

Most natural diamonds luminesce blue. Different colours of luminescence result from the presence of defects. The nitrogen aggregation centre N3 (a triangular arrangement of three nitrogens) has a cathodoluminescence band at 2.985*e*V with an accompanying zero phonon line at 415nm (blue). Platelet defects and radiation damage centres are a cause of green luminescence. Zones of non luminescence are believed to indicate an absence of nitrogen.

The blue luminescence of diamond is attributed to the spacing of acceptor and donor centres in diamond (Davies, 1979). Boron is the only recognised acceptor in diamond and in Type IIb diamond concentrations (30ppm) allow P-type semiconductor behaviour. In Type Ia diamond the acceptor-donor pair acts as an N-type semiconductor, although with high activation energies (Collins & Lightowlers, 1979).

The spacing of acceptor and donor pairs strongly affects the cathodoluminescence behaviour of the diamond and is related to thermal equilibrium. Where growth is rapid, donor-acceptor separation is large and luminescence has phonons of low energy (wavelengths close to the green and red end of the optical spectrum). During equilibrium growth, the spacing of the pairs is closer and the luminescence is of a higher energy (i.e. blue wavelengths). The relatively rapid growth of synthetic diamonds for example is probably the principle cause of their green luminescence.

Individual growth bands within diamonds record a crystal stratigraphy. There are two principle growth forms in most diamonds. The {111} faces result from faceted octahedral growth and are termed normal growth (Lang, 1979). "Cuboid" or {100} surfaces are non faceted, with a hummocky appearance. These surfaces may result from the dissolution of diamonds along cube (100) directions to form rounded surfaces. An alternative explanation is

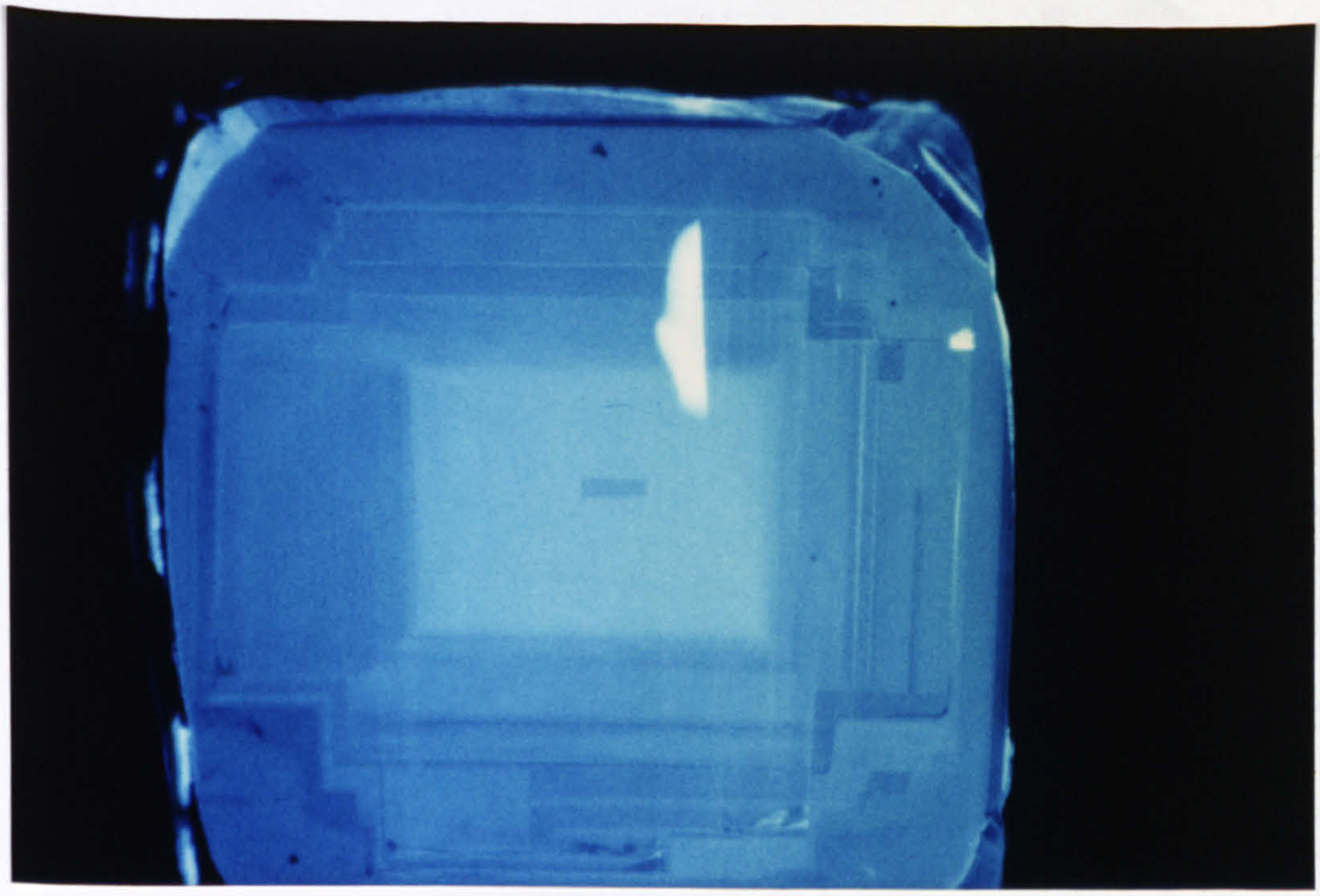

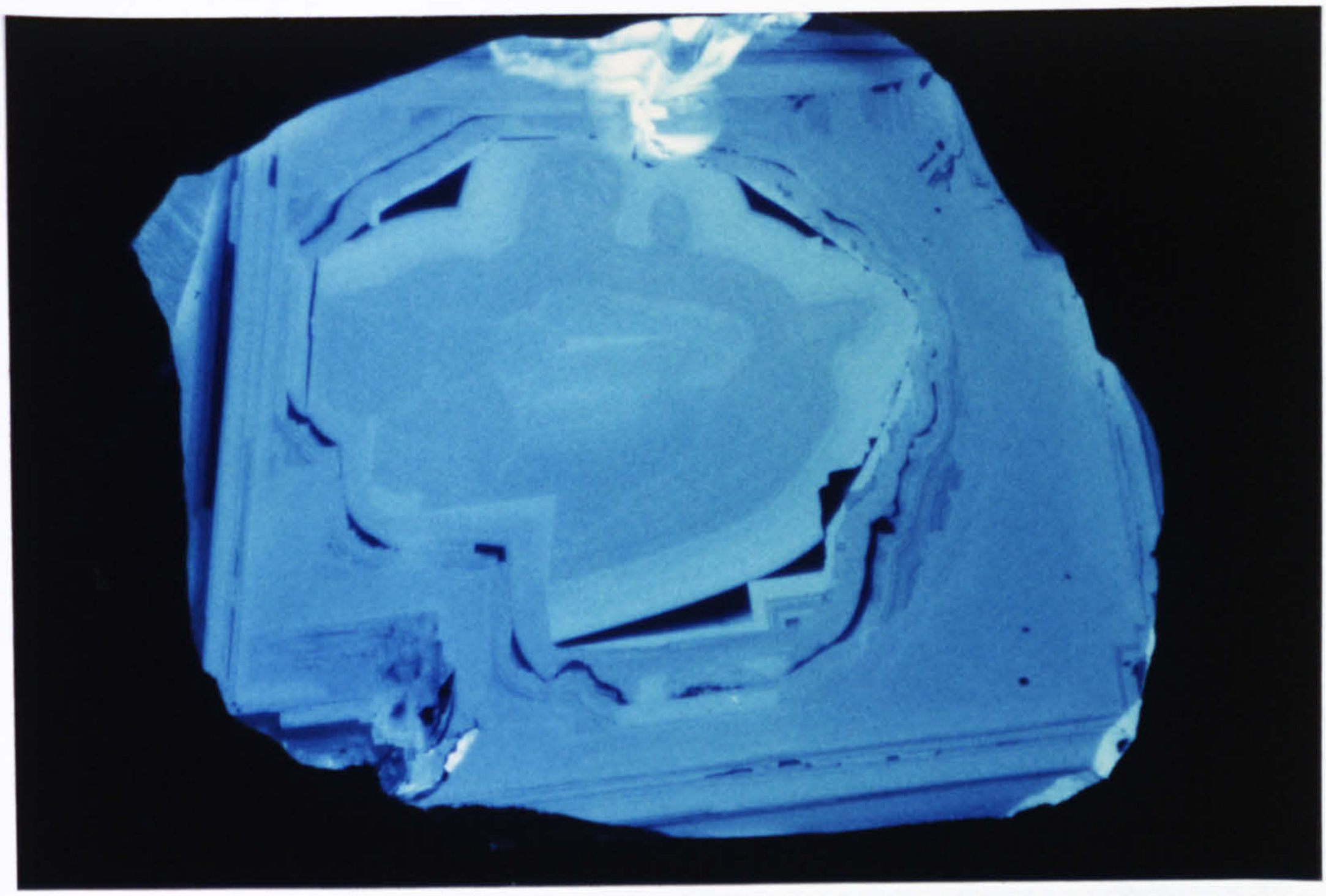

Fig. 4.9.

Cathodoluminescence Image of Diamond 1063.1.

This diamond shows a central zone of green luminescence and cuboid growth. The surfaces of the central zone are hummocky and are bounded by zones of non luminescence. The rim of the diamond shows octahedral growth and blue luminescence. The diamond is 4mm across.

Fig. 4.10.

Cathodoluminescence Image of diamond 1064.5.

The core of this diamond luminesces green, but shows octahedral growth. The blue luminescing rim of the diamond shows a cruciform growth pattern which results from etching along (100) directions.this diamond is 3.2mm across.

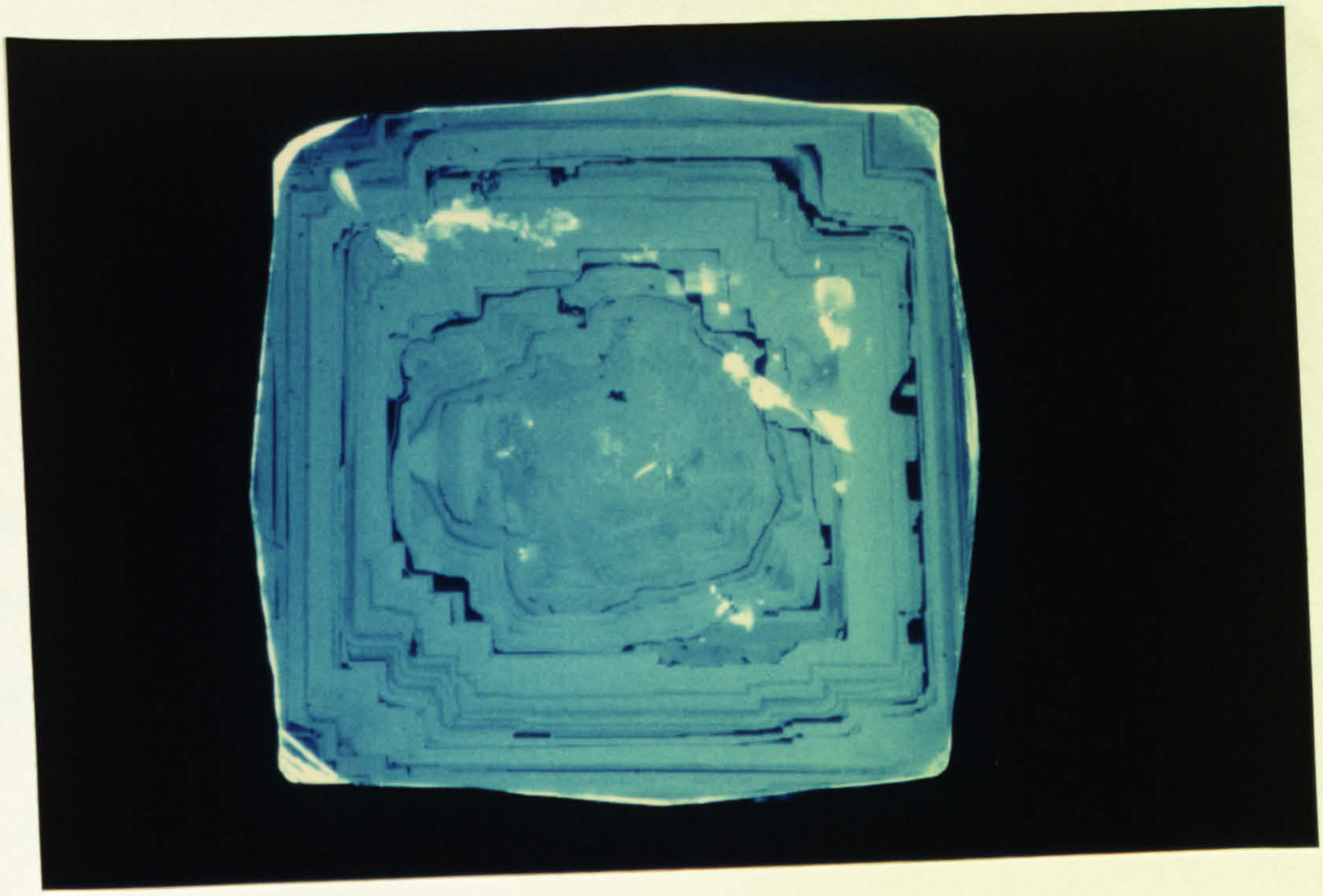

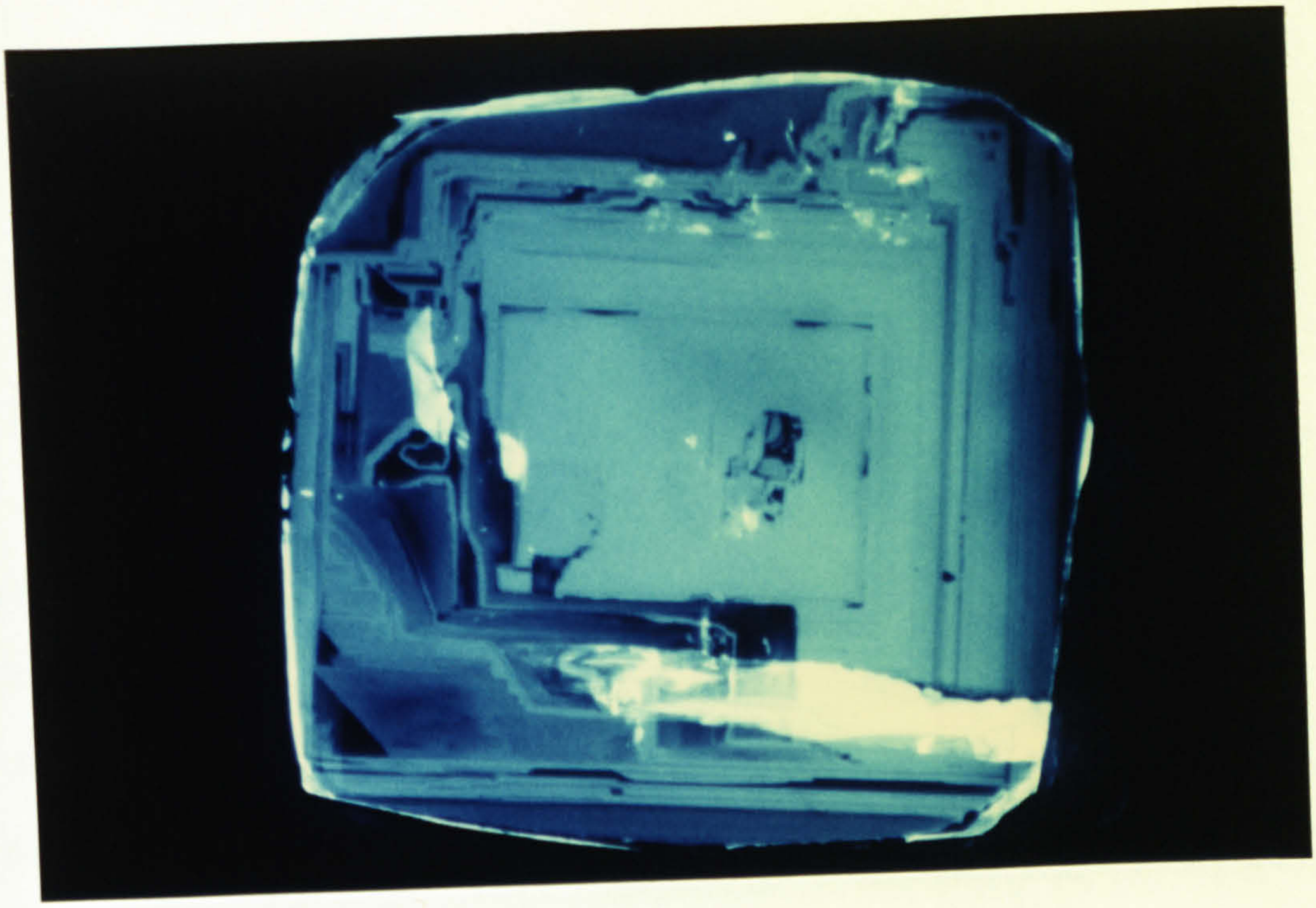

Fig. 4.11.

Cathodoluminescence Image of Diamond 1063.2.

This diamond shows faceted octahedral growth and blue-green luminescence. One part of the diamond is etched along (100) and shows further growth in the form of hummocky cuboid surfaces with blue luminescence. A zone of non luminescence separates the two growth phases. The diamond is 3mm across.

Fig. 4.12.

Cathodoluminescence Pattern of Diamond 1061.2.

There are three phases of growth in this diamond each phase shows cuboid growth and blue luminescence. Each growth zone is separated by a zone of non luminescence. The diamond is 4mm across.

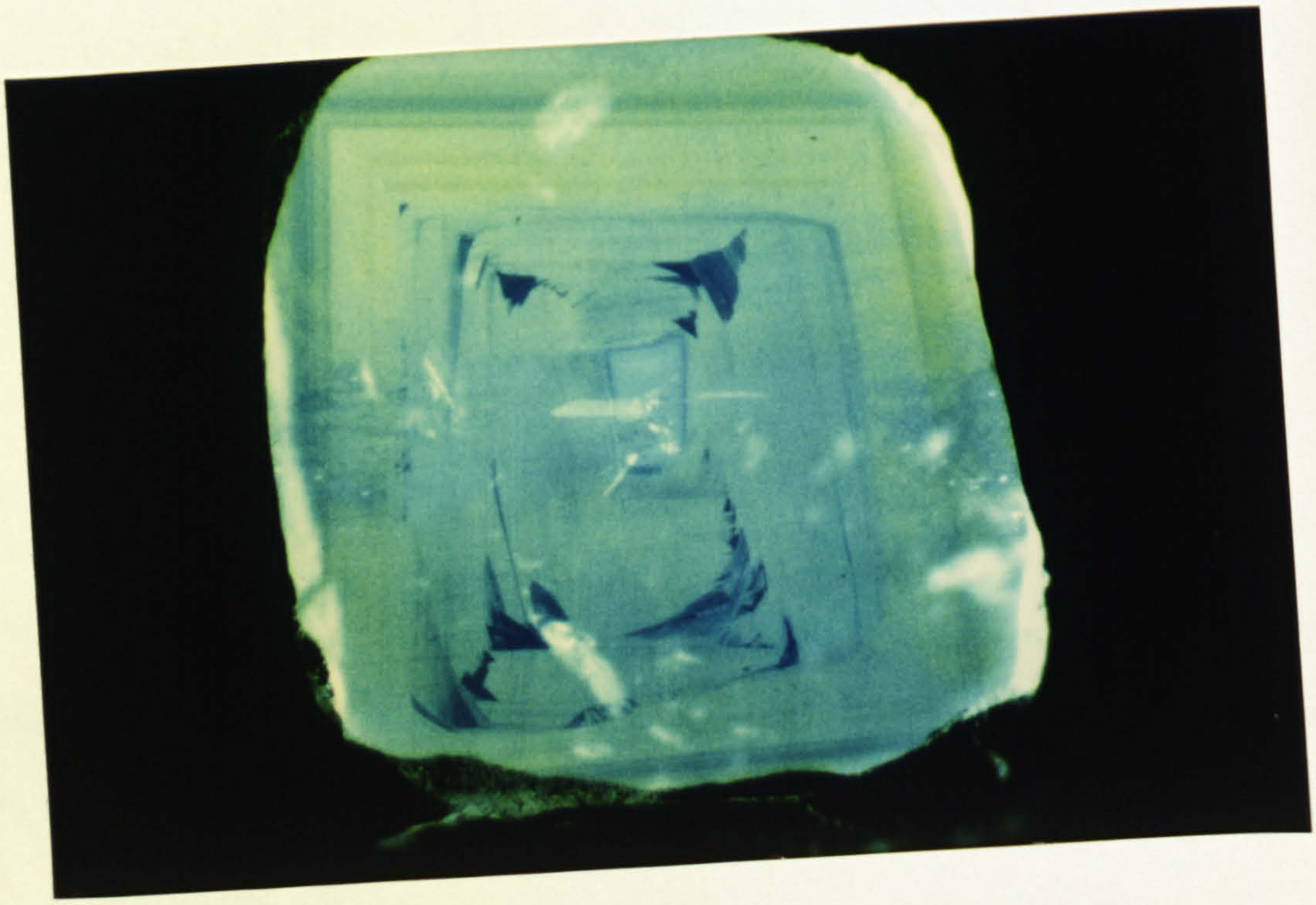

Fig 4.13.

Cathodoluminescence of Diamond 1063.9.

This diamond, which is 3.2mm across, is dominated by octahedral growth and shows green luminescence. The diamond core luminesces blue. Cuboid etching is followed by overgrowths which have a deep blue luminescence.

that individual growth increments do not completely cover the previous diamond surfaces and, as a result, a rounded surface is formed. Where the diamond has been dissolved, the previous growth increments are usually truncated.

The cathodoluminescence patterns of the large diamonds from Bultfontein showed that 20 out of the 30 diamonds had octahedral growth and dominantly blue luminescence. Individual diamonds showed variation in colour from a blue to green and in the intensity of luminescence. The width of growth increments varied from 5 to 50μm.

The remaining 10 diamonds showed a more complicated luminescence pattern, with distinct cuboid zones. A noticeable change in the colour of luminescence occurs across some diamonds, giving rise to green cores and blue rims as shown in figures 4.9 and 4.10. Also different sets of growth zones are often separated by zones of non luminescence and examples of these are seen in figures 4.11 and 4.12. In one case (see figure 4.13) the luminescence is reversed, the outer growth is green and the octahedral sectors in the core deposited on cuboid surfaces are blue.

The dissolution of diamond which occurs in cuboid cores may be in response to minor fluctuations in redox conditions which cause oxidation or reduction of carbon. Because only 10 out of 30 diamonds showed cuboid cores this may imply that most diamond growth occurred in a stable redox environment. A limited study of the cathodoluminescence of inclusion-bearing diamonds also shows sector growth and variations of colour and intensity similar to the larger diamonds. Although the inclusion-bearing diamonds are smaller than the diamonds used for cathodoluminescence the growth patterns are similar especially in respect of the cuboid cores. This similarity would suggest that, although no paragenesis could be assigned to the large diamonds, they are probably peridotitic and also grew under conditions of fluctuating oxygen fugacity.

Those diamonds with cuboid growth may be evidence of an earlier but distinct growth environment in which different temperature and redox conditions gave rise to cuboid growth. Subsequently octahedral growth became important. On this basis one might speculate, if there was a time gap between cuboid and octahedral growth, that the octahedral diamonds formed later than those with cuboid cores.

For the 30 diamonds studied for cathodoluminescence individual luminescence wavebands as seen in the cathodoluminescence of the (100) surfaces were not determined. In consequence no data are available about the impurities which cause the luminescence pattern in each diamond.

4.4.2 Nitrogen Characteristics.

Infra red traverses across thin diamond plates of 11 out of the 30 diamonds were used to determine the nitrogen aggregation state. All the diamonds studied were Type Ia but there was a variation in the amounts of IaA, IaB and platelet nitrogen.

The nitrogen concentrations (up to 3000ppm) and A/B ratios were higher than those measured in inclusion-bearing diamonds and varied across the diamond plates. The changes in nitrogen are not regular and do not vary systematically with cathodoluminescence pattern. However the IaB content is always greater at the centre of the diamond. Figure 4.14 shows the variation in nitrogen concentration and the state of aggregation (as defined by the ratio A/B) across the diamond shown in figure 4.10. The correlation coefficient of the A/B ratio for this diamond has a value of 0.72 (a value of 1.0 would be expected if there was a perfect correlation). Although the concentration of nitrogen at the core of the diamond is apparently high the correlation coefficient for this diamond is 0.16, indicating poor correlation. The A/B ratio shows an increase towards the rim of the diamond, where most nitrogen is aggregated in the IaA aggregate.

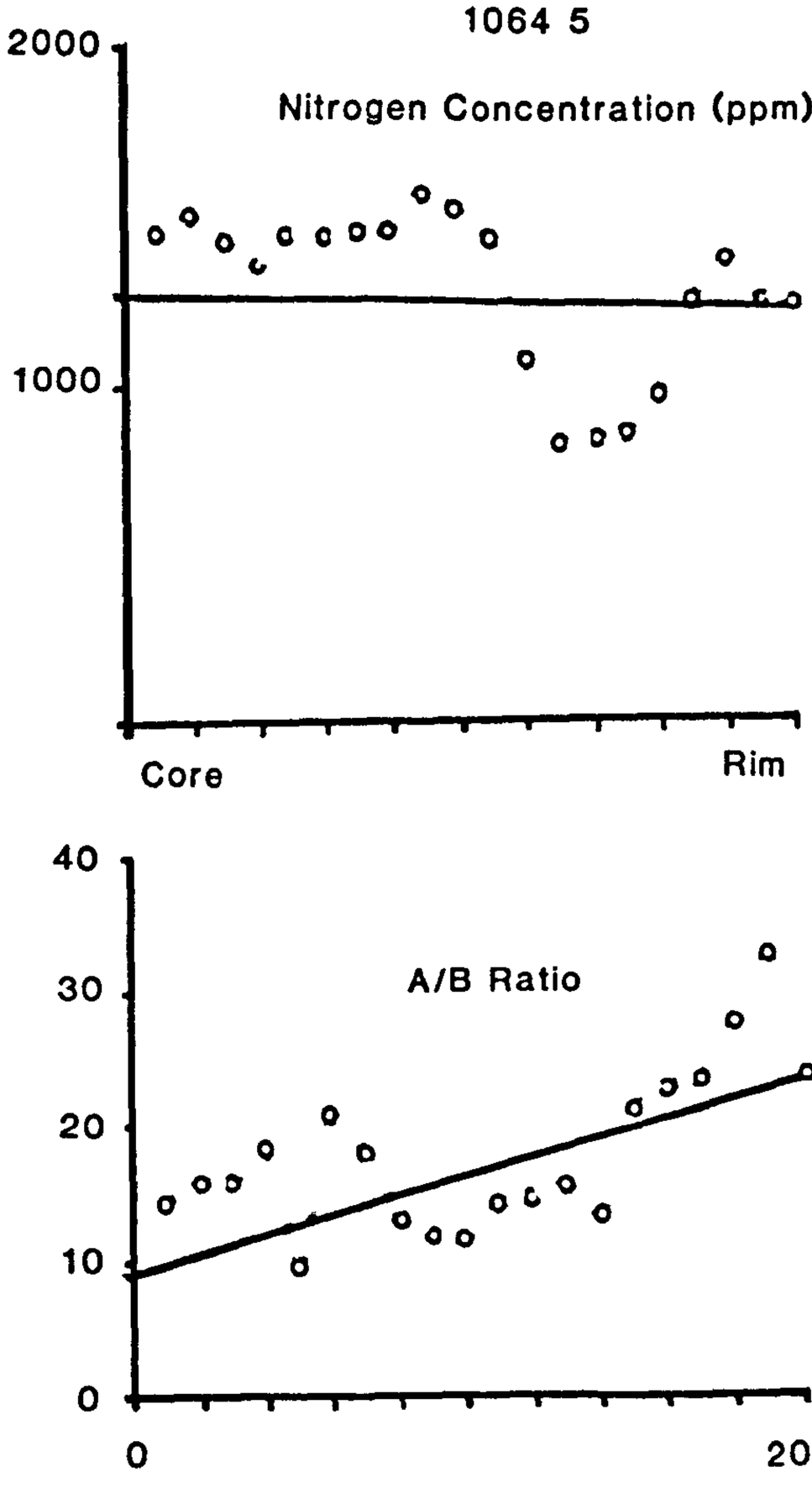
1064 5
Nitrogen Concentration (ppm)
2000
1000
Core
Rim
A/B Ratio
40
30
20
10
0
0
2000

Fig 4.14.

Nitrogen Characteristics in Diamond 1064.5.

The nitrogen concentration of this diamond is shown to be constant by a least squares fit. The A/B ratio shows an increase towards the rim of the diamond. This correlates with a high IaA content in the blue luminescent zone.The length of traverse is 2000μm.

1061 2

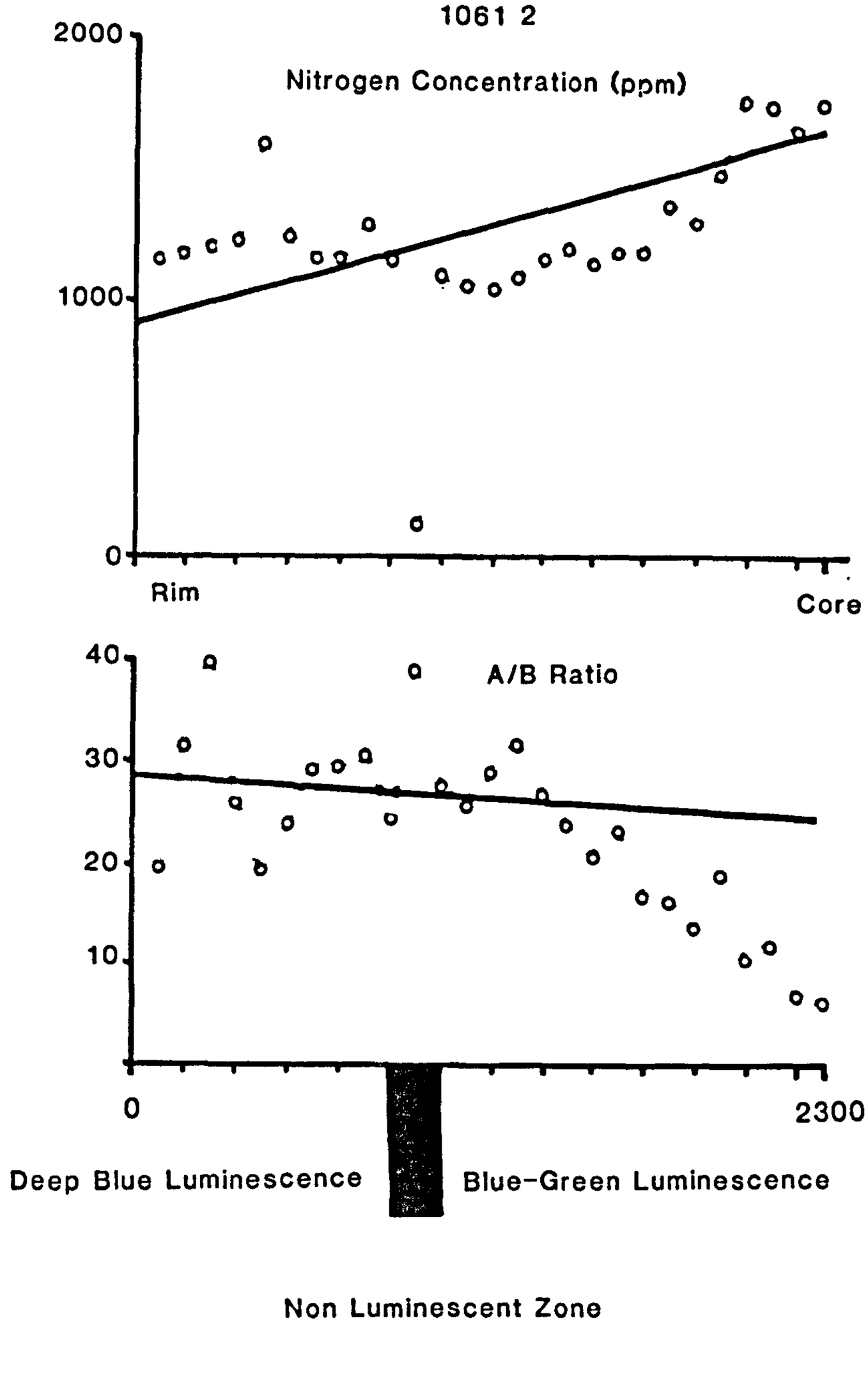
Nitrogen Concentration (ppm)
2000
1000
0
Rim
Core
A/B Ratio
40
30
20
10
0
2300
Deep Blue Luminescence
Blue-Green Luminescence
Non Luminescent Zone

Fig 4.15.

Nitrogen Characteristics of Diamond 1061.2.

The nitrogen concentration in this diamond is shown by a least squares fit to be highest at the diamond core. A low value of nitrogen occurs in a zone of non luminescence. The least squares fit to the A/B ratio shows a constant value with a slight decrease in the diamond core, indicating more IaB.The length of traverse is 2300μm.

Figure 4.15 is a traverse of the diamond shown in figure 4.12 the correlation coefficient for the A/B ratio for this diamond is 0.99 indicating a close correlation of A/B ratio with distance across a diamond. The correlation coefficeint for the total nitrogen content with distance is 0.59 and shows that there a variation in the A/B ratio and also in the absolute nitrogen concentration. The nitrogen concentration is lowest in a zone of non luminescence.

Calculations from Evans and Qi show that for the diamond in figure 4.14 at 1000^{o}C a period of 3.6 x 10^{12} years would be required to aggregate the nitrogen at the core with a A/B ratio of 20, while at the edge of the diamond the period is 8.3 x 10^{11} years. At 1200^{o}C these differences are 2.9 x 10^{8} and 6.8 x 10^{7} years respectively and implies a period of diamond growth of at least 200ma.

4.4.3 Carbon Isotope Variation of a Single Diamond.

Carbon isotope differences between the cores and opaque coats of diamond have been reported by Swart *et al.*(1983) and Boyd *et al.* (1987). Differences in the $\delta\ ^{13}C$ values across Type II diamonds have been determined by Milledge *et al.*, (1983) and differences in $\delta\ ^{13}C$ in different growth sectors in synthetic stones are also known (Milledge *et al.*, 1987).

It has been argued in section 4.3 that the carbon isotope data for the Bultfontein inclusion-bearing diamonds were derived from a limited carbon reservoir, with carbon isotope fractionation processes controlling the $\delta\ ^{13}C$ values. A study of the carbon isotope variation across a single diamond crystal might allow this hypothesis to be further assessed.

The cathodoluminescence of the diamond studied shows a cyclic pattern of several blue zones of cuboid growth overlain by octahedral zones of green luminescence, as can be seen from figure 4.16. The diamond was 4.0 x 3.5mm in size and a (100) section was polished to produce a thin plate of 4.0 x 2.5mm.

Unfortunately this diamond contained no diagnostic inclusions, so there is a possibility that the stone is eclogitic.

The $^{12}C/^{13}C$ ratio was determined by ion microprobe using a Cs^+ ion source, outlined in Chapter 2. Precision of each analysis was 1σ 0.5 ‰ and results are believed to be accurate to within 1 ‰. The isotope ratio at each point was determined by 100 measurements at the ^{13}C and ^{12}C peaks counting for 5 seconds and 1 second respectively. Each analysis comprised 10 blocks of 10 ^{13}C and ^{12}C measurements.

To standardise the ion probe measurements, a homogeneous synthetic diamond was used (6.0 x 3.0mm). 52 measurements were taken and a piece of this diamond was analysed using the conventional method for isotope analysis (see Chapter 2). The isotope ratios for the Bultfontein diamond were then expressed as δ values relative to PDB, shown in Table 4.6.

Carbon isotope values range from δ ^{13}C of -5.7 to -10.9 ‰ vs PDB. This range is greater than any analytical error and furthermore the variation in carbon isotope composition corresponds with cathodoluminescence zones shown in figures 4.16 and 4.17. At the centre of the diamond values are initially -6.5 ‰ and there is then a gradual decrease with each luminescence zone until a minimum value is reached, close to -10 ‰. There is then an abrupt change to values between -6 to -7 ‰ on the rim of the diamond.

To explain these variations in terms of fluctuating oxygen fugacity solely using the CH_4 oxidation model from a limited reservoir is difficult. Changes in isotope ratio of the order of -4 to -5 ‰ correspond to a fractionation factor of 4, assuming an initial upper mantle vapour composition of -5 ‰. From figure 4.8 an increase in the oxygen fugacity of 1 to 2 log units will change the fractionation factor from 0 to 4 and will cause a -4 ‰ depletion of the precipitated diamond. The range of values from the single diamond that was studied suggests that precipitation of carbon from a limited reservoir of δ ^{13}C = -5 ‰ was followed by diamond precipitation by increasing oxygen fugacity

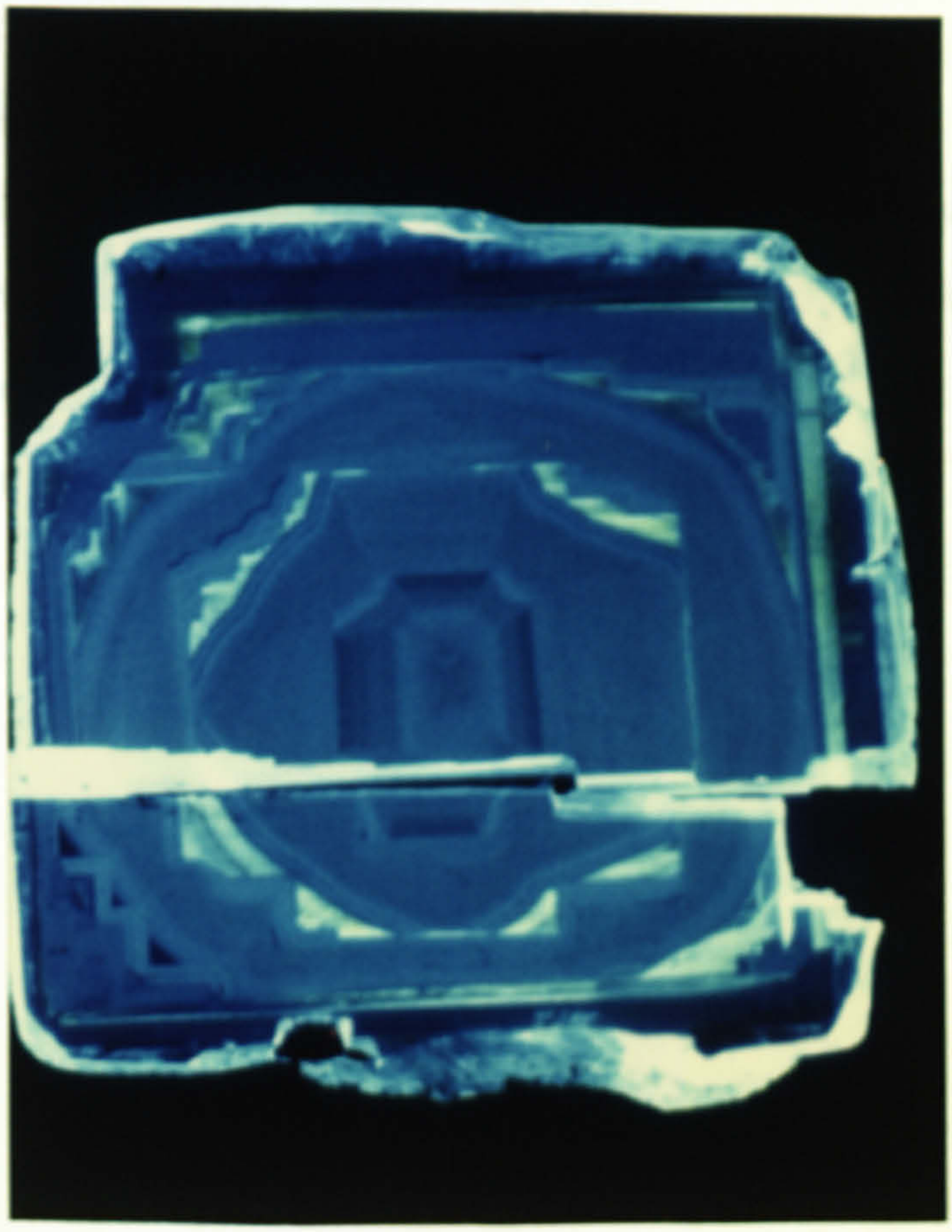

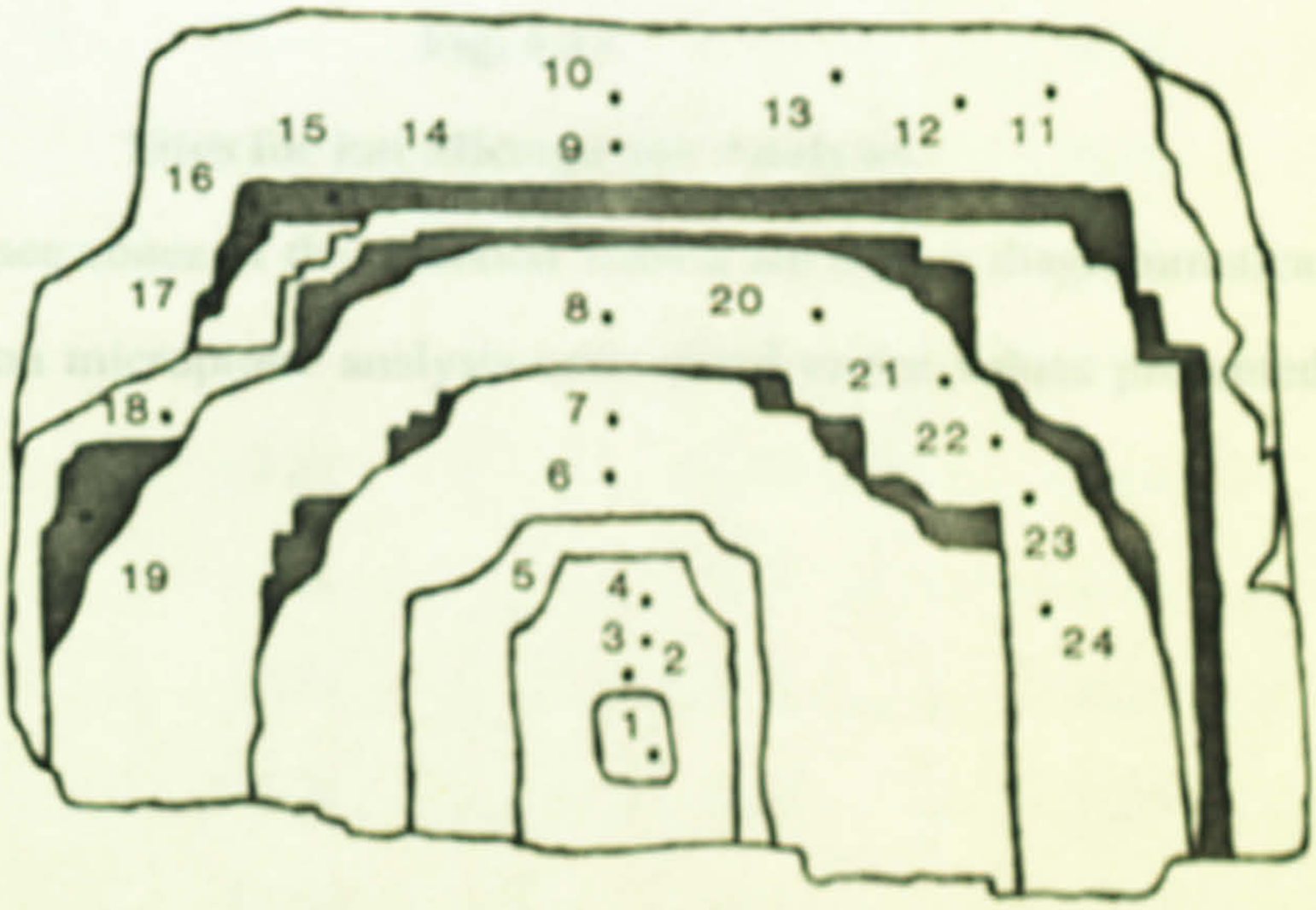

Cathodoluminescence Zones for Diamond 1064 2.

Fig. 4.16.

Cathodoluminescence Pattern for Diamond 1064.2.

This diamond is unique in that it shows cyclic growth. there are four zones of blue luminescence which show hummocky cuboid growth. each growth phase is separated by a zone of octahedral growth which luminesces bright green. The diamond is a thin plate 4.0mm x 2.5mm in size.

Fig. 4.17.

Sites for ion Microprobe Analysis.

The luminescence zones of the diamond 1064.2 are shown diagrammatically. The sites for ion microprobe analysis correspond to the values presented in Table 4.6.

Table 4.6

Analysis	$\delta\,^{13}C_{STD}$	$\delta\,^{13}C_{PDB}$	2σ	X_{std}
1	18.76	-6.45	0.16	0.2
2	16.89	-8.32	0.16	1.0
3	17.00	-8.21	0.18	0.8
4	16.34	-8.87	0.20	0.5
5	19.42	-5.79	0.18	0.9
6	15.03	-10.17	0.18	0.5
7	15.69	-9.03	0.18	0.5
8	14.49	-10.72	0.18	0.5
9	18.87	-6.34	0.24	0.1
10	18.54	-7.28	0.40	0.7
11	18.91	-6.29	0.80	0.8
12	19.02	-6.19	0.20	0.1
13	18.36	-6.84	0.12	0.7
14	17.16	-8.05	0.20	0.1
15	16.17	-9.04	0.20	0.3
16	18.03	-7.18	0.18	0.3
17	18.14	-7.08	0.22	0.3
18	15.74	-9.47	0.22	0.7
19	16.28	-8.93	0.20	0.4
20	14.86	-10.35	0.14	0.4
22	14.31	-10.87	0.12	0.6
23	14.75	-10.46	0.12	0.7
24	14.86	-10.35	0.14	0.4

involving CO_2 thereby producing $\delta\ ^{13}C$ values of -10 $^{o}/_{oo}$. Although the isotope variations favour a change in Δ from $\Delta_{CH4\text{-}c}$ to $\Delta_{CO2\text{-}c}$ during diamond growth it has been argued that CO_2 will not be present in the mantle as a free vapour phase because CO_2 may react to produce carbonates could in a solid or molten form. Also the fractionation effects between carbon and carbonate are probably small. However if the carbonate coexists with free CO_2 (i.e CO_2 was in excess) the fractionation effects attributed to CO_2 reduction reactions could take place. During the final stages of diamond growth the $\delta\ ^{13}C$ values become -6 $^{o}/_{oo}$, corresponding to a return to diamond precipitation by CH_4 reduction.

4.5 Growth conditions of Bultfontein diamonds.

The following conclusions are drawn from the nitrogen and carbon characteristics of the Bultfontein diamonds.

1. The nitrogen aggregation state of the Bultfontein diamonds changes with inclusion type. Two groupings of nitrogen characteristics are seen, one group of diamonds which contains olivine, orthopyroxene and peridotite paragenesis garnets has a relatively high IaB and platelet content. The other group also contains olivine, orthopyroxene and garnet bearing diamonds. In addition chromite-bearing diamonds and diamonds which contain peridotite paragenesis clinopyroxene occur in the second group. The rate of nitrogen aggregation depends on the temperature and the initial concentration of nitrogen. Diamonds with a high IaA and low platelet content have the highest nitrogen concentrations. The diamonds with the high IaB and platelet contents have the lowest nitrogen concentrations. The two groups of diamonds may have formed in a separate environments with different nitrogen contents.

2. Studies of the nitrogen variation across large diamonds show that the IaB content at the cores is greater than on the rims. The higher IaB content at the

centre of the diamond is interpreted as indicating a long period of diamond growth for diamonds which have a fixed nitrogen content.

3. Carbon isotope studies show a mean $\delta\ ^{13}C$ value of -4.66 $^{o}/_{oo}$. The Bultfontein diamonds are skewed towards heavier isotopic compositions. The $\delta\ ^{13}C$ values of each inclusion type vary such that olivine, orthopyroxene and chromite-bearing diamonds are all skewed towards heavier compositions. Chromite-bearing diamonds are the most ^{13}C enriched. Sulphide and eclogite suite diamonds have $\delta\ ^{13}C$ values of normal distribution. The $\delta\ ^{13}C$ data are interpreted as the results of isotope fractionations resulting from carbon precipitation from a C-O-H vapour with continued equilibrium of diamond and vapour. The skewness of peridotite suite diamonds towards heavier isotopic values results from the precipitation of carbon by CH_4 oxidation reactions. The eclogite and sulphide bearing diamonds are probably derived from the precipitation of a small volume of carbon from either a single limited reservoir or precipitation of a large volume of carbon from an infinite reservoir.

4. A single diamond crystal shows a maximum variation of $\delta\ ^{13}C$ across individual growth zones of 4 $^{o}/_{oo}$. The $\delta\ ^{13}C$ values correspond to fractionation effects that would be expected from an increase of oxygen fugacity of 1 to 2 log fO_2 units which would change the carbon bearing species present from CH_4 to CO_2. The diamond initially precipitated by CH_4 oxidation and then by CO_2 reduction as the oxygen fugacity increased. Because CO_2 is likely to form a carbonate in the mantle rather than exist as a free vapour phase this type of reaction may only occur if CO_2 was in excess after reaction to produce carbonate.

5. Cathodoluminescence patterns of larger diamonds show that most of the diamond growth was octahedral. Some of the diamonds had cuboid cores and may have grown under conditions of fluctuating oxygen fugacity. Inclusion bearing

diamonds also show complicated cathodoluminescence patterns that include cuboid surfaces. Nitrogen aggregation (IaB) and platelet contents of inclusion-bearing diamonds and the cuboid cores of the larger diamonds are similar. These results suggest that those diamonds with cuboid cores grew first and were then followed by a more dominant octahedral growth, these changes may have occurred in response to fluctuating temperature and oxygen fugacity.

Chapter 5.

Origin of Bultfontein diamonds.

5.1 Introduction.

In Chapters 3 and 4 the diamonds from Bultfontein were shown to have characteristics that distinguish them from other mines in the Kaapvaal Craton. This information will be used to place some constraints on diamond formation. The principle distinctive features of Bultfontein are: A dominantly peridotite inclusion suite in which chromites are more abundant than sulphides; The equilibrium temperatures suggest a formation of diamond below $1000^{o}C$; The nitrogen aggregation characteristics of the inclusion-bearing diamonds show a dominance of Type IaA nitrogen; The $\delta\ ^{13}C$ values for Bultfontein diamonds are skewed towards heavy values and these are interpreted as having precipitated by CH_4 oxidation reactions under conditions of fluctuating oxygen fugacity.

In addition the cathodoluminescence and detailed infra red studies of the Bultfontein diamonds show that diamond growth may have occurred over a long period of time. Cuboid cores and inclusion-bearing diamonds may have grown first under conditions of fluctuating redox conditions. Octahedral diamonds grew later in a more stable redox environment. The $\delta\ ^{13}C$ study of a single diamond crystal shows a variation in $\delta\ ^{13}C$ value across a diamond consistent with carbon precipitation from a C-O-H vapour.

5.2 Regional Inclusion Abundances.

Table 5.1 shows the inclusion abundances for six localities on the Kaapvaal Craton (data from Harris and Gurney, unpubl.). All of the localities show inclusions of both eclogite and peridotite paragenesis, although the relative abundance of each varies. Orapa and Premier show a high abundance of eclogite suite inclusions. The position of each locality on the craton is also shown in Table 5.1 with Monastery, Finsch, Orapa and Koffiefontein marginal to the craton (M),

Table 5.1

Inclusion Abundances for the Kaapvaal Craton.

Locality	1	2	3	4	5	6
Peridotite	56.2	29.3	38.7	10	88.4	18.3
Eclogite	1.1	1.7	27.5	69.4	4.8	20.6
Sulphides	40.1	62.1	33.5	20.0	6.2	61.1
Clouds	2.6	6.8	0.3	0.1	0.7	0.0
Position	M	M	C	M	C	M

Data From Harris & Gurney (unpubl.1989)

1 Finsch 2 Koffiefontein
3 Premier 4 Orapa
5 Bultfontein 6 Monastery

whereas Premier and Bultfontein are central (C). As can be seen from Table 5.1 the inclusion abundances do not vary systematically with position on the craton.

The distinctive features of the Bultfontein diamonds reflect the conditions of pressure, temperature and redox conditions of formation. Boyd and Gurney (1982) suggest that diamonds form in thickened parts of cratons where the temperatures of formation are sufficiently low to enable diamond to be stable. In such a "keel" the diamond stability curve will be domed upwards. Where the keel is thickest and the geothermal gradient is lowest, diamonds can form between depths equivalent to 120 and 180km. Towards the edges of the cratons, where the geothermal gradients are higher, diamond is stable at increasingly greater depths. The Bultfontein diamonds have low temperatures of origin consistent with an origin in the thickest part of the craton. However, the regional inclusion abundances do not reflect a depth of origin, although the occurrence of high pressure phases in mines such as Monastery and Jagersfontein supports a deep origin for diamonds on the edges of the craton.

5.3 Geochemistry of Peridotite Suite Diamonds.

The composition of peridotite suite diamonds and their relationship to mantle composition will first be discussed with particular reference to Bultfontein. Peridotite suite inclusions are very refractory because of their high chrome and magnesium contents. The mineralogy consists of olivine, orthopyroxene, sub calcic chrome-rich garnet and chromite. Clinopyroxene is rare. At Bultfontein the abundance of chromites is anomalously high.

The composition of peridotite suite garnet inclusions is similar to sub-calcic garnets from heavy mineral concentrates from kimberlites. Gurney (1984) has suggested that these two sets of minerals have the same origin, namely they are derived from a harzburgite layer that exists at the base of cratons (see also Boyd and Gurney, 1982). Subsequently Danchin and Boyd (1976), Dawson *et al.* (1978) and Nixon *et al.* (1987) suggest that such a harzburgite layer may result

whereas Premier and Bultfontein are central (C). As can be seen from Table 5.1 the inclusion abundances do not vary systematically with position on the craton.

The distinctive features of the Bultfontein diamonds reflect the conditions of pressure, temperature and redox conditions of formation. Boyd and Gurney (1982) suggest that diamonds form in thickened parts of cratons where the temperatures of formation are sufficiently low to enable diamond to be stable. In such a "keel" the diamond stability curve will be domed upwards. Where the keel is thickest and the geothermal gradient is lowest, diamonds can form between depths equivalent to 120 and 180km. Towards the edges of the cratons, where the geothermal gradients are higher, diamond is stable at increasingly greater depths. The Bultfontein diamonds have low temperatures of origin consistent with an origin in the thickest part of the craton. However, the regional inclusion abundances do not reflect a depth of origin, although the occurrence of high pressure phases in mines such as Monastery and Jagersfontein supports a deep origin for diamonds on the edges of the craton.

5.3 The Geochemistry of Peridotite Suite Diamonds.

The composition of peridotite suite diamonds and their relationship to mantle composition will first be discussed with particular reference to Bultfontein. Peridotite suite inclusions are very refractory because of their high chrome and magnesium contents. The mineralogy consists of olivine, orthopyroxene, sub calcic chrome-rich garnet and chromite. Clinopyroxene is rare. At Bultfontein the abundance of chromites is anomalously high.

The composition of peridotite suite garnet inclusions is similar to sub-calcic garnets from heavy mineral concentrates from kimberlites. Gurney (1984) has suggested that these two sets of minerals have the same origin, namely they are derived from a harzburgite layer that exists at the base of cratons (see also Boyd and Gurney, 1982). Subsequently Danchin and Boyd (1976), Dawson *et al.* (1978) and Nixon *et al.* (1987) suggest that such a harzburgite layer may result

from komatiite volcanism. Harzburgite nodules which consist of olivine, orthopyroxene and garnet, all of which have similar compositions to diamond inclusions, have been recorded at Premier, Liquabong (Lesotho) and, more recently at Jagersfontein. The inclusions at Bultfontein are consistent with an origin in a harzburgite layer that results from komatiite volcanism. Alternative suggestions for harzburgites of high magnesium and low calcium contents include an origin as serpentinised ocean crust (Schulze, 1984) and an origin as a cumulate in subducted crust (Ringwood,1977). The high magnesium content of olivines and orthopyroxenes is related to a komatiite origin in both these cases.

The high abundance of chromite inclusions at Bultfontein is anomalous. The oxygen fugacity controls the amount of divalent (Cr^{2+}) and trivalent (Cr^{3+}) chrome available. The abundance of chromite at Bultfontein would imply a relatively high oxygen fugacity, since chromite consists of 2/3 trivalent chrome. For low oxygen fugacities divalent chrome would enter olivine and/or orthopyroxene. At Bultfontein, however, the amount of Cr^{2+} in olivines is similar to other mines on the Kaapvaal Craton, with the exception of Finsch mine where there is no detectable Cr^{2+} in olivines and the abundance of chromites is less than at Bultfontein. If the fO_2 conditions at Finsch were high chromite abundance (Cr^{3+}) would be greater.

Apart from chromites the major chrome bearing phase in Bultfontein diamonds is garnet, where chrome enters the garnet as knorringite.

As shown by Danckwerth and Newton (1978) in alumina spinels there is a univariant reaction which produces garnet and olivine:

$$MgAl_2O_4 + 2Mg_2Si_2O_6 = Mg_2SiO4 + Mg_3Al_2Si_3O_{12}$$

Spinel + Orthopyroxene = Olivine + Pyrope

This spinel to garnet transition has a shallow $\delta P/\delta T$ slope and is therefore a useful indicator of the pressure of origin for xenoliths. The spinel to garnet transition is believed to be between 80 and 50km depth, for temperatures of $1000^{o}C$.

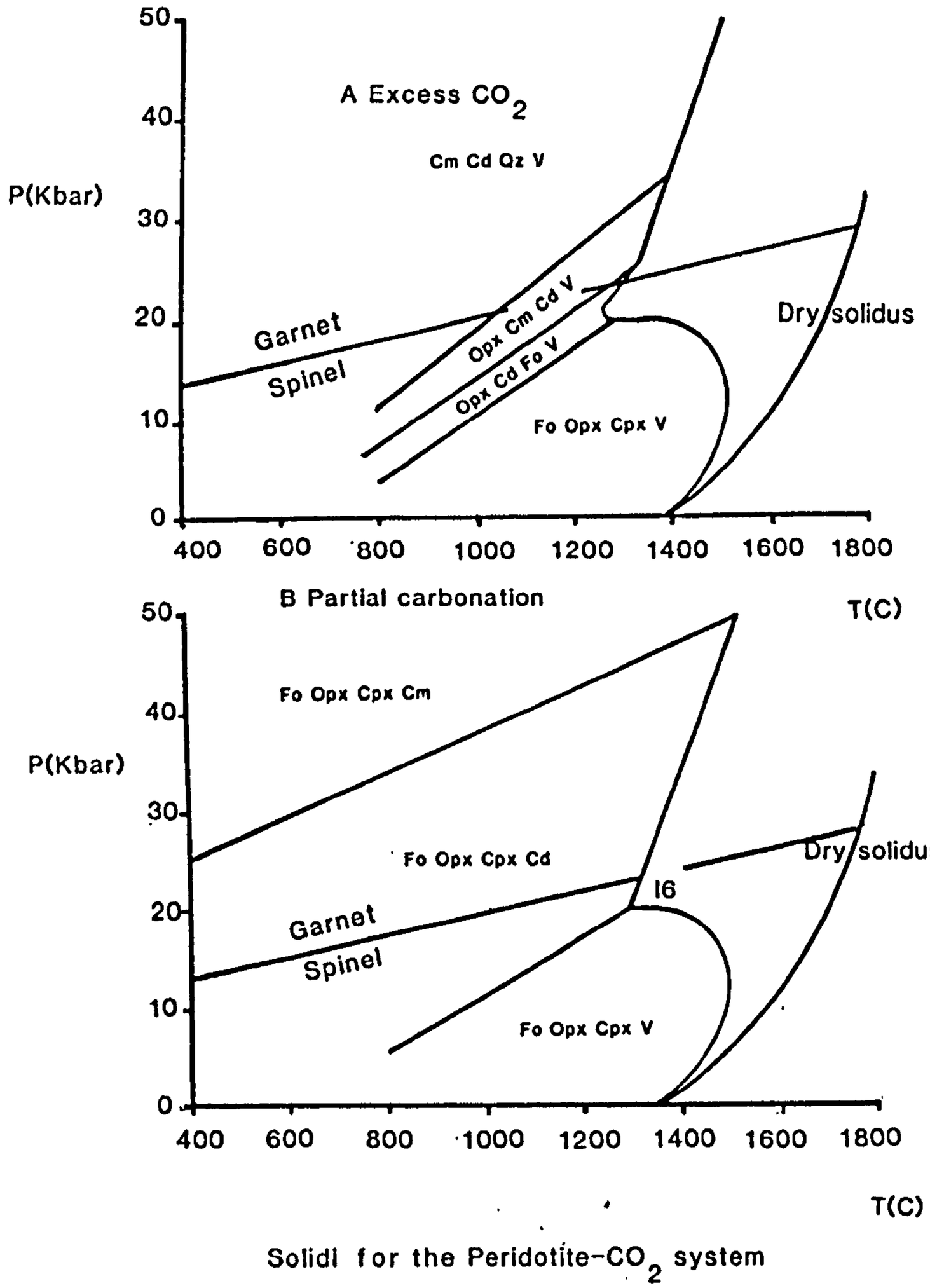

Solidl for the Peridotite-CO_2 system

Fig. 5.1.

Solidi for Carbonated Peridotite.

The effect of CO_2 on simple peridotite systems is shown. The phases present are forsterite (Fo), enstatite (Opx), diopside (Cpx) and quartz (Qz). CO2 can exsit as a vapour (V) or as carbonate. The carbonate is present as either dolomite (Cd) or magnesite (Cm). Also shown is the spinel-garnet transition of Danckwerth and Newton. In the first case (A), excess CO_2 causes carbonation of the mantle minerals at high pressure. Where there is insufficient CO_2 to cause complete carbonation of the mantle (B), carbonate exists with olivine and orthopyroxene. In both cases the solidus is reduced and has a minimum value at an invariant point, I6. I6 is the intersection of the solidus and the carbonate producing reaction which divides the mantle into a low pressure field where free CO_2 can exist and a high pressure field where carbonate can exist.

Danckwerth and Newton (1978) suggest that, assuming ideal solution, additional components such as FeO and Cr_2O_3 may increase the temperature of this transition. For chrome end members, therefore, an analogous reaction might be:

$$MgCr_2O_4 + 2Mg_2Si_2O_6 = Mg_2SiO_4 + Mg_3Cr_2Si_3O_{12}$$

Chromite + Orthopyroxene = Olivine + Knorringite

Such a reaction might explain the high abundance of chromites at Bultfontein. It is also notable that at Bultfontein the colourless inclusions show an abundance of orthopyroxene over olivine. The dual abundance of orthopyroxenes and chromites might be explained by the low pressure side of the reaction above. The garnets (knorringite) and olivines would indicate a higher pressure of origin, which in turn indicate that the Bultfontein diamonds may be derived from a range of depths of formation within the lithosphere.

Harte *et al.* (1980) in their study of peridotite suite inclusions explained the sub-calcic nature of the peridotite suite garnets in terms of CO_2-H_2O interactions with the mantle resulting from carbonation reactions. Wyllie (1977 and 1987), Wyllie and Huang (1975) and Eggler *et al.* (1976) have experimentally studied the processes of carbonation of the mantle by C-O-H vapour. They concluded that in model mantle systems excess CO_2 will form carbonate in the mantle at high pressure, and at low pressure free vapour CO_2 can exist with mantle minerals. These relationships are shown in figure 5.1a and 5.1b. The two fields of carbonate and free CO_2 are separated by the reaction:

$$Fo + Cpx + CO_2(V) = Opx + Cd_{ss}$$

This reaction (see figure 5.1a) intersects the solidus at an invariant point, termed I6. If there is less than 0.5wt.% CO2 present then the mantle is only partially carbonated and at high pressures the assemblage is that shown in figure 5.1b, and is:

$$Cpx + Ol + Opx + Cd_{ss}$$

The phase relationships show that with the addition of H_2O to the system the peridotite solidus is lowered. As a consequence the solidi may intersect geothermal gradients and melting of the mantle may occur. The lowest temperatures of melting occur when X_{H2O} is close to unity. Melting of the mantle and diamond might therefore be expected if H_2O bearing fluids are introduced into the mantle, with only a small amount of CO_2 present.

In the Harte *et al.* (1984) model melts that are produced would have a kimberlite composition. These authors point out however that the kimberlite melt which caused diamond formation is not necessarily the one which transported the diamonds to the surface, a conclusion borne out by the subsequent demonstration of the ages of diamond by Richardson *et al.* (1984).

Most models of mantle melting assume an initial lherzolite composition. Peridotite paragenesis inclusions are more Mg and Cr rich than the equivalent minerals in lherzolite and these minerals are of harzburgite composition. Harzburgite residues can be produced by the partial melting of lherzolite. McKenzie (1984, 1985 & 1987) points out that at mantle pressures the first formed melts will be mobile and that as soon as the degree of melting is high enough to produce interconnecting frameworks the melt (and any dissolved volatiles) will disappear. The harzburgite compositions of diamond inclusions could not, therefore, have been produced by a single melt of harzburgite. Subsequent melts would, however, produce a residue that becomes progressively more Mg and Cr enriched.

Sulphide inclusions are rare at Bultfontein, but the nickel contents show them to be of peridotite paragenesis. In Table 5.1 it can be seen that sulphides are more abundant at other peridotite dominant mines and that at these mines the temperatures of diamonds formation are higher. The abundance of sulphides is seen to increase such that at mines which show a high temperature of formation the sulphides are more abundant. This may relate to depth of origin, such that low

temperature low pressure environments have little sulphur or low sulphur/high oxygen fugacities that prevent sulphide formation.

5.4 Geochemistry of Eclogite Suite Inclusions.

Eclogite and sulphide suite inclusions have a low abundance at Bultfontein. Eclogite can be produced from garnet lherzolites (mantle compositions) by partial melts (e.g. O'Hara, 1967) and eclogite paragenesis diamonds may therefore originate as direct melts from undepleted mantle (Hatton and Gurney, 1987). An alternative explanation is that the eclogites represent subducted oceanic crust (e.g MacGregor, 1983). Jaques *et al.* (1989) for example have suggested that light $\delta\ ^{13}C$ values of eclogite suite diamonds represent organic carbon subducted with oceanic crust. The $\delta\ ^{13}C$ values at Bultfontein are similar to the isotopic compositions of peridotite suite diamonds and it is concluded that the eclogite suite diamonds at Bultfontein have a mantle origin, although nitrogen data suggests that the origin was separate to peridotite suite diamonds.

The nitrogen aggregation states for these diamonds suggests a low temperature of formation or formation later than the peridotite suite diamonds.

5.5 Oxygen fugacity conditions for Peridotite Paragenesis Diamonds.

The carbon isotope data for the Bultfontein diamonds is used to interpret the redox conditions of the upper mantle. Since carbon in the mantle can be present as elemental carbon, CO_2 , CH_4, CO and CO_3^{2-} the oxygen conditions are crucial for determining the carbon bearing gas species present.

There are two methods of investigating the redox conditions of the mantle. Electrochemical methods can be used (Ulmer *et al.*, 1976) where the electromotive force (e.m.f.) generated by a known buffer and the e.m.f. generated in the sample of interest are compared using electrolytes of ZrO_2 or Cr_2O_3 (Pehlke *et al.*, 1975).

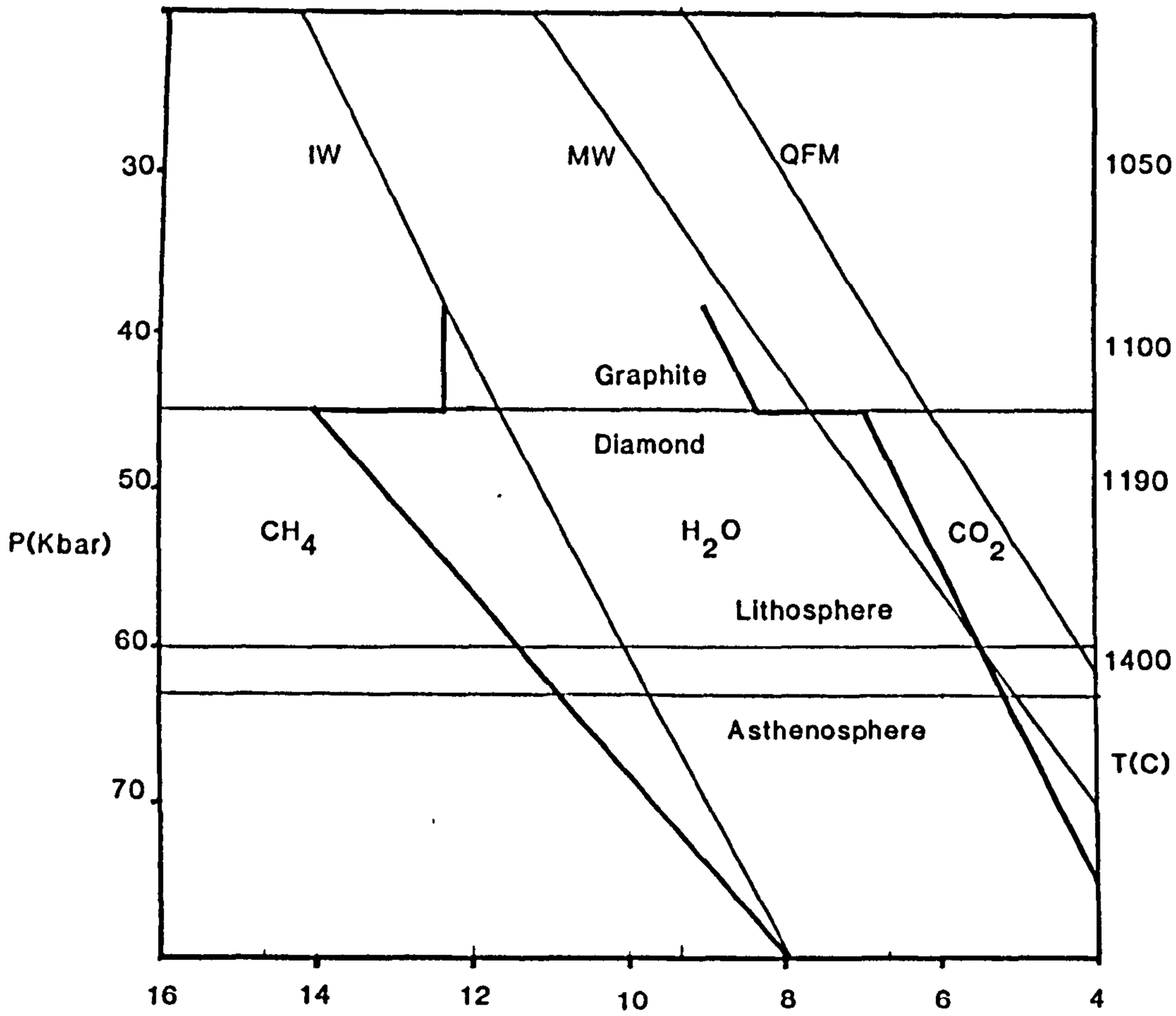

Gas Species as a Function of P, T and FO_2

Fig. 5.2.

Gas Species as a Function of P, T and fO_2.

Gas species in the lithosphere and the asthenosphere are shown as a function of fO_2. Diamond is stable over a wide range of fO_2 between the stable buffers of IW and QFM (see text), H_2O is also stable over this range (Haggerty, 1986).

example the exchange equilibria in the rocks between Ti and Fe, and Fe^{2+} and Fe^{3+} which define unique solutions of T^oC and fO_2 (Buddington & Lindsley, 1964).

Investigations of fO_2 are usually depicted in terms of synthetic buffers defined by equilibrium reactions. As shown in figure 5.2, the limits of most investigations into the upper mantle fO_2 values are the quartz-fayalite-magnetite buffer (QFM) representing total ferric to ferrous iron transition, the iron-wustite buffer (IW) which represents metal saturation and intermediate between these two the magnetite-wustite buffer (MW).

The studies of Mattioli and Wood (1986) on a group of mantle derived nodules show fO_2 values close to QFM ($\pm$ 1.5 $\log_{10}$ units) for ilmenite nodules, spinel-ilmenite intergrowths and megacrysts. For Cr rich nodules the values of fO_2 are much lower and are near to IW. Spinel-ilmenite pairs analysed by Haggerty and Tompkins (1983) demonstrate a range of values from close to MW to QFM. Peridotite nodules from alkali basalts (Haggerty and Tompkins, 1983) have more reduced fO_2 values close to the IW buffer. These relationships can be seen in figure 5.2.

Arculus and Delano (1980) showed by intrinsic measurement of the fO_2 values for spinels that some peridotite and megacryst fO_2 values are close to the IW buffer. In consequence Brett (1984) suggested that the mantle may be in equilibrium with the metal saturated core.

Intrinsic measurements of the fO_2 of MORB glasses by Christie *et al.* (1984) showed substantially more reduced fO_2 than the QFM value for MORB basalts, which these authors concluded represents oxidation by diffusive loss of H_2 due to proximity of the Earth's surface at ocean ridges. Just how representative of the mantle fO_2 the values for MORB basalts are is therefore doubtful.

The general range of oxygen fugacity values suggest that there may be a layering within the upper mantle in terms of redox conditions in addition to compositional layering. Haggerty and Tompkins (1983) suggest that depleted

The general range of oxygen fugacity values suggest that there may be a layering within the upper mantle in terms of redox conditions in addition to compositional layering. Haggerty and Tompkins (1983) suggest that depleted lithosphere is also reduced as a consequence of mantle degassing that accompanies the removal of basaltic components. These values of fO_2 are probably close to IW, consistent with the analyses of Cr rich nodules by Mattioli and Wood. Because the asthenosphere is considered to be "fertile", that is not depleted in basaltic components, Haggerty and Tompkins suggest that it is oxidised and has an fO_2 value close to QFM. The geochemical layering of the upper mantle probably varies laterally and the thickness of depleted reduced lithosphere ranges from a minimum at spreading centres to a maximum thickness beneath cratons (Haggerty and Tompkins, 1983).

Diamond is stable over a range of oxygen fugacity conditions (Haggerty, 1986) and can be precipitated either from CO_2 reduction or CH_4 oxidation, as shown in figure 5.2. In reduced areas of the mantle where CH_4 is the dominant carbon bearing phase a minor fO_2 increase could cause carbon precipitation by reactions 2 and 4 in chapter 4 (page 113). Where oxygen fugacity is higher and CO_2 is the main carbon bearing phase carbon precipitation is by CO_2 reduction (reactions 1 and 3, page 113). However free CO_2 will react with mantle minerals to form carbonates and CO_2 reduction reactions are unlikely to be important in diamond precipitation. Precipitation of carbon in both cases is by a change in redox conditions. Diamond formation can therefore occur where there is an interface between zones of contrasting oxygen fugacity, for example between oxidising fluids and reduced harzburgite.

Taylor and Green (1988) have determined the effect of C-O-H volatiles on the melting behaviour of pyrolite. Above continental geotherms and at low fO_2 melting will only occur if methane is eliminated from the volatile species by fO_2 increase since CH_4 bearing fluids have high solidi. Shi *et al.* (in prep) and Saxene and Fei (1988) have shown that through an

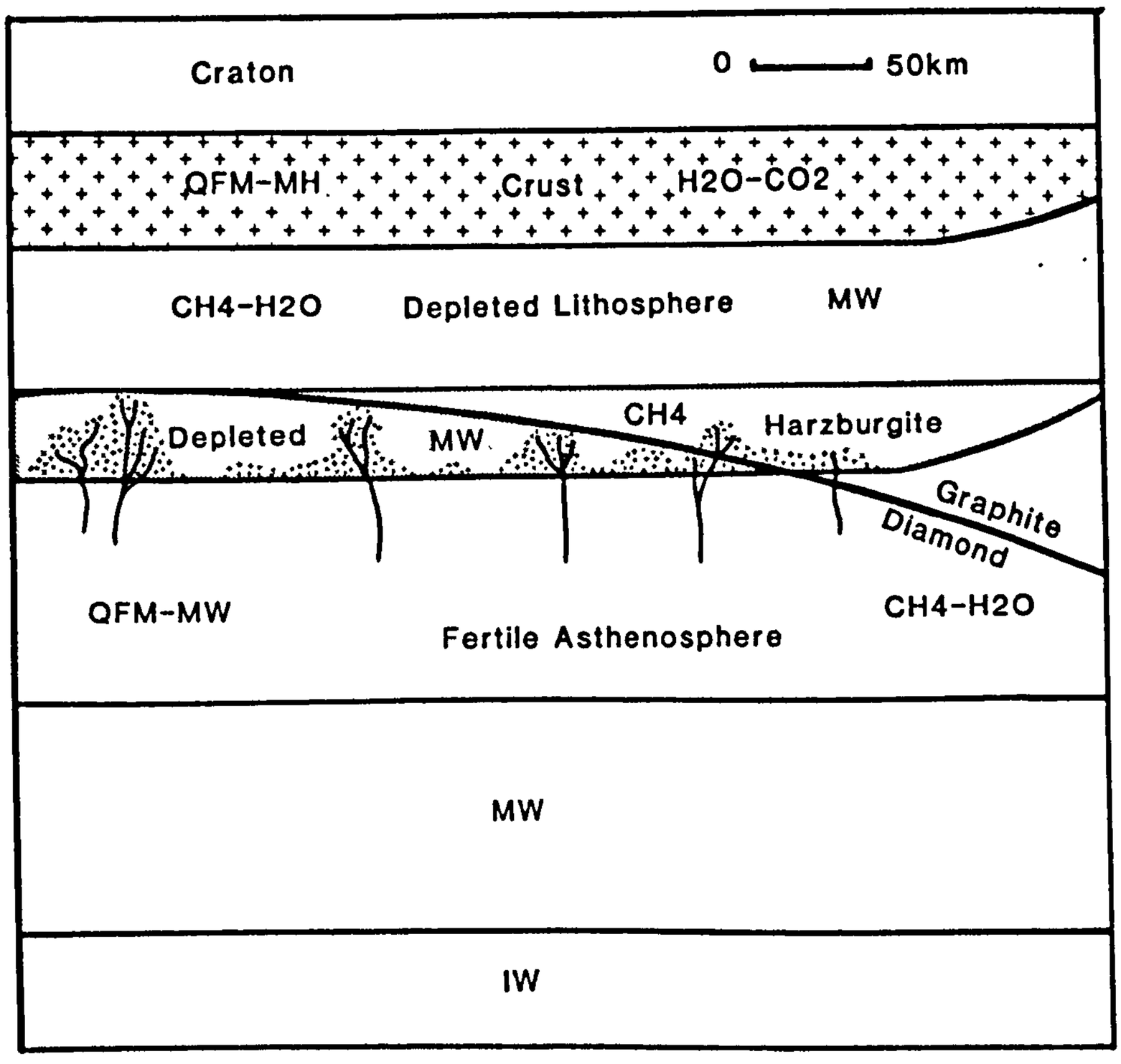
Craton
0
50km
QFM-MH
Crust
H2O-CO2
CH4-H2O
Depleted Lithosphere
MW
Depleted
MW
CH4
Harzburgite
Graphite
Diamond
QFM-MW
Fertile Asthenosphere
CH4-H2O
MW
IW

Fig. 5.3.

Model for Diamond Growth.

The diagram shows a thickened cartonic area with a depleted harzburgite layer at the base as a remnant of komatiite volcanism. The redox conditions of the layered mantle are shown and range from IW (iron wustite), in equilibrium with the core, and MH (magnetite haematite) in the crust. In the depleted lithosphere H_2O-CH_4 is the dominant vapour phase, in the more reduced harburgite layer CH_4 dominates. The asthenosphere is relatively oxidised and migrating fluids from the asthenosphere into the depleted areas can cause carbon precipitation by methane oxidation (Haggerty, 1986). The carbon can be stable as diamond if it is precipitated below the diamond stability curve. Where the craton is thickest and the geothermal gradient is lowest, the diamond stability curve may be domed upward allowing diamond formation at shallower levels. the diamonds from Bultfontein suggest such a formation at shallow depths within a harburgite layer by methane oxidation.

increase of oxygen fugacity redox melting can occur. Carbon precipitation may accompany such fO_2 changes.

The Bultfontein diamonds apparently formed by CH_4 oxidation, this would imply an increase in redox conditions. Volatile rich melts have been recognised as a potential source of mantle metasomatism (Harte, 1987). In addition, metasomatising fluids are a good way of introducing C-O-H volatiles into different parts of the mantle. For example introduction of a CO_2 and H_2O rich fluid might promote redox melting and carbon precipitation by CH_4 oxidation.

5.6 The Formation of Bultfontein Diamonds.

The Bultfontein diamonds are dominated by peridotite paragenesis inclusions. These are magnesium and chrome rich. To explain this chemistry many authors have suggested that peridotite suite diamonds originate in a harzburgite layer that is a remnant from komatiite volcanism. Such a layer is likely to be reduced and will probably have an oxygen fugacity value close to IW. As shown in figure 5.3 the geothermal gradients of cratons are low and the diamond stability curve will be domed upwards to relatively shallow depths within a depleted harzburgite layer. At shallow depths it is possible that chromites rather than garnets are stable and the relatively high abundance of chromites at Bultfontein may reflect a shallow depth of origin for a large number of diamonds. The Bultfontein peridotite suite diamonds also show two separate lines of evidence that favour a low temperature of origin, namely low equilibrium temperatures for inclusion pairs and of low overall IaB nitrogen content.

The carbon isotope compositions of Bultfontein peridotite suite diamonds suggest that diamond precipitation occurred by continued equilibrium during methane oxidation reactions. This implies that redox conditions in the mantle were initially reduced and were then progressively oxidised. Such an increase in redox conditions could result from the introduction of volatiles into a reduced

area. From figure 5.3 it can be seen that the asthenosphere is relatively oxidised and asthenospheric volatiles introduced into a depleted harzburgite in the lithosphere could precipitate diamond which may contain magnesium and chrome rich inclusions.

If an H_2O- rich vapour is introduced into the harzburgite there are three effects. Initially this may cause partial carbonation of the mantle and will lower the solidi sufficiently to intersect geothermal gradients, thereby causing melting. This in turn decreases the calcium content of garnet and removes any clinopyroxene that is present (sub-calcic garnets and a very low abundance of clinopyroxenes are observed at Bultfontein.). The third effect is that the redox state of the mantle is altered and carbon precipitated.

The cathodoluminescence pattern of Bultfontein diamonds shows evidence for cuboid cores which may result from a fluctuation of oxygen fugacity. One possible explanation of the $\delta\ ^{13}C$ variation across a single diamond is that redox conditions changed to high fO_2 values to where CO_2 is stable. The $\delta\ ^{13}C$ variations can only be produced, however, if CO_2 is in excess after carbonation reactions. An alternative explanation is that isotopically light carbon is introduced into the diamond growth area. Both explanations favour the introduction of carbon species in volatile rich fluids, either as a vapour or as a carbonate melt.

It is concluded that the Bultfontein peridotite paragenesis diamonds originated over a range of depths within a reduced, depleted harzburgite layer beneath the Archean Kaapvaal Craton. Introduction of C-O-H volatiles caused carbon precipitation by CH_4 reduction and carbon was precipitated from a limited carbon reservoir that became progressively depleted in ^{12}C. The period of diamond growth was extensive and initially this was characterised by variable fO_2.

The nitrogen and carbon isotope data for the eclogite suite diamonds show a low temperature of origin and precipitation of carbon from an infinite reservoir with a mode $\delta\ ^{13}C$ close to -5 $^{o}/_{oo}$.

Chapter 6

Garnet-Rich Inclusions from Sao Luiz Mine.

6.1 Introduction.

Diamonds from the Sao Luiz mine were recovered from river gravels associated with the Sao Luiz River, which drains via the Aripuena River into the Amazon. The deposit is located in north east Mato Grosso, close to Aripuena (see figure 6.1).

The diamonds are concentrated in gravels with a grade of 200-300 carats per 100 tonnes. Diamonds also occur in a group of Cretaceous kimberlites of the Aripuena Province and Tertiary sediments, all within 20km of the Sao Luiz River. The concentrations of diamonds in the kimberlites and Tertiary sediments are too low for economic extraction. Diamonds from all three sources have similar characteristics and it is assumed that the diamonds in the Sao Luiz River gravels and the Tertiary sediments were derived from the Aripuena Kimberlites.

Most of the kimberlites in the Aripuena Province occur in a graben structure and have kimberlite tuffs and non-volcanic sediments that are typical of the crater zone (see chapter 2). These kimberlites have undergone very little erosion. To the north of the province kimberlites of the same age occur which show characteristics of the diatreme zone and these have been subject to a greater degree of erosion. Near to the more deeply eroded kimberlites is an isolated area of Tertiary sediments, the Chapadao Sao Luiz, which is the dissected remnant of sediments derived from the kimberlites. In the Chapadao Sao Luiz, diamonds and heavy minerals such as ilmenite occur. The present river system has eroded the Chapadao to form the river gravels in the Sao Luiz River.

The Aripuena Kimberlite Province was intruded in to the Guyana-Guapore Shield in the Cretaceous (90Ma). As shown in figure 6.1 the Guyana-Guapore shield consists of four, Precambrian tectonometamorphic provinces.

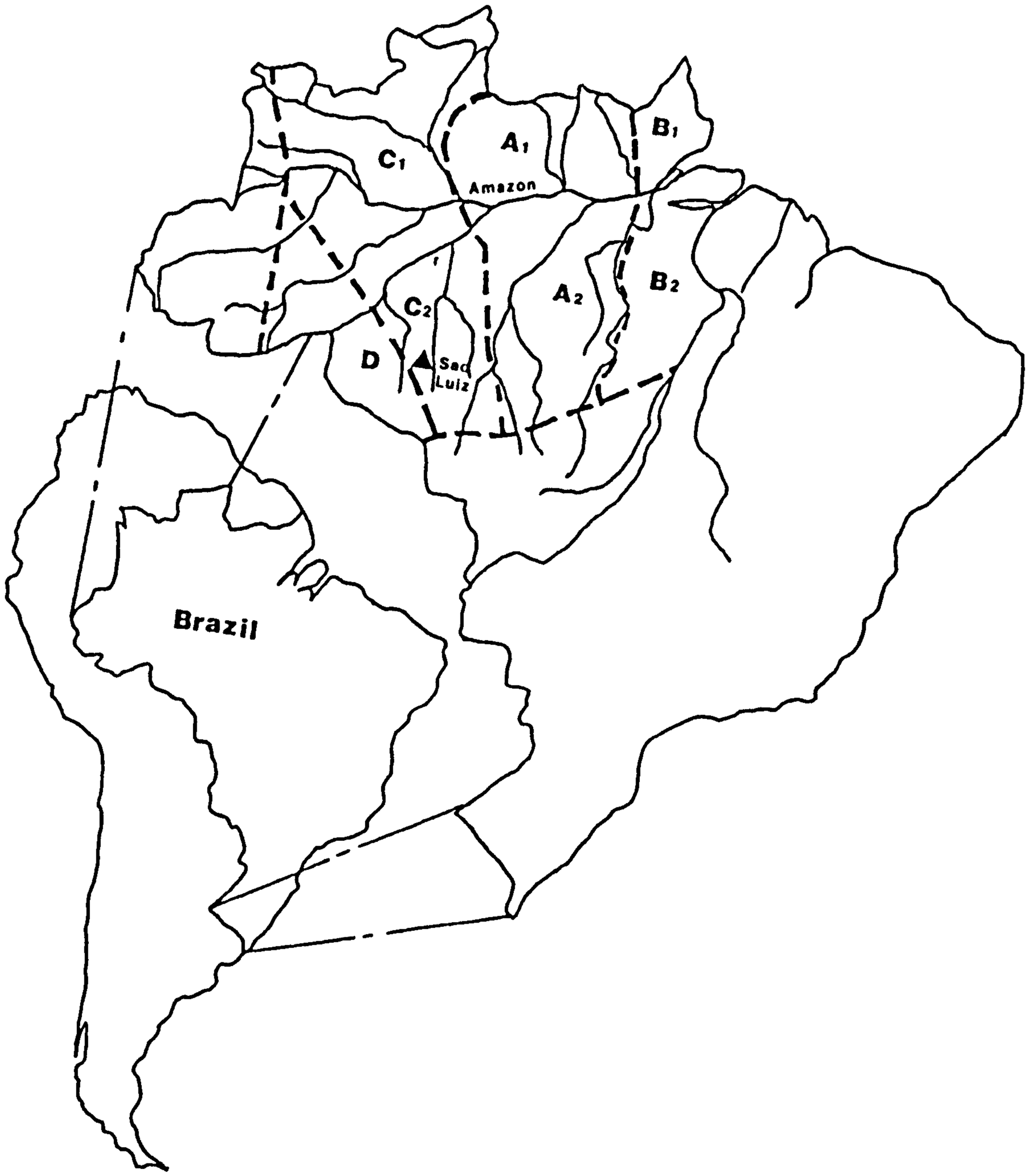
A1
B1
C1
Amazon
A2
B2
C2
D
Sao Luiz
Brazil

Fig 6.1

Tectonic Provinces of the Guyana-Guapore Craton.

Four belts are defined in the shield region of the Guyana-Guapore Craton, shown on the map of Brazil. The Xingu-Mapuera Belt (A1-A2), the Itacuanos-Maroni Belt (B1-B2), the Rio Negro-Jupuena Belt (C1-C2) and the Rondonian Belt (D). The four belts are believed to continue across the Amazon river system but the continuity is obscured by alluvium. The Xingu-Mapuera and the Itacuanos-Maroni Belts are believed to be re-mobilised Archean greenstones and granite gneisses. The Rio Negro-Jupuena Belt is thought to be an island arc terrain that was trapped during the collision of two continental areas, the Rondonian Belt (also remobilised Archean) and the Xingu-Mapuera Belt. The Aripuena Kimberlite Province, which is the source of the Sao Luiz diamonds occurs in the south west of the Rio Negro-Jupuena Belt, and is indictated by the symbol SL.

The oldest province is the Xingu-Mapuea Belt which consists of granite gneisses and greenstones of Archean origin, although Rb-Sr ages have been reset to 2000-1800Ma. The Itacuanas-Maroni Belt occurs to the east and this is a remobilised Archean Terrain with a metamorphic age of 2000 to 1800Ma. To the west of the Xingu-Mapuena Belt is the Rio Negro-Jureuna Belt which has a metamorphic age of 1450 to 1750Ma. The Rondonian Belt lies to the extreme west of the Shield and this comprises granites and greenstones with an age of 1000 to 1200Ma and it is also believed to be a remobilised Archean terrain.

The Rio Negro-Juruena Belt has been tenatively identified as an Island Arc Terrain (A. J. Carrington pers. comm.) accreted during the continent to continent collision of the Xingu-Mapuea Belt and the Rondonian belt. The Aripuena Kimberlite Province is intruded into the Rio Negro-Juruena Belt, close to its boundary with the Rondonian Belt. These kimberlites are therefore not intruded into an Archean Craton but are intruded into a cratonic area that has been remobilised in the Proterozoic.

Off-craton kimberlites are normally considered to be non diamondiferous. The low concentrations of diamonds in the Aripuena Kimberlites have however, been concentrated by sedimentary processes at Sao Luiz. Sao Luiz diamonds, therefore, provide a unique opportunity to study diamonds from an off craton environment and one not normally associated with economic diamond production.

6.2 Inclusion Divisions.

The inclusions in the Sao Luiz diamonds comprise two groups: garnet and garnet-rich inclusions that are discussed in this chapter, and other silicate and oxide inclusions, discussed in Chapter 7. The garnet inclusions were recovered from diamonds primarily for isotopic age dating (Nd/Sm) and a fraction of this sample was analysed by electron microprobe. In total sixty garnet-rich inclusions were examined and these were all visually identified optically as orange to pale orange eclogite paragenesis garnets.

Table 6.1

Principal Types of Garnet-Rich Inclusions from Sao Luiz.

Group I	
	Contain garnet with ~ 3.0 Si atoms per 12 Oxygens.
IA	Homogeneous (garnet only)
IB	Composite with clinopyroxene accompanying garnet.
Group II	
	Contain garnet with > 3.0 Si atoms per 12 oxygens.
IIA	Homogeneous (garnet only)
IIB	Composite with high-jadeite clinopyroxene accompanying garnet.

The study of the garnet-rich inclusions was supplemented by an examination of ten diamonds which contained orange garnets.

The analyses of the garnet-rich inclusions are shown in Appendix 3 together with the nitrogen aggregation state and the $\delta\ ^{13}C$ values for the ten garnet-bearing diamonds.

As can be seen from Table 6.1, two principal divisions of the garnet-rich inclusions are established on the basis of silica content.

In Group I inclusions the garnet silica contents are normal, that is approximately 3.0 Si atoms per 12 oxygens in the garnet formula. Group II garnets have more than 3.1 Si atoms per formula unit and these are believed to represent high pressure solid solutions between garnet and pyroxene within a garnet structure (Major, 1967). The Group II inclusions will be referred to as high-silica garnets. Similar high-silica garnets are rare as inclusions in diamond but have been documented in diamonds from Monastery (Moore & Gurney, 1985) and at Jagersfontein (Gurney *et al.*, unpubl.).

Both Group I and Group II are further subdivided. Some of the inclusions are composite and have clinopyroxene present in addition to the garnet-rich phase. Group IB garnets consist of normal-silica garnet and clinopyroxene. Group IIB garnets have high-silica garnet and clinopyroxene, in addition some normal-silica garnet may be present.

6.2.1 Group IA inclusions.

The silica contents in these 3 inclusions range from 2.89 to 3.0 silicon atoms for every twelve oxygens in the garnet formula. The garnets have sodium contents of up to 0.04 sodium atoms per formula unit. Calcium and titanium values are up to 1.12 and 0.22 atoms per formula unit respectively. Magnesium values show a restricted range of between 0.33 and 0.38 Mg/R^{2+} (see Appendix 3 for details). In figure 6.2 the concentrations of sodium, titanium and calcium are shown. As can be seen the sodium, titanium and calcium contents tend to increase

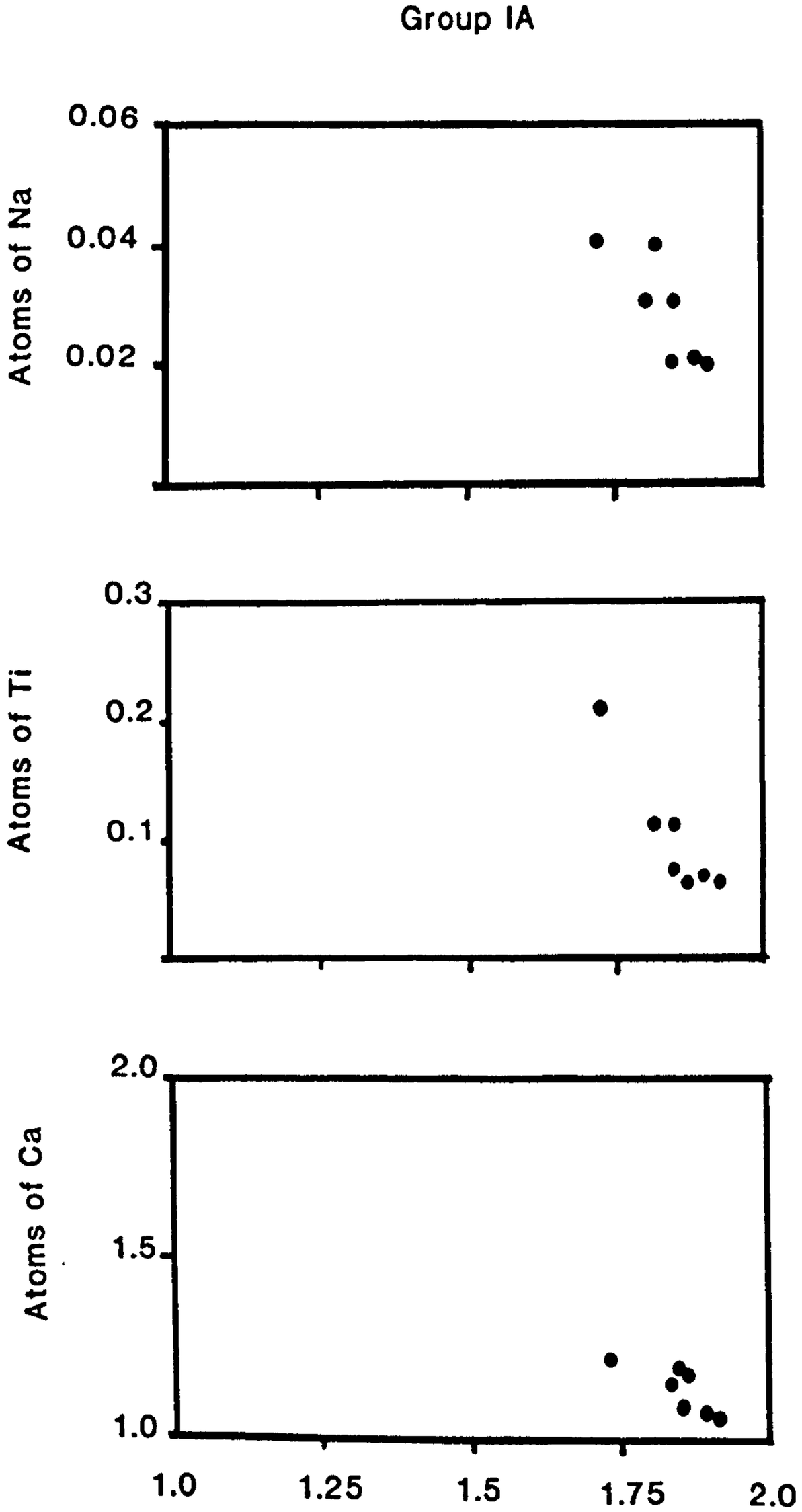
Group IA
0.06
0.04
0.02
Atoms of Na
0.3
0.2
0.1
Atoms of Ti
2.0
1.5
1.0
Atoms of Ca
1.0
1.25
1.5
1.75
2.0
Atoms of Al

Fig 6.2

Sodium, calcium and Titanium Contents for Group IA Garnets.

Atoms of sodium, calcium and titanium for each formula unit (12 oxygens) are shown against the number of aluminium atoms.

with decreasing aluminium content. Titanium is usually expected to replace aluminium in octahedral coordination, the total Ti + Cr + Al in the octahedral sites is 1.92 to 1.98, which may be compared to 2.0 cations in the garnet formula. Some sodium may accompany the substitution of quadrivalent Ti in order to maintain the charge balance, although there is not enough sodium present to balance all of the titanium in the R^{3+} site. The number of R^{2+} and sodium ions present in the garnet structure ranges from 2.88 to 3.08 (see Table 6.2), while the number of ions in the R^{3+} site (Al, Ti and Cr) ranges from 1.92 to 1.98. In some inclusions therefore the octahedral sites are not fully occupied by trivalent (Al, Cr) or quadrivalent (Ti) cations. Some of the excess divalent cations may therefore be in octahedral coordination, and this could be another means of maintaining the charge balance when Ti substitutes for Al.

6.2.2 Group IB inclusions.

The clinopyroxene and garnet in these 15 inclusions are separated by smooth, sinuous boundaries which show little evidence for crystallographic control. The garnets have similar composition to those in Group IA, except that they are more magnesian (Mg/R^{2+} 0.38 to 0.42). As shown in figure 6.3, the sodium content is highest at low aluminium values, and such inclusions have titanium concentrations of around 0.1 cations. The concentrations of sodium in these inclusions are too low for all the titanium (Ti^{4+}) present to be balanced. As in Group I inclusions, the titanium probably enters into octahedral coordination, but again not all of the octahedral sites are occupied. Some excess divalent cations may therefore be present in the octahedral sites (see Table 6.2).

The clinopyroxenes (Appendix 3) have a high jadeite ($NaAlSi_2O_6$) content, where the clinopyroxene is largely homogeneous with up to 10 mol.% jadeite, shown as high sodium and aluminium contents. The clinopyroxene shows textural and chemical evidence for the breakdown from high jadeite to lower jadeite compositions (2-3 mol.%). This reaction is accompanied by the exsolution

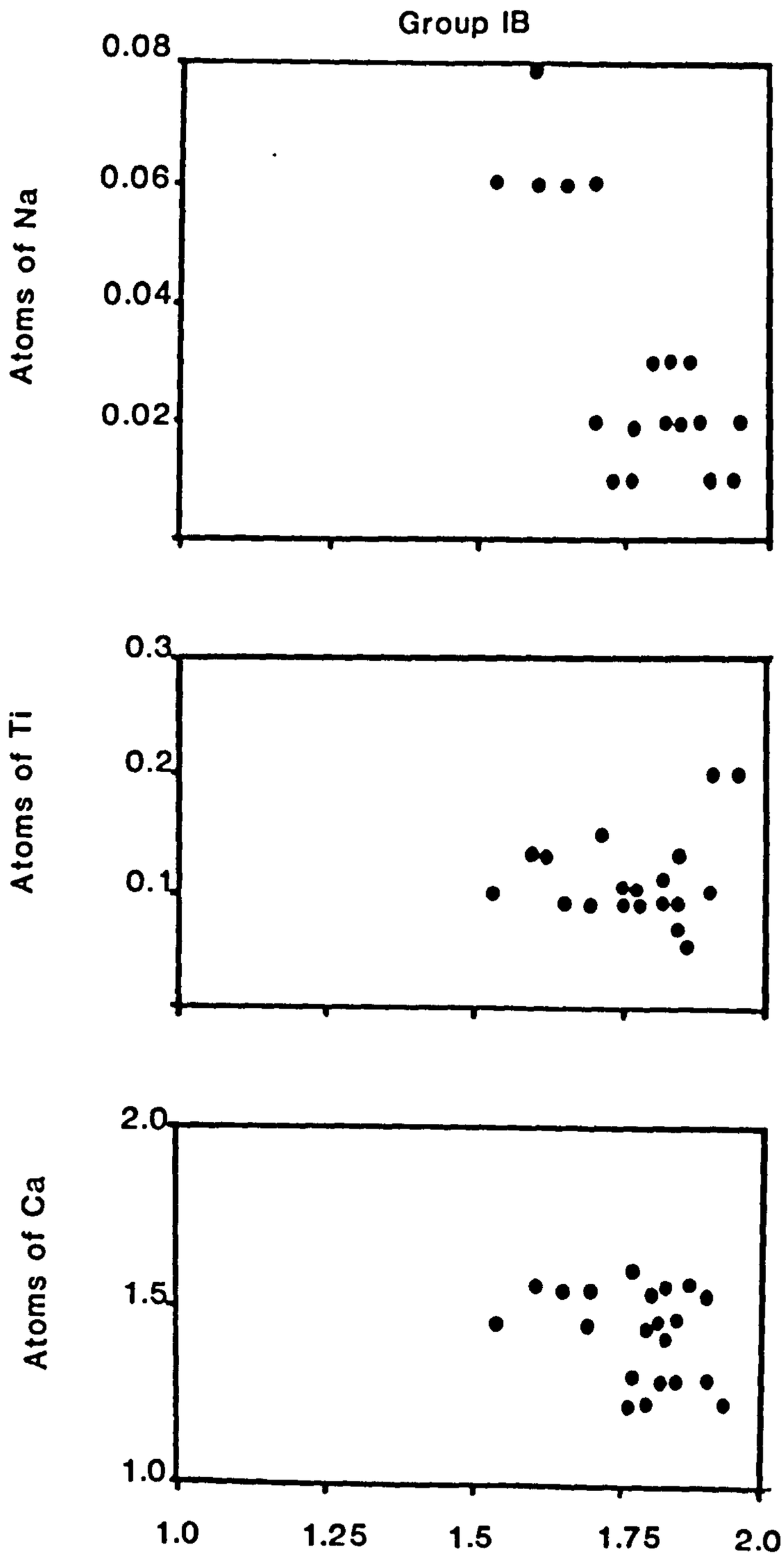
Group IB
0.08
0.06
0.04
0.02
Atoms of Na
0.3
0.2
0.1
Atoms of Ti
2.0
1.5
1.0
Atoms of Ca
1.0
1.25
1.5
1.75
2.0
Atoms of Al

Fig 6.3

Sodium, Calcium and Titanium contents for Group IB Garnets.

The number of sodium, calcium and titanium atoms per twelve oxygens. Titanium is assumed to enter into octahedral coordination to replace aluminium.

of an unidentified aluminosilicate phase. This unidentified phase consists of 25 wt.% aluminium (Al_2O_3) and 60 wt.% silica (SiO_2). During electron microprobe analysis the counts at the sodium peak are initially high. This phase possibly represents the jadeite ($NaAlSi_2O_6$) component of the pyroxene which has been exsolved to form complicated networks in the low-jadeite pyroxene. The clinopyroxene compositions show a range of Fe/Fe+Mg ratios of 0.50 to 0.67, with Ca/Ca+Mg ratios of 0.44 to 0.51. In addition there are minor amounts of Ti present (up to 0.04 cations). The aluminium contents are too high, compared with sodium, for all the aluminium present to represent the jadeite component. Some aluminium probably enters into the tetrahedral sites normally occupied by silicon, as the values of Si atoms per formula unit are lower than would be expected in a normal pyroxene formula and the number of aluminium atoms in tetrahedral coordination is probably up to 0.04 per 6 oxygens.

6.2.3 Group IIA inclusions.

The 3 garnet inclusions in this group have a higher silicon content than Group I, with up to 3.3 silicon atoms per twelve oxygens. These compositions are interpreted as solid solutions between garnet and clinopyroxene but within a garnet structure. Such minerals are termed majorite and were first identified experimentally by Ringwood and Major (1966a and b) and Ringwood (1967). The garnets show low aluminium contents which indicate the substitution of silicon atoms into octahedral sites. As shown in figure 6.4, around 0.1 Ti atoms are also present, which are probably incorporated into the octahedral (R^{3+}) sites. Sodium values of up to 0.08 suggest that sodium may replace a divalent cation such as Ca, Mg, Fe or Mn in eightfold coordination, in order to balance some of the Ti or Si present. From Appendix 3 and Table 6.3 it can be seen that, even with the incorporation of excess silica, there are not enough R^{3+} and R^{4+} ions to fill all of the octahedral sites. Some divalent cations which are in excess may also enter into the octahedral site. The Mg/R^{2+} values range from 0.35 to 0.42 and the most

Group IIA

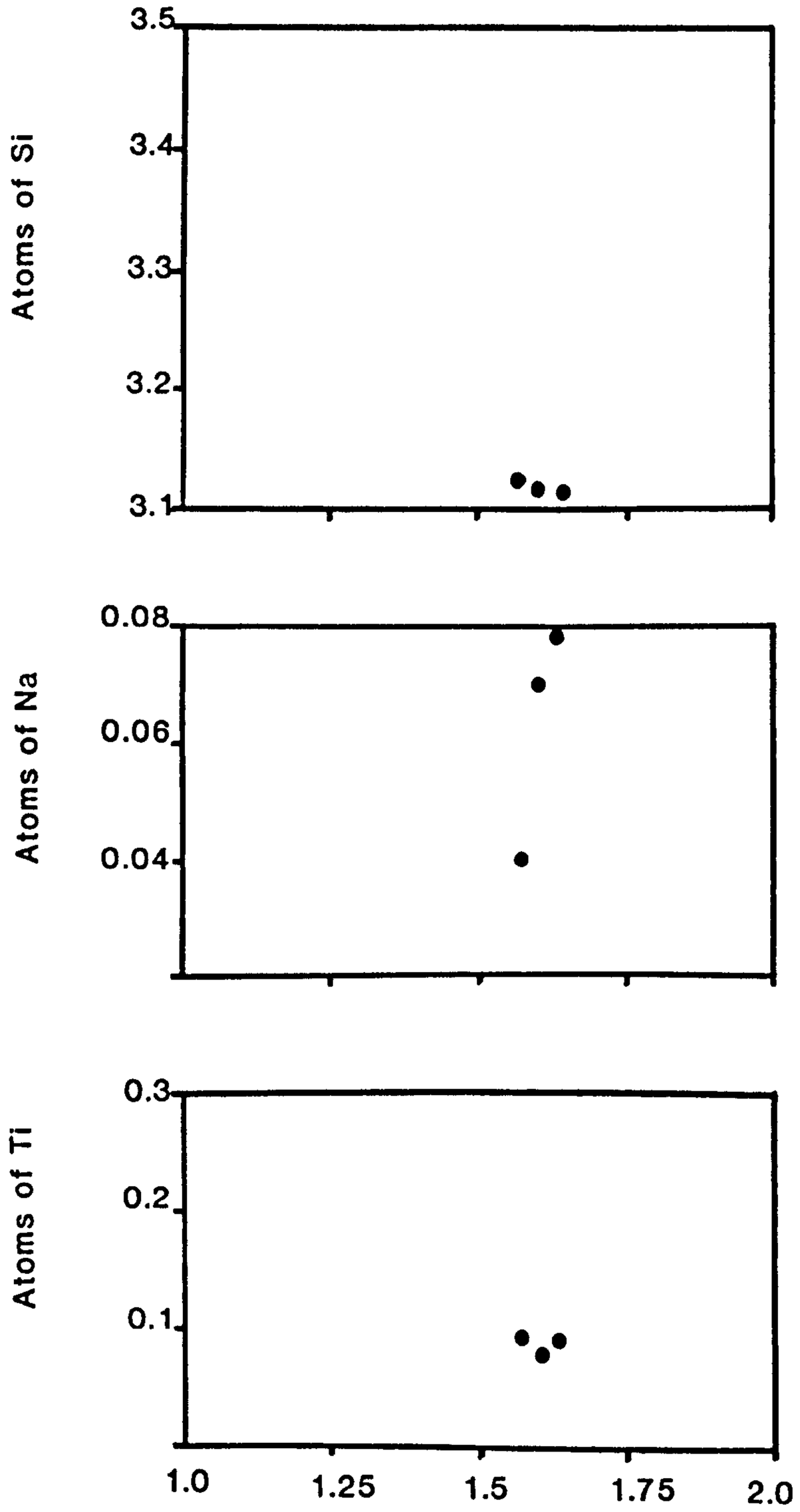
Atoms of Si
3.5
3.4
3.3
3.2
3.1
Atoms of Na
0.08
0.06
0.04
Atoms of Ti
0.3
0.2
0.1
1.0
1.25
1.5
1.75
2.0
Atoms of Al

Fig 6.4

Silicon, Sodium and Titanium Contents for Group IIA High Silica Garnets.

The limited data for inclusions of this type suggests that silicon atoms replace aluminium in octahedral coordination. The silicon substitution is possibly accompanied by sodium substitution which replaces a divalent cation (Mg or Fe) in eightfold coordination.

magnesian inclusions have the highest silica, which may indicate that Mg enters into the octahedral site, thereby helping to maintain the charge balance in view of the excess R^{4+} cations.

6.2.4 Group IIB inclusions.

These 11 inclusions are composite and contain both high-silica garnet and clinopyroxene. Generally the high-silica garnet is surrounded by a discontinuous rim of clinopyroxene. Garnet of normal-silica composition is sometimes present and this tends to mantle cores of the high-silica garnet suggesting decomposition of the solid solution phase. Only one inclusion shows direct evidence for crystallographically controlled exsolution and this consists of a core of high-silica garnet surrounded by garnet of normal-silica content with parallel clinopyroxene lamellae. Figure 6.5 shows the silicon, sodium and titanium contents of the high-silica garnets. As with Group I inclusions up to 0.08 Na atoms per twelve oxygens are present. The excess (> 3.0 cations) silicon and all of the titanium are assumed to substitute for aluminium in octahedral coordination. As with Group IIA, the total excess of Si, together with all of the Al, Cr and Ti leave a deficiency in the octahedral site and this may be balanced by the excess divalent cations.

The separate clinopyroxene phase is jadeite rich, up to 45 mol %. There is also evidence for a complex breakdown of the pyroxene into lower jadeite pyroxene, again accompanied by the networks of an unidentified aluminosilicate as observed in Group IB. The silicon contents of the clinopyroxenes also show (Appendix 3) that there are less than 2.0 Si atoms per 6 oxygens in the pyroxene formula and implies that some aluminium enters into tetrahedral coordination. The Mg/Mg+Fe ratios range from 0.67 to 0.77 with Ca/Ca+Mg values of 0.46 to 0.52. These values show more magnesian compositions that the Group IB inclusions.

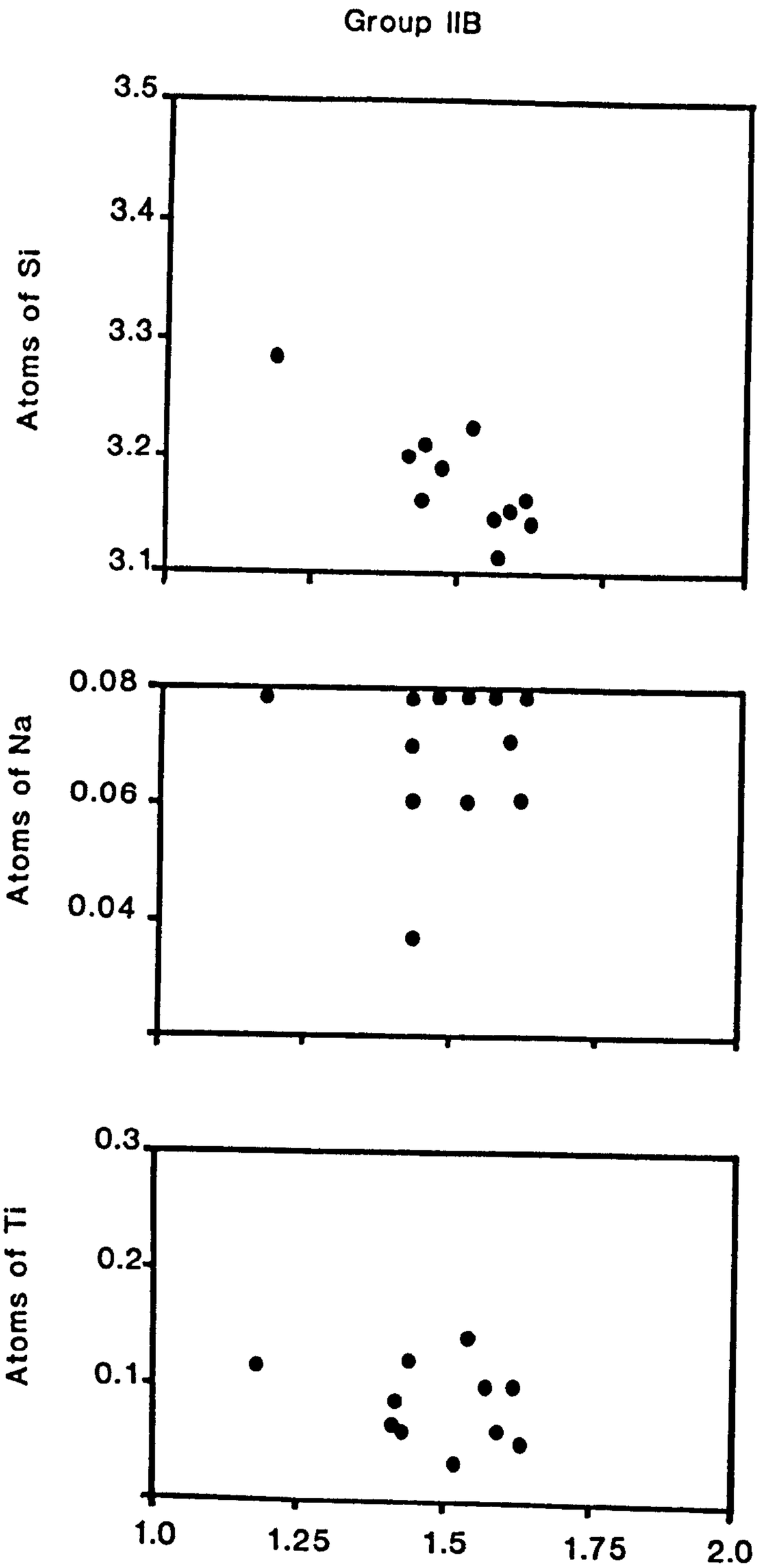
Group IIB
3.5
3.4
3.3
3.2
3.1
Atoms of Si
0.08
0.06
0.04
Atoms of Na
0.3
0.2
0.1
Atoms of Ti
1.0
1.25
1.5
1.75
2.0
Atoms of Al

Fig 6.5

Silicon, Sodium and Titanium Contents for Group IIB High Silica Garnets.

Silicon atoms replace aluminium in octahedral sites, and up to 3.3 silicon atoms per twelve oxygens are present. Sodium contents are highest for high silicon and low aluminium values. Titanium values are high for low aluminium values and titanium is also probably incorporated into octahedral sites. The sodium probably replaces divalent cations such as Mg and Fe in eightfold coordination.

6.3 Site Occupation in Garnet Inclusions.

In garnet structured minerals, for a formula unit with twelve oxygens there are the following cation sites: three cubic sites, commonly occupied by divalent cations, two octahedral sites, typically occupied by Al, but also with Ti^{4+}, Cr^{3+} and Fe^{3+} sometimes present and three tetrahedral sites, occupied by Si.

The data presented in the previous sections is summarised in Tables 6.2 and 6.3 and demonstrates the following points:

Increasing Ti is associated with decreasing Al in Group I garnets, indicating Ti substitution for Al in octahedral sites. In the high-silica garnets Ti concentrations are not unusual in comparison with normal-silica garnets and Si cannot be correlated with a change in Ti. Cr concentrations are low for all garnet inclusions. In Group II inclusions increased excess Si is correlated with decreased Al, and the Si probably occupies octahedral sites.

The sum of Al, Cr and Ti and also excess Si commonly falls short of the 2.0 cations in the garnet structure. The sum of Na and divalent cations (assuming all Fe is Fe^{2+}) commonly exceeds the 3.0 cations expected in cubic sites. Some of the excess divalent cations may therefore occupy octahedral sites in the garnet structure. The charge balance of excess Si and Ti in octahedral sites may be partly accounted for by Na substitution in cubic sites, however, Na contents are insufficient to balance all the quadrivalent cations present. Both the lack of R^{3+} cations in octahedral sites and the excess R^{4+} cations can be accounted for by R^{2+} cations, in place of Al in octahedral sites.

To illustrate the above figure 6.6 compares the number of Si atoms with the number of Al, Cr and Ti atoms that can occupy the octahedral sites in garnet structure and the number of Na and R^{2+} cations that can occupy the cubic sites. The typical values for a garnet two cations in octahedral sites and three cations in cubic sites and three Si cations per twelve oxygens. As figure 6.6 shows, as the amount of silica in the garnets is increased (values above 3.0 Si atoms) the sum of

Table 6.2

Cations in Group I Inclusions.

Group IA

Sample	Si^{4+}	Al+Cr+Ti	R^{2+}+Na
4	2.98	1.93	3.10
11	2.95	1.97	3.04
44	2.92	1.94	3.10

Group IB

1	2.96	1.94	3.07
2	2.98	1.91	3.10
5	2.99	1.95	3.05
12	2.94	1.93	3.12
13	3.00	1.86	3.12
14	2.96	1.95	3.07
15	3.09	1.76	3.16
16	3.07	1.76	3.13
18	3.08	1.75	3.13
25	3.08	1.73	3.16
32	2.97	1.86	3.13
34	2.97	1.92	3.08
37	2.96	1.99	3.08
39	3.00	1.98	3.03
42	2.99	1.93	3.07

Table 6.3

Cations in Group II Inclusions.

Sample	Si^{4+}	Al+Cr+Ti	R^{2+}+Na
Group IIA			
9	3.10	1.74	3.10
27	3.12	1.65	3.18
46	3.15	1.67	3.09
Group IIB			
7	3.28	1.33	3.18
10	3.11	1.68	3.18
19	3.20	1.51	3.12
21	3.07	1.70	3.23
22	3.14	1.68	3.11
29	3.22	1.57	3.17
43	3.21	1.52	3.21
45	3.14	1.72	3.04
47	3.19	1.68	3.15
48	3.18	1.48	3.35
50	3.18	1.62	3.15

Ti, Al and Cr cations, normally associated with the octahedral sites, decreases. The number of divalent cations and Na cations increases. These trends of variation support the suggestion that excess silicon and excess divalent cations enter into octahedral coordination, together with aluminium, titanium and chromium. Following the median lines of the trends shown in figure 6.6, when the value of excess silicon is 3.3 (i.e all Si sites are occupied but 0.3 Si atoms are in excess) the sum of titanium, aluminium and chromium cations is only 1.25, whilst the sum of sodium, calcium, magnesium, iron and manganese is 3.4.. The number of cations per site in garnet structure approximately balances, as follows:

$$R^{2+}_3((R^{2+})_{0.4}(Ti,Al,Cr^{3+})_{1.25}(Si^{4+})_{0.3}))Si_3O_{12}$$

Where the cubic site is occupied by Na, Ca, Fe, Mg and Mn and the octahedral site is occupied by Al, Ti, Cr, Fe, Mg, and excess Si. Mg and Fe probably enter into octahedral coordination rather than Na and Ca because of the large ionic radii (1.18 and 0.91Å respectively) for the latter two ions.

In order to maintain a charge balance, the excess Si and Ti cations must balance the Na and excess divalent cations in each inclusion, from Appendix 3 the excess Si and Ti cations are mostly balanced.

It is possible that some of the iron in the garnet inclusions from Sao Luiz is ferric (Fe^{3+}), which may mean that some of the iron may enter into the octahedral sites. In Group I inclusions it can be seen from Table 6.2 that not all of the deficit in octahedral sites is balanced by Si and some of these sites may be occupied by Fe^{3+}, up to 10% of the iron in Group I inclusions may therefore be Fe^{3+}. In Group II inclusions however, in order to occupy all of the octahedral sites, up to 48% of the iron present must be Fe^{3+}, which would imply very oxidised conditions of diamond formation, also the charge on each inclusion would not be balanced. From Appendix 3, the analyses totals are close to 100%, if ferric iron is present, lower totals would be expected. Ferric iron is not considered to be important in Group II inclusions.

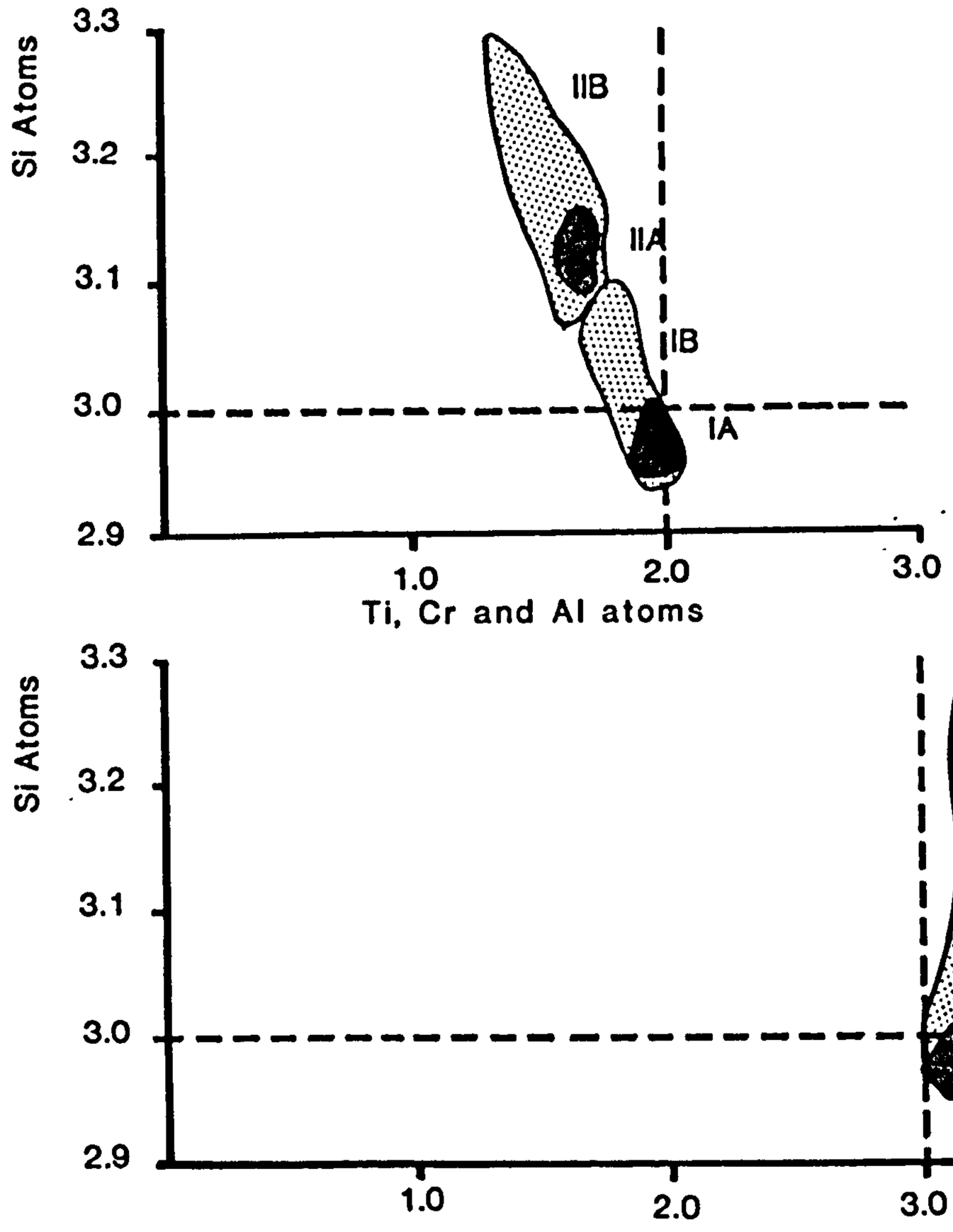

Cations in Garnet Structure

for

Group I and II garnet-like inclusions

Fig 6.6

Cations in Garnet Structure for Sao Luiz Inclusions.

The two diagrams show the number of cations that would be expected in fourfold sites (R^{4+}), sixfold sites (R^{3+}) and in eightfold sites (R^{2+}) in a normal garnet structure. In an ideal garnet there are three quadrivalent cation in fourfold coordination, two trivalent cations in sixfold coordination and three divalent cations in eightfold coordination. In the Sao Luiz diamonds the ions expected to enter into the sixfold site are Ti, Al and Cr. The ions expected to enter the eightfold sites are Na, Ca, Mg, Fe and Mn. There are too many divalent ions (including monovalent sodium) to occupy all of the R^{2+} site, also there are not enough ions of Ti, Al and Cr to occupy all of the R^{3+} sites. With excess silica the number of trivalent ions decreases and the number of divalent ions increases. This suggests that with solid solution of pyroxene in garnet the sixfold sites in a garnet structure are occupied by Al, Si, Ti and divalent cations (Probably Mg and Fe).

The substitution mechanisms for the Sao Luiz inclusions therefore probably involve the substitution of silicon atoms for aluminium atoms in octahedral coordination. Titanium also enters into octahedral coordination. Calcium and sodium remain in eightfold sites but divalent iron and magnesium may also enter into octahedral coordination. The basic substitution mechanism is:

$$(Mg,Fe)^{2+} + Si^{4+} = 2Al^{3+}$$

At high pressures several important substitution mechanisms for garnets have been suggested, principally to explain the high sodium content in garnets in eclogite nodules, but these are equally applicable to the garnets from Sao Luiz. Sobolev and Laurent'ev (1971) related the increase of sodium in garnet to a coupled substitution involving replacement of aluminium in octahedral sites by silicon. Monovalent sodium accompanies the silicon present in order to maintain a charge balance:

$$Na^{+[8]}Si^{4+[6]} = Ca^{2+[8]}Al^{3+[6]}$$

This substitution could potentially explain the high sodium contents of the Sao Luiz inclusions, however, as can be seen from figures 6.4 and 6.5, the amount of sodium is insufficient to balance the number of silicon atoms present. In addition to silicon, titanium is an important substitution ion in the Sao Luiz garnet-like inclusions of both Group I and II.

The presence of P^{5+} in some garnets has been suggested as a mechanism for the substitution of sodium without the need for silica to enter octahedral sites in the garnet structure (Bishop *et al.*, 1976, Thompson, 1976). The coupled substitution in this reaction is:

$$Ca^{2+[8]}Si^{4+[6]} = Na^{+[8]}P^{5+[6]}$$

The Sao Luiz garnets show some P^{5+} to be present but this has a constant value irrespective of the diamond group. The only change in the phosphorus content is where calcium values are high, this is most likely to be a result of X-Ray interference of the P Kα I and Ca Kβ II peaks during microprobe analysis.

6.4 Textural features of Garnet phases.

The textures of the normal garnet and high-silica garnet inclusions from Sao Luiz are divided into six categories as shown in figure 6.7.

The first two divisions only occur in Group I inclusions. Group IA inclusions have a homogeneous texture (Texture 1). With Group IB inclusions clinopyroxene as well as garnet is present (Texture 2). As can be seen in figure 6.8 clinopyroxene forms blebs and discontinuous rims surrounding garnet in these inclusions.

The third textural type consists of high-silica garnet in which high-jadeite clinopyroxene is sometimes present. The phases are separated by smooth sinuous boundaries as shown in figure 6.9. In addition, the pyroxene sometimes shows a breakdown from high-jadeite to low-jadeite compositions by exsolution of the jadeite component.

The fourth texture was only observed in the inclusion shown in figure 6.10. This texture consists of a core of high-silica garnet that is surrounded by a complex intergrowth of normal-silica garnet and high-jadeite pyroxene. Some of the pyroxene is in the form of lamellae and may represent crystallographically controlled exsolution of pyroxene from high-silica garnet. Other pyroxene forms complicated textures within normal-silica garnet that are reminiscent of symplectite intergrowths.

The fifth texture is shown in figure 6.11 and consists of a core of high-silica garnet surrounded by normal-silica garnet and pyroxene. The boundary between the high-silica garnet and the normal-silica garnet is very irregular. The normal-silica garnet may originate as a breakdown product of the high-silica garnet. However the breakdown is not crystallographically controlled and the reaction front separating the breakdown products from the host phase is not distinct. The clinopyroxene is separated from the other phases by smooth, embayed boundaries.

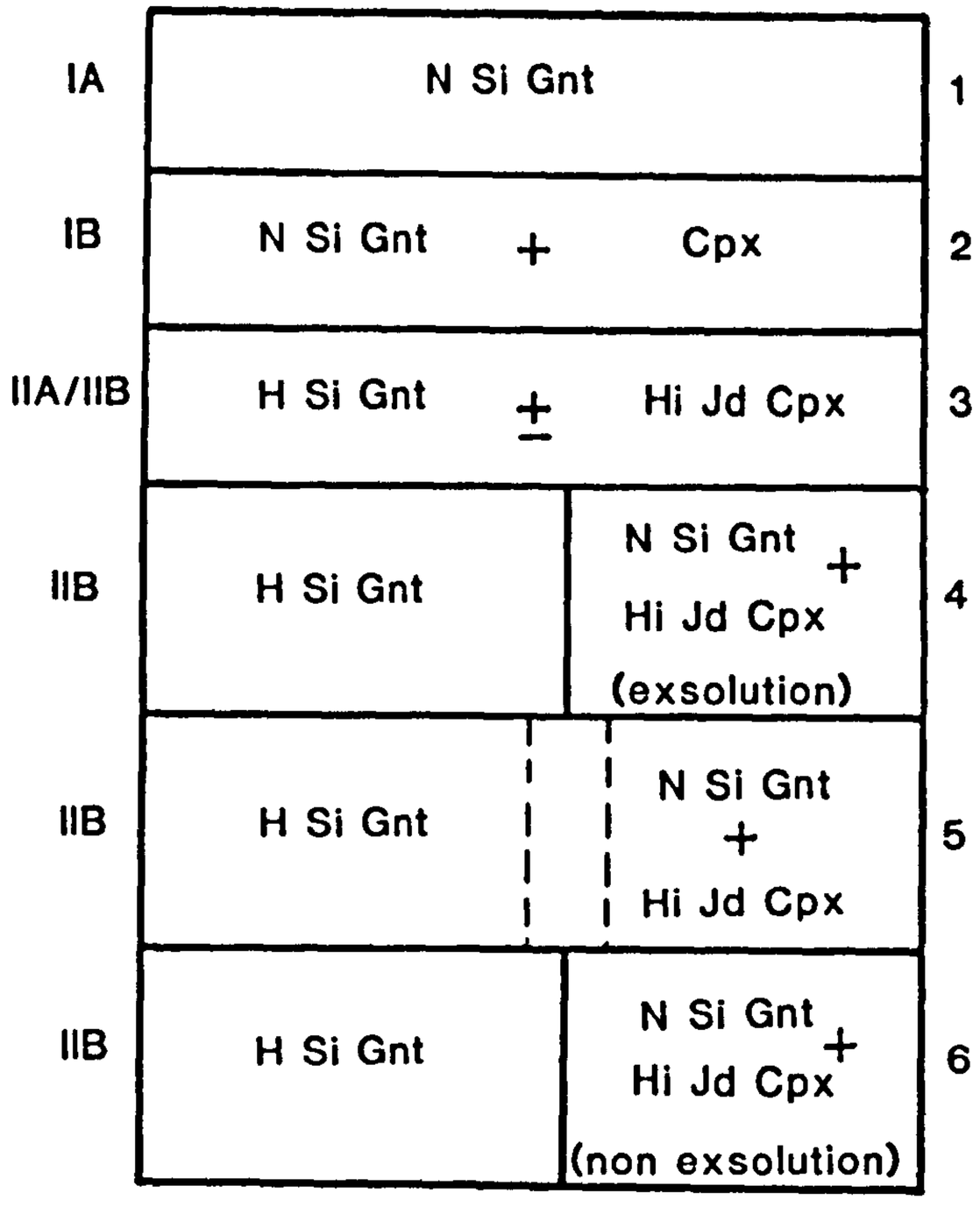
IA
N Si Gnt
1
IB
N Si Gnt + Cpx
2
IIA/IIB
H Si Gnt ± Hi Jd Cpx
3
IIB
H Si Gnt
N Si Gnt + Hi Jd Cpx (exsolution)
4
IIB
H Si Gnt
N Si Gnt + Hi Jd Cpx
5
IIB
H Si Gnt
N Si Gnt + Hi Jd Cpx (non exsolution)
6

Fig 6.7

Textual Subdivisions of Sao Luiz Inclusions

Six divisions are made on the basis of textures observed in garnets and high silica garnets.

Group I inclusions have the textures 1 and 2 and consist of normal-silica garnet (N Si Gnt) and low-jadeite pyroxene (Cpx). Group II inclusions have textures of types 3 to 6 and consist of high-silica garnet (H Si Gnt) with high-jadeite clinopyroxene (Hi Jd Cpx). Normal-silica garnet is present in addition to high-silica garnet in textures 4, 5 and 6.

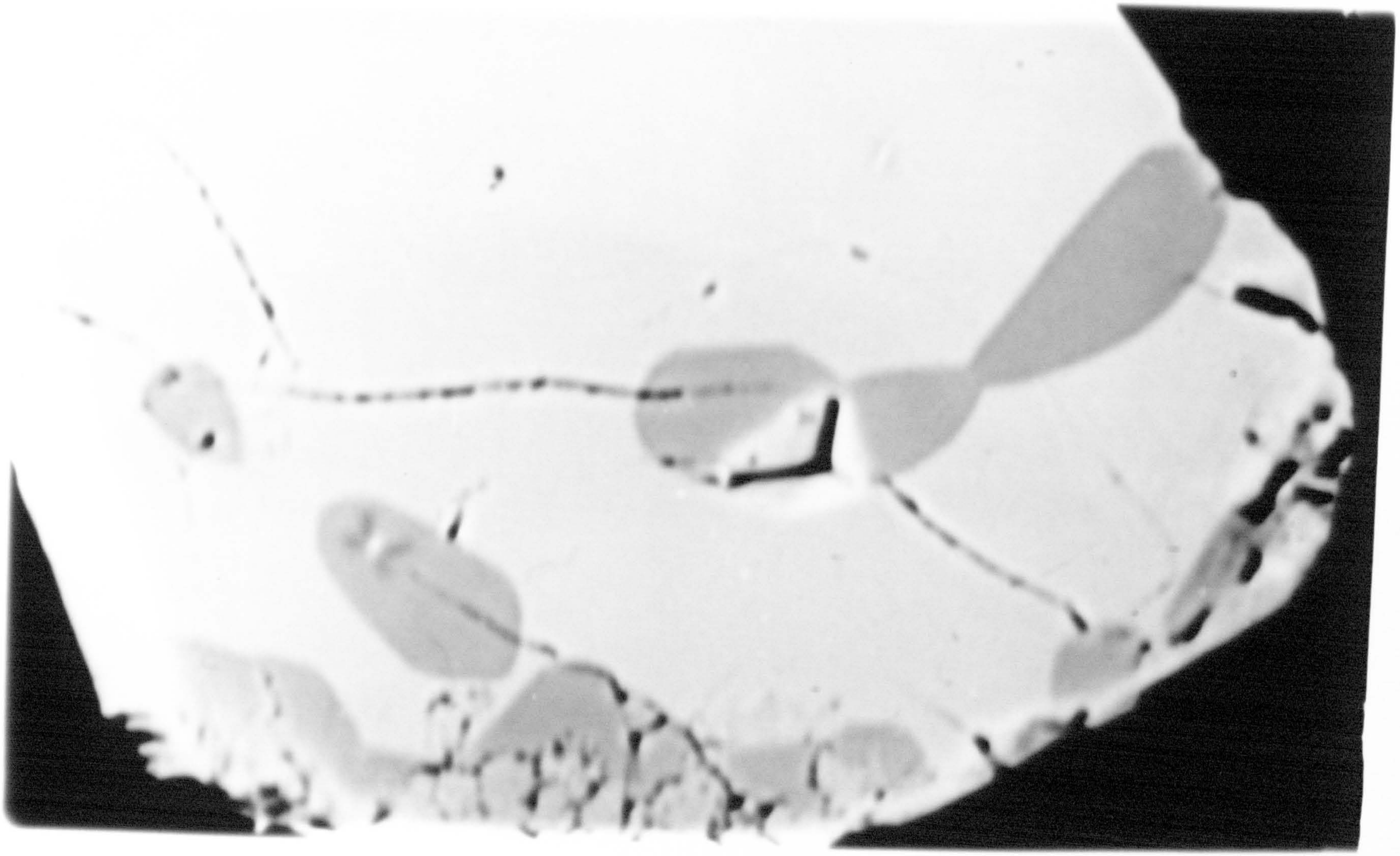

Fig 6.8

Back Scattered Electron Image of a Group IB Inclusion, Texture Type 2.

The light grey ares are garnet with normal-silica content, while the dark grey areas are jadeite-rich pyroxene. On the edge of the inclusion the pyroxene shows decomposition to a pyroxene which has a lower-jadeite content. This inclusion shows evidence of a complicated network of exsolution to a very dark jadeite. The inclusion has a diameter of 150μm.

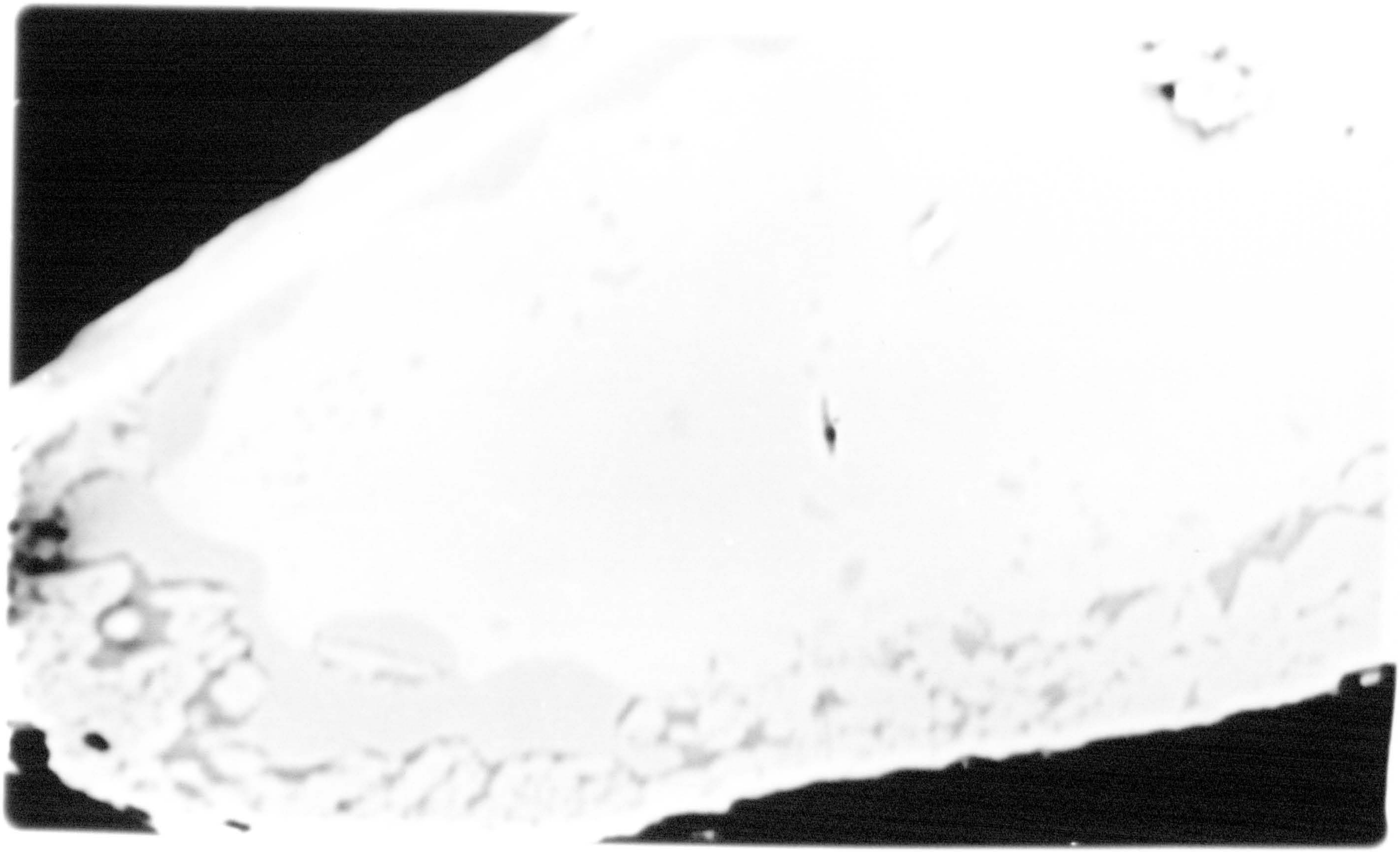

Fig 6.9

Back Scattered electron Image of Group IIB Inclusion, Texture Type 3.

This inclusion consists of high-silica garnet and jadeite rich pyroxene. The light grey high-silica garnet contains some dark grey pyroxene and is surrounded by a discontinuous rim of pyroxene. The pyroxene is separated from the high-silica garnet by smooth cuspate boundaries. There is evidence for the breakdown of pyroxene in the form of medium grey low-jadeite pyroxene and networks of black jadeite component on the rim of the inclusion. The inclusion is 200μm long.

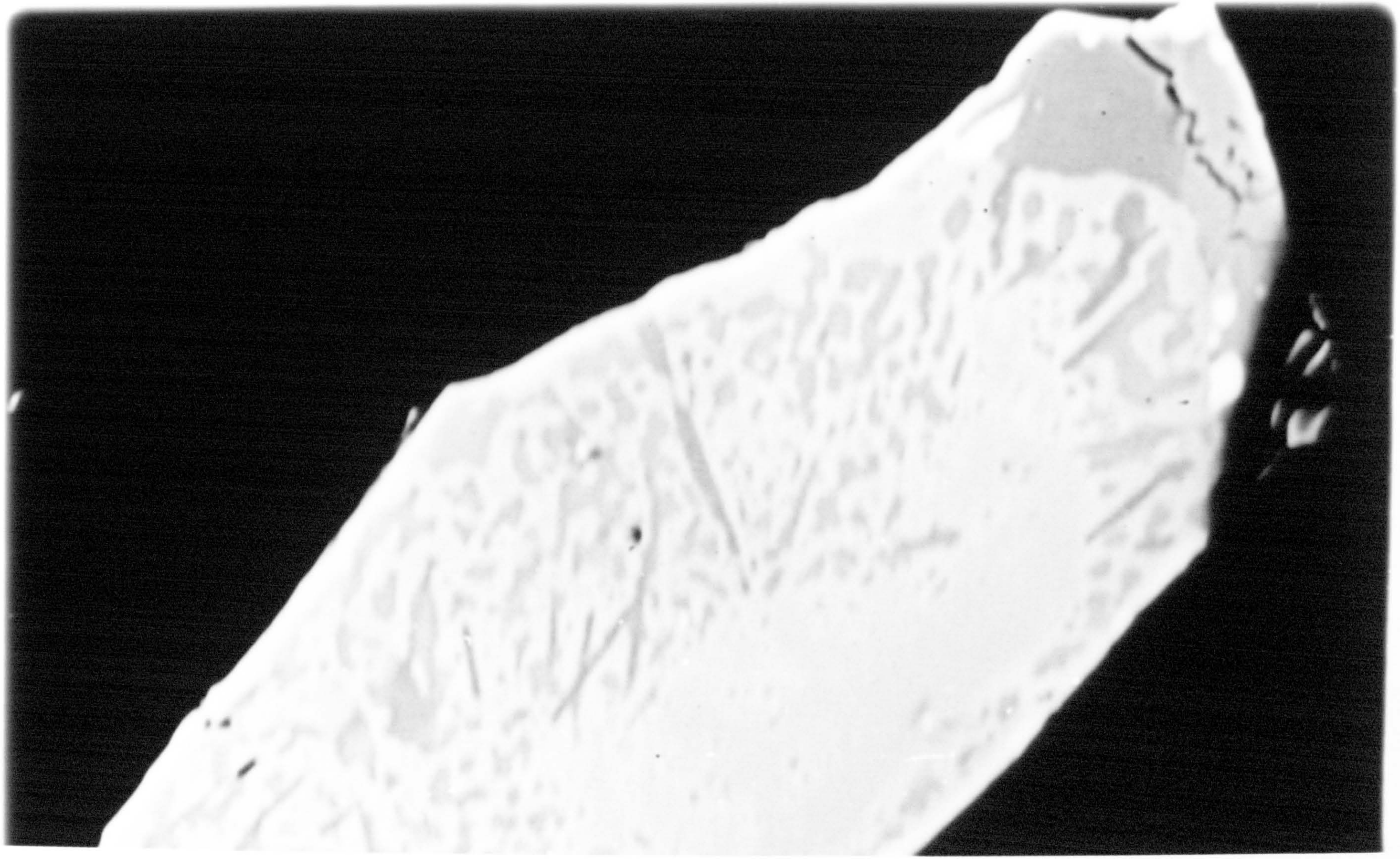

Fig 6.10

Back Scattered Electron Image of a Group IIB inclusion, Texture Type 4.

Only one inclusion of this texture was observed. This texture consists of a light grey core of high silica garnet surrounded by a complicated intergrowth of normal silica garnet and dark grey jadeite rich pyroxene. Some of the pyroxene is in the form of lamellae which suggest crystallographically controlled exsolution while other pyroxene occurs as blebs that suggest symplectite intergrowths. The inclusion is 150μm long.

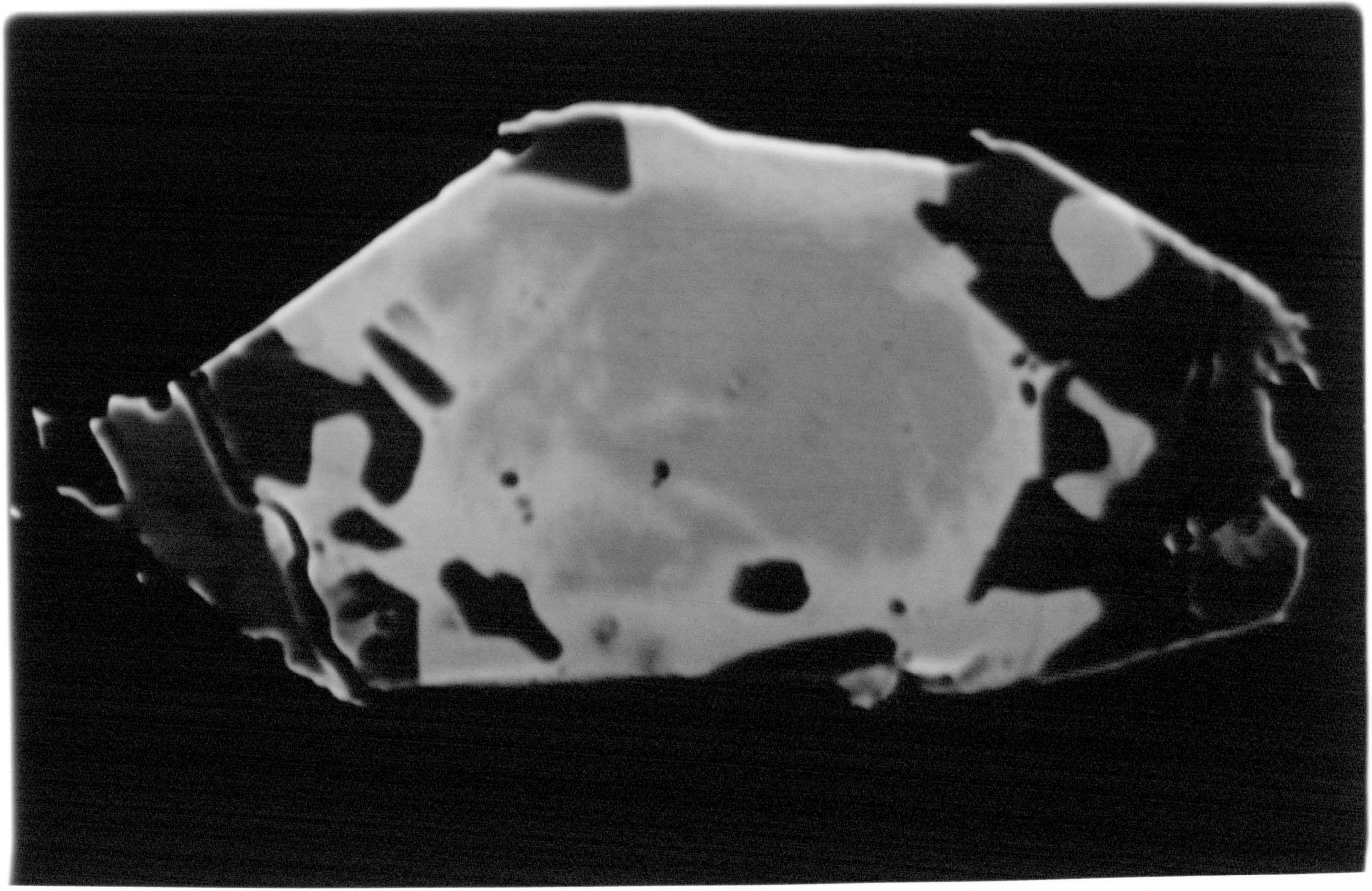

Fig 6.11

Back Scattered Electron Image of Group IIB Inclusion of Texture Type 5.

This inclusion is 150μm long and comprises an embayed core of medium grey high-silica garnet that is surrounded by a light grey area of normal-silica garnet. The edge of the inclusion has dark grey areas of jadeite-rich pyroxene that are bounded by smooth, rounded surfaces. The irregular boundary between the high- and low-silica garnet is interpreted as resulting from the breakdown of the high-silica phase.

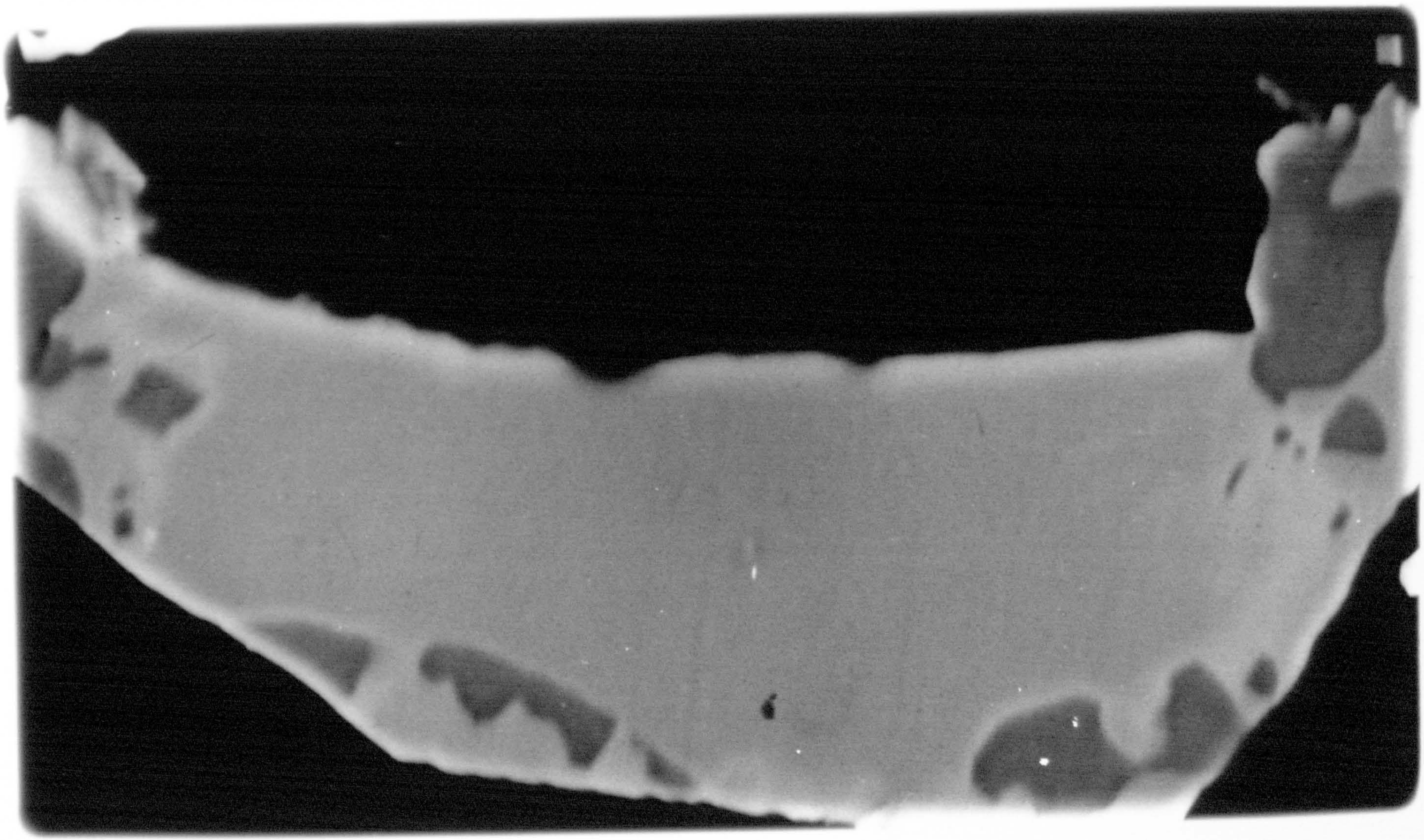

Fig 6.12

Back Scattered Electron Image of a Group IIB inclusion, Texture 6.

The core of this inclusion consists of high-silica garnet and is surrounded by dark grey jadeite-rich pyroxene and normal-silica garnet. The boundaries between high- and low-silica garnet are smooth and curved and are interpreted as reaction fronts that represent the breakdown of high-silica garnet to medium grey normal-silica garnet and jadeite-rich pyroxene. The inclusion is 150μm long.

The sixth texture, which is shown in figure 6.12, is interpreted as a breakdown product of high-silica garnet to produce normal-silica garnet and clinopyroxene. The decomposition products are separated from the high-silica garnet by a smooth boundary, which is different in character to that in category five (see figure 6.11) in that it is smooth and sinuous.

The relationship between the six types of texture is uncertain. In three dimensions it is possible that all six textures can be found in one single inclusion.

In addition to these six textural categories, there is a complicated texture observed in the pyroxenes of the composite grains. This occurs in both Group I and Group II inclusions and consists of reaction fronts separating jadeite-rich from jadeite-poor pyroxene. A network of the jadeite component (unresolved by microprobe) occurs in the jadeite-poor phase, this texture is considered first in the next section.

6.5 Discussion of Texture and Evolutionary History.

The textures which occur in the pyroxenes of composite inclusions are concluded to be a result of the decomposition of high-jadeite pyroxene by the exsolution of the jadeite component. This process is probably independent of the process which controls the distribution of pyroxene and garnet phases in the composite grains.

Composite inclusions are not unique to the Sao Luiz diamonds, see for example Sobolev (1977) for a discussion on composite grains in diamonds from Siberia. There are three possible explanations for the textures seen in the composite grains:

A) All of the clinopyroxene present results from the decomposition of a high-silica garnet at lower pressures.

B) Pyroxene and garnet phases were present at the time of diamond formation and subsequently underwent decomposition in the diamond to produce a range of textures.

C) Textures in the inclusions were produced before enclosure in the diamond. The latter possibility is unlikely because in the inclusions which show the most complicated textures the clinopyroxenes are concentrated around the rim of the inclusions. Decomposition of the high-silica garnet would be expected to occur at the diamond-inclusion interface, as observed in sulphide inclusions, and suggests that any exsolution occurred after enclosure. The inclusions also show an imposed morphology which is interpreted as formation by the mutual growth of diamond and inclusion (see Chapter 2).

In deciding between the first and second possibilities it is necessary to look at the cation contents of garnet phases. From figure 6.13 the compositions of the garnet-like inclusions and clinopyroxenes from Sao Luiz are shown in terms of the cation proportions. In ideal garnet structures there are 2.0 R^{3+} ions, 3.0 R^{2+} ions and 3.0 R^{4+} ions for every 12 oxygens in the garnet formula. In ideal clinopyroxene there are 2.0 ions for every 6 oxygens in both the R^{4+} and R^{2+} sites, which when doubled (for 12 oxygens) is 4.0. Solid solutions between garnet and pyroxene would lie between the two ideal compositions shown.

If Group I garnets and Group I pyroxenes originated from the decomposition of the high-silica garnets of Group II then a linear relationship would be expected between the Group II garnets and the exsolved products, in addition the exsolved pyroxene phase would be expected to have R^{4+} values greater than Group II garnets and the exsolved garnet phase would have higher R^{3+} values. The clinopyroxenes and garnets of Group I do not show the linear relation with Group II and are therefore not derived.

The Group II pyroxenes are very jadeite rich and if the Group II clinopyroxenes and garnets were exsolution products then a linear relationship would be expected from a high pressure phase that was initially rich in jadeite components (Na and Al) and which would have a silica value even lower than the Group II garnets. No such phases are found in the Sao Luiz diamonds. It is therefore unlikely that the Group II clinopyroxenes

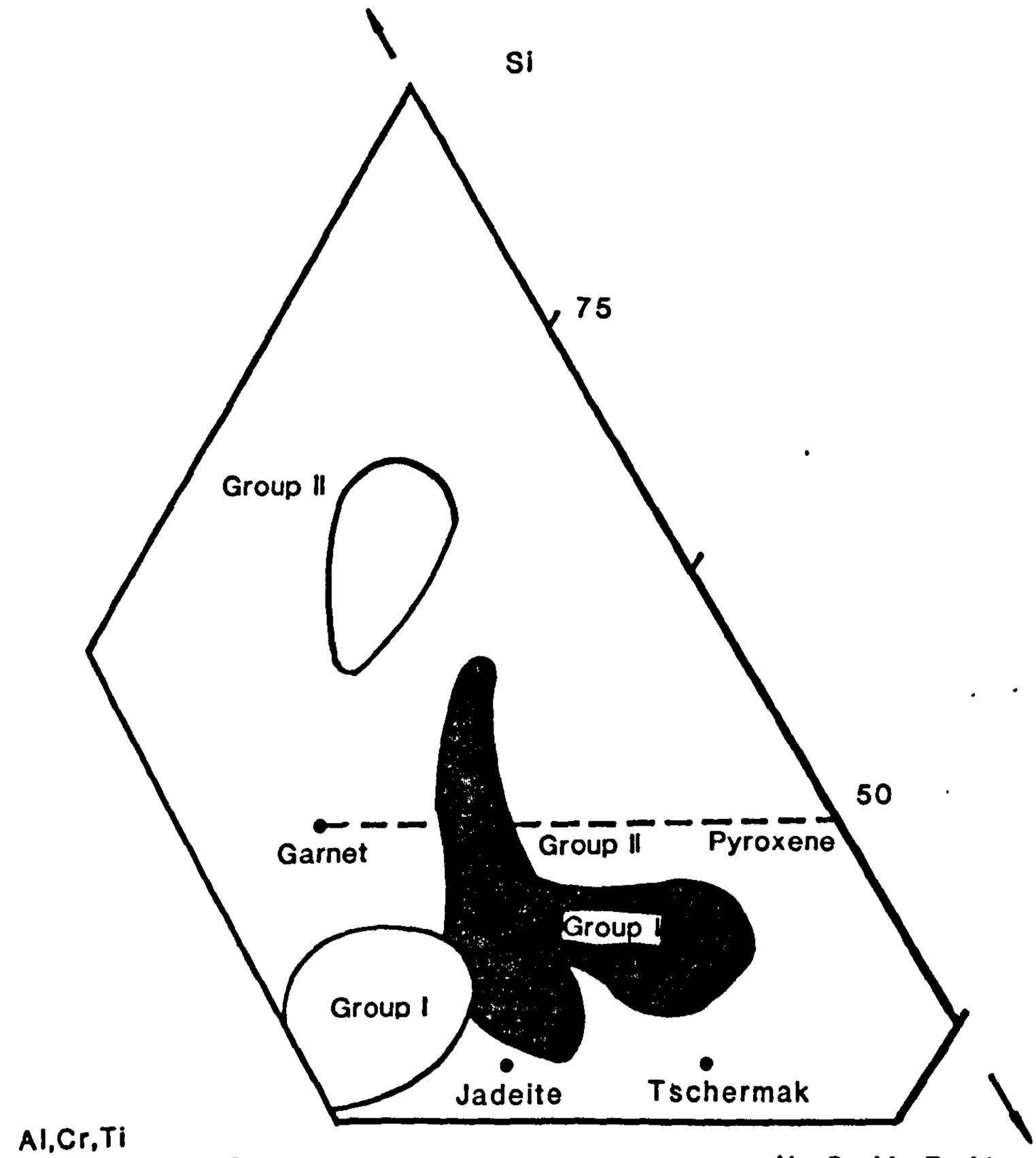

Group I and II Garnet and Pyroxene

inclusions

Fig 6.13

Cation Proportions for Composite Inclusions from Sao Luiz.

The compositions of garnets and pyroxenes of Group I and II inclusions are plotted in terms of their cations. The sum of cations expected to enter into the eightfold site in garnet (for 12 oxygens) is 3.0 and these cations are Na, Ca, Fe, Mg and Mn. The sum of cations expected in the sixfold site in garnet is 2.0 and these ions are Al, Cr and Ti. The number of silicon atoms will be 3.0 in a pure end member garnet. In ideal pyroxene there will be 4.0 silicon atoms per 12 oxygens and 4.0 other cations (Na, Ca, Al, Mg, Fe and Mn). The ideal compositions for garnet are shown, together with diopside, jadeite and Tschermak pyroxene end members. The Sao Luiz garnet-like inclusions of Group II have higher silicon contents than would be expected for a simple solid solution between garnet and pyroxene. The Group II pyroxenes (shaded) have a range of compositions from high-jadeite to low-jadeite compositions. The Group I garnets and pyroxenes (shaded) plot below the line of garnet and pyroxene solution. A linear relationship between the garnets, high-silica garnets and pyroxenes would be expected if the Group I inclusions were breakdown products of Group II, this is not the case at Sao Luiz. It is therefore suggested that the garnet and pyroxene-rich phases were separate before inclusion into the diamond.

and garnets are exsolution products.

The non linear relationships exclude the first possibility referred to earlier. As the second proposal does not require a linear relationship for its formation this proposal may best account for the mineralogical observations. In order to investigate this possibility the element distribution across mutual boundaries was investigated. Si, Ca, Al and Fe peaks were made using a step scanning mode on the Camebax microprobe to determine the concentrations of these elements.

The concentration gradients of aluminium and silica in an inclusion which shows a category five texture are shown in figure 6.14. At the edge of the high-silica garnet core there is a marked increase in the concentration of silica which corresponds to a thin rim of pyroxene. This pyroxene has a different composition to the very jadeite rich pyroxene that forms the outside part of the inclusion. The pyroxene surrounding the high-silica garnet core is interpreted as a breakdown of the high-silca garnet to produce normal-silica garnet and pyroxene. The concentration gradients of calcium and iron at this boundary are much more irregular, with calcium concentrations highest at the centre of the high-silica garnet. The iron contents are highest in the two pyroxene zones and are also very high at the interface between normal-silica garnet and pyroxene. The calcium and iron concentration gradients probably represent the relatively slow diffusion of iron and calcium in the garnet and pyroxene.

In the Group IIB inclusion, texture three, shown in figure 6.15, there is a similar steep concentration gradient of silica and aluminium at the boundary between pyroxene and high-silica garnet. The iron and calcium contents however remain constant in the garnet phase.

Even though the evidence in figure 6.13 shows that the pyroxene and garnet-rich phases were included separately into the diamond, the distribution of elements within the garnet phase shows that there has been some sub-solidus decomposition of the high-silica garnet after enclosure to form garnet of normal silica composition.

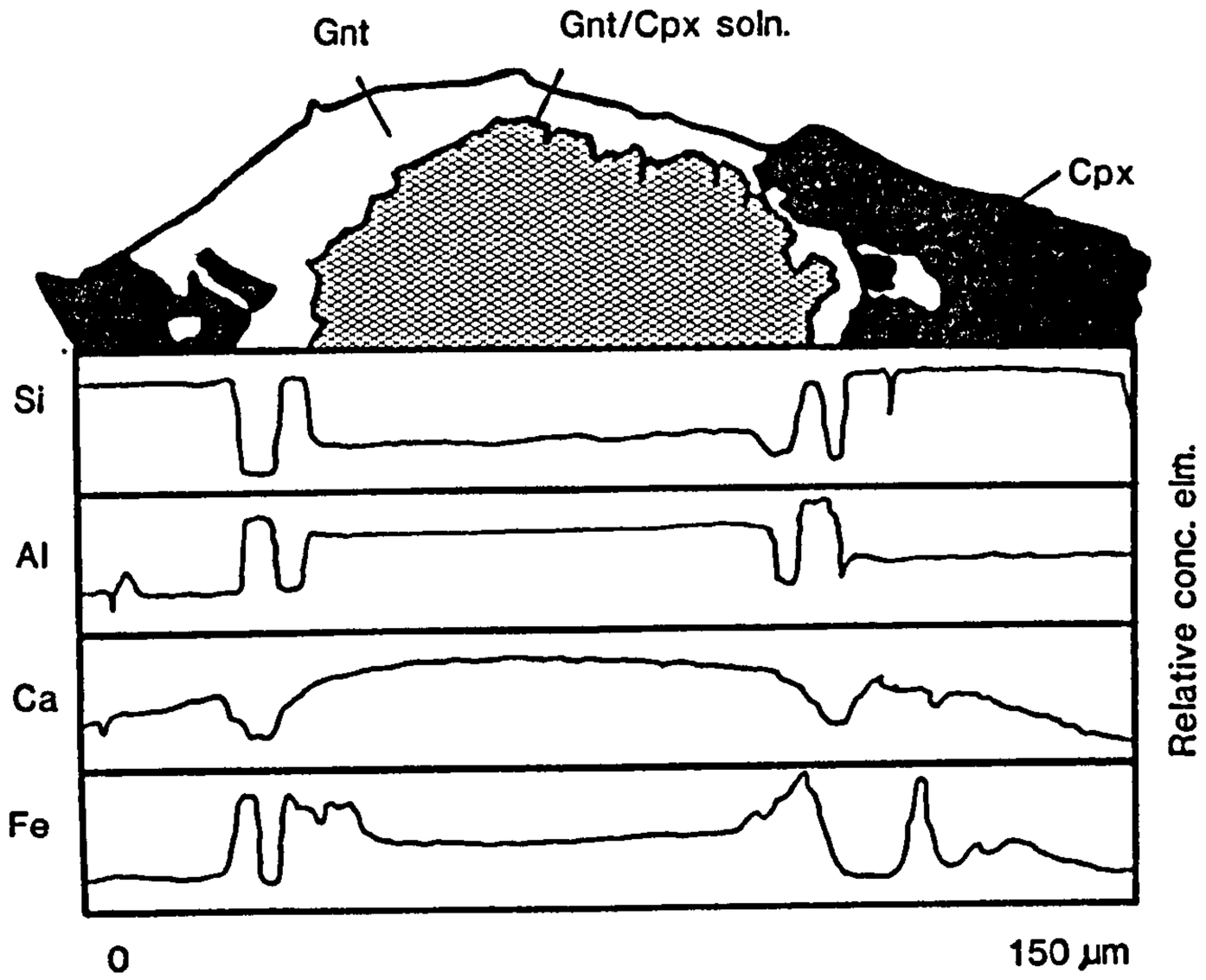
Gnt
Gnt/Cpx soln.
Cpx
Si
Al
Ca
Fe
0
150 μm
Relative conc. elm.

Fig 6.14

Element Distribution in Composite Grains.

The aluminium and silicon contents of garnet show sharp changes in concentration across phase boundaries. The core of high silica garnet has high silicon and low aluminium which changes to low aluminium and high silicon in an area of pyroxene immediately surrounding the core. These values change to lower silicon, higher aluminium in the normal silica garnet. Calcium and iron show more shallow compositional gradients. Calcium concentrations increase into the high silica garnet while the iron content of high silica garnet increases close to the boundaries with jadeite rich pyroxene.

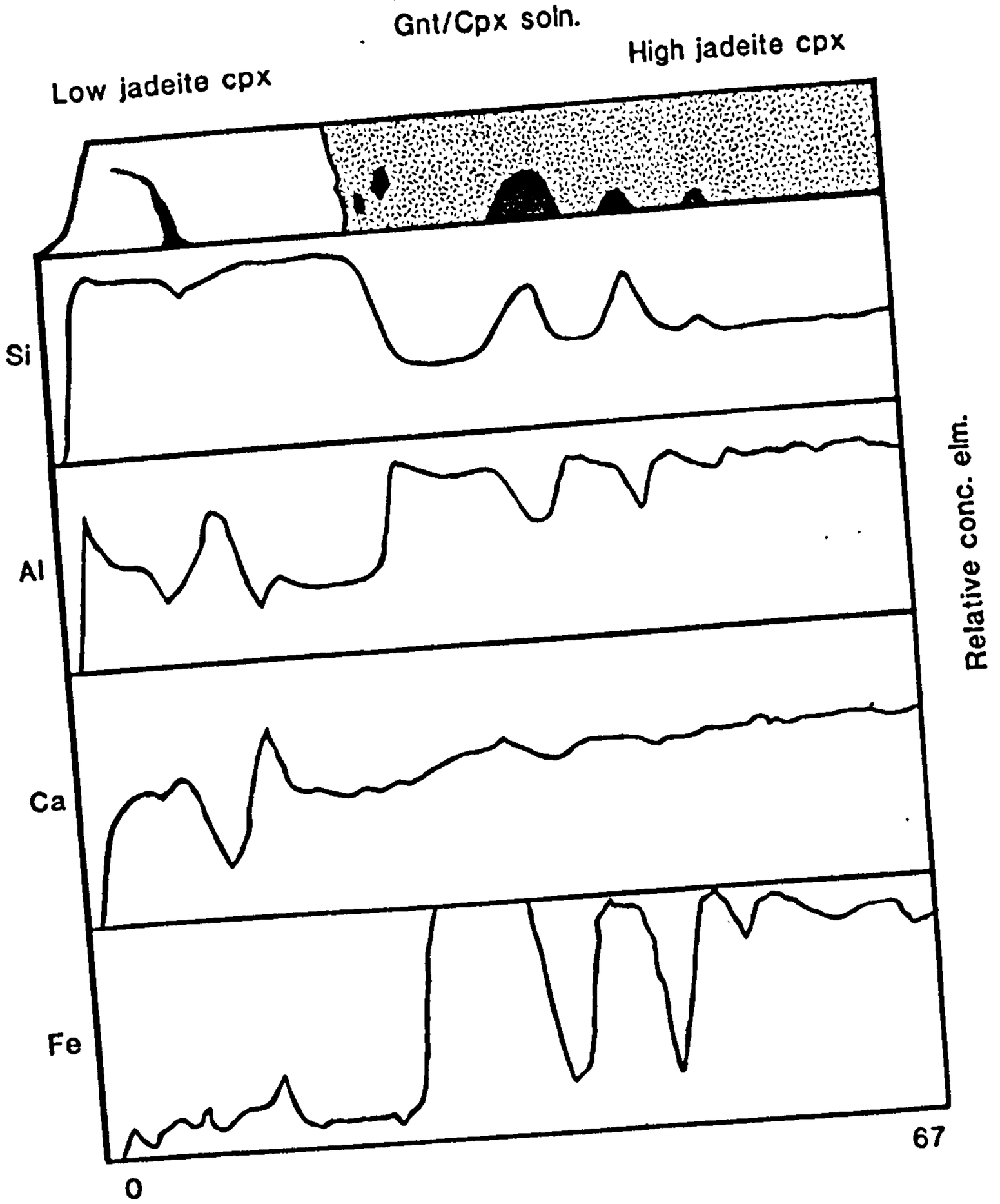
Gnt/Cpx soln.
High jadeite cpx
Low jadeite cpx
Si
Al
Ca
Fe
0
67
Relative conc. elm.

Fig 6.15

Element Distribution in Composite Grains.

Aluminium and silicon show sharp, steep compositional gradients across the boundaries between the high silica garnet and pyroxene phases, although the boundaries are less steep than in Fig 6.14. Partly this is due to breakdown of high jadeite pyroxene by diffusion of aluminium and silicon which modifies the distribution of elements. Calcium shows a compositional profile that increases into the high silica garnet phase, while the iron content is constant in the garnet phase.

6.6 Phase Relationships and Temperature.

The two major divisions of the garnet inclusions from the Sao Luiz mine are based on the silica to oxygen content. For garnet this ratio is 1:4 and for pyroxene this is 1:3. A close chemical association between the two phases is also known from experimental work (e.g O'Hara & Yoder, 1967) principally because aluminium can enter into pyroxene. Ringwood (1967) has shown that at high pressures pyroxene becomes soluble in garnet and at very high pressures the pyroxene is completely dissolved in a garnet-structured phase. The pyroxene solid solution begins at approximately 95kbar and is completed at 150kbar. For the system $MgO\text{-}Al_2O_3\text{-}SiO_2$, the pyroxene component enters garnet as follows:

$$Mg^{[8]}(Mg,Si)^{[6]}Si^{[4]}{}_3O_{12}$$

The silicon of the pyroxene enters into octahedral coordination; these sites are normally occupied by aluminium in the garnet structure. Ringwood has shown that these relationships apply to the systems of $MgO\text{-}Al_2O_3\text{-}SiO_2$ and $CaO\text{-}Al_2O_3\text{-}SiO_2$ and also in more complicated, natural, systems such as eclogite.

The solid solution of garnet and pyroxene occurs with silicon entering the octahedral sites in a garnet structure. The measurement of the activity of garnet end members enables the degree of solid solution, and hence pressure to be determined. For magnesian end members this is:

$$a^{py}_{grt} = (X_{Mg})^3(X_{Al})^2$$

Where aluminium completely occupies the octahedral site the term X_{Al} will be equal to one, which should be the case for normal-silica garnets. As solution increases the value of X_{Al} will decrease linearly and for example at 0.5 the solution consists of 50% of garnet and 50% pyroxene.

The X_{Al} values for the Sao Luiz garnets show a range between 0.9 and 0.75 for the Group II garnets, which indicates formation over a range of pressures between 110 and 130kbar, equivalent to 330 and 390km.

Table 6.4

Temperature estimates for Group IIB Inclusions.

	Fe/Mg_{GT}	X_{Ca}	Fe/Mg_{PX}	LnK_D	T^oC
1	0.60	0.29	0.25	0.85	1345
2	0.47	0.18	0.23	0.69	1312
12	0.71	0.34	0.29	0.89	1376
13	0.53	0.14	0.27	0.66	1282
14	0.58	0.27	0.25	0.85	1342
15	0.67	0.33	0.42	0.47	1665
18	0.76	0.36	0.39	0.65	1558
24	0.61	0.25	0.31	0.88	1362
25	0.78	0.36	0.42	0.62	1589
34	0.69	0.36	0.29	0.87	1399
37	0.59	0.21	0.31	0.65	1379
39	0.80	0.20	0.40	0.67	1351
42	0.83	0.31	0.37	0.62	1405

Table 6.5

Temperature estimates for Group IIB Inclusions.

Fe/Mg_{GT}	X_{Ca}	Fe/Mg_{PX}	LnK_D	T^oC
10	0.70	0.39	0.49	0.38	1822
19	0.44	0.29	0.28	0.43	1631
21	0.43	0.33	0.38	0.12	1991
22	0.66	0.37	0.40	0.51	1668
29	0.64	0.27	0.39	0.50	1565
43	0.42	0.28	0.28	0.43	1632
48	0.46	0.30	0.28	0.49	1613

Temperature Estimates

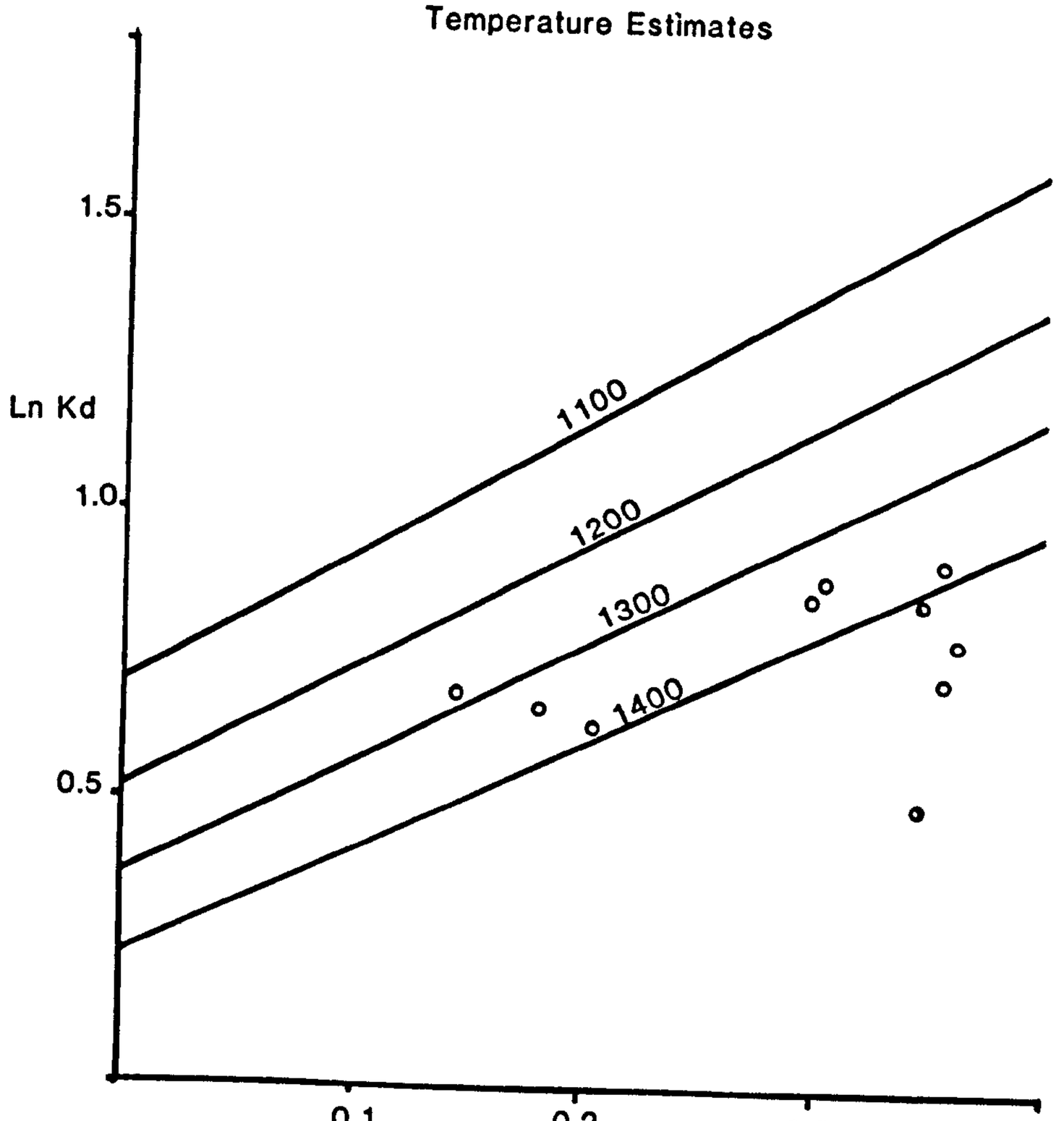

Fig 6.16

Temperature Estimates.

Shown are lnK_D and $X_{x\alpha}$ values for Group IB inclusions which have garnet of normal-silica content coexisting with pyroxene in the same inclusions. Temperature estimates are based on the geothermometer of Ellis and Green (1979). The precision of electron microprobe analyses (see Appendix 5) means that the temperature estimates are accurate to $\pm$ 25°C, whilst the uncertainty of the geothermometer itself means that the estimates are only accurate to $\pm$ 70°C (see Carswell and Gibb, 1987)

The temperatures of equilibration for the composite inclusions from Sao Luiz have been estimated using the geothermometer of Ellis and Green (1979), corrected for calcium. Thirteen inclusions from Group IB were studied (see figure 6.16 and Table 6.4). The range of K_D values corresponds to a range of temperatures of 1282 to 1665^{o}C. All but one of the K_D values indicate temperatures in excess of 1300^{o}C. The temperature of the asthenosphere is believed to have values between 1350 and 1500^{o}C for depths of 100 and 400km (see for example McKenzie, 1984), and the temperature estimates for the Group IB inclusions are therefore quite consistent with an asthenosphere origin. The temperature estimates all provide equilibration temperatures above the values of the closure temperature (1150^{o}C) of Harte and Sautter (1988).

The temperature estimates for seven Group IIB inclusions using the same method gave a range of temperature values from 1613 to 1991^{o}C (Table 6.5). The Fe-Mg partitioning behaviour between high-silica garnet and pyroxene is unknown and the actual temperatures of equilibrium for these inclusions may differ substantially from these estimates. However the high temperature estimates are, to some extent, compatible with the high pressure of origin indicated by the silica content of these inclusions. Temperatures at the base of the asthenosphere, assuming an adiabatic gradient of 0.6 ^{o}C/km are would be 1500 to 1600^{o}C. Both the pressure and temperature estimates for the garnet inclusions favour an origin for the Sao Luiz diamonds within the asthenosphere.

6.7 Trace element analyses.

Four homogeneous inclusions of Groups IA and IIA were studied for trace element concentration using O^- ions in the Cameca IMS 4F ion microprobe at Edinburgh. A comparison was made with the trace element contents of peridotite suite garnets from diamonds (Shimizu & Richardson, 1987) as well as garnet nodules and melt residues (Shimizu & Allegre, 1978; Prinzhoefer & Allegre, 1985).

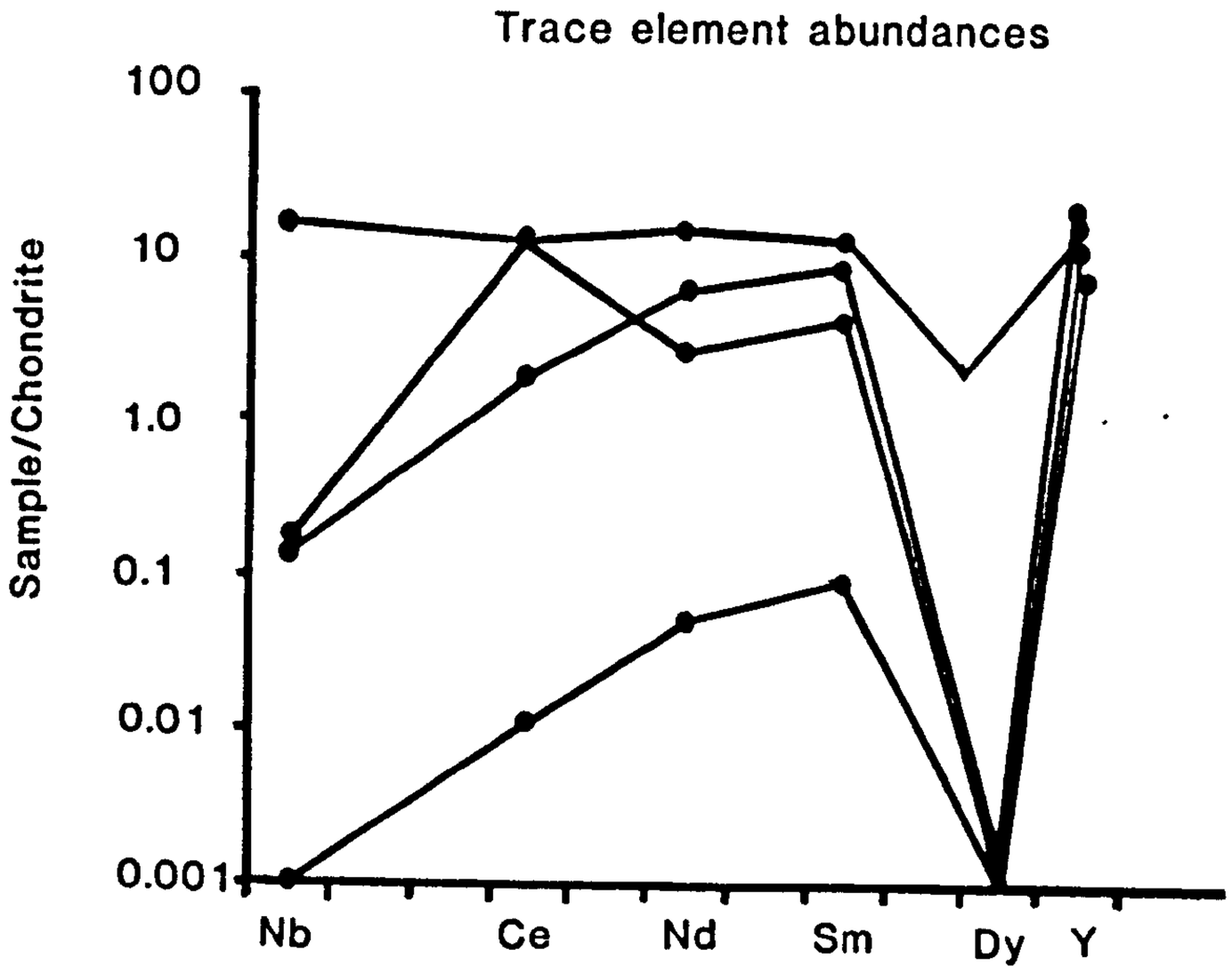
Trace element abundances
Sample/Chondrite
100
10
1.0
0.1
0.01
0.001
Nb
Ce
Nd
Sm
Dy
Y

Fig. 6.17.

Trace element Abundances.

These trace element analyses of Group IA and IIA inclusions were determined by ion microprobe analysis using a O- primary ion beam.There are a variety of patterns from LREE depleted patterns to patterns enriched relative to chondrites (C1). The variability of trace element patterns shown below does not correlate with variability of major element chemistry. All the inclusions examined are also rich in HFSE (High Field Strength Elements) such as Zr and Ti.

	BZ20	BZ23	B12	BZ38	Precision
Ti	6899.64	10726.12	10167.62	5224.89	4.81
Y	18.06	36.74	36.01	19.55	0.49
Zr	213.34	211.31	125.56	63.94	1.71
Ce	0.01	8.73	1.95	7.73	0.01
Sm	0.10	1.02	2.15	2.02	0.01
Dy	0.00	nd	nd	0.48	0.11
Tb	0.02	0.01	0.02	0.02	0.0.01
Nd	0.04	2.35	4.56	6.65	0.38
Nb	0.13	0.13	0.08	6.47	0.11

The inclusions BZ20 and BZ12 are Group I and BZ23 and BZ38 are Group II.

From the four traces no single pattern of trace element concentrations was established and the concentrations ranged from very depleted to enriched patterns. The results are shown in figure 6.17. The variable HFSE (High Field Strength Elements, such as Zr and Ti) patterns are different from the predicted world-wide depleted pattern of HFSE in the mantle which Salters and Shimizu (1988) have suggested. In addition LREE (Light Rare Earth Elements) have patterns which vary from depleted to enriched compositions.

Although the inclusions studied were homogeneous the three dimensional relationships are unknown. Some of the inclusions may be composite with pyroxene. Therefore the LREE and HFSE may not represent the equilibrium conditions of formation but redistribution of elements following enclosure by the diamond.

6.8 Nitrogen and Carbon Characteristics of Garnet-Bearing Diamonds.

Unfortunately most of the garnets studied had already been removed from their enclosing diamond and this material was not available for study. Ten diamonds containing eclogite paragenesis garnets were examined. After determination of colour, morphology and surface features, the inclusions were extracted, and the fragments of these diamonds were retained for a preliminary study of nitrogen aggregation and carbon isotope analysis by the methods outlined in Chapter 2.

All the diamonds were brown and showed rounded surfaces on which plastic deformation lines were visible. Seven diamonds were macles and the remaining three were octahedra. A high degree of crystallographically controlled etching was observed in the form of trigon etch pits. The etch pits were frequently found to be close to macle lines and other planes of weakness, such as broken cleavage surfaces. The etch included hexagonal pits and also pyramidal pits with apices oriented along the four fold crystal directions.

Table 6.6

Cations in Garnet Inclusions from Ten Sao Luiz Diamonds.

Sample	Si^{4+}	Al+Cr+Ti	R^{2+}+Na
121	2.98	1.95	3.06
122	3.13	1.72	3.15
123	2.99	1.93	3.08
124	3.05	1.77	3.17
125	3.05	1.81	3.08
126	2.97	1.98	3.03
127	3.13	1.75	3.03
128	2.96	1.99	3.04
129	3.12	1.83	2.99
130	2.96	1.99	3.09

Table 6.7

Temperature Estimates for Three Group IB Inclusions.

	Fe/Mg_{Gt}	X_{Ca}	Fe/Mg_{Px}	lnK_D	T^oC
121	0.77	0.34	0.27	1.05	1297
123	0.82	0.40	0.31	0.97	1412
126	0.78	0.45	0.14	0.97	1458

The inclusions were pale to dark orange in colour and had an imposed cubo-octahedral morphology. The chemical analyses for these inclusions are shown in Appendix 3. Six of the inclusions are Group I and four are Group II. Three of the Group I inclusions are composite (Group IB) and consist of garnet and pyroxene with a 20 mol.% jadeite content in the latter,the remaining three are homogeneous. Only one Group II inclusion is composite and this consists of a high-silica garnet with a pyroxene of 20 mol.% jadeite content, the remaining three Group II inclusions are homogeneous. The composite inclusions of both groups show textures of category 2 and 3 (see above) there being little evidence for sub-solidus decomposition of the high-silica garnets.

In Table 6.6 the number of Si atoms per 12 oxygens are compared with the number of Al, Ti and Cr cations and also the number of R^{2+} and Na cations. As shown earlier the excess Si enters into octahedral coordination in the Group II inclusions. From Table 6.6 the number of R^{2+} and Na cations in the Group II garnets exceeds the number of cubic sites available in garnet structure and some of the excess divalent cations probably enter into the octahedral sites to maintain a charge balance.

The temperature of formation of the three Group IB inclusions has been estimated using the method of Ellis and Green, to enable the a direct comparision to be made with the compositie inclusions described above. Table 6.7 shows the temperature estimates for the three Group IB inclusions. A range of values of equilibration temperatures of 1297 to 1412^{o}C were calculated (for 50kbar) and these are again compatible with an asthenosphere origin for these inclusions.

The infra red studies of these ten diamonds show a total nitrogen concentrations range from 76 to 271ppm. All of the diamonds are Type IaA, with 1282/1180 ratios greater than 0.3. The amount of IaB nitrogen present in each diamond varies and, as shown in Appendix 3, all but two of the diamonds have 1282/1180 ratios of less than 1.0, indicating a high IaB content. Three of the

diamonds contain composite inclusions which enable temperatures of equilibration to be made, and the time taken to aggregate the IaB nitrogen in these three diamonds can therefore be calculated using the procedure shown in Chapter 4. These calculations give periods of 76 to 152 million years to aggregate the IaB nitrogen present and imply only a very short residence time at high temperatures.

The carbon isotope composition of the ten diamonds showed a range in δ ^{13}C values of between -6.42 $^{o}/_{oo}$ and -12.57 $^{o}/_{oo}$ vs PDB, as shown in Appendix 3 and seen in figure 6.18. In the 6 normal-silica garnets the mean δ ^{13}C value is -9.52 $^{o}/_{oo}$ (with a range of values from -6.70 to -12.57$^{o}/_{oo}$). In high-silica garnets there is a narrower range of values from -6.70 tp -10.98 $^{o}/_{oo}$) the mean δ ^{13}C value for diamonds being -8.18 $^{o}/_{oo}$. All the δ ^{13}C values are isotopically lighter than the average mantle (-5 $^{o}/_{oo}$).

If the carbon in the athenosphere has the isotopic value of -5 $^{o}/_{oo}$ then the light δ ^{13}C values for the Sao Luiz diamonds may have resulted from isotopic fractionation processes, such as those described in Chapter 4. Alternatively if the asthenosphere is extremely heterogeneous the 10 results may indicate a several limited carbon reservoirs of different isotopic compositions. Because the sample of diamonds analysed for δ ^{13}C was so small the true distribution of carbon isotopic compositions is unknown. If the light isotopic values are a function of fractionation processes then the Δ_{V-C} value must be close to 5, in order to produce the δ ^{13}C value of -11 $^{o}/_{oo}$ from a mean mantle source. Deines (unpubl.) has recorded two groups of δ ^{13}C in diamonds which contain high-silica garnets from Jagersfontein. The high-silica garnets at Jagersfontein have very ^{13}C depleted signatures around -21 $^{o}/_{oo}$, while normal-silica garnets are more ^{13}C enriched (-6 $^{o}/_{oo}$). It is unlikely that the range in isotope compositions for Sao Luiz and Jagersfotein could have been produced by any known upper mantle fractionation process for carbon with a mean composition of -5 $^{o}/_{oo}$. The most likely explanation for the range in carbon isotope compositions therefore is that in the asthenosphere carbon is derived

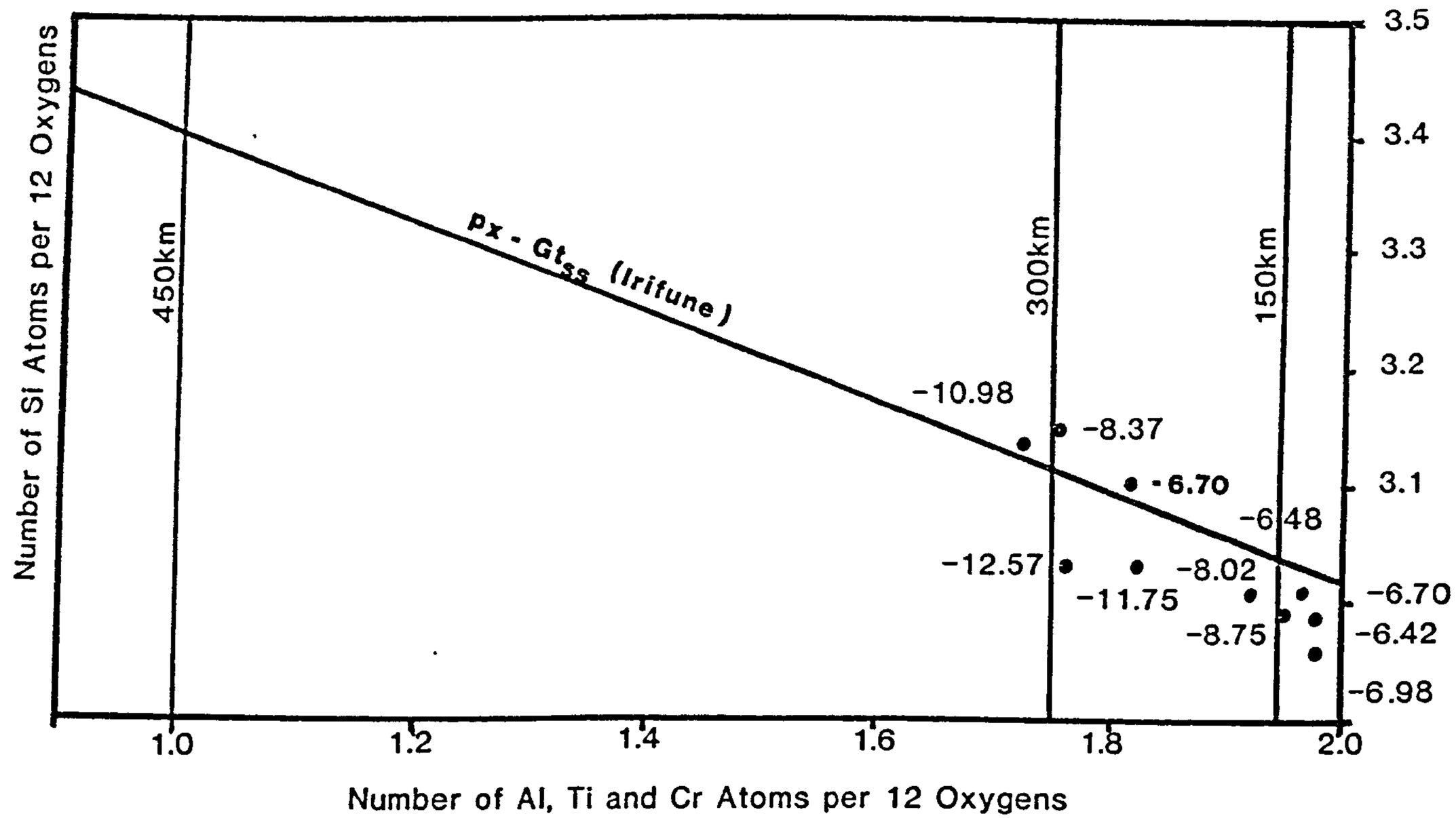
Number of Si Atoms per 12 Oxygens
3.5
3.4
3.3
3.2
3.1
450km
300km
150km
px - Gtss (Irifune)
-10.98
-8.37
-6.70
-6.48
-12.57
-8.02
-11.75
-8.75
-6.70
-6.42
-6.98
1.0
1.2
1.4
1.6
1.8
2.0
Number of Al, Ti and Cr Atoms per 12 Oxygens

Fig 6.18.

Degree of Solid Solution of Pyroxene in Garnet.

The solid solution of pyroxene in garnet is shown by an increase in silicon in octahedral coordination, shown by a decrease in aluminium content. The result of experiments by Irifune are shown compared with some compositions from Sao Luiz garnets. Also shown are $\delta\ ^{13}C$ values which show a significant variation with depth of origin, garnets derived from relatively shallow depths have a limited range of $\delta\ ^{13}C$ at -6 $^{o}/_{oo}$, deeper origin garnets have lighter carbon isotope signatures.

from a limited number of reservoirs of different isotopic compositions.

6.9 Origin of Sao Luiz Garnet-like Inclusions.

The garnet-like inclusions from Sao Luiz have several features that suggest a deep origin, probably within the asthenosphere.

1. The garnet-like inclusions from Sao Luiz have complicated chemistries. Two main divisions are made on the basis of silica content. The high-silica garnets represent complicated solid solutions between pyroxene and garnet. Silicon atoms enter into octahedral sites in the garnet structure, with titanium and divalent cations (Mg and Fe) also entering these sites. Monovalent sodium and divalent calcium are probably restricted to eightfold sites, since their ionic radii are too large to permit entry into the octahedral sites.

2. Some of the inclusions are composite and contain garnet and pyroxene in the same inclusion. In these composite grains the garnet and pyroxene phases cannot be produced by the decomposition of an initial high-silica garnet, and it is concluded that the pyroxene and garnet were incorporated into the diamond separately. Some composite grains show evidence for re-equilibrium in the form of small segregations of garnet and pyroxene which overprint the Si and Al distributions between the main garnet and pyroxene-rich phases.

3. The silica contents of the garnet-like phases indicate a range of depths of origin from pressures of 65kbar to 150kbar, equivalent to depths of 180 and 450km, which are considered to be asthenospheric. The temperatures of equilibrium of composite inclusions with normal-silica garnet show a range from 1282 to 1616^{o}C. The temperature estimates are also compatible with an asthenosphere origin.

4. A preliminary study of the nitrogen and carbon characteristics of the Sao Luiz diamonds shows variable nitrogen aggregation states and light isotopic compositions. The diamonds showed a high amount of Type IaB nitrogen, again compatible with an asthenosphere origin, at high temperature. The carbon isotope compositions show a range of $\delta\ ^{13}C$ values that are all lighter than the assumed mean mantle $\delta\ ^{13}C$ value of -5 $^{o}/_{oo}$. Data from Jagersfontein mine shows an even greater range in $\delta\ ^{13}C$ for similar inclusions. Although it is possible that the $\delta\ ^{13}C$ values may be a result of isotope fractionation processes, it is more likely that the different isotopic values indicate a number of limited reservoirs within the asthenosphere, each with a separate isotopic value.

In conclusion it is suggested that the Sao Luiz garnet-bearing diamonds originate within the asthenosphere from a range of depths between 180 and 450km. Temperature estimates show a high temperature of origin consistent with the asthenosphere. Garnet and pyroxene phases were probably separate before inclusion into the diamond, although some may have undergone subsequent sub-solidus re-equilibration following enclosure. Although the carbon isotopic data is limited it is also suggested that a number of isotopically distinct carbon reservoirs exist in the asthenopshere.

Chapter 7.

Non Garnetiferous Inclusions from Sao Luiz.

7.1 Introduction.

In addition to the garnetiferous inclusions described in Chapter 6, another parcel of 462 diamonds from Sao Luiz was studied for inclusions. The diamonds ranged in size from -9+7 to -4+3. Table 7.1 shows the inclusion abundances in these diamonds as estimated by optical examination. As shown in Table 7.1 the inclusions are divided into peridotite and eclogite, with the peridotite suite dominated by colourless inclusions and those containing more than one inclusion (multiple). The eclogite suite inclusions are dominated by oxides. Sulphide-bearing diamonds are also common. There are no orange garnet inclusions in these diamonds and therefore no direct evidence of the relationship to the garnet inclusions discussed in Chapter 6, because garnet-bearing diamonds had been removed from this parcel prior to study.

A preliminary study of 50 diamonds from the parcel of 462 was made. The diamonds were chosen randomly from peridotite, eclogite and sulphide-bearing diamonds. The diamonds chosen contained inclusions as follows; ten with colourless inclusions, ten with more than one inclusion, twenty containing oxide inclusions and ten containing sulphides. At the subsequent analytical stage the sulphide-bearing diamonds were found to contain oxides. Their appearance prior to removal was related to their location in black rosette fractures, a characteristic of sulphide-bearing diamonds.

In addition to the inclusion study all of the 462 diamonds were examined for their colour, morphology and surface features; these observations are summarised in section 7.2. The chemistry of the inclusions is discussed in sections 7.3 and 7.4.

Table 7.1

Optically Estimated Abundances of Sao Luiz Inclusions.

		No.	%
Peridotite.			
	Colourless	133	28
	P. Gnt	0	0
	Cpx	6	1
	Chromite	0	0
	Multiple	87	19
Eclogite.			
	Orange Gnt.	0	0
	Cpx	0	0
	MgO-FeO	155	34
	Multiple	12	3
Sulphides.		64	14
Clouds.		5	1

Table 7.2

Colour and Morphology of Sao Luiz Diamonds

	Octa (%)	Macles (%)	Aggr. (%)	Irreg. (%)
Colourless	11	34	0.5	0.2
Yellow	5	20	0	0.2
Brown	6	21	0.7	0.5
Total	22	75	1.3	0.9

7.2 Morphology, Colour and Surface Features.

The morphologies of the 462 inclusion-bearing diamonds from Sao Luiz are summarised in Table 7.2. Most of the diamonds are macles (75%), while 22% are octahedra. Aggregates and irregular diamonds form the remaining 3%. 46% of the diamonds are colourless, with brown diamonds (25%) and yellow-brown diamonds (27%) also being important. The yellow-brown colour of the Sao Luiz diamonds is unusual because it is not a true body colour but is probably due to staining of internal fractures by iron oxides. The oxides result from the alteration of magnesiowustite inclusions (MgO-FeO) to haematite (Fe_2O_3) and magnetite (Fe_3O_4) (see later).

Forty three of the fifty diamonds studied showed plastic deformation. Thirteen of these diamonds were brown and twelve had a yellow-brown body colour, both these groups showed plastic deformation features. The remaining twenty five diamonds were colourless and only eighteen were plastically deformed.

All except one of the diamonds showed evidence of crystallographic etch. The etch patterns include negative trigons and hexagonal etch pits, with the hexagon edges parallel to the (111) growth direction. Some pyramidal pits were also observed with apices of the pyramids parallel to the (100) direction and edges of the pits parallel to the (111) direction. Frequently the etch pits were concentrated along weaknesses such as plastic deformation lines.

7.2 Oxide inclusions.

In Table 7.3 the number of oxide inclusions identified by microprobe analysis are shown compared with the number of oxide inclusions identified optically. In total 24 oxides were analysed, this includes 18 from the original 20 oxide bearing inclusions, 6 inclusions initially identified as sulphides. The diamonds ranged in size from -9+7 to -6+5, three of the diamonds were colourless

Table 7.3

Inclusion Abundances at Sao Luiz.

	Colourless	Multiple	Oxide	Sulphide
No. of Diamonds	10	10	20	10
Inclusions recovered				
Colourless	8	3	0	0
Multiple	0	1	0	0
Oxide	0	0	17	0
Sulphides	0	0	6	0
Inclusion lost	2	6	3	4

octahedra, the remaining 21 were macles. 11 of the macles were colourless, while 5 were brown and 5 had a yellow-brown colour. The magnesiowustite analyses are summarised in Appendix 4.

Whilst in the diamonds the magnesiowustites had an iridescent, blue-green appearance, but when released they had a black to dark brown body colour. The inclusions were all cubo-octahedra with a maximum dimension of 200μm. Frequently, the inclusions were surrounded by fractures and in some cases, where the fractures extended to the diamond surface, alteration had occurred. Care was taken to avoid analysing such inclusions and, with one exception, the inclusions analysed were unaltered.

Microprobe analyses of the inclusions showed them to be solid solutions between MgO and FeO and accordingly these are termed magnesiowustites. They showed a range of Fe/Fe+Mg values from 0.16 to 0.61, giving an FeO/FeO+MgO content of 0.32 to 0.72. In addition to FeO and MgO, up to 1.0 wt.% Cr_2O_3 and 0.2 wt.% Al_2O_3 are present. There is little evidence for correlation between the iron and magnesium contents and the aluminium and chromium contents. Both aluminium and chromium contents are shown in figure 7.1. As shown in figure 7.2 nickel concentrations of up to 1.0 wt.% NiO were determined. The nickel contents do not vary systematically with iron and magnesium content and both high and low nickel values occur in inclusions with similar iron contents. In 11 of the magnesiowustite inclusions were, discrete inclusions (<2μm) of nickel-iron metal (with approximate compositions of Fe 70:Ni 30). The analyses for such magnesiowustites invariably show high totals (see Appendix 4) in response to there being too much Ni^{2+} to balance the oxygen calculated during microprobe analysis. Accordingly it is possible that some of the nickel may in fact be present as metal rather than oxide (see Chapter 8),

One sample of magnesiowustite was altered to more oxidized phases, most probably due to contact with external fluids. The altered

Magnesiowustite Composition

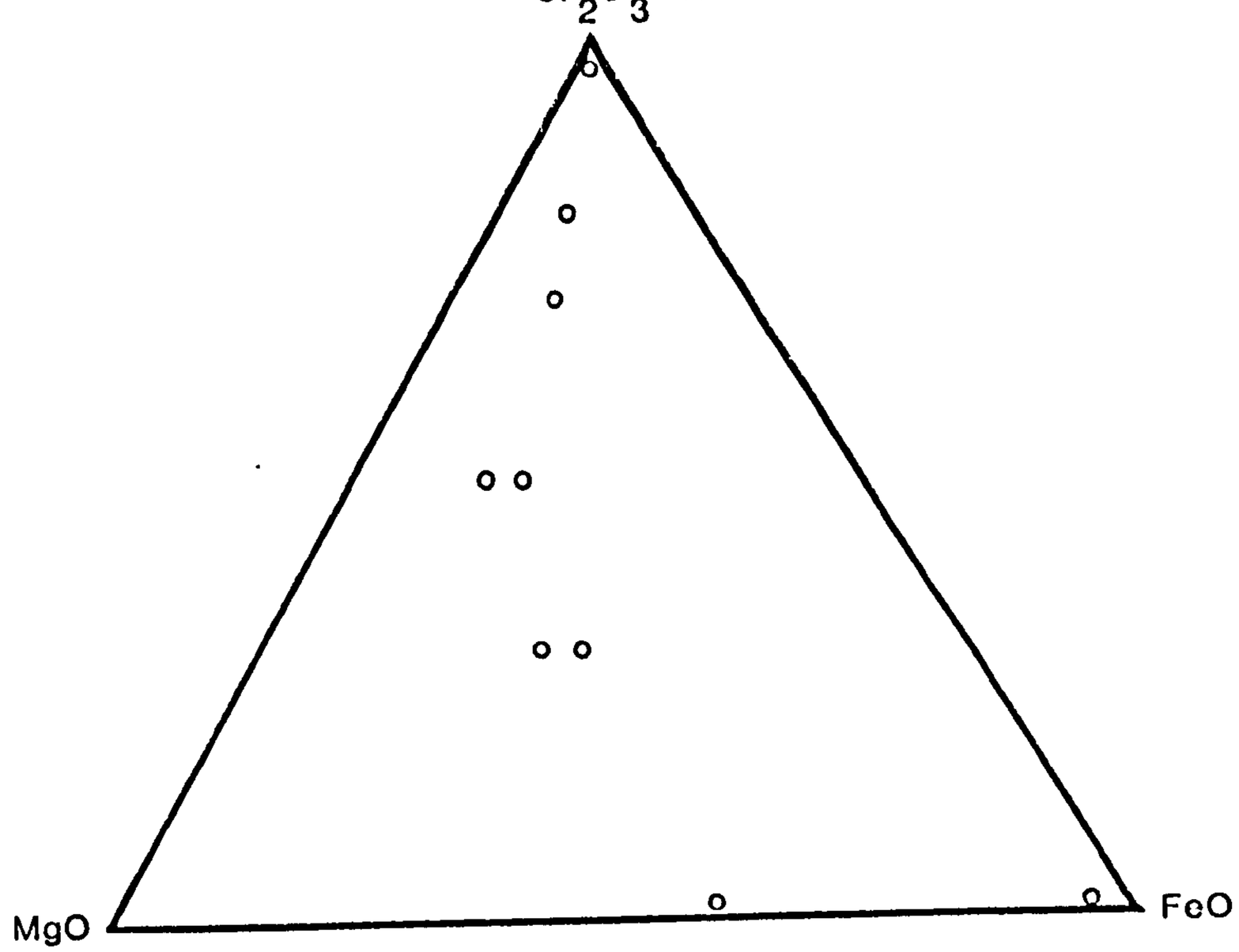

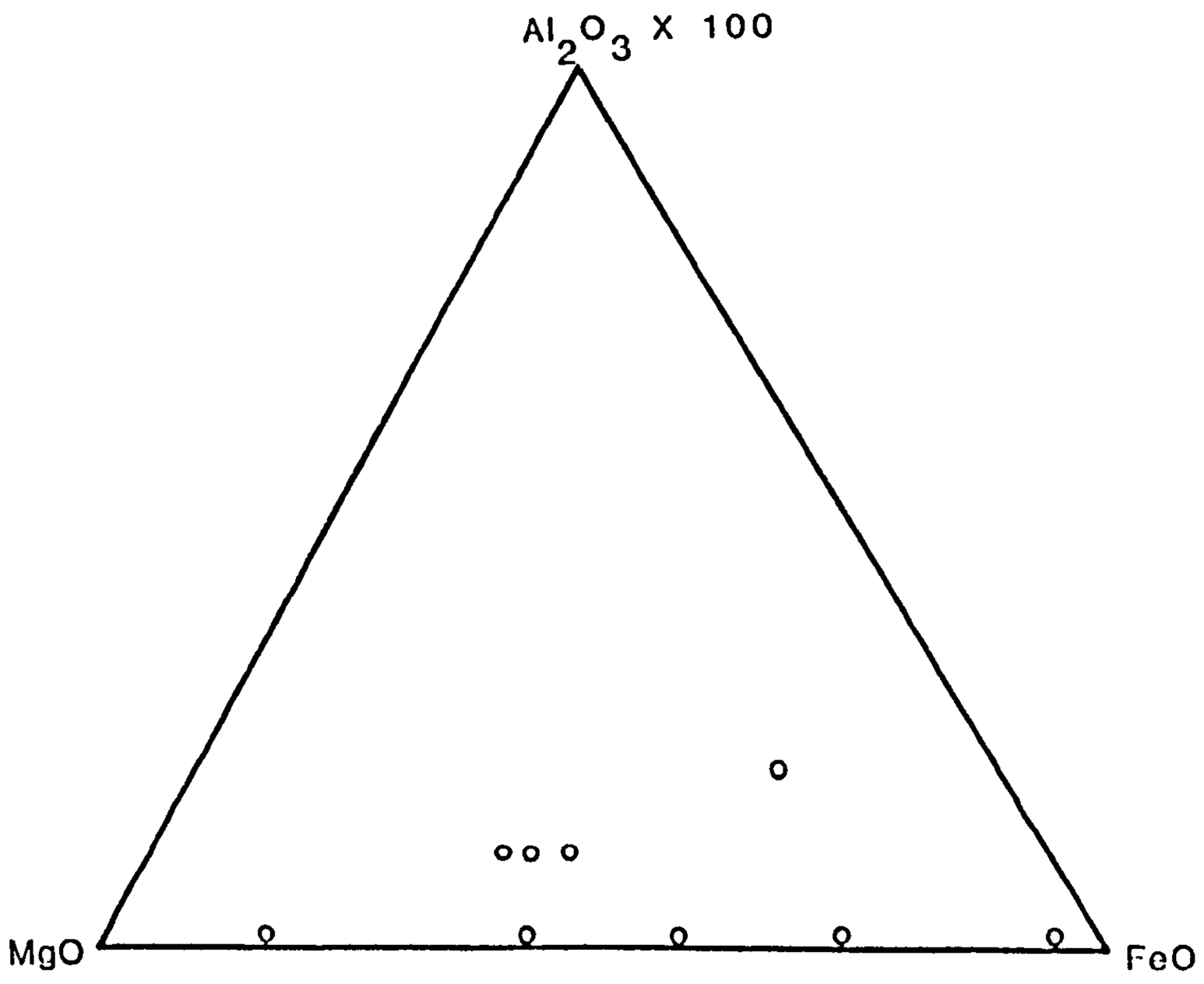

Fig. 7.1.

Magnesiowustite Compositions.

MgO, FeO, Cr_2O_3 and Al_2O_3 contents of magnesiowustite inclusions from Sao Luiz. The chrome contents are highest in the inclujons that show the highest MgO contents. Aluminium is high in the inclusions that have high iron contents. The amount of aluminium is insufficient to replace all of the chrome and so there is not a simple substitution of aluminium for chrome with increased iron.

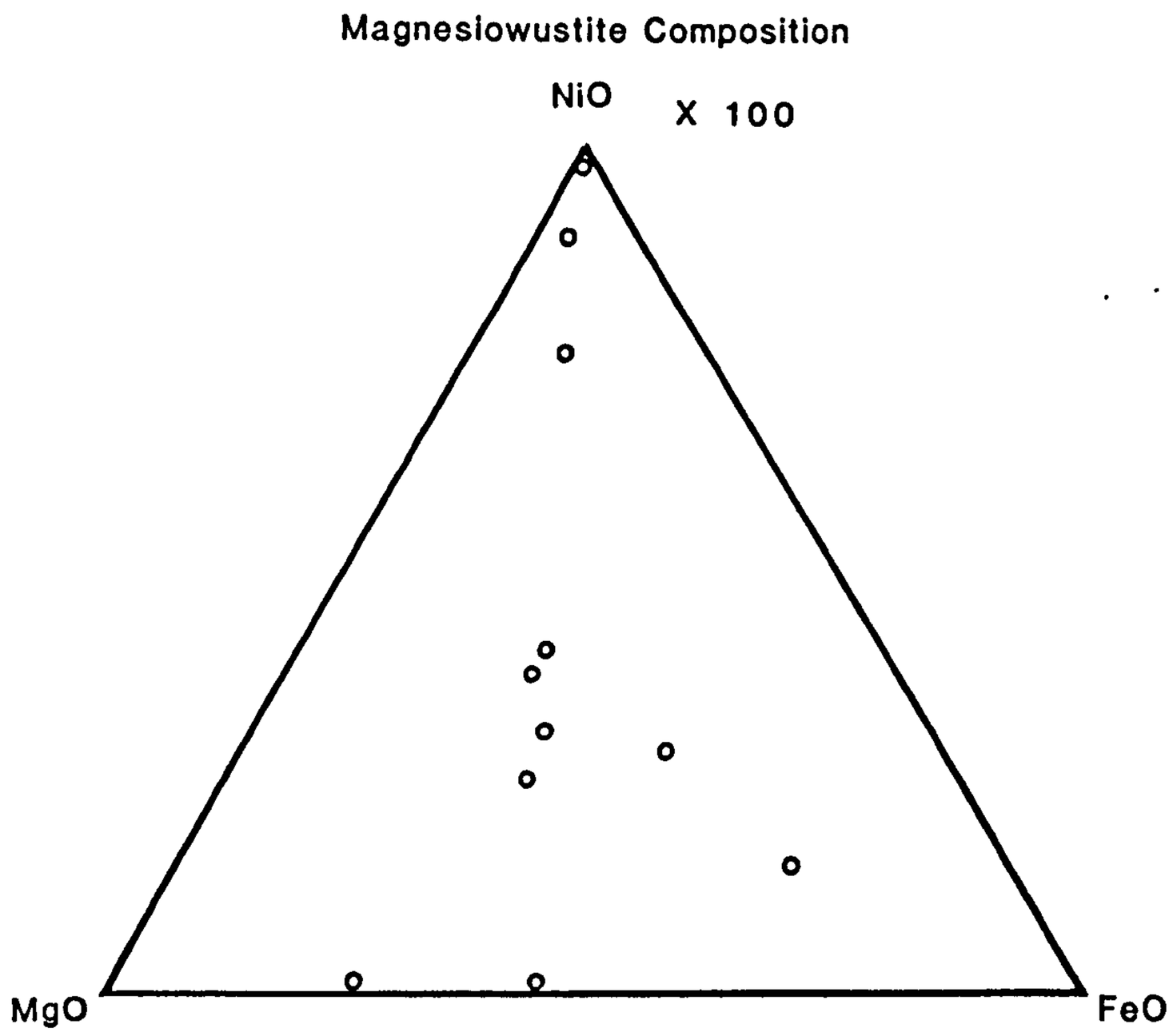
Magnesiowustite Composition
NiO
X 100
MgO
FeO

Fig 7.2.

Magnesiowustite Compositions.

MgO, FeO and NiO contents of magnesiowustite inclusions from Sao Luiz are shown. The inclusions show a wide range in FeO and MgO contents and also a significant variation in NiO content. There is no systematic variation of NiO with FeO content and inclusions of similar iron content show varied Ni contents

inclusions contained both haematite (Fe_2O_3) and magnetite (Fe_3O_4), which form two halves of the inclusion.

Magnesiowustites have been documented in diamonds from four other localities: Orroroo in South Australia (Scott-Smith *et al.*, 1984); at Monastery and Koffiefontein in South Africa (Gurney *et al.*, 1989) and at Sloan, a kimberlite on the Colorado-Wyoming State Line district of the U.S.A. (Otter *et al.*, 1989). At Orroroo the magnesiowustite inclusions showed an average FeO/FeO+MgO content of 0.21. The example from Monastery mine was very iron rich with a value of 0.93 but at Koffiefontein, three magnesiowuistite inclusions had values of 0.21. The magnesiowustite inclusions from Sloan had values of 0.19. The range of FeO/FeO+MgO values at Sao Luiz varies between 0.23 and 0.74, demonstrating a very much greater range of composition particularly towards Fe enrichment with the exception of the single inclusion from Monastery.

7.4 Colourless inclusions.

Of the original ten diamonds 8 inclusions were recovered. In addition three inclusions were recovered from diamonds containing multiple inclusions. The inclusions showed a variety of compositions which include $CaSiO_3$ (6), pure silica (SiO_2)(2), diopside ($CaMgSi_2O_6$)(1), olivine ($(Mg,Fe)_2SiO_4$)(1), two silicon carbide (SiC) inclusions and one unidentified calc silicate. Special attention was paid to extraction and recovery procedure for all the inclusions. These inclusions are all considered to be syngenetic.

The six inclusions of $CaSiO_3$ composition are facetted cubo-octahedra which luminesced a faint yellow colour during microprobe analysis. Their compositions are very pure with a limited amount of magnesium (0.46 wt.%), trace amounts of Ti (0.02 wt %) and Fe (0.08 wt.%), although the latter values are close to the WDS detection limits of electron microprobes. Although the inclusions have a $CaSiO_3$ composition, the mineral structure is unknown.

The silica inclusions do not have a cloudy, amorphous appearance that would be expected from an epigenetic inclusion but are transparent and have an imposed morphology. The 2 inclusions recovered have a very pure composition and consist of SiO_2 with small amounts of MnO (0.01 wt.%), FeO (0.07 wt.%) and Al_2O_3 (0.04 wt.%), these latter values are again close to the WDS detection limits. Using a Weissenburg X-ray camera with Ni filtered Cu radiation one of the SiO_2 was identified as α quartz. As α quartz is not stable at the same pressures as diamond the implication is that this inclusion is epigenetic. The colour of the inclusion and the very careful way in which the inclusion was recovered from the diamond suggests a primary origin and may indicate that the silica phase has inverted from a high pressure phase (stishovite or coesite). The second silica inclusion coexisted with magnesiowustite which has an MgO/MgO + FeO ratio of 56%.

One of the colourless inclusions analysed had an end member diopside composition with only 0.2 Fe atoms present in the pyroxene formula (6 oxygens). No other minor elements were detected and the crystal system was undetermined.

The single olivine present has a composition of Fo_{85}, the olivine also contains significant manganese (0.13 wt.%), calcium (0.14 wt.%) but limited chrome (0.04 wt.%). The crystal system is again undetermined. The composition is much more iron rich than olivines generally found in peridotite suite diamonds.

The two moissanite (SiC) inclusions were recovered from two diamonds. Both inclusions were colourless to pale blue, facetted, whole crystals which were exceptionally hard and difficult to polish. In initial examination, the microprobe analyses of this phase gave compositions of 150% SiO_2. Measurement of the number of counts at the carbon K α X-ray peak showed approximately 200 to 300 counts per second on the inclusion and approximately 50 counts per second at the background level. This corresponds to an approximate composition of 80% Si and 20% C. Recalculating the silicon with a carbon anion gave an approximate composition of moissanite (SiC).

Moissanite has been reported as an inclusion in diamonds from Argyle (Jaques *et al.*, 1989), at Sloan (Otter & Gurney, 1989) and at Monastery (Moore & Gurney, 1989). The moissanite inclusions from Sloan have since been proved to be laboratory contaminants and given that the inclusions from Monastery were analysed in the same laboratory it is possible that the moissanite inclusions from Monastery are also a contaminant. However Jaques (pers comm., 1989) has noted imposed crystal surfaces on the moissanites from Argyle, and considers his specimens to be syngenetic.

An unidentified alumino-silicate phase of 43 wt.% SiO_2 and 35 wt.% Al_2O_3 was found. This phase had a calcium content of 18.9 wt.% and has a composition close to that of anorthite. This phase may have composition close to $Ca_2Al_2SiO_7$ (see section 7.6, below).

7.5 Nitrogen and carbon characteristics.

The nitrogen characteristics of 50 inclusion-bearing diamonds from Sao Luiz were determined using infra red absorption spectroscopy. Spectra were measured and decomposed using the methods described in Chapter 2.

The nitrogen characteristics are summarised in Appendix 4 and Table 7.4. There are 37 diamonds that are Type II, 5 are Type IaA and the remaining 8 are Type IaB, with 1282/1180 ratios less than 0.3. In the Type Ia diamonds the range of total nitrogen concentrations is from 29 to ****ppm, with one very high value of 7800ppm. The Type IaA diamonds have a range of total nitrogen contents of 127 to 7800ppm, with a mean value of 1491ppm (without this high value the mean is 670ppm). The Type IaB diamonds have a range of total nitrogen values of 29 to 1354ppm, with a mean value of 928ppm. No relationship between mineral chemistry and nitrogen aggregation state was found. The composition of the inclusion from the diamond with the very high total nitrogen content was not determined because the inclusion was too small, although the inclusion was visually identified as a magnesiowustite. The very high nitrogen content of this

Table 7.4

Summary of Nitrogen Characteristics.

Inclusion	IaA	IaB	II
Oxide	4	3	17
Colourless	0	1	8
Multiple	4	1	12
Total Nitrogen (mean ppm)	1491(670*)	928	0

* Excluding very high value of 7800ppm.

diamond contrasts with the high abundance of Type II diamonds from this locality.

From Chapter 4, the rate of nitrogen aggregation state is shown to be dependent on the initial concentration of nitrogen, the temperature and the time available for aggregation. In 5 of the Type IaB diamonds all of the nitrogen is in the IaB aggregate. The IaB content in the IaA diamonds is up to 89%. The time taken to aggregate IaB nitrogen from IaA can be calculated. At temperatures of 1400^{0}C, for example, the time required to aggregate 50% IaB from IaA, with a mean nitrogen value of 1491ppm, will be 1.75 million years, whilst for initial nitrogen concentrations of 928ppm the time required to aggregate 50% of the nitrogen available to IaB is 2.5 million years. Thus, given the high temperatures suggested for the Sao Luiz inclusion suite as a whole, the residence time for these diamonds only needs to be short in order to produce the high Type IaB nitrogen contents observed.

At Sao Luiz the distinctive nitrogen contents may represent at least two different environments of formation, one where there is no nitrogen present, the other where relatively high nitrogen concentrations exist. However there appears to be no correlation between nitrogen content and the inclusion composition. Three possible explanations for this anomaly are suggested: Firstly, that the mechanism of diamond precipitation at depth excludes nitrogen. Secondly that there is no nitrogen present during diamond formation. Thirdly, that nitrogen in the diamond is held in defects that are not infra-red active. The rapid aggregation of IaA to IaB nitrogen favours a rapid aggregation from IaB nitrogen to defects, for example voidites, that are invisible to infra-red. This fact favours the third explanation.

The carbon isotope composition of 2 diamonds containing colourless inclusions and 3 diamonds containing magnesiowustites shows a very small range of $\delta\ ^{13}C$ values of -5.02 to -4.14 $^{o}/_{oo}$ vs PDB. The limited data are close to the $\delta\ ^{13}C$ value of -5 $^{o}/_{oo}$ associated with the carbon of the upper mantle (see Chapter

4). There is, for example, no discernible variation of the $\delta\ ^{13}C$ value with iron content in the magnesiowustite or the mineralogy of the colourless inclusions. The diamonds which contain garnet-like inclusions (see Chapter 6) have $\delta\ ^{13}C$ values ranging from -6.42 to -12.57 $^{o}/_{oo}$ and are generally isotopically lighter. The magnesiowustites and non-garnet silicate inclusions require a deeper origin than the garnet inclusions. The differences in $\delta\ ^{13}C$ may reflect a differences in carbon isotope composition of the mantle between 200 and 400km and deeper mantle at depths greater than 400km.

7.6 Expected Phase Relationships in the Deep Mantle.

The magnesiowustites, the coexisting silica and the calcium and aluminium bearing phases in the Sao Luiz diamonds are distinctive and have only rarely been documented in diamonds from other localities. High pressure experimental work has shown that such phases are stable in the deep mantle. The compositions of the non-garnetiferous inclusions from Sao Luiz will therefore be compared with the expected compositions from the mantle.

The structure of the mantle has been determined by seismic discontinuities which allow division of the mantle into upper and lower parts. The lower part is below 650km (Ringwood, 1977). There is another discontinuity at 400km and both this discontinuity and the one at 650km are believed to represent changes of mineral structure with higher pressures. In figure 7.3, taken from Ringwood (1982), the changes expected for pyrolite composition are shown. At depths of up to 200km the mantle consists of olivine, orthopyroxene, clinopyroxene and garnet. At greater depths the pyroxene phases become dissolved in garnet. Between 400 and 550km a single garnet structured phase exists with β olivine, which has an inverse spinel structure. The olivine has a spinel structure below 550km and at 600km the garnet structure decomposes to form calcium ferrite structured $NaAlSiO_4$ and ilmenite structured $(Mg,Fe)SiO_3$. At even greater depths spinel and ilmenite structured phases dissociate to form perovskite structured

Table 7.5

Calculated Density of Magnesiowustite Inclusions.

	Xfe_{mw}	Xfe_{pv}	Mean ρ_{mw}	$\rho_{mw}-\rho_{pv}$
BZ65	0.44	0.03	4.98	0.81
BZ66	0.73	0.06	5.72	1.56
BZ67	0.58	0.05	5.33	1.20
BZ70	0.42	0.03	4.91	0.73
BZ72	0.45	0.04	4.97	0.80
BZ73	0.42	0.04	4.91	0.74
BZ78	0.32	0.03	4.66	0.48
BZ80	0.36	0.04	4.76	0.59

Xfe_{mw} Mole Fraction of iron in magnesiowustite.

Xfe_{pv} Mole fraction of iron in perovskite phase.

Mean ρ_{mw} Mean density of magnesiowustite.

$\rho_{mw}-\rho_{pv}$ Differences in density of magnesiowustite and perovskite.

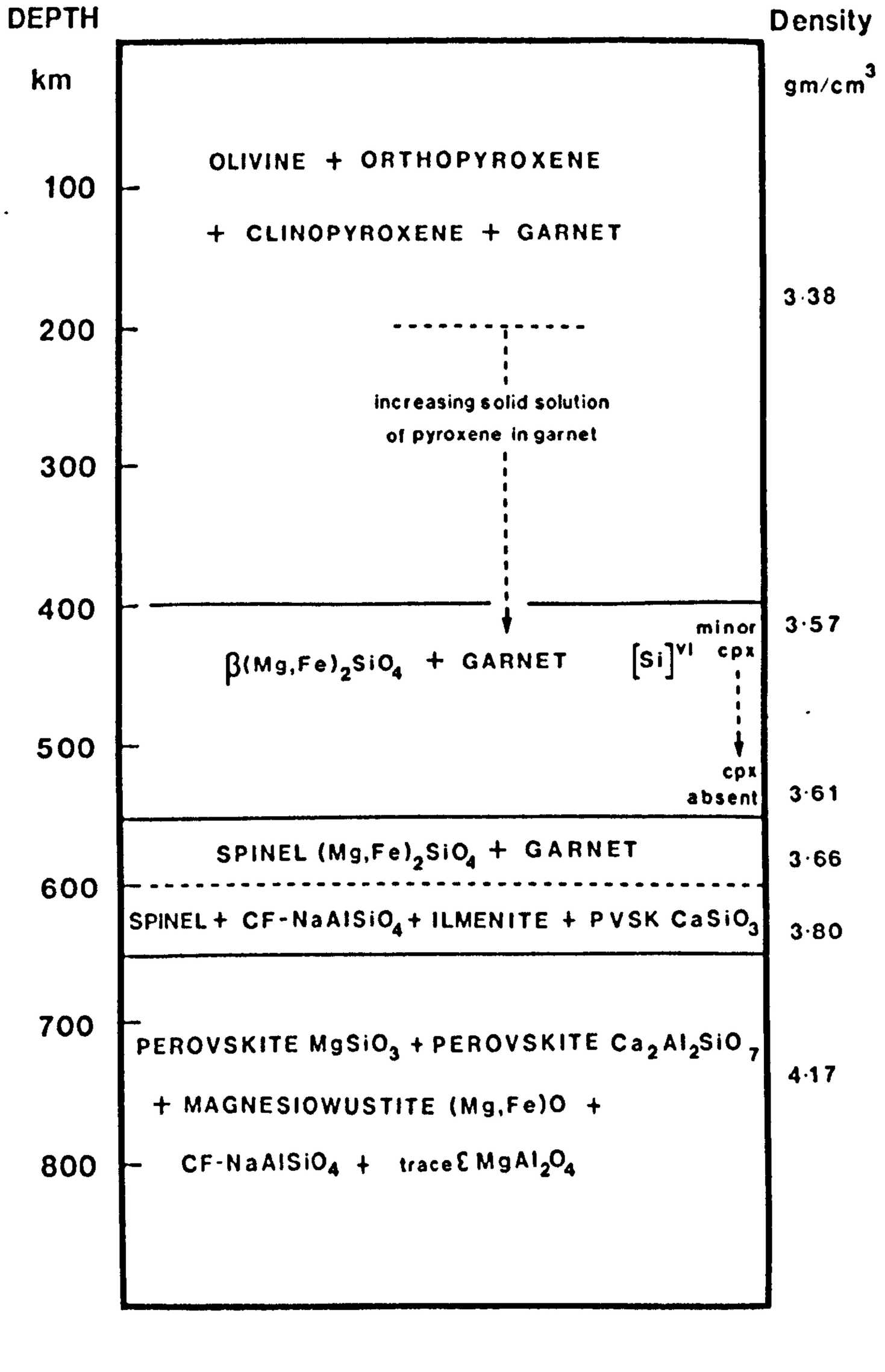
PYROLITE
DEPTH
km
Density
gm/cm3
100
200
300
400
500
600
700
800
OLIVINE + ORTHOPYROXENE
+ CLINOPYROXENE + GARNET
3·38
increasing solid solution
of pyroxene in garnet
β(Mg,Fe)2SiO4 + GARNET
[Si]VI
minor cpx
cpx absent
3·57
3·61
SPINEL (Mg,Fe)2SiO4 + GARNET
3·66
SPINEL + CF-NaAlSiO4 + ILMENITE + PVSK CaSiO3
3·80
PEROVSKITE MgSiO3 + PEROVSKITE Ca2Al2SiO7
+ MAGNESIOWUSTITE (Mg,Fe)O +
CF-NaAlSiO4 + trace MgAl2O4
4·17

Fig 7.3.

Phase Changes in Rocks of Pyrolite Composition at High Pressure.

The phase changes for pyrolite mantle are shown according to Ringwood (1982). The mantle assemblage of olivine, orthopyroxene, garnet and clinopyroxene transforms into a higher pressure assemblage at depths greater than 200km. Pyroxene becomes dissolved into a garnet-structured phase and at 400 and 500km the assemblage present is garnet and β olivine, which has an inverse spinel structure. At depths greater than 550km the olivine has a spinel structure and below 650km olivine dissociates into perovskite-structured enstatite ($(Mg,Fe)SiO_3$) and magnesiowustite (Mgo-FeO).

$(Mg,Fe)SiO_3$ and magnesiowustite (MgO-FeO) of rocksalt structure. These general relationships also apply to rocks of eclogite and harzburgite compositions at depths greater than 550km.

It is important to note that the changes in phases at high pressures do not necessarily correspond to the depths of seismic velocity change. Experimentally derived density and seismic velocity measurements would imply a narrower range of seismic discontinuity at 650km than is actually recorded and phase boundaries alone are therefore not responsible for the 650km seismic discontinuity (a subject discussed in more detail by Richter and Jeanloz, 1979). Also calculated velocity profiles indicate translations at depths shallower than those measured, although changes in chemistry, particularly a change in iron and silicon content, could account for the wide range of seismic velocity increase (as suggested by Lees *et al.*, 1983).

The non-garnetiferous inclusions from Sao Luiz consist of magnesiowustites, silica, olivine, diopside and calcium-bearing phases ($CaSiO_3$, anorthite and diopside). The inclusions from the Sao Luiz diamonds would therefore appear to be derived from a range of depths below 400km. The inclusion chemistry will be compared in detail to the chemistry of phases expected in the system MgO-FeO-SiO_2 at high pressure.

Figure 7.4 shows the phase changes in the system MgO-FeO-SiO_2 for a range of pressures equivalent to depths of 630 to 755km. Two pseudobinary systems are also shown for olivine ($(Mg,Fe)_2SiO_4$) and enstatite ($(Mg,Fe)SiO_3$) compositions. The simple transition of olivine and enstatite to high pressure phases would produce perovskite structured ($(Mg,Fe)SiO_3$) and magnesiowutite. The inclusions from Sao Luiz show a range of iron contents and, in one case, also show a bimineralic assemblage of SiO_2 and magnesiowustite. Significantly no inclusions of ($(Mg,Fe)SiO_3$) composition were recovered (see page 241). Figure 7.4 shows that iron rich magnesiowustite compositions and the assemblage of magnesiowustite and silica can only be produced if the initial bulk composition is

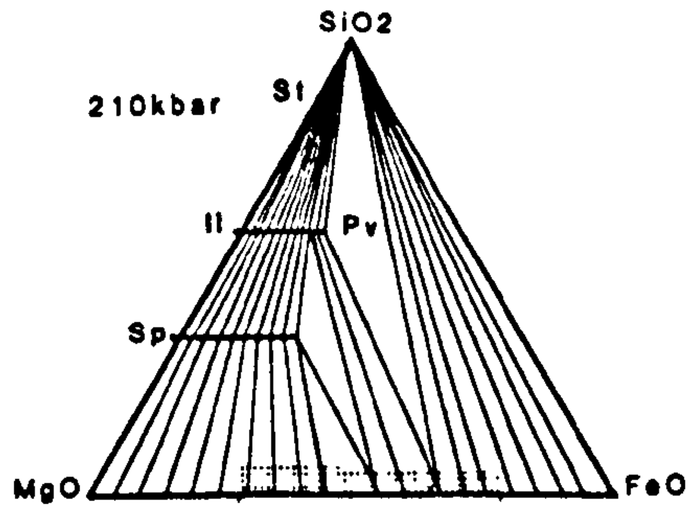

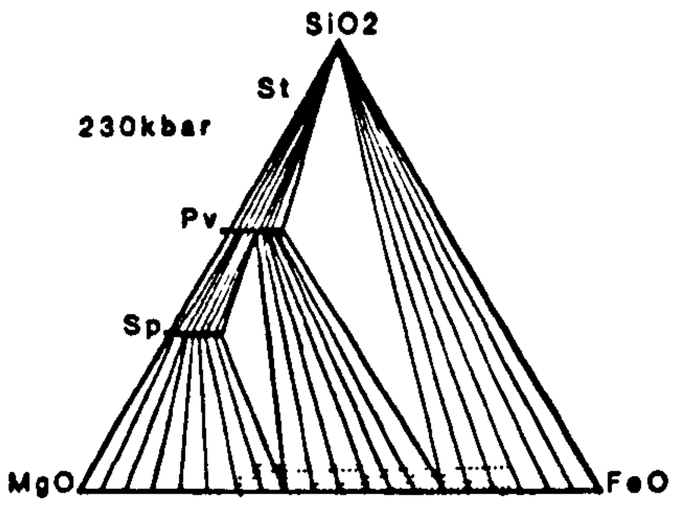

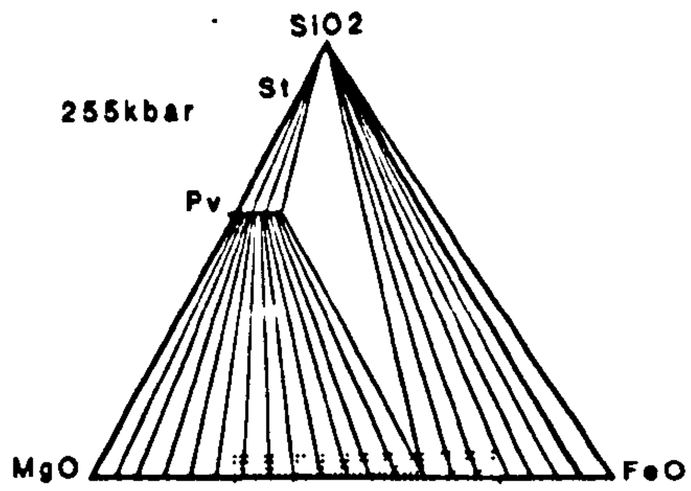

Phase Relations in the System MgO-SiO2-FeO

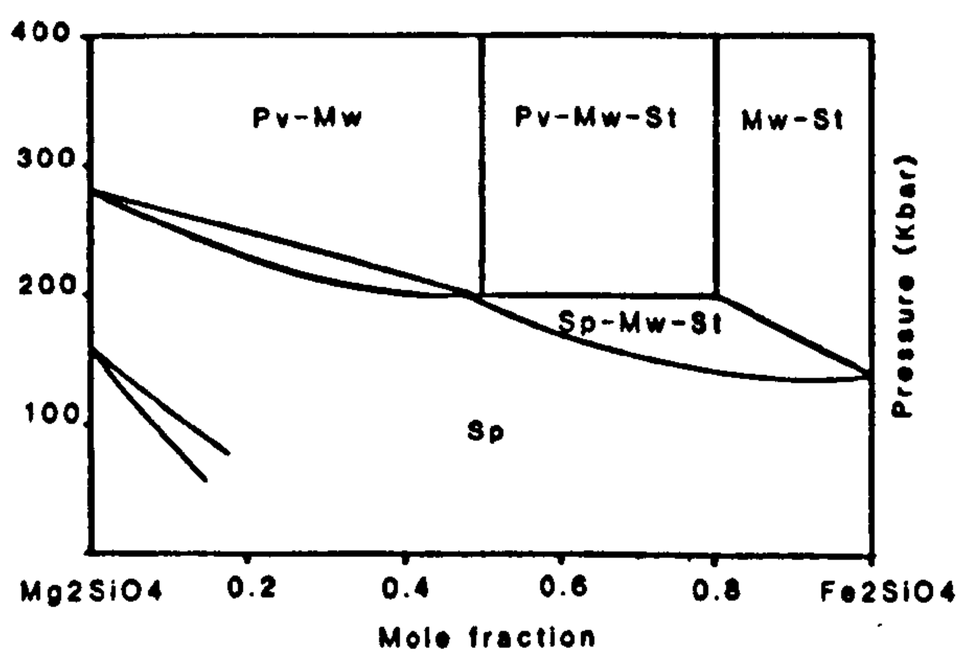

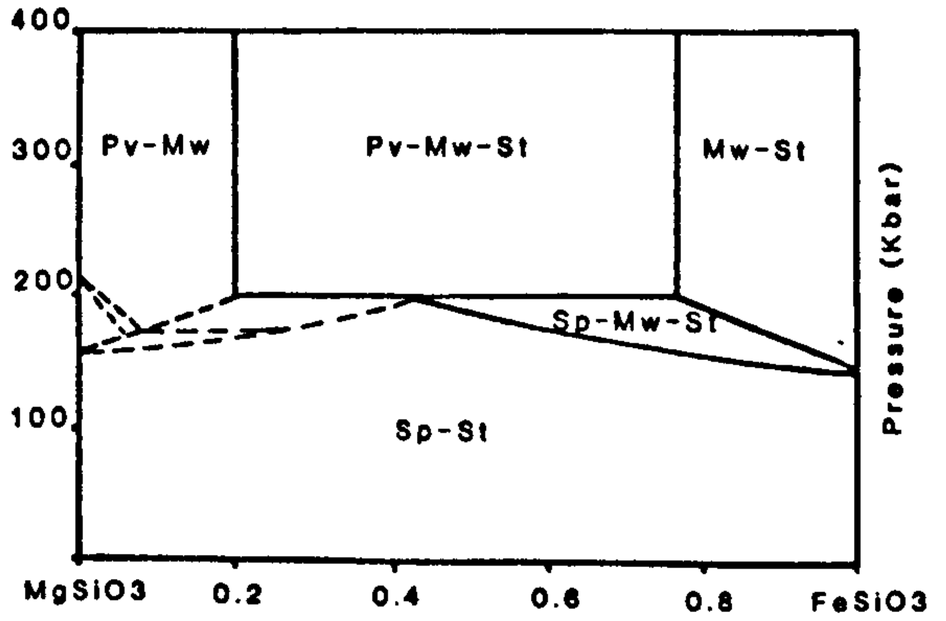

Fig 7.4.

The System MgO-SiO_2-FeO at High Pressure.

Three ternary phase diagrams are shown in the system MgO-SiO_2-FeO (from Yagi *et al*, 1979) together with pseudobinary systems for olivine and orthopyroxene compositions, for a range of pressures equivalent to 630 to over 700km depth. Mantle minerals would be expected to form various assemblages of perovskite-structured $(Fe,Mg)SiO_3$ (PV), spinel-structured $(Mg,Fe)_2SiO_4$ (Sp), Stishovite (SiO_2) (St) and magnesiowustite (Mg,Fe)O (MW), with changes depending on pressure. Assemblages of magnesiowustite and perovskite with high magnesium contents would be expected for mantle compositons at the high pressures shown. The Sao Luiz inclusions show magnesiowustites ranging from 0.28 to 0.78 Mg/Mg+Fe (Shaded). A magnesiowustite coexisting with silica has an Mg/Mg+Fe of 0.56, which is not possible on the diagrams. This suggests a more iron rich composition than direct derivation from normal mantle minerals.

iron rich. The unaltered upper and lower mantle would probably have an Fe/Fe+Mg content of 0.2 (Ringwood, 1982) which contrasts with the iron rich environment favoured for the Sao Luiz diamonds.

The density of magnesiowustite phases is very iron dependent. Bell *et al.* (1979) have shown that there is a significant partitioning of iron and magnesium between the perovskite-structured enstatite and rock-salt-structured oxide (magnesiowustite) with iron strongly partitioned into the oxide phase. Using the data of Mao *et al.* (1979), and with the estimated distribution coefficients, also implied in figure 7.4, simple calculations of density dependence on the mole fraction of iron were performed. This determination also allowed the composition of the perovskite-structured enstatite coexisting with the magnesiowustite to be determined.

In Table 7.5 the results of these calculations are shown. The range of densities for magnesiowustite is 4.66 to 5.72 gcm^{-3} (for iron contents of Fe/Fe+Mg values 0.32 and 0.72 respectively). The most iron rich compositions, with densities of 5.72 gcm^{-3}, would sink because they have a density greater than the surrounding perovskite (4.16gcm^{-3}). These iron rich phases would not therefore be expected in the lower mantle and they are probably only present in the Sao Luiz diamonds because enclosure in the diamond (density 3.51 gcm^{-3}) has protected and prevented such phases from sinking.

Inclusions of olivine composition are found in the Sao Luiz diamonds. The magnesiowustite phases may therefore have originated below 650km, whilst olivines formed at shallower depths (less than 400km).

Calcium in the mantle normally occurs in garnet and clinopyroxene. At pressures greater than 200km calcium enters into garnet structured majorite. The high pressure experimental work of Liu and Ringwood (1975) has shown that there is a triple disassociation of these complex garnet solid solutions into; ilmenite-structured $(Mg,Fe)SiO_3$; calcium ferrite-structured $NaAlSiO_4$ and perovskite-structured $CaSiO_3$, between 600 and 650km. Below 650km (220kb)

PAGE
MISSING
IN
ORIGINAL

calcium enters into a complex $Ca_2Al_2SiO_7$ phase of perovskite related structure (Liu, 1979). The calcium-bearing compositions from Sao Luiz consist of $CaSiO_3$, diopside and an anorthite composition phase. These may represent a limited pressure range where $CaSiO_3$ is stable (600 to 650km). According to Liu (1977) $CaSiO_3$ may persist to greater depths if there is insufficient aluminium to form the $Ca_2Al_2SiO_7$ phase. This situation may be explained by the reaction sequence:

$$Ca_3Al_2Si_3O_{12} = 3CaSiO_3 + Al_2O_3 = Ca_2Al_2SiO_7 + CaSiO_3 + SiO_2 .$$

In this reaction, end member grossular dissociates to form $CaSiO_3$ and Al_2O_3. The complex calc-silicate phase forms from the reaction of the $CaSiO_3$ with Al_2O_3, but excess $CaSiO_3$ and SiO_2 behind. If the garnet phase belongs to the majorite series and, therefore, has a high pyroxene component in solid solution, then the amount of $CaSiO_3$ produced in the above reactions will be even greater. Such a reaction would be additionally enhanced if aluminium is taken up into calcium ferrite structured $NaAlSiO_4$ or ε-$MgAl_2O_4$.

7.7 Formation of Sao Luiz Inclusions.

1. A suite of inclusion-bearing diamonds from Sao Luiz was examined and the inclusions were extracted from a small proportion of these stones. The inclusions consist of magnesiowustite, $CaSiO_3$, silica, olivine and diopside. In addition two inclusions of moissanite (SiC) composition were recovered. Magnesiowustites inclusions have been found at four other localities; Orroroo, Koffiefontein, Monastery and Sloan. The composition of these inclusions suggest that some diamonds are derived from very deep sources.

2. The inclusions in the Sao Luiz diamonds have compositions that are consistent with a high pressure of origin. High pressure experiments have shown that olivine

in the mantle transforms to magnesiowustite and perovskite structured enstatite at pressures equivalent to 650km. Calcium in the mantle occurs as $CaSiO_3$ composition phases at depths below 450km. This implies that some Sao Luiz diamonds originated at depths below 450km and that most of these were probably derived from depths below 650km. These depths of origin are greater than those of the garnet-like inclusions described in Chapter 6.

3. The compositions of the silicate and oxide inclusions from Sao Luiz have been compared with the compositions of a pyrolite mantle. In pyrolite the phase that would be stable at depths below 650km are perovskite structured enstatite and magnesiowustite. However, no enstatite inclusions were found at Sao Luiz. The range of Fe/Fe+Mg ratios for the magnesiowustite inclusions is much greater than would be expected from the pyrolite model. An inclusion pair of silica and magnesiowustite also implies an iron rich composition. It is concluded that the Sao Luiz diamonds therefore formed in an environment that was enriched in iron relative to the mantle through partial melts of perovskite structured phases.

4. Most of the Sao Luiz diamonds are Type II. Diamonds which do show aggregated nitrogen have high IaB contents, confirming estimated high temperatures of formation (see also Chapter 6). At temperatures in excess of $1400^{o}C$ only short mantle residence times are required to aggregate all of the IaA nitrogen present. The rapid aggregation of nitrogen into defects, such as voidites, that are invisible to infra red may explain the abundance of Type II diamonds.

Chapter 8

Origin of the Sao Luiz diamonds.

8.1. Phase relations.

The nature and composition of the inclusions in the Sao Luiz diamonds indicate a considerable variation in depth of origin. The garnet inclusions, described in Chapter 6, alone have a range in depths of origin. The garnets of normal silica content have an origin at depths shallower than 200km and are indistinguishable from eclogite paragenesis garnets from other localities. The high-silica garnets indicate a greater depth of origin from 200 to 400km.

The oxide and non-garnet silicate inclusions from Sao Luiz (Chapter 7) have a much deeper origin, with $CaSiO_3$ composition phases likely to originate at depths greater than 450km and magnesiowustite inclusions probably originating at depths greater than 650km.

On the basis of mineralogy the mineral inclusions from Sao Luiz represent a new assemblage of minerals which relate to different depth zones in the mantle. The garnet inclusions have similar compositions to eclogite paragenesis garnets, but have higher silica contents, these diamond can be termed "garnetiferous" because they contain mainly garnet (garnet and pyroxene would be expected in eclogite paragenesis diamond) and originate in an area of the mantle where garnet-structured minerals are an important phase.

The magnesiowustites show a range in Fe/Fe + Mg ratios from 0.16 to much more iron rich values of 0.61. The colourless inclusions include $CaSiO_3$ composition phases, which are not normally found as a diamond inclusion. These inclusions form a separate paragenesis, dominated by magnesiowustite, and can be termed the "magnesiowustite" suite.

The are some mineralogical and chemical differences in the inclusions and the compositions that might be expected for the mantle. The magnesiowustites

have compositions that are more iron rich than would be expected in the pyrolite, harzburgite or eclogite mantle models. $CaSiO_3$ composition phases would only be expected to form over a small depth range 450 to 500km because at depths greater than 550km calcium enters into the $Ca_2Al_2SiO_7$ phase. The $CaSiO_3$ phases at Sao Luiz may have formed at depths greater than 650km if bulk aluminium contents were low. At depths greater than 650km, perovskite structured enstatite would be expected to form most of the mantle, yet no inclusions of this composition have been recovered from the Sao Luiz diamonds.

These observations provide two distinct environments for the origin of the Sao Luiz diamonds; for the shallow diamonds (up to 450km) the origin of the diamonds may be from a melt from pyrolite or eclogite compositions. For deeper diamonds, formation by be through the direct melting of primary, peridotite, mantle. Both these possibilities are considered below.

Basaltic liquids may crystalise to produce eclogites at high pressure (e.g O'Hara & Yoder, 1967). Scarfe and Takahashi (1986) have studied the melting of a sheared periodotite, that approximates to a pyrolite mantle composition, at high pressure. The liquids produced are calcium and iron rich relative to the starting composition. Scarfe and Takahashi have shown that at high pressures such melts will crystalise to form high-silica garnets of similar compositions to those found in diamonds from Monastery mine by Moore and Gurney (1985).

Ohtani *et al.*(1986) carried out experimental work on the melting of chondritic mantle compositions in the system CFMAS. At pressures of up to 15Gpa olivine is the liquidus phase with olivine, orthopyroxene and garnet as the subsolidus assemblage. Above 15Gpa majorite (high-silica garnet) is the liquidus phase with majorite and β-olivine as the subsolidus assemblage. Figure 8.1 shows the Ca/Al ratios for the starting compositions of Ohtani *et al.* and that of liquidus majorite at 20Gpa. The melt is clearly most enriched in calcium relative to the starting composition. Given that virtually all of the calcium and aluminium is located in the majorite or melt at these pressure, the majorite crystals must

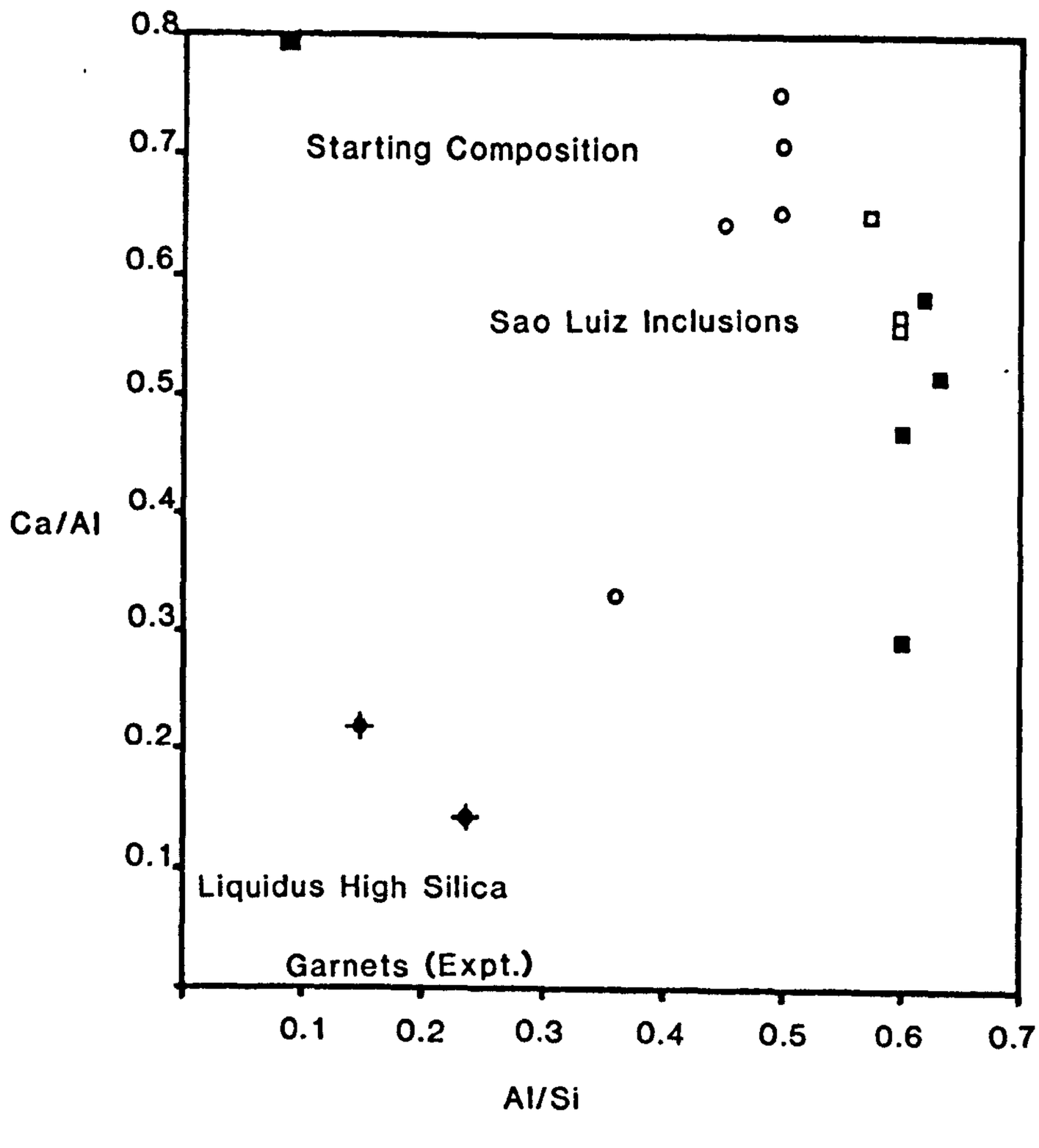
0.8
0.7
0.6
0.5
0.4
0.3
0.2
0.1
Ca/Al
Starting Composition
Sao Luiz Inclusions
Liquidus High Silica
Garnets (Expt.)
0.1
0.2
0.3
0.4
0.5
0.6
0.7
Al/Si

Fig 8.1

Ca/Al and Al/Si Ratios for Sao Luiz Garnetiferous Inclusions.

Ca/Al and Al/Si values are shown for Group IA (open squares), Group IB (filled squares) and Group IIB (open circles) garnetiferous inclusions. Also shown are high-silica garnets that coexist with experimental melts of chondritic starting compositions at high pressure (closed circles) (Ohtani *et al.*, 1986). On melting of chondritic material with high initial Ca/Al ratio, the liquidus phase is a high silica garnet of low Ca/Al value. The Ca/Al ratio of the liquid increases during crystallisation of the high silica garnet.

develop higher Ca/Al with progressive crystallisation of the liquid until they match the bulk Ca/Al at the point of final disappearance of the liquid. The Sao Luiz high-silica garnets have Ca/Al ratios that range from 0.33 to 0.75 (compared with a bulk starting value for the mantle of 0.8) and could have formed from the crystallisation of a melt from a chrondrite in the lower part of the upper mantle. The Al/Si ratio of these phases are different from those anticipated by crystallisation of melts from chondrite, it is possible that if b-olivine is precipitated as well as garnet-structured phases then the Al/Si ratios may differ from those determined experimentally.

Kato *et al.* (1988) show that Y, Zr, Hb and Hf partition into such melts produced at high pressure. Some of the Zr and Y contents of the Sao Luiz inclusions are moderately enriched (sample/chondrite values > 1.0) and suggests an origin consistent with small degrees of melt direct from a pyrolite mantle source.

In deeper diamonds magnesiowustite inclusions have higher Fe/Fe+Mg values (0.16 to 0.61) than would be expected from the mantle below 650km. Also the assemblage of magnesiowustite and silica is only stable with more iron rich bulk compositions according to experimental studies (see, for example, figure 7.4). Below 650km the mantle is predicted to consist of perovskite structured $(Mg,Fe)SiO_3$, with an Fe/Mg+Fe ratio of 0.2 (Ringwood, 1982). No inclusions of $(Mg,Fe)SiO_3$ composition were recovered from the Sao Luiz diamonds. This lack of perovskite-structured $(Mg,Fe)SiO_3$ may be associated with a high Fe/Fe+Mg value, since phase equilibrium studies show perovskite-structured $(Mg,Fe)SiO_3$ is restricted to magnesium rich compositions.

The Sao Luiz magnesiowustites can be compared with studies of melting processes in the deep mantle such as those studied by Ito and Takahashi (1987). In this study the sub-solidus assemblage for pyrolite compositions consists of perovskite-structured $(Mg,Fe)SiO_3$ and magnesiowustite. Calcium and aluminium may be present in perovskite related $Ca_2Al_2SiO_7$ and $CaSiO_3$ phases. During

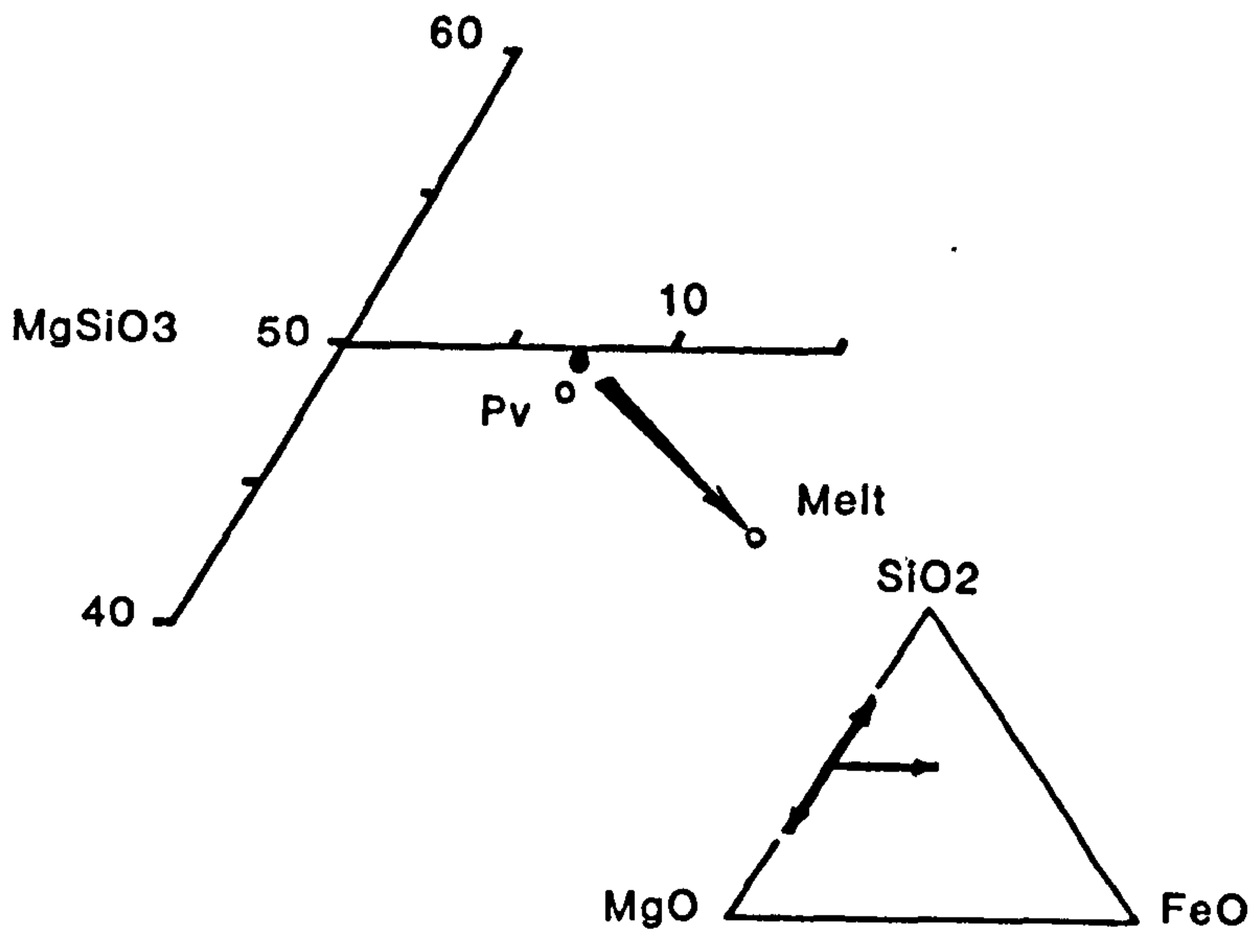
60
MgSiO3
50
10
Pv
Melt
40
SiO2
MgO
FeO

SiO2

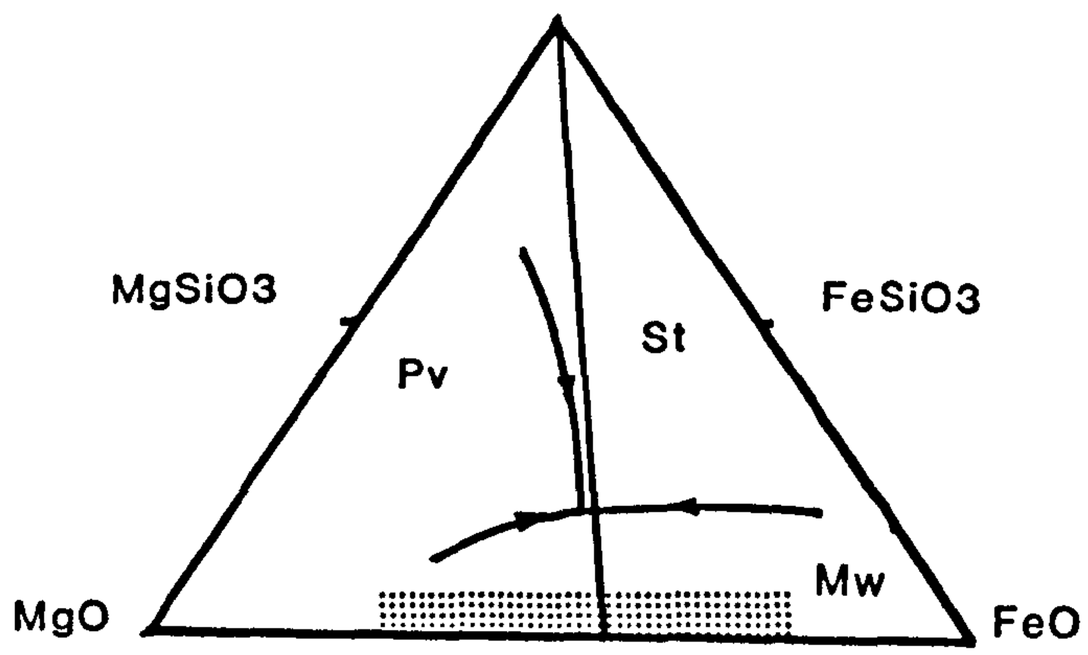
MgSiO3
FeSiO3
Pv
St
Mw
MgO
FeO

Fig 8.2

Melting Relationships in the System FeO-SiO_2-MgO.

The melting relationships of a perovskite ($Mg_{0.9}Fe_{0.1}SiO_3$) are shown (Heinz & Jeanloz, 1987) at pressures equivalent to 650km. The products of melting are perovskite (Pv) and a more iron rich glass. The phases present at high pressure are magnesiowustite, stishovite and perovskite. Melts of mantle perovskite would be expected to yield iron-rich and could crystalise stishovite, iron-rich perovskite and iron-rich magnesiowustite. The assemblages from Sao Luiz are shown as a shaded area of magnesiowustite and a tie line between stishovite and magnesiowustite.

melting calcium and iron partition into the melt, as is also shown by Watt and Ahrens (1982), whilst aluminium and magnesium remain in the perovskite-structured residue (Kao *et al.*, 1988).

The experimental melting of a perovskite-structured enstatite of $(Mg_{0.9}Fe_{0.1})SiO_3$ composition by Heinz and Jeanloz (1987) produced an iron rich glass at pressures equivalent to 650km, this relationships is shown in figure 8.2. In the lower part of figure 8.2 the range of magnesiowustite compositions found in Sao Luiz diamonds is shown together with a tie line between the single coexisting magnesiowustite and silica. Heinz and Jeanloz's phase diagram for the system FeO-SiO_2-MgO shows that melts from perovskite structured mantle might be expected to crystalise iron rich magnesiowustites and possibly SiO_2, as they cool towards a eutectic point, whether this provides an explanation for the Sao Luiz compositions is unclear because the experimental data provide no information on the coexisting liquid and mineral phase compositions.

In more complicated systems which involve calcium, the calcium might also be expected to partition into the melt. Thus with differentiation, $CaSiO_3$ composition phases would be expected to precipitate from the liquid. The abundance of $CaSiO_3$ composition phases at Sao Luiz may therefore fit with a hypothesis involving formation of diamond in differentiated perovskite melts.

8.2 Redox conditions.

In the magnesiowustite group there are two important inclusion compositions in the Sao Luiz diamonds that provide particular information on the redox conditions of formation. These are magnesiowustites (MgO/FeO) and moissanite (SiC). Of particular importance is that within the magnesiowustites there are small inclusions of iron nickel alloy. Because this alloy must coexist with the wustite component of the magnesiowustite their relationship typifies the reaction between ferrous and metallic iron in the iron-wustite buffer (IW):

$$2Fe + O_2 = 2FeO$$

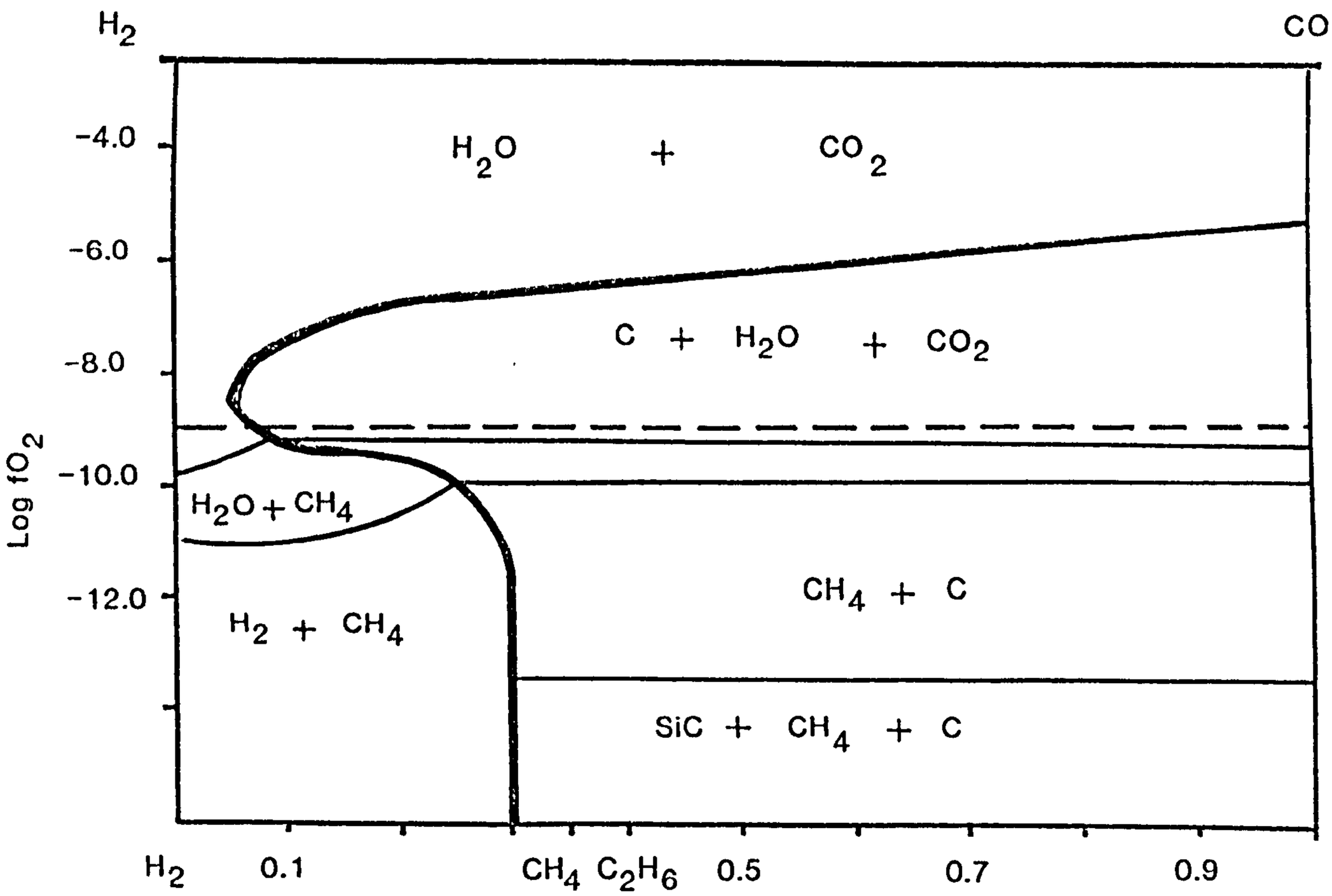
H_2
CO_2
-4.0
-6.0
-8.0
-10.0
-12.0
Log fO_2
H_2O + CO_2
C + H_2O + CO_2
$H_2O + CH_4$
CH_4 + C
H_2 + CH_4
SiC + CH_4 + C
H_2
0.1
CH_4 C_2H_6
0.5
0.7
0.9
Xc ($C/C+H_2$)

Fig 8.3

Log fO_2 - X_c Diagram for 1400^{0}C at 30Kbar.

The oxygen fugacity and the X_c ($C/C+H_2$) values show the stabilities for carbon-bearing species expected over a wide range of oxygen fugacity conditions. The iron-wustite buffer is shown as a broken line. The carbon saturation curve divides the diagram into two areas (from Taylor, 1986). To the left of the carbon saturation curve carbon only exists in a fluid (as CH_4 or CO_2, depending on fO_2). To the right of this curve carbon, as graphite or diamond, can coexist with fluid. Carbon can be precipitated under very reduced conditions by an increase in the $C/C+H_2$ ratio (by H_2 loss) and it is possible that some of the deep Sao Luiz diamonds formed in this way. Most silicon is stable as silica (SiO_2), except for very reduced conditions where silicon carbide is stable (SiC), as shown.

The iron-nickel alloy inclusions were too small to enable any calculations of the fO_2 to be made. Moissanite will only be stable under very reduced redox conditions, usually -8 log fO_2 units less than IW at 1000°C (Taylor, 1986). Under such conditions this mineral can be precipitated by silica reduction reactions such as:

$$SiO_2 + C = SiC + O_2$$

Reactions such as:

$$SiO_2 + CH_4 = SiC + 2H_2O$$

are unlikely to be important, since H_2O will not be a stable species in the gas phase at such low oxygen fugacities, as can be seen in figure 8.3.

Figure 8.3 shows the redox state plotted against the amount of carbon present ($C/C+H_2$). Frost (1979) has shown that as $C/C+H_2$ increases at a constant fO_2 the carbon precipitation curve is reached and carbon is precipitated (either as graphite or diamond). According to Taylor (1986) the $C/C+H_2$ ratio can be increased by loss of H_2 from the mantle and carbide may form under particularly reduced conditions. The deep Sao Luiz inclusions may have therefore precipitated as a result of H_2 loss rather than by a change in oxygen fugacity. Taylor (1986) has pointed that the presence of silicon carbide (SiC) can indicate that primoidal carbide was incorporated into the earth during accretion. It is more likely, however, that carbide formed in a reduced CH_4-H_2 fluid because it is doubtful that carbide would remain stable in a relatively oxidised mantle throughout the age of the earth. Brett (1984) also suggests that such a reduced fluid may indicate a redox equilibrium between the lower mantle and the metallic earth core and again indicates very reduced conditions for diamond formation.

At depths shallower than 650km the oxidation state of the mantle is difficult to determine because none of the inclusions in the garnetiferous group at

Sao Luiz are minerals that occur in synthetic buffers. The range of oxygen fugacity conditions for asthenosphere derived material implies values of between the QFM and IW (see also Chapter 5). From figure 8.3 it can be seen that under these conditions an increase in the of -2 log fO_2 units from IW (broken line) will precipitate carbon. Under such fO_2 conditions carbide phases will not be stable.

Below 400km the oxygen fugacity is controlled by the iron content in olivine phases. Saxena (1989) has shown that ferrous iron (Fe^{2+}) can control both the amount of CH_4 and carbon present through the following equilibria:

$$C + 2H_2O = CH_4 + O_2 \quad (1)$$

$$2Fe + O_2 = 2FeO \quad (2)$$

$$FeSiO_3 + FeO = Fe_2SiO_4 \quad (3)$$

Through reaction 1, methane increases to form 80% of the vapour present at the expense of carbon as diamond (Saxena, 1980). The iron content of olivine remains virtually constant and only increases from Fo87 to Fo86, this value being the maximum iron saturation.

Within the asthenosphere high-silica garnet phases will be stable at depths between 200 and 400km and at these depths, as suggested by Haggerty and Tompkins (1983), the asthenosphere may be relatively oxidised. Between 400 and 650km, where olivine compositions are stable, methane will probably be the dominant carbon-bearing species. The interface of CH_4 from the base of the asthenosphere to the more oxidised areas at the top of the asthenosphere may therefore cause carbon precipitation and the formation of garnetiferous diamonds at Sao Luiz.

The studies of the carbon isotopes of Sao Luiz diamonds were insufficient to establish the effects of redox conditions on diamond precipitation. The diamonds containing garnet inclusions had a range of $\delta\ ^{13}C$ compositions with values less than the assumed mantle composition. These values may suggest a number of separate carbon reservoirs in the asthenosphere. However, the $\delta\ ^{13}C$ values are also consistent with the values that would be expected from carbon

precipitation by CO_2 reduction reactions and could have formed at the interfaces of reduced and relatively oxidised areas of the asthenosphere. The diamonds which contain deeper inclusions have $\delta\ ^{13}C$ that are close to the assumed mantle compositions. These values are consistent with an origin by CH_4 reactions, possibly involving H_2 loss.

8.3 Mantle Dynamics.

Within the deep mantle melts will probably propagate along grain boundaries. If diamonds form from such melts, then a transport mechanism is required to transfer these diamonds either to the base of the lithosphere, or to a position in the asthenosphere, where they can be sampled by kimberlites or lamproites. The most likely two mechanisms proposed are; a) convecting cells within the mantle, or b) migrating melts from the mantle.

There has been much recent debate concerning the possibility of whole mantle convection. If this kind of convection does occur covering a range from 2700km to 200km then diamonds originating below 650km could well become incorporated in convection cells.

Lees *et al.* (1983) and Richter and Jeanloz (1979) have suggested that the 650km seismic discontinuity results from chemical differences in the perovskite-structured mantle. Richter and McKenzie (1981) have calculated that a difference in density of 2% between the upper and lower mantle is sufficient to prevent whole mantle convection. It seems unlikely therefore that diamonds have been transported from below 650km by such a mechanism.

The migration of primitive lower mantle as melt has been suggested as a mechanism for formation of ocean island basalts (OIB) and continental flood basalts (see, for example, Menzies & Hawksworth, 1987 and Hoffman and White, 1982). Such melts, if they migrate as diapirs, may transport diamonds with them. Olsen and Yuen (1982) have suggested that the melts derived from the lower

mantle only need to be 4% lighter than the surrounding perovskite in order to breach the 650km discontinuity.

8.4 Summary.

The diamonds from Sao Luiz formed over a great range of depth under different redox conditions. Within the asthenosphere. There are two distinct groups, diamonds containing garnet-like inclusions (garnetiferous) formed between 200 and 400km, with precipitation at the interface between oxidised and reduced asthenosphere. Diamonds which are dominated by oxide and non-garnet silicate inclusions (magnesiowustite) originate at depths from 450km to below 650km. Most of these diamonds are formed under very reduced conditions, probably as a result of partial melts from perovskite-structured mantle. Diamond precipitation is probably by H_2 loss from CH_4. The mechanism for transporting these diamonds to higher levels is unknown, but it is possible that migrating diapirs from the lower mantle may transport diamonds from into the convecting upper asthenosphere.

References.

ALLSOPP, H. L. & BARRETT, D. R., 1975, "Rb-Sr Age Determinations on South African Kimberlites."in *Physics and Chemistry of the Earth, vol 9*, pp 605-617.

ARCULUS, R. J. & DELANO, J. W., 1980. " Implications for the Primitive Atmosphere of the Oxidation State of the Earths Upper Mantle," *Nature*, 288, pp 72-74,

ARCULUS, R. J. & DELANO, J. W., 1981. "Intrinsic Oxygen Fugacity Measurements: Techniques and Results for Spinels from Upper Mantle Peridotites and Megacryst Assemblages." *Geochimica et Cosmochimica Acta*, 45, pp 899-913.

ARCULUS, R. J. & DELANO, J. W., 1987, " Oxidation State of the Upper Mantle: Present Conditions, Evolution and Controls." in *Mantle Xenoliths*, ed. P. H. Nixon, J. Wiley & Sons ltd.

ARCULUS, R., DAWSON, J. B. MITCHELL, GUST, P. A. & HOLMES, R. D., 1984, "Oxidation State of the Upper Mantle as Recorded by Megacryst Ilmentite, Kimberlite and Type A and B spinel lherzolites." *Contributions to Mineralogy and Petrology*, 85, pp 85-95.

ARNDT, N. T. & NESBITT, E. G., 1982, " What is a Komatiite ?" in *Komatiites* ed N. T. Arndt & E. G. Nesbitt, Geo. Allen & Unwin: London.

BAILEY, D. K., 1982, "Mantle Metasomatism: Continuing Chemical Change Within the Earth." *Nature*, 296, pp 525-530.

BELL, P. M., YAGI, T. & MAO, H. K., 1979, "Iron-Magnesium Distribution between Spinel [$(Mg,Fe)_2SiO_4$], Magnesiowustite [(Mg,Fe)O] and Perovskite [$(Mg,Fe)SiO_3$]." *Carnegie Institute of Washington Year-book*, 78, pp 618-621.

BICKLE, M. J., 1982, "The Magnesium Contents of Komatiitic Liquids." in *Komatiites* ed N. T. Arndt & E. G. Nesbitt, Geo. Allen & Unwin: London.

BICKLE, M. J., FORD, C. E. & NISBET, E. G., 1977, " The Petrogenesis of Peridotite Komatiites: Evidence from High Pressure Partial Melting Experiments." *Earth and Planetary Science Letters*, 37, pp 97-106.

BISHOP, A. C., 1967, *An Outline of Crystal Morphology*, Hutchison, London.

BISHOP, F. C., SMITH, J. V. & DAWSON, J. B., 1976, "Na, P, Ti and Coordination of Si in Garnet from Peridotite and Eclogite Xenoliths.", *Nature*, 260, pp 696-697.

BRETT, R. , 1988, "Chemical Equilibration of the Earth's Core and Upper Mantle." *Geochimica et Cosmochimica Acta*, 48, pp 1183-1188.

BOBRIEVICH, A. P., BONDARENKO, M. N., GREVESHERVICH, R. K., SMIRNOV, G. F. & YURKEVICH, R. K., 1959, "The Diamond Deposits of Yakutia." *State Scientific and Technical Publishing House for Literature on Geology and the Conservation of Mineral Resources, Moscow, (in Russian).*

BOYD, F.R.,1973, "A pyroxene Geotherm."*Geochimica et Cosmochimica Acta*, 37, pp2533-2546.

BOYD, F.R. & FINNETY, A.A., 1980, "Conditions of Origin of Natural Diamonds of Peridotite Affinity." *Journal of Geophysical Research*, 85, pp 6911-6918.

BOYD, F. R. & GURNEY, J. J., 1982, "Low Calcium Garnets: Keys to Craton Structure and Diamond Crystallisation." *Carnegie Institute of Washington Year-book*, 81, pp 261-267.

BOYD, F. R., GURNEY, J. J. & RICHARDSON, S. H., 1985, "Evidence for a 150-200km Thick Lithosphere from Diamond Inclusion Thermobarometry." *Nature*, 315, pp 387-389.

BOYD, S. R., MATTEY, D. P., PILLINGER, C. T., MILLEDGE, H.J., MENDELSSOHN, M. & SEAL, M., 1987, "Multiple Growth Events During Diamond Genesis: An Integrated Study of Carbon and Nitrogen isotopes and Nitrogen Aggregation State in Coated Stones." *Earth and Planetary Science Letters*, 86, pp 341-353.

BUDDINGTON, A. F. & LINDSLEY, D. H., 1964, "Iron-Titanium Oxide Minerals and Synthetic Equivalents." *Journal of Petrology*, 5,pp311-357.

BUNDY, F. P., 1980, "The P T Phase and Reaction Diagram for Elemental Carbon." *Journal of Geophysical Research*, 85 (B12), pp6930-6936.

BURSHILL, L. A. & GLAISHER, R. W., 1985, " Aggregation and Dissolution of Small and Extended Defect Structures in Type Ia Diamond." *American Mineralogist*, 70, pp 608-618.

BURGESS, R., TURNER, G., LAURENZI, M. & HARRIS, J. W., 1989, "^{40}Ar-^{39}Ar laser Probe Dating of Individual Clinopyroxene Inclusions in the Premier Eclogitic Diamonds." in press: *Earth and Planetary Science Letters.*

CARSWELL, D. A. & GIBB, F. G. F, 1987, "Evaluation of Mineral Thermometers and Barometers Applicable to Garnet Lherzolite Assemblages." *Contributions to Mineralogy and Petrology*, 95, pp 499-511.

CAWTHORN, R. G., 1975, "Degrees of Melting in Mantle Diapirs and the Origin of Ultrabasic Liquids." *Earth and Planetary Science Letters*, 27, pp 113-120.

CAWTHORN, R. G. & McIVER, J. R., 1977, "Nickel in Komatiites." *Nature*, 266, pp 716.

CHRENKO, R. M., TUFT, R. E. & STRONG, H. M., 1977, "Transformation of the State of Nitrogen in Diamond.", *Nature*, 270, pp 141-144.

CHRISTIE, D. M., CARMICHAEL, I. S. & LANGMUIR, C. H., 1986, "Oxidation State of Mid Ocean Ridge Basalt Glasses.", *Earth and Planetary Science Letters*, 79, pp 397-411.

CLARKE, D. B., & O'HARA, M. J., 1979, "Nickel and the Existance of High MgO Fluids in Nature." *Earth and Planentary Science Letters*, 44, pp 153-158.

CLAYTON, R. N., 1986, "High Temperature Isotopes in the Early Solar System." in *Stable Isotopes in High Temperature Geological Processes*. eds J. W. Valley, H. P. Taylor & J. R. O'Neil.

CLEMENT, C. R. , 1978, "A Comparative Geological Study of some Major Kimberlite Pipes in the Northern Cape and Orange Free State." Phd Thesis, University of Cape Town.

COLE, D. R. & OHMOTO, H., 1986, "Kinetics of Isotope Exchange at Elevated Temperatures and Pressures." in *Stable Isotopes in High Temperature Geological Processes* ed J. W. Valley, J. R. O'Neil & H. P. Taylor. Reviews in Mineralogy, Vol 16, Min. Soc. Am.

COLLINS, A. T., 1980, "Vacancy Enhanced Aggregation of Nitrogen in Diamond." *Journal of Physics C. Solid state Physics*, 13, pp 2641-2650.

COLLINS, A. T. & LIGHTOWLERS, E. C., 1979, "Electrical Properties" in *Properties of Diamond* ed J. E. Field, Academic Press, London: New York: San Fransisco.

COX, K. G., BELL, J. D. & PANKHURST, R. J., 1979, *The Interpretation of Igneous Rocks*. Geo. Allen & Unwin: London.

COWARD, M. P. & FAIRHEAD, J. D., 1980, "Gravity and Structural Evidence for the Deep, Structure of the Limpopo Belt, Southern Africa.", *Tectonophysics*, 68, pp 31-48.

CRAIG, J. R., 1974, "The Fe-Ni-S System." in *Sulfide Mineralogy: Min. Soc. Am. short course notes, vol 1*. ed P. H. Ribbe.

DANCKWERTH, P. A. & NEWTON, R. C., 1978, "Expermimental Determination of the Spinel Peridotite to Garnet Peridotite Reaction in the System $MgO-Al_2O_3-SiO_2$ in the Range 900-1100°C and Al_2O_3 Isopleths of Enstatite." *Contributions to Mineralogy and Petrology*, 66, pp 189-201.

DANCHIN, R. V. & BOYD, F. R., 1976, "Ultramafic Nodules from the Premier Kimberlite Pipe, South Africa." *Carnegie Institute of Washington Yearbook*, 75, pp531-538.

DAVIES, G., 1979, "Cathodoluminescence." in *Properties of Diamond* ed J. E. Field, Academic Press, London: New York: San Fransisco.

DAVIES, G., 1981, "Decomposing the IR Spectra of Diamonds." *Nature*, 290, pp 40-41.

DAVIES, G. & HARRIS, J. W., 1980, "Some Features of Nitrogen Aggregation in Diamonds from Different Sources and Specific Growth Environment." *Diamond Conference Abstracts, Bristol 1980.*

DAWSON, J. B., 1980, *Kimberlites and their xenoliths*. Springer-Verlag, Berlin.

DAWSON, J. B., 1982, "Contrasting Types of Mantle Metasomatism." *Terra Cognita*, 2, pp232-233.

DAWSON, J. B., 1984, "Petrogenesis of Kimberlite" in *Kimberlite Occurrence and Origin*, eds J. E. Glover & P. G. Harris. The Geology Department and University Extension, University of Western Australia, Publication no. 8.

DAWSON, J. B., 1987, "The MARID Suite of Xenoliths and Their Relationship to the Mantle"in *Mantle Xenoliths* ed P. H. Nixon, John Wiley & Sons.

DAWSON, J. B., SMITH, J. V. & DELANEY, J. S., 1978, "Multiple Spinel-Garnet Transitions in the Upper Mantle: Evidence from a Harzburgite Xenolith. *Nature*, 273, pp741-743.

DEINES, P., 1980, "The Carbon Isotopic Composition of Diamonds: Relationship to Diamond Shape, Colour Occurrence and Vapour Composition.", *Geochimica et Cosmochimica Acta*, 44, pp 943-961.

DEINES, P., GURNEY, J. J. & HARRIS, J. W., 1984, "On the Existance of ^{13}C Depleted Carbon in the Mantle, Evidence from Diamond Studies." *Geochimica et Cosmochimica Acta*, 45, pp 325-342.

DEINES, P., GURNEY, J. J. & HARRIS, J. W., 1984, "Associated Chemical and Carbon Isotopic Composition in Diamonds from the Finsch and Premier kimberlite, South Africa." *Geochimica et Cosmochimica Acta*, 48, pp 325-342.

DEINES, P., HARRIS, J. W. & GURNEY, J. J. ,1984, "Nitrogen and ^{13}C Content of Finsch and Premier Diamonds and their Implications." unpublished.

DEINES, P., HARRIS, J. W. & GURNEY, J. J., 1987, "Carbon Isotopic Composition, Nitrogen Content and Inclusion Composition of Diamonds from the Roberts Victor kimberlite, South Africa: Evidence for ^{13}C Depletion on the Mantle." *Geochemica et Cosmochimica Acta*, 51, pp 1227-1243.

DEINES, P. & WICKMAN, F. E., 1973, "The Isotopic Composition of Graphitiic Carbon from Iron Meteorites and Some Remarks on Troilite Sulfur of Iron Meteorites." *Geochimica et Cosmochimica Acta*, 37, pp 1295-1319.

DEINES, P. & WICKMAN, F. E., 1975, "A Contribution to the Stable Carbon Isotope Geochemistry of Iron Meteorites.", *Geochimica et Cosmochimica Acta*, 39, pp 547-557.

EGGLER, D. H., 1978 "The Effect of CO_2 Upon Partial Melting of Peridotite in the System Na_2O-CaO-Al_2O_3-MgO-SiO_2-CO_2 to 30kbar with an Analysis of Melting in a Peridotite-H_2O-CO_2 System." *American Journal of Science*, 278, pp305-343.

EGGLER, D. H., 1976, "Does CO_2 Cause Partial Melting in the Low Velocity Layer of the Mantle ?" *Geology*, 4, pp 69-72.

EGGLER, D. H., HOLLOWAY, J. R & MYSEN, B. O, 1976, "High CO_2 Solubilities in Mantle Magmas: comment and reply." *Geology*, 4, pp 199.

ELLIS, D. J. & GREEN, D. H., 1979, "An Experimental Study of the Effect of Ca upon Garnet-Clinopyroxene Fe-Mg Exchange Equilibria." *Contributions to Mineralogy and Petrrology*, 71, pp 13-22.

EVANS, T. & QI, Z., 1982, "The Kinetics of the Aggregation of Nitrogen Atoms in Diamond." *Proceedings of the Royal Society of London*, A381, pp 159-178.

FIELD, J. E., 1979, *Properties of Diamond*, Academic Press, London: New York: San Fransisco.

FOLEY, S. F., 1989, "Emplacement Features of Lamprophyre and Carbonitic Lamprophyre Dykes at Aillik Bay, Labrador." *Geological Magazine*, 126(1), pp29-42.

FROST, B. R., 1979, "Mineral Equilibria Involving Mixed Volatiles in a C-O-H Fluid phase: The Stabilities of Graphite and Siderite." *American Journal of Science*, 279, pp1033-1059

FRICK, U. & PEPIN, R. O., 1981, "Microanalysis of Nitrogen Isotope Abundances: Association of Nitrogen with Noble Gase Carriers in Allende." *Earth and Planetary Science Letters*, 56, pp64-81.

GREEN, D. H. & WALLACE, M. E., 1988, "Mantle Metasomatism by Ephemeral Carbonatite Melts." *Nature*, 336, pp 459-461.

GURNEY, J. J., 1984, "Correlation Between Garnets and Diamonds from Kimberlite." in *Kimberlite Occurrence and Origin* eds J. E. Glover & P. G. Harris, The Geology department and University Extension, University of Western Australia, Publication No. 8.

GURNEY, J. J., HARRIS, J. W. & RICKARD, R. S., 1984, "Silicate and Oxide inclusions in Diamond from the Orapa Mine, Botswana." in *Kimberlites II: the mantle and crust mantle relationships*. ed J. Kornprobst. Elsevier: Amsterdam.

GURNEY, J. J., HARRIS, J. W. & RICKARD, R. S., 1979, "Silicate and Oxide inclusions in Diamond from the Finsch Kimberlite Pipe." in *Kimberlites, Diamonds and Diatremes, theier geology, petrology and geochemistry*. ed H. O. A. Meyer & F. R. Boyd: American Geophysical Union: Washington.

GURNEY, J. J., HARRIS, J. W. & RICKARD, R. S., 1984, "Minerals Associated with Diamond from the Roberts Victor Mine." in Kimberlites II: the Mantle and Crust-Mantle Relationships. ed J Kornprobst. Eslevier: Amsterdam.

GURNEY, J. J., HARRIS, J. W., RICKARD, R. S. & MOORE, R. O., 1985, "Inclusions in Premier Mine Diamonds." *Transactions of the Geological Society of South Africa*, 88, pp 301-310.

GURNEY, J. J., HARRIS, J. W., RICKARD, R. S. & CARDSO, P., 1986, "Mineral Inclusions in Diamonds from the Koffiefontein Mine." *4th International Kimberlite Conference extended abstracts*.

GURNEY, J. J. & HARTE, B., 1980, "Chemical Variation in Upper Mantle Nodules from Southern African Kimberlites." *Philosophical Transactions of the Royal Society of London*, A297, pp273-293.

HAGGERTY, S. E., 1976, "Opaque Mineral Oxides in Terrestrial Igneous Rocks." in *Min Soc. Am. short course notes vol 3. Oxide Minerals* ed D. Rumble.

HAGGERTY, S. E., 1979, "Spinels in High Pressure Regimes." in *The Mantle Sample: Inclusions on kimberlites and other volcanics*. ed H. O. A. Meyer & F. R. Boyd, American Geophysical Union, Washington.

HAGGERTY, S. E., 1986,"Diamond Genesis in a Multiply Constrained Model." *Nature*, 320, pp 34-37.

HAGGERTY, S. E. & NAGIEB, S., 1989, "Diamonds in Non-kimberlitic, Non-lamproitic Diatremes from NW Syria." *28th I.G.C. Abstracts*.

HAGGERTY, S. E. & TOMPKINS, L. A., 1983,"Redox State of the Earth's Upper Mantle from Kimberlite Ilmenites." *Nature*, 303, pp 295-300.

HARLEY, S. L., 1984,"An Experimental Study of the Partitioning of Fe and Mg Between Garnets and Orthopyroxene." *Contributions to Mineralogy and Petrology*, 86, pp 359-373.

HARRIS, J. W., 1968,"The Recognition of Diamond Inclusions: Part 1 Syngenetic Mineral Inclusions." *Industrial Diamond Review*, 28, pp 402-410.

HARRIS, J. W., 1968,"The Recognition of Diamond Inclusions: Part 2 Epigenetic Mineral Inclusions." *Industrial Diamond Review*, 28, pp 458-461.

HARRIS, J. W., 1987,"Recent Physical, Chemical and Isotopic Research of Diamond." in *Mantle Xenoliths* ed P. H. Nixon, John Wiley & Sons.

HARRIS, J. W. & COLLINS, A. T., 1985,"Studies of Argyle Diamonds." *Industrial Diamond Review*, 3, pp 128-130.

HARRIS, J. W., HAWTHORNE, J. B. & OOSTERVELD, M. M., 1984, "A Comparison of Diamond Characteristics from the De Beers Pool Mines, Kimberley, South Africa." *Annals Science of the University of Clermont Ferrand*, II, 74, pp 1-13.

HARRIS, J. W., HAWTHORNE, J. B., OOSTERVELD, M. M. & WHERMEYER, G., 1975,"A Classification Scheme for Diamond and a Comparative Study of Southern African Characteristics." in *Physics and Chemistry of the Earth, vol 9* ed L. H. Ahrens, J. B. Dawson, A. R. Duncan & A. J. Erlank, Pergammon Press, Oxford & New York.

HARRIS, J. W. & GURNEY, J. J., 1979, "Inclusions in Diamond." in *The Properties of Diamond* ed J. E. Field, Academic Press, London, New York & San Fransisco.

HARRIS, J. W. & GURNEY, J. J., "Inclusion Abundances in Diamonds from Southern Africa." unpublished.

HARRIS, J. W. & VANCE, E. R., 1972, "Induced Graphitisation and Crystalline Inclusions in Diamond." *Contributions to Mineralogy and Petrology*, 35, pp 227-234.

HART, S. R. & DAVIES, K. E., 1978,"Nickel Partitioning Between Olivine and Silicate Melt." *Earth and planetary Science Letters*, 40, pp 203-219.

HARTE, B., 1983,"Mantle Peridotites and Processes: the Kimberlite Sample." in *Continental basalts and Mantle Xenoliths* ed M. J. Norry & J. G. Fitton, Shiva Publishing, Nantwich.

HARTE, B., 1987, "Metasomatic Events Recorded in Mantle Xenoliths: an Overview." in *Mantle Xenoliths* ed P. H. Nixon, John Wiley & Sons.

HARTE, B., GURNEY, J. J. & HARRIS, J. W., 1980, "The Formation of Peridotite Suite Diamond Inclusions." *Contributions to Mineralogy and Petrology*, 72, pp 181-190.

HAWTHORNE, J. B., 1975, "Model of a Kimberlite." in *Physics and Chemistry of the Earth Vol. 9.* ed L. H. Ahrens, J. B.dawson, A. R. Duncan & A. J. Erlank, Pergammon Press.Oxford: New York.

HEINZ, D. & JEANLOZ, R., 1987, "Measurement of the Melting Curve of $Mg_{0.9}Fe_{0.1}SiO_3$ at Lower Mantle Conditions and it's Geophysical Implications." *Journal of Geophysical Research*, 92, B11, pp11,437-11,444.

HERVIG, R. L. & SMITH, J. V., 1982,"Temperature Dependent Distribution of Cr Between Olivine and Orthopyroxene in Lherzolite Xenoliths." *Contributions to Mineralogy and Petrology*, **81**, pp 184-189.

HERVIG, R. L., SMITH, J. V. & DAWSON, J. B., 1986, "Lherzolite Xenoliths in Kimberlite and Basalt: Petrogenetic and Crystallogenetic Significance of Some Minor Trace Elements in Olivine, Pyroxene and Garnet." *Transactions of the Royal Society of Edinburgh*, **71**, pp 181-201.

HERVIG, R. L., SMITH, J. V., STEELE, I. M., GURNEY, J. J., MEYER, H. O. A. & HARRIS, J. W., 1980, "Diamonds: Minor Elements in Silicate Inclusions: Pressure and Temperature Implications." *Journal of Geophysical Research*, **85**, pp 6919-6929.

HOFFMAN, A. W. & WHITE, W. M., 1982, "Mantle Plumes from Ancient Oceanic Crust." *Earth and Planetary Science Letters*, **57**, pp 421-436.

IRVING, A. J., 1978, "A Review of Experimental Studies of Crystal/Liquid Trace Element Partitioning." *Geochimica et Cosmochimica Acta*, **42**, pp 743-770.

ITO, K. & MATSUI, Y., 1977, "Silicate Ilmentites and Post Spinel Transformations." in *High Pressure Research: Applications in Geophysics*. ed M. H. Manghnani & S Akimoto, Academic Press, London, New York & san Fransisco.

ITO, E. & TAKAHASHNI, E., 1987, "Melting of Peridotite at Uppermost Mantle Conditions." *Nature*, 328, pp514-517.

JANSE, A. J. A., 1984, "Kimberlites Where and When ?" in *Kimberlite Occurrence and Origin* ed J. E. Glover & P. G. Harris, The Geology department and University extension: The University of Western Australia, pupl 8.

JAQUES, A. L., HALL, A. E., SHERATON. J. W., SMITH, C. B, SUN, S-S., DREW, R. W., FOUDOULIS, C. & ELLINGSEN, C., 1986, "Composition of Crystalline Inclusions and C Isotope Composition of Argyle and Ellendale Diamonds." *Proceedings of the 4th International Kimberlite Conference* (preprint).

JAVOY, M. PINEAU, F. & DEMAIFFE, D., 1984, "Nitrogen and Carbon Isotopic Composition in the Diamonds of Mbuji Magi (Zaire)." *Earth and Planetary Science Letters*, 68, pp 399-412.

JEANLOZ, R. & RICHTER, F. M., 1979, "Convection, Composition and Thermal State of the Lower Mantle." *Journal of Geoophysical Research*, 84, pp 5497-5504.

JURENWICZ, A. J. G. & WATSON, E. B., 1988, "Cations in Olivine, Part 1: Calcium Partioning and Calicum Magnesium Distribution Between Olivines and Coexisting Melts With Petrologic Applications." *Contribiutions to Mineralogy and Petrology*, 99, pp 176-185.

JURENWICZ, A. J. G. & WATSON, E. B., 1988, "Cations in Olivine, Part 2: Diffusion in Olivine Xenocrysts, With Applications to Petrology and Mineral Physics." *Contributions to Mineralogy and Petrology*, 99, pp 186-201.

KATO, T., RINGWOOD, A. E. & IRIFUNE, T., 1988, "Constraints on Element Partition Coefficients Between $MgSiO_3$ Perovskite and Liquid Determined by Direct Measurements." *Earth and Planettary Science Letters*, 90, pp65-68.

KENNEDY, C. S. & KENNEDY, G. C., 1976, "The Equilibrium Boundary Between Graphite and Diamond." *Journal of Geophyusical Research*, 81, pp 2467-2470.

KAISER, W. & BOND, W. L., 1959, "Nitrogen, a Major Impurity in Common Type I Diamond." *Physical Review*, 115(4) pp 857-863.

KRAMERS, J. D., 1977,"Lead and Stromtium Isotopes in Cretaceous Kimberlites and Mantle Derived Xenoliths from Southern Africa." *Earth and Planetary Science Letters*, 34, pp 419-431.

KRAMERS, J. D., 1979, "Lead, Uranium, Strontium, Potassium and Rubidium in Inclusion Bearing Diamonds and Mantle Derived Xenoliths from Southern Africa." *Earth and Planetary Science Letters*, 42, pp 58-70.

KRAMERS, J. D., SMITH, C. B., LOCK, N. P., HARMON, R. S. & BOYD, F. R., 1981, "Can Kimberlite be Genertated from an Ordinary Mantle ?" *Nature*, 291, pp 53-56.

KYSER, T. K., 1986, "Stable Isotope Variations in the Mantle." in *Stable Isotopes in High Temperature Geological Processes.* ed J. W. Valley, H. P. Taylor & J. R. O' Neil.

LANG, A. R., 1979, "Diamond Structure." in *Properties of Diamond* ed J. E. Field, Academic press, London, New York & San Fransisco.

LAWLESS, P. J., 1978, "Some Aspects of the Mineral Chemistry of the Peridotite Xenolith Suite from the Bultfontein Diamond Mine, Kimberley, South Africa.", Phd. thesis, University of Cape town.

LAWLESS, P. J., GURNEY, J. J. & DAWSON, J. B., 1979, "Polymict peridotites from the Bultfontein and De Beers mine, Kimberley, South Africa." in *The Mantle Sample: inclusions in kimberlite and other volcanics* ed F. R. Boyd & H. O. A. Meyer, American Geophysical Union, Washington.

LEES, A. C., BUKOWINSKI, M. S. T. & JEANLOZ, R., 1983, "Reflection Properties of Phase Transitions and Compositional Change Models of the 670 Discontinuity." *Journal of Geophysical Research*, 88, pp 8145-8159.

LEWIS, H. C., 1897, *Genesis and Matrix of the Diamond.* Longmans, Green & Co, London.

LUI, L. G., 1976, "The High Pressure Phases of $MgSiO_3$." *Earth and Planetary Science Letters*, 31, pp 200-208.

LUI, L. G., 1976, "The Post Spinel Phase of Forsterite." *Nature*, 262, pp 770-772

LUI, L. G., 1977, "High Pressure $NaAlSiO_4$: The First Silcate Calcium Ferrite Isotype." *Geophysical Research Letters*, 4, pp 183-186.

LUI, L. G. ,1977, "The Post Spinel Phase of Twelve Silicates and Germanates." in *High Pressure Research: Applications in Geophysics* ed M. H. Manghnani & S. Akimoto, Academic Press, London, New York & San Fransisco.

LUI, L. G., 1978, "A New High Pressure Phase of $Ca_2Al_2SiO_7$ and Implications for the Earth's Interior." *Earth and Planetary Science Letters*, 40, pp 401-406.

LUI, L. G., 1978, "A New High Pressure Phase of Spinel." *Earth and Platnetary Science Letters*, 41, pp 398-404.

LUI, L. G., 1979, "On the 650km Seismic Discontinuity." *Earth and Planetary Science Letters*, 42, pp 202-208.

LUI, L. G. & RINGWOOD, A. E., 1975, "Synthesis of a Perovskite Type Polymorph of $CaSiO_3$." *Earth and Planetary science Letters*, 28, pp209-211.

MacGREGOR, I. D. & MANTON, W. I., 1986, "Roberts Victor Eclogites: Ancient Oceanic Crust." *Journal of Geophysical Research*, 91, pp 14063-14079.

McKENZIE, D. P., 1967, "Some Remarks on Heat Flow and Gravity Anomalies." *Journal of Geophysical Research*, 72(24),pp 6261-6273.

McKENZIE, D. P., 1984, "The Generation and Compaction of Partially Molten Rock." *Journal of Petrology*, 25, pp 713-765.

McKENZIE, D. P., 1985, "The Extraction of Magma from the Crust and Mantle." *Earth and Planetary Science Letters*, 74, pp 81-91.

McKENZIE, D. P., 1987, "The Compaction of Igneous and Sedimentary Rocks." *Journal of the Geological Society of London*, 144(2), pp 299-309.

McKENZIE, D. P. & O'NIONS, R. K., 1983, "Mantle Reservoirs and Ocean Island Basalts." *Nature*, 301, pp 229-231.

MATTIOLI, G. & WOOD, B. J., 1987, "Upper Mantle Oxygen Fugacity Recorded by Spinel Lherzolites." *Nature*, 322, pp 626-628.

MAO, H. K., BELL, P. M. & YAGI, T., 1979, "Iron Magnesium Fractionation for the Earth." *Carnegie Institute of Washington Yearbook*, 78, pp 621-625.

MENZIES, M. A. & HAWKSWORTH, C. J. ,1987, "Upper Mantle Processes and Composition." in *Mantle Xenoliths* ed P. H. Nixon, John Wiley & Sons.

MEYER, H. O. A., 1975, "Chromium and the Genesis of Diamond." *Geochimica et Cosmochimica Acta*, 39, pp929-936.

MEYER, H. O. A., 1987, "Inclusions in Diamonds." in *Mantle Xenoliths* ed P. H. Nixon, John Wiley & Sons.

MEYER, H. O. A. & BOYD, F. R., 1972, "Composition and Origin of Crystalline Inclusions in Natural Diamond." *Geochimica et Cosmochimica Acta*, 36, pp 1255-1273.

MILLEDGE, H. J., MENDLESSOHN, M., SEAL, M., ROUSE, J. E., SWART, P. K. & PILLINGER, C. T., 1983, "Carbon Isotopic Variation in Spectral Type II Diamonds." *Nature*, 303, pp 791-792.

MITCHELL, R. H., 1986, *Kimberlites: Mineralogy, Chemistry and Geology*. Plenum Press, New York.

MOORE, R. O. & GURNEY, J. J., 1985, "Pyroxene Solid Solution in Garnets Included in Diamond." *Nature*, 318, pp 553-555.

MUNKE, G., 1979, "Physics of Diamond." in *Properties of Diamond* ed J. E. Field. Academic Press, London: New York: San Fransisco

NICKEL, K. G. & GREEN, D. H., 1985, "Empirical Geothermobarometry for Garnet Peridotites and Implications for the Nature of the Lithosphere, Kimberlites and Diamonds." *Earth and Planetary Science Letters*, 73, pp 158-170.

NIXON, P. H., Van CATSSTERNEN, P. W. C., BOYD, F. R. & HAWKSWORTH, 1987, "Harzburgites with Garnets of Diamond Facies from South African Kimberlites." in *Mantle Xenoliths* ed P. H. Nixon, John Wiley & Sons.

NIXON, P. H. & DAVIES. G. R., 1987, "Mantle Xenolith Perspectives." in *Mantle Xenoliths* ed P. H. Nixon, John Wilery & Sons.

OHTANI, E., KATO, T. & SAWAMOTO, H., 1986, "Melting of a Model Chondritic Mantle at 20Gpa." *Nature*, 322, pp352-354.

O'HARA, M. J. & YODER, H. S., 1967,"Formation and Fractionation of Basic Magmas at High Pressures." *Scottish Journal of Geology*, 3(1) pp 67-117.

O'NEIL, J. R., 1986,"Theoretical and Experimental Aspects of Isotopic Fractionation." in *Stable Isotopes in High Temperature Geological Processes* ed J. W. Valley, H. P. Taylor & J. R. O'Neil, Reviews in Mineralogy vol 16, Min. Soc. Am.

ORLOV, Y. L., 1973, *The Mineralogy of Diamond*. John Wiley & Sons, New York.

OLSON, P. & YUEN, P. A., 1982, "Thermochemical Plumes and Phase Transitions." *Journal of Geophysical Research*, 87, pp 3992-4002.

PEHLKE, R. D, MAZANDARANY, F. N & RADSILOWSKI, R. H., 1975, "Solid Oxide emf cell Determination of the Standard Free Energy of Cr_2O_3 and Applications to Chromium Bearing Mineral Systems." *Geochimica et Cosmochimica Acta*, 39, pp 833-845.

PHILLIPS, D., ONSTUTT, T. C. & HARRIS, J. W., 1989, "$^{40}Ar/^{39}Ar$ Laser Probe Dating of Diamond Inclusions from the Premier kimberlite." *Nature*, 340, pp 460-462.

PRINZ, M., MANSON, D. V., HLAVA, P. F & KIEL, K., 1975, "Inclusions in Diamonds: Garnet lherzolite and Eclogite Assemblages." in *Physics and Chemistry of the Earth vol 9* ed L. H. Ahrens, J. B Dawson, A. R. Duncan & A. J. Erlank, Pergammon Press, Oxford & New York.

PRINZHOEFER, A. & ALLEGRE, C. J., 1985,"Residual Peridotites and the Mechanisms of Partial Melting." *Earth and Planetary Science Letters*, 74, pp 2561-261.

REID, A. M., BROWN, R. W., DAWSON, J. B., WHITFIELD, G. G. & SIEBERT, J. C., 1976, "Garnet and Pyroxene Compositions in Some Diamondiferous Eclogites." *Contributions to Mineralogy and Petrology*, 58, pp 203-220.

RICHARDSON, S. H., 1986, "Latter Day Origin of Diamonds of Eclogite Paragenesis." *Nature*, 322, pp 623-626.

RICHARDSON, S. H., ERLANK, A. J. & HART, S. R., 1985, "Kimberlite Borne Garnet Peridotie Xenoliths from Old Enriched Subcontinental Lithosphere." *Earth and Planetary Science Letters*, 75, pp 116-128.

RICHARDSON, S. H., GURNEY, J. J., ERLANK, A. J. & HARRIS, J. W., 1984, "Origin of Diamonds in Old, Enriched Mantle." *Nature*, 310, pp 198-202.

RICHTER, F. M. & McKENZIE, D. P., 1981, "On Some Consequences and Possible Causes of Layered Mantle Convection." *Journal of Geophysical Research*, 86, pp 6133-6142.

RINGWOOD, A. E., 1967, "The Pyroxene-Garnet Transformation in the Earths Mantle." *Earth and Planetary Science Letters*, 2. pp 255-263.

RINGWOOD, A. E., 1975, *Composition and Petrology of the Earths mantle.* McGraw-Hill, New York.

RINGWOOD, A. E., 1977, "Synthesis of Pyrope-Knorringite Solid Solution Series." *Earth and Planetary Science Letters*, 36, pp443-448.

RINGWOOD, A. E., 1982, "Phase Transformations and Differentiation in the Subducted Lithosphere: Implications for Mantle Dynamics, Basalt Petrogeneis and Crustal Evolution." *Journal of Geology*, 90, pp 611-643.

RINGWOOD, A. E. & MAJOR, A., 1967a, "Some High Pressure Phase Transformations of Geophysical Significance." *Earth and Planetary Science Letters*, 2, pp 106-110.

RINGWOOD, A. E. & MAJOR, A., 1967b, "Synthesis of Majorite and Other High Pressure Garnets and Perovskite." *Earth and Planetary Science Letters*, 12, pp 411-418.

ROBERTSON, D., FOX, J. J. & MARTIN, A. E., 1934, "Two Types of Diamond." *Philosophical Transactions of the Royal Society*, A232, pp458-463.

SALTERS, V. J. M. & SHIMIZU, N., 1988, "World Wide Occurrence of HFSE Depleted Mantle." *Geochimica et Cosmochimica Acta*, 52, pp 2177-2182.

SAUTTER, V. & HARTE, B., 1988, "Diffusion Gradients in an Eclogite Xenolith in the Roberts Victor Kimberlite: (1) Mechanism and Evolution of garnet exsolution in Al_2O_3 Rich Clinopyroxene." *Journal of Petrology*, 29, pp1325-1352.

SCARFE, C. M. & TAKAHASHI, E., 1986, "Melting of Garnet Peridotite to 13Gpa and the Early History of the Upper Mantle." *Nature*, 322, pp354-356.

SAXENA, S. K., 1989, "Oxidation State of the Mantle." *Geochimica et Cosmochimica Acta*, 53, pp 89-95.

SAXENA, S. K. & FEI, Y., 1988, "Fluid Mixtures in the C-O-H System at High Pressure and Temperature." *Geochimica et Cosmochimica Acta*, 52, pp 505-512.

SCHULZE, D. J., 1986, "Calcium Anomalies in the Mantle and a Subducted Metaserpentine Origin for Diamond." *Nature*, 319, pp483-485.

SCOTT-SMITH, B. H., DANCHIN, R. V., HARRIS, J. W. & STRACKE, K. J., 1984, "Kimberlites Near Orroroo, South Australia." in *Kimberlites I: Kimberlites and related rocks* ed J Kornprobst. Elsevier, Amsterdam.

SELLSCHOP, J. P. F., 1979, "Nuclear probe Studies in Physical and Chemical Studies of Natural Diamond." in *Properties of Diamond* ed J. E. Field, Academic Press, London, New York & San Fransisco.

SHEE, S. R., GURNEY, J. J. & ROBINSON, D. N., 1982, " Two diamond Bearing Peridotite Xenoliths From Finsch Mine, South Africa." *Contributions to Mineralogy and Petrology*, 81, pp 79-87.

SHI, P., HARTE, B. & BIGGAR, G. M., 1989, "Redox Partial Melting." Unpublished.

SHIMIZU, N. & ALLEGRE, C. J., 1978, "Geochemistry of Transition Elements in Garnet Lherzolite Nodules in Kimberlites." *Contributions to Mineralogy and Petrology*, 67, pp 41-50.

SHIMIZU, N. & RICHARDSON, S. H., 1987, "Trace element Abundance Patterns of Garnet Inclusions in Peridotite Suite Diamonds." *Geochimica et Cosmochimica Acta*, 51, pp 755-758.

SMITH, C. B., 1983, "Pb, Sr and Nd Isotopic Evidence for Sources of Southern African Kiimberlites." *Nature*, 304, pp 51-54.

SMITH, C. F. H., 1912, *Gemstones*, Revised F. C. Phillips, 1958, Methuen, London.

SOBOLEV, N. V., 1984, "Crystalline Inclusions in Diamonds from New South Wales." in *Kimberlite Occurrence and Origin* eds J. E. Glover & P.

G. Harris, The Geology Department and University Extension, University of Western Australia, Publication No. 8.

SOBOLEV, N. V., 1977, *Deep Seated Inclusions in Kimberlites and the Problem of the Compositon of the Upper Mantle.* America Geophysical Union, Washington.

SOBOLEV, N. V., GALIMOV, E. M., IVANOSKAYA, I. N. & YEFIMOVA, E. S., 1979, "The Carbon Isotopic Composition of Diamonds Containing Crystallographic Inclusions." *Doklady Akedemia Nauk, SSSR*, 207, pp164-167. (in Russian)

SOBOLEV, N. V., LAURENT'YEV, Yu. G. POKHILENKO, N. & USOVA, L. V., 1973, "Chrome Rich Garnets from the Kimberlites of Yakutia and their Paragenesis." *Contributions to Mineralogy and Petrology*, 40, pp 39-52.

SOBOLEV, V. S., SOBOLEV, N. V. & LAURENT'EV, Yu. G., 1971, Isomorphic Sodium Admixture in Garnets formed at High Pressures." *Contributions to Mineralogy and Petrology*, 31, pp 1-12.

SWART, P. K., PILLINGER, C. T., MILLEDGE, H. J. & SEAL, M., 1983, "Carbon Isotopic Variation Within Individual Diamonds." *Nature*, 303, pp 793-794.

TAYLOR, W. R., 1985, "Studies ofthe Model System C-O-H + Peridotite." University of Tasmania PhD Thesis (unpubl.)

TAYLOR, W. R. & GREEN, D. H., 1988, "Measurement of Reduced Peridotite C-O-H Solidus and Implications for Redox Melting of the Mantle." *Nature*, 332,pp 349-352.

THOMPSON, R. N., 1975, "Is Upper Mantle Phosphorous Contained in Sodic Garnet ?" *Earth and Planetary Science Letters*, 26, pp 417-424.

TSAI, H. M., SHIEH, Y. N. & MEYER, H. O. A., 1979, "Mineralogy and $^{34}S/^{35}S$ Ratios of Sulphide Associated with Kimberlite, Xenoliths

and Diamonds." in *The Mantle Sample, Inclusions in Kimberlites and Other Volcanics.* eds F. R. Boyd & H. O. A. Meyer, American Geophysical Union, Wsahington D. C..

ULMER, G. C., ROSENHAUER, M. WOERMAN, E. GINDER, J., DRORY WOLF, A.& WASILENSKI, . ,1976, "Applicabilty of Electrochemical Oxygen Fugacity Measurementss to Geothermometry." *American Mineralogist*, 61, pp 653-660.

VANCE, E. R., HARRIS, J. W. & MILLEDGE, H. J., 1973, "Possible Origins for α Particle Damage in Diamonds from Kimberlite and Alluvial Sources."

VALLEY, J. W., TAYLOR, H. P. & O'NEIL, J. R., 1986, *Stable Isotopes in High temperature Geological Processes.* Reviews in Mineralogy, Vol 16, Mineralogical society of America.

VILJOEN, M. J., VILJOEN, R. P. & PEARTON, T. N., 1982, "The Nature and Distribution of Archean Komatiite Volcanics in South Africa." in *Komatiites* ed N. T. Arndt & E. G. Nesbitt, Geo Allen & unwin, London.

WAGNER, P. A., 1914, *The Diamond Fields of Southern Africa.*, C. Struik, Cape Town (2nd impression , 1971).

WATT, J. P. & AHRENS, T. J., 1982, "The Role of Iron Partitioning in Mantle Composition, Evolution and Scale of Convection." *Journal of Geophysical Research*, 87, pp5631-5644.

WEDLAKE, R. J., 1979, "Technology of Diamond Growth." in *Properties of Diamond* ed J. E. Field Academic Press, London: New York: San Fransisco.

WHYTE, F. A. & WOOD, G. M., 1986, *Mass Spectrometry: Applications in Science and Engineering.* Wiley Interscience: John Wiley & sons, New York.

WILLIAMS, A. F., 1932, *The Genesis of Diamond.* Benn, London.

WOOD, B. J., 1974, "The Soluability of Alumina in Orthopyroxene Coexisting with Garnet." *Contributions to Mineralogy and Petrology*, 46, pp 1-15.

WOOD, B. J. & BANNO, S., 1973, "Garnet Orthopyroxene and Orthopyroxene Clinopyroxene Relationships in Simple and Complex Systems." *Contributions to MIneralogy and Petrology*, 42, pp 109-124.

WOODS, G. S., 1986, "Platelets and the Infra Red Absorption of Type Ia Diamond." *Proceedings of the Royal Society of London*, A407, pp219-238.

WYATT, B. A. & LAWLESS, P. J., 1984, "Ilmenite in Polymict Xenoliths from the Bultfontein and De Beers mines, South Africa." in *Kimberlites II: The Mantle and Crust Mantle Relationships* ed J. B. Komprobst, Elsevier, Amsterdam.

WYLLIE, P. J., 1987, "Metasomatism and Fluid Generation in Mantle Xenoliths." in *Mantle Xenoliths* ed P. H. Nixon, John Wiley & Sons.

WYLLIE, P. J., 1980, "The Origin of Kimberlite." *Journal of Geophysical Research*, 85, pp6902-6910.

WYLLIE, P. J., 1977, "Mantle Fluid Compositions Buffered by Carbonates in Peridotite-CO_2-H_2O." *Journal of Geology*, 85, pp 187-207.

WYLLIE, P. J. & HUANG, W. L., 1976, "High CO_2 Solubilities in Mantle Magmas." *Geology*, 4, pp 21-24.

WYLLIE, P. J. & HUANG, W. L., 1976,"Does CO_2 Cause Partial Melting in the Low Velocity Layer of the Mantle ?" *Geology*, 4, pp712,787-788.

WYLLIE, P. J. & HUANG, W. L., 1975, "Peridotite, Kimberlite and Carbonatite Explained in the System CaO-MgO-SiO_2-CO_2.", *Geology*, 3, pp 621-624.

WYLLIE, P. J. & HUANG, W. L., 1975, "Influence of CO_2 in the Generation of Carbonatites and Kimberlites." *Nature*, 257, pp 297-299.

YAGI, T. MAO, H. K. & BELL, M. K., 1979,"Lattice Parmeters and Specific Volume for the Perovskite Phase of Orthopyroxene Composition, (Mg,Fe)SiO_3." *Carnegie Institue of Washington Yearbook*, 78, pp 612.

YAGI, T., MAO, H. K. & BELL, P. M., 1979, "Hydrostatic Compression of Perovskite Structure." *Carnegie Institue of Washington Yearbook*, 78, pp 613-614.

YAGI, T., BELL, P. M. & MAO, H. K., 1979, "Phase Relations in the System MgO-SiO_2-FeO Between 150-700kbar at 1000°C." *Carnegie Institute of Washington Yearbook*, 78, pp 614-618.

YAMAOKA, S., KANDA, H. & SETAKA, N., 1980, "Etching of Diamond Octahedrons at High Temperatures and Pressures with Controlled Oxygen Partial Pressure." *Journal of Material Science*, 15, pp332-336.

YEFIMOVA, E. S. & SOBOLEV, N. V., 1983, "Sulfide Inclusions in Diamond and Specific Features of Their Paragenesis." *Dok. Akad. Nauk. SSR*, 237, pp 1474-1478.

Appendix 1.

The averaged, tabulated analyses for Bultfontein inclusions are shown. Chemical analyses were determined by wave dispersive (WDS) X ray analysis. Inclusions which were identified by energy dispersive (EDS) analysis are not shown.

Chromites.

	B1A	B2A	B2D	B2E	B3A	B3B
MGO	13.53	13.53	15.98	16.32	15.85	15.69
SIO2	0.00	0.00	0.10	0.00	0.00	0.00
AL2O3	6.80	7.10	9.80	8.60	8.60	8.60
TIO2	0.07	0.06	0.03	0.04	0.03	0.01
CR2O3	64.70	64.30	63.90	65.10	65.00	65.20
FEO	14.40	13.81	9.91	9.73	10.04	10.01
NIO	0.09	0.07	0.11	0.07	0.09	0.10
TOTAL	99.59	98.87	99.83	99.86	99.61	99.61
SI	0.02	0.02	0.03	0.02	0.02	0.02
TI	0.00	0.00	0.00	0.00	0.00	0.00
AL	2.10	2.20	2.90	2.60	2.60	2.60
CR	13.00	13.00	12.00	13.00	13.00	13.00
FE2	2.68	2.69	1.98	1.79	1.98	1.98
FE3	0.42	0.31	0.12	0.21	0.12	0.12
MG	5.30	5.30	6.00	6.20	6.00	6.00
NI	0.02	0.01	0.02	0.01	0.02	0.02
TOTAL	23.54	23.53	23.05	23.83	23.74	23.74
F/F+M	0.37	0.36	0.26	0.24	0.26	0.26

	B6A	B7B	B10A	B10B	B11A	B12A
MGO	13.49	14.82	16.41	14.65	14.83	14.53
SIO2	0.00	0.00	0.00	0.00	0.00	0.00
AL2O3	7.80	7.80	8.40	7.18	7.40	7.00
TIO2	0.17	0.11	0.06	0.28	0.17	0.25
CR2O3	63.70	64.80	64.80	64.53	65.30	65.50
FEO	14.28	11.98	9.59	12.19	11.64	12.12
NIO	0.10	0.07	0.13	0.11	0.08	0.10
TOTAL	99.54	99.58	99.39	99.93	99.42	99.50
SI	0.00	0.02	0.02	0.02	0.02	0.01
TI	0.00	0.00	0.00	0.00	0.00	0.00
AL	2.40	2.40	2.50	2.20	2.20	2.10
CR	13.00	13.00	13.00	13.00	13.00	13.00
FE2	2.78	2.29	1.77	2.28	2.28	2.38
FE3	0.32	0.31	0.23	0.32	0.22	0.22
MG	5.20	5.70	6.20	5.70	5.70	5.60
NI	0.02	0.01	0.03	0.02	0.02	0.02
TOTAL	23.72	23.73	23.75	23.54	23.44	23.33
F/F+M	0.37	0.31	0.24	0.31	0.30	0.32

Chromites

	B12B	B13A	B13B	B15A	B18A	B19A
MGO	15.68	13.95	16.38	15.96	15.89	16.45
SIO2	0.10	0.10	0.10	0.00	0.07	0.00
AL2O3	7.90	7.40	9.30	8.50	8.77	8.70
TIO2	0.05	0.91	0.03	0.05	0.07	0.05
CR2O3	64.60	64.90	64.60	65.20	64.68	65.50
FEO	11.22	13.55	9.60	9.82	9.36	9.52
NIO	0.12	0.10	0.12	0.10	0.11	0.13
TOTAL	99.67	100.91	100.13	99.63	98.95	100.35
SI	0.03	0.02	0.04	0.02	0.02	0.02
TI	0.00	1.60	0.00	0.00	0.00	0.00
AL	2.40	2.00	2.80	2.50	2.60	2.60
CR	13.00	12.00	12.00	13.00	13.00	13.00
FE2	1.98	3.18	1.78	1.88	1.88	1.77
FE3	0.42	0.58	0.22	0.22	0.12	0.23
MG	6.00	4.80	6.20	6.10	6.10	6.20
NI	0.02	0.02	0.02	0.02	0.02	0.03
TOTAL	23.85	23.04	23.06	23.74	23.74	23.85
F/F+M	0.29	0.35	0.24	0.26	0.25	0.24

	B20A	B21A	B21B	B22A	B25A	B26A
MGO	15.53	16.35	15.71	16.49	15.47	13.97
SIO2	0.00	0.10	0.08	0.00	0.00	0.00
AL2O3	7.40	8.60	8.36	8.70	8.35	7.20
TIO2	0.00	0.01	0.05	0.06	0.03	0.05
CR2O3	65.30	64.60	64.81	65.20	64.75	64.50
FEO	11.68	9.62	9.57	9.75	10.20	13.34
NIO	0.13	0.11	0.40	0.12	0.09	0.09
TOTAL	100.04	99.39	98.98	100.32	98.88	99.15
SI	0.02	0.03	0.02	0.02	0.02	0.02
TI	0.00	0.00	0.00	0.00	0.00	0.00
AL	2.20	2.60	2.50	2.60	2.50	2.20
CR	13.00	13.00	13.00	13.00	13.00	13.00
FE2	2.07	1.78	1.92	1.78	2.08	2.58
FE3	0.43	0.22	0.08	0.22	0.12	0.32
MG	5.90	6.20	6.00	6.20	5.90	5.40
NI	0.03	0.02	0.08	0.02	0.02	0.02
TOTAL	23.65	23.85	23.60	23.84	23.64	23.54
F/F+M	0.30	0.24	0.25	0.24	0.27	0.35

Chromites

	B27A	B28A	B29A	B30A	B31A	B32A
MGO	16.46	14.47	15.87	15.70	14.98	16.22
SIO2	0.00	0.00	0.00	0.00	0.00	0.00
AL2O3	8.90	6.40	7.80	8.70	6.50	8.90
TIO2	0.06	0.03	0.02	0.07	0.01	0.08
CR2O3	64.50	66.00	64.50	64.60	66.00	64.20
FEO	9.69	11.95	10.05	10.33	11.31	9.72
NIO	0.11	0.08	0.11	0.09	0.09	0.14
TOTAL	99.72	98.93	98.35	99.49	98.89	99.26
SI	0.02	0.02	0.02	0.01	0.02	0.02
TI	0.00	0.00	0.00	0.00	0.00	0.00
AL	2.60	1.90	2.40	2.60	2.00	2.70
CR	13.00	13.00	13.00	13.00	13.00	13.00
FE2	1.78	2.38	1.88	1.98	2.18	1.77
FE3	0.22	0.22	0.22	0.22	0.22	0.23
MG	6.20	5.60	6.10	6.00	5.80	6.20
NI	0.02	0.02	0.02	0.02	0.02	0.03
TOTAL	23.84	23.14	23.64	23.83	23.24	23.95
F/F+M	0.24	0.32	0.26	0.27	0.29	0.24

	B33A	B117A	B117B	B118B	B118B	B118C
MGO	14.99	13.57	13.58	15.19	15.20	15.37
SIO2	0.10	0.00	0.00	0.00	0.00	0.00
AL2O3	7.70	7.00	6.90	7.60	7.70	7.80
TIO2	0.07	0.04	0.04	0.27	0.29	0.27
CR2O3	65.50	66.00	65.80	65.80	65.60	65.10
FEO	10.45	13.18	13.19	10.65	10.73	10.76
NIO	0.11	0.06	0.10	0.14	0.10	0.14
TOTAL	98.92	99.85	99.61	99.65	99.62	99.44
SI	0.04	0.02	0.02	0.02	0.01	0.01
TI	0.00	0.00	0.00	0.00	0.00	0.00
AL	2.30	2.10	2.10	2.30	2.30	2.40
CR	13.00	13.00	13.00	13.00	13.00	13.00
FE2	2.18	2.79	2.68	2.17	2.18	2.07
FE3	0.02	0.01	0.12	0.13	0.12	0.23
MG	5.80	5.20	5.30	5.80	5.80	5.90
NI	0.02	0.01	0.02	0.03	0.02	0.03
TOTAL	23.36	23.13	23.24	23.45	23.43	23.64
F/F+M	0.27	0.35	0.35	0.28	0.28	0.28

Chromites

	B119A	B120A	B120B	B121A	B121B	B122A
MGO	15.65	14.13	13.40	14.30	14.68	14.63
SIO2	0.20	0.00	0.00	0.00	0.00	0.00
AL2O3	8.10	6.80	7.70	7.80	6.90	7.50
TIO2	0.02	0.16	0.19	0.12	0.08	0.05
CR2O3	65.30	66.30	66.60	66.30	66.50	66.50
FEO	9.81	12.11	12.23	11.30	11.43	11.32
NIO	0.13	0.09	0.06	0.11	0.06	0.08
TOTAL	99.21	99.59	100.18	99.93	99.65	100.08
SI	0.06	0.01	0.01	0.01	0.02	0.02
TI	0.00	0.00	0.00	0.00	0.00	0.00
AL	2.40	2.10	2.30	2.40	2.40	2.30
CR	13.00	13.00	13.00	13.00	15.00	13.00
FE2	1.97	2.48	2.89	2.48	5.99	2.38
FE3	0.13	0.12	0.29	0.08	3.19	0.02
MG	6.00	5.50	5.10	5.50	2.00	5.60
NI	0.03	0.02	0.01	0.02	0.01	0.02
TOTAL	23.59	23.23	23.02	23.33	22.23	23.34
F/F+M	0.26	0.32	0.34	0.30	0.58	0.30

Garnets

	B34A	B35A	B39A	B101A	B103A	B105A
NA2O	0.01	0.02	0.02	0.01	0.01	0.01
MGO	24.65	25.06	23.82	26.19	24.58	25.67
SIO2	42.62	42.54	43.41	43.50	42.24	42.67
AL2O3	17.74	20.45	21.24	21.65	17.24	18.13
CAO	1.04	1.31	2.53	0.97	0.71	0.95
TIO2	0.04	0.00	0.02	0.00	0.00	0.01
CR2O3	8.72	5.41	3.75	3.75	9.36	8.52
MNO	0.24	0.19	0.23	0.21	0.26	0.23
FEO	4.93	4.71	5.19	4.61	5.40	4.73
TOTAL	99.99	99.69	100.11	100.89	99.80	100.92
SI	3.02	2.99	3.04	3.00	3.01	3.00
TI	0.00	0.00	0.00	0.00	0.00	0.00
AL	1.48	1.70	1.75	1.76	1.45	1.50
CR	0.49	0.30	0.21	0.20	0.53	0.47
FE2	0.29	0.28	0.30	0.27	0.32	0.28
MN	0.01	0.01	0.01	0.01	0.02	0.01
MG	2.61	2.63	2.48	2.69	2.61	2.69
CA	0.08	0.10	0.19	0.07	0.05	0.07
TOTAL	7.99	8.01	7.98	8.01	8.00	8.02

	B105A	B106A	B114A	B115A	B116B	B123A
NA2O	0.01	0.01	0.02	0.02	0.02	0.02
MGO	25.67	24.87	23.71	25.45	25.23	24.85
SIO2	42.53	42.76	41.68	42.57	42.31	42.46
AL2O3	18.13	18.07	14.03	19.09	17.99	19.22
CAO	0.95	0.89	1.60	0.97	0.78	1.08
TIO2	0.01	0.00	0.06	0.00	0.01	0.01
CR2O3	8.52	8.53	12.65	6.89	8.81	6.43
MNO	0.23	0.00	0.00	0.22	0.27	0.23
FEO	4.73	4.67	5.51	4.28	4.56	4.76
TOTAL	100.78	99.80	99.26	99.49	99.98	99.06
SI	2.99	2.99	3.03	3.01	3.00	3.02
TI	0.00	0.00	0.00	0.00	0.00	0.00
AL	1.50	1.52	1.20	1.59	1.50	1.61
CR	0.47	0.48	0.73	0.38	0.49	0.36
FE2	0.28	0.28	0.33	0.25	0.27	0.28
MN	0.01	0.00	0.00	0.01	0.02	0.01
MG	2.69	2.65	2.57	2.68	2.66	2.63
CA	0.07	0.07	0.12	0.07	0.06	0.08
TOTAL	8.02	8.00	8.00	8.00	8.00	8.00

Garnets

	B124A	B128B	B149A	B149B	B150A
NA2O	0.02	0.02	0.01	0.02	0.00
MGO	23.18	25.37	24.19	24.53	25.96
SIO2	41.84	42.75	40.12	41.70	42.56
AL2O3	15.73	18.96	16.73	16.87	20.18
CAO	2.37	0.71	2.97	2.93	2.32
TIO2	0.08	0.00	0.08	0.09	0.03
CR2O3	11.05	7.01	9.95	9.95	5.56
MNO	0.28	0.21	0.23	0.23	0.20
FEO	4.89	4.17	4.48	4.59	4.72
TOTAL	99.44	99.20	98.76	100.91	101.530
SI	3.02	3.02	2.92	2.96	2.90
TI	0.00	0.00	0.00	0.00	0.00
AL	1.34	1.58	1.44	1.41	1.78
CR	0.63	0.39	0.57	0.56	0.30
FE2	0.30	0.25	0.27	0.27	0.27
MN	0.02	0.01	0.01	0.01	0.01
MG	2.49	2.68	2.62	2.60	2.63
CA	0.18	0.05	0.23	0.22	0.17
TOTAL	7.99	7.99	8.07	8.04	8.06

Olivines.

	B42A	B57A	B67A	B70B	B74A	B131A
MGO	51.99	51.75	53.18	51.68	50.72	52.86
SIO2	41.63	41.53	41.58	40.78	41.03	41.96
AL2O3	0.00	0.05	0.02	0.03	0.03	0.02
CAO	0.00	0.01	0.00	0.01	0.04	0.00
TIO2	0.00	0.00	0.00	0.01	0.00	0.00
CR2O3	0.01	0.05	0.06	0.05	0.03	0.06
MNO	0.08	0.09	0.08	0.08	0.11	0.07
FEO	4.92	5.41	4.48	5.81	6.76	4.69
NIO	0.36	0.35	0.31	0.32	0.32	0.39
TOTAL	99.10	99.24	99.71	98.77	99.07	100.05
SI	1.01	1.11	1.00	1.00	1.00	1.01
AL	0.00	0.00	0.00	0.00	0.00	0.00
CR	0.00	0.00	0.00	0.00	0.00	0.00
FE2	0.10	0.10	0.09	0.12	0.14	0.09
MN	0.00	0.00	0.00	0.00	0.00	0.00
MG	1.88	1.67	1.91	1.88	1.85	1.89
CA	0.00	0.00	0.00	0.00	0.00	0.00
TOTAL	2.99	2.88	3.00	3.00	2.99	2.99

	B132A	B133A	B136A
MGO	52.74	51.63	51.46
SIO2	41.33	41.32	40.89
AL2O3	0.04	0.01	0.02
CAO	0.00	0.00	0.00
TIO2	0.00	0.01	0.01
CR2O3	0.01	0.08	0.04
MNO	0.06	0.01	0.08
FEO	4.27	5.73	6.15
NIO	0.37	0.39	0.23
TOTAL	98.87	99.18	99.88
SI	1.00	1.00	1.00
AL	0.02	0.00	0.00
CR	0.00	0.00	0.00
FE2	0.12	0.12	0.12
MN	0.02	0.00	0.00
MG	1.86	1.87	1.87
CA	0.00	0.00	0.00
TOTAL	3.00	2.99	3.00

Orthopyroxenes.

	B48A	B70A	B70C	B78A	B111C	B129A
NA2O	0.05	0.36	0.04	0.00	0.02	0.04
MGO	36.97	35.89	35.98	37.04	36.87	36.52
SIO2	58.11	57.39	57.98	57.26	58.32	58.17
AL2O3	0.17	0.95	0.92	0.67	0.86	0.96
CAO	0.23	0.36	0.32	0.18	0.11	0.12
TIO2	0.00	0.02	0.03	0.00	0.00	0.00
CR2O3	0.08	0.75	0.69	0.39	0.67	0.72
MNO	0.07	0.95	0.09	0.07	0.07	0.09
FEO	3.42	3.44	3.53	3.13	2.59	2.70
NIO	0.18	0.12	0.10	0.13	0.13	0.13
TOTAL	99.28	100.23	99.68	98.87	99.64	99.35
SI	1.99	1.96	1.98	1.97	1.99	1.99
AL	0.01	0.04	0.04	0.03	0.03	0.04
CR	0.00	0.02	0.02	0.01	0.02	0.02
FE2	0.10	0.10	0.10	0.09	0.07	0.08
MN	0.00	0.03	0.00	0.00	0.00	0.00
MG	1.89	1.83	1.83	1.90	1.87	1.86
CA	0.01	0.01	0.01	0.01	0.00	0.00
TOTAL	4.00	4.00	3.99	4.01	3.99	3.98

	B139A	B140A	B141A	B143A	B146A
NA2O	0.00	0.02	0.03	0.03	0.02
MGO	36.91	36.83	35.87	35.77	36.51
SIO2	57.66	57.95	57.93	57.69	57.81
AL2O3	0.82	0.94	0.86	0.77	0.84
CAO	0.00	0.18	0.30	0.41	0.17
TIO2	0.00	0.18	0.28	0.05	0.02
CR2O3	0.65	0.64	0.70	0.58	0.66
MNO	0.08	0.08	0.10	0.10	0.07
FEO	2.58	2.64	3.28	3.49	3.45
NIO	0.11	0.15	0.10	0.11	0.08
TOTAL	98.81	99.61	99.45	99.00	99.63
SI	1.98	1.98	1.98	1.99	1.98
TI	0.00	0.00	0.01	0.00	0.00
AL	0.03	0.04	0.03	0.03	0.03
CR	0.02	0.02	0.02	0.02	0.02
FE2	0.07	0.07	0.09	0.10	0.10
MN	0.00	0.00	0.00	0.00	0.00
MG	1.89	1.87	1.83	1.84	1.86
CA	0.00	0.01	0.01	0.02	0.01
TOTAL	3.99	3.99	3.98	3.99	3.99

Clinopyroxene.

	B75A	B77A	B79A
NA2O	1.64	6.35	3.73
MGO	17.31	14.29	13.95
SIO2	54.44	55.69	55.57
AL2O3	2.18	3.75	3.66
CAO	18.96	16.35	16.13
TIO2	0.49	0.39	0.41
CR2O3	1.48	3.47	3.47
MNO	0.21	0.13	0.11
FEO	2.06	2.25	2.24
TOTAL	98.77	100.67	99.27
SI	1.98	1.86	2.01
TI	0.01	0.01	0.01
AL	0.09	0.15	0.15
FE2	0.06	0.06	0.07
MN	0.01	0.00	0.00
MG	0.94	0.71	0.75
CA	0.74	0.59	0.62
NA	0.06	0.53	0.13
TOTAL	3.93	4.00	3.85

Eclogite Paragenesis Inclusions.

	B135(PX)	B142(PX)	B148(GT)
NA2O	4.68	2.13	0.17
MGO	11.06	14.74	18.24
SIO2	55.38	54.00	42.06
AL2O3	8.41	2.56	23.84
CAO	15.30	17.48	4.14
TIO2	0.38	0.32	0.13
CR2O3	0.05	0.05	0.06
MNO	0.06	0.14	0.21
FEO	3.68	8.10	13.91
TOTAL	99.00	99.52	102.79
SI	1.99	1.99	2.96
TI	0.01	0.01	0.01
AL	0.00	0.00	1.98
FE2	0.11	0.25	0.82
MN	0.00	0.00	0.04
MG	0.59	0.81	1.91
CA	0.59	0.69	0.31
NA	0.16	0.08	0.03
TOTAL	3.82	3.94	8.08

Appendix 2.

The infra red absorption at 7.3μm and the values of the A and B aggregate are shown together with the $\delta\ ^{13}C$ composition. Diamonds which show no absorption are Type II.

Chromites.

	A(ppm)	B(ppm)	μ7.3	$\delta^{13}C$
B1	789.4	359.0	7.1	-2.50
B3	747.1	607.0	1.2	-2.79
B4	315.7	54.0	3.7	-4.70
B5	147.5	122.0	0.7	-2.01
B6	92.9	48.0	0.9	-4.35
B7	134.5	94.0	1.4	-2.50
B8	141.1	65.0	1.6	-5.98
B9	273.8	14.0	2.2	-5.73
B10	90.0	58.9	0.3	-1.86
B11	490.7	203.0	0.5	-1.86
B12	448.7	340.0	7.8	-5.97
B13	45.0	29.4	0.6	-5.78
B14	70.2	9.0	0.4	-4.28
B15	521.1	40.2	3.8	-4.79
B18	249.7	54.4	1.8	-4.77
B19			Type II	-4.65
B20	236.4	154.5	1.8	-4.85
B21	109.2	36.2	0.9	-4.75
B22	53.8	33.6	1.2	-4.51
B23	290.2	113.2	6.1	-0.48
B24	411.8	33.9	9.0	-1.07
B27	567.4	156.3	4.1	-4.62
B29	356.5	274.4	4.4	-2.88
B33	172.5	28.9	0.5	-1.74

Chrome Pyrope Garnets.

	A(ppm)	B(ppm)	μ7.3	$\delta^{13}C$
B34	101.1	116.9	1.4	-4.58
B36	104.4	54.35	1.0	-5.04
B103	266.4	18.2	0.4	-6.39
B105		Type II		-6.17
B106	28.5	18.12	2.2	-6.46

Olivine and Orthopyroxene.

	A(ppm)	B(ppm)	μ7.3	$\delta^{13}C$
B46	28.66	268.4	2.6	-4.46
B50	215.9	0.0	1.0	-3.77
B54	92.0	114.1	0.4	-4.78
B57	162.5	8.6	2.2	-3.78
B56	87.5	18.2	1.2	-4.65
B60		Type II		-5.54
B63	30.2	184.6	1.4	-5.41
B64		Type II		-4.59
B65	725.3	253.6	4.4	-5.48
B66		Type II		-4.81
B67	968.0	181.2	5.0	-5.10
B69	248.8	95.11	1.6	-5.35
B71	6.4	88.6	1.8	-5.23

Chrome Diopsides.

	A(ppm)	B(ppm)	μ7.3	$\delta^{13}C$
B40	77.4	56.9	1.2	-3.90
B42	804.1	54.6	1.8	-5.11

Sulphides.

	A(ppm)	B(ppm)	μ7.3	$\delta^{13}C$
B85	745.3	126.8	1.8	-5.56
B88	855.7	108.7	3.2	-4.73
B89	1562.0	181.2	4.5	-5.12
B90		Type II		-1.77
B92	1150.0	317.9	0.6	-4.06
B96	109.4	185.7	2.4	-5.64
B98	130.2	81.9	0.8	-5.16
B99	116.7	108.1	0.6	-7.96

Appendix 3

Garnet-bearing diamonds from Sao Luiz.

Appendix 3.1

Individual tabulated analyses for Sao Luiz garnetiferous inclusions. All chemical compositions were determined by wave dispersive X-ray analysis.

Group IA Garnets.

	BZ4 1	BZ4 3	BZ4 4	BZ4 5	BZ11 1	BZ11 2
NA2O	0.25	0.29	0.27	0.26	0.48	0.43
MGO	10.40	10.67	10.62	10.68	9.13	9.01
SIO2	39.10	39.60	39.70	39.40	39.40	39.60
P2O5	0.19	0.18	0.19	0.19	0.33	0.34
AL2O3	20.59	21.51	21.61	21.63	0.94	20.75
K2O	0.02	0.00	0.00	0.00	0.00	0.02
CAO	12.84	12.89	12.93	12.94	13.88	13.70
TIO2	1.14	1.13	1.15	1.14	1.95	1.96
CR2O3	0.10	0.08	0.09	0.11	0.05	0.06
MNO	0.27	0.27	0.29	0.29	0.32	0.31
FEO	13.00	13.06	13.10	12.89	13.69	13.75
	97.90	99.69	99.94	99.52	100.17	99.92
SI	2.98	2.96	2.96	2.95	2.95	2.97
TI	0.07	0.06	0.06	0.06	0.11	0.11
AL	1.85	1.89	1.90	1.90	1.85	1.83
CR	0.01	0.00	0.00	0.01	0.00	0.00
FE2	0.83	0.81	0.82	0.81	0.86	0.86
MN	0.02	0.02	0.02	0.02	0.02	0.02
MG	1.18	1.19	1.18	1.19	1.02	1.01
CA	1.05	1.03	1.03	1.04	1.11	1.10
NA	0.02	0.02	0.02	0.02	0.03	0.03
K	0.00	0.00	0.00	0.00	0.00	0.00
P	0.01	0.01	0.01	0.01	0.02	0.02
TOTAL	8.00	8.01	8.00	8.01	7.98	7.96

	BZ11 4	BZ11 5	BZ11 5	BZ11 7	BZ11 8	BZ44 1
NA2O	0.50	0.46	0.50	0.46	0.53	0.53
MGO	9.18	9.11	9.24	9.07	9.39	9.64
SIO2	40.00	39.20	39.80	39.30	39.00	38.90
P2O5	0.33	0.33	0.30	0.33	0.33	0.19
AL2O3	21.03	21.04	21.34	20.81	21.23	19.43
K2O	0.00	0.01	0.01	0.01	0.00	0.00
CAO	13.77	13.73	13.67	13.72	13.79	13.93
TIO2	1.94	1.94	1.95	1.97	1.94	3.87
CR2O3	0.04	0.05	0.06	0.05	0.02	0.08
MNO	0.32	0.32	0.34	0.30	0.30	0.31
FEO	13.76	13.68	13.89	13.94	13.68	13.34
	100.88	99.87	101.09	99.96	100.21	100.21
SI	2.97	2.95	2.95	2.95	2.92	2.92
TI	0.11	0.11	0.11	0.11	0.11	0.22
AL	1.84	1.86	1.86	1.84	1.87	1.72
CR	0.00	0.00	0.00	0.00	0.00	0.00
FE2	0.85	0.86	0.86	0.87	0.86	0.84
MN	0.02	0.02	0.02	0.02	0.02	0.02
MG	1.02	1.02	1.02	1.02	1.05	1.08
CA	1.10	1.10	1.09	1.10	1.11	1.12
NA	0.04	0.03	0.04	0.03	0.04	0.04
K	0.00	0.00	0.00	0.00	0.00	0.00
P	0.02	0.02	0.02	0.02	0.02	0.01
TOTAL	7.97	7.98	7.97	7.98	8.00	7.97

Group IB Garnets.

	BZ1	BZ1	BZ1	BZ1	BZ1	BZ2 .
NA2O	0.38	0.38	0.40	0.41	0.39	0.24
MGO	12.18	12.18	12.22	12.23	12.42	15.67
SIO2	40.20	40.20	40.60	40.20	40.50	40.60
P2O5	0.22	0.20	0.20	0.23	0.25	0.13
AL2O3	20.99	20.99	21.10	21.14	21.36	21.05
K2O	0.02	0.00	0.01	0.01	0.00	0.00
CAO	11.07	11.07	11.06	11.10	11.11	6.81
TIO2	2.08	2.08	2.07	2.09	2.03	1.68
CR2O3	0.12	0.12	0.13	0.14	0.13	0.11
MNO	0.30	0.30	0.28	0.26	0.26	0.33
FEO	13.22	13.22	13.19	13.17	13.13	13.00
	100.78	100.74	101.26	100.98	101.58	99.61
SI	2.96	2.96	2.97	3.25	2.95	2.98
TI	0.11	0.11	0.11	0.13	0.11	0.09
AL	1.82	1.82	1.82	2.01	1.84	1.82
CR	0.01	0.01	0.01	0.01	0.01	0.01
FE2	0.81	0.81	0.81	0.89	0.80	0.80
MN	0.02	0.02	0.02	0.02	0.02	0.02
MG	1.34	1.34	1.33	0.27	1.35	1.71
CA	0.87	0.87	0.87	0.96	0.87	0.54
NA	0.03	0.03	0.03	0.03	0.03	0.02
K	0.00	0.00	0.00	0.00	0.00	0.00
P	0.01	0.01	0.01	0.02	0.02	0.01
TOTAL	7.99	7.99	7.98	7.58	7.99	8.00

	BZ2	BZ2	BZ2	BZ2	BZ2	BZ5
NA2O	0.24	0.30	0.24	0.23	0.22	0.25
MGO	15.78	15.82	15.83	15.76	15.52	11.32
SIO2	40.60	42.40	41.10	40.60	40.60	40.70
P2O5	0.16	0.11	0.11	0.15	0.14	0.16
AL2O3	21.05	20.87	21.32	21.14	20.91	21.83
K2O	0.01	0.01	0.01	0.00	0.01	0.01
CAO	6.78	6.97	6.79	6.81	6.83	12.67
TIO2	1.67	1.67	1.67	1.66	1.69	0.90
CR2O3	0.10	0.07	0.10	0.12	0.12	0.11
MNO	0.31	0.25	0.30	0.31	0.28	0.26
FEO	13.03	12.87	13.00	12.85	12.95	12.62
	99.72	101.36	100.46	99.63	99.27	100.84
SI	2.98	3.05	2.99	2.98	2.99	2.99
TI	0.09	0.09	0.09	0.09	0.09	0.05
AL	1.82	1.77	1.83	1.83	1.81	1.89
CR	0.00	0.00	0.00	0.01	0.01	0.01
FE2	0.80	0.77	0.79	0.79	0.80	0.77
MN	0.02	0.02	0.02	0.02	0.02	0.02
MG	1.73	1.69	1.71	1.72	1.70	1.24
CA	0.53	0.54	0.53	0.54	0.54	1.00
NA	0.02	0.02	0.02	0.02	0.02	0.02
K	0.00	0.00	0.00	0.00	0.00	0.00
P	0.01	0.01	0.01	0.01	0.01	0.01
TOTAL	8.00	7.96	7.99	8.00	7.99	7.99

Group IB Garnets.

	BZ5	BZ5	BZ5	BZ5	BZ5	BZ12
NA2O	0.20	0.27	0.23	0.25	0.25	0.34
MGO	11.22	11.25	10.95	11.08	10.99	10.69
SIO2	40.70	40.90	40.40	40.70	40.90	39.60
P2O5	0.14	0.17	0.12	0.16	0.18	0.18
AL2O3	21.69	21.77	21.32	21.42	21.37	20.75
K2O	0.00	0.01	0.01	0.00	0.01	0.02
CAO	12.73	12.58	12.76	12.67	12.76	13.01
TIO2	0.10	0.92	0.91	0.92	0.87	1.92
CR2O3	0.10	0.13	0.11	0.10	0.11	0.06
MNO	0.27	0.24	0.25	0.26	0.26	0.28
FEO	12.77	12.76	12.64	12.47	12.63	13.62
	99.91	101.00	99.72	100.03	100.34	100.48
SI	3.02	3.01	3.01	3.01	3.02	2.95
TI	0.01	0.05	0.05	0.05	0.05	0.11
AL	1.90	2.01	1.87	1.87	1.86	1.82
CR	0.00	0.01	0.01	0.00	0.01	0.00
FE2	0.79	0.84	0.79	0.77	0.78	0.85
MN	0.02	0.02	0.02	0.02	0.02	0.02
MG	1.24	1.32	1.21	1.22	1.21	1.19
CA	1.01	0.22	1.02	1.00	1.01	1.04
NA	0.01	0.02	0.02	0.02	0.02	0.02
K	0.00	0.00	0.00	0.00	0.00	0.00
P	0.01	0.01	0.01	0.01	0.01	0.01
TOTAL	8.01	7.70	7.99	7.98	7.98	8.01

	BZ12	BZ12	BZ12	BZ13	BZ13	BZ13
NA2O	0.34	0.34	0.16	0.16	0.18	0.17
MGO	10.38	10.40	15.52	15.62	15.79	15.81
SIO2	38.90	39.20	40.10	40.50	40.80	41.00
P2O5	0.17	0.18	0.14	0.11	0.31	0.12
AL2O3	20.46	20.60	20.06	20.09	20.28	20.05
K2O	0.00	0.00	0.01	0.00	0.00	0.00
CAO	13.07	12.96	5.51	5.50	5.46	5.43
TIO2	1.94	1.89	1.85	1.82	1.80	1.80
CR2O3	0.06	0.09	0.25	0.24	0.23	0.26
MNO	0.28	0.30	0.27	0.27	0.28	0.28
FEO	13.49	13.60	15.15	15.11	15.01	15.08
	99.10	99.56	99.03	99.42	100.14	100.01
SI	2.94	2.95	2.99	3.00	3.00	3.02
TI	0.11	0.11	0.10	0.10	0.10	0.10
AL	1.82	1.83	1.76	1.75	1.76	1.74
CR	0.00	0.00	0.01	0.01	0.01	0.02
FE2	0.85	0.86	0.94	0.94	0.92	0.93
MN	0.02	0.02	0.02	0.02	0.02	0.02
MG	1.17	1.17	1.72	1.72	1.73	1.73
CA	1.06	1.04	0.44	0.44	0.43	0.43
NA	0.02	0.02	0.01	0.01	0.01	0.01
K	0.00	0.00	0.00	0.00	0.00	0.00
P	0.01	0.01	0.01	0.01	0.02	0.01
TOTAL	8.01	8.01	8.01	8.00	7.99	7.99

Group IB Garnets.

	BZ14	BZ14	BZ14	BZ14	BZ14	BZ15
NA2O	0.38	0.42	0.40	0.42	0.42	0.84
MGO	12.31	12.37	12.44	12.43	12.52	10.71
SIO2	40.00	40.00	40.30	40.20	40.30	41.10
P2O5	0.22	0.22	0.24	0.23	0.22	0.23
AL2O3	20.87	21.03	20.95	21.13	21.02	18.66
K2O	0.01	0.00	0.00	0.00	0.00	0.00
CAO	11.02	11.07	11.10	11.01	11.02	12.69
TIO2	2.14	2.12	2.13	2.08	2.12	1.37
CR2O3	0.18	0.18	0.20	0.17	0.16	0.09
MNO	0.29	0.25	0.26	0.28	0.26	0.25
FEO	12.76	12.84	12.83	12.79	12.56	12.97
	100.18	100.50	100.85	100.74	100.61	98.91
SI	2.96	2.95	2.96	2.95	2.96	3.10
TI	0.12	0.12	0.12	0.12	0.12	0.08
AL	1.82	1.83	1.81	1.83	1.82	1.65
CR	0.01	0.01	0.01	0.01	0.01	0.00
FE2	0.79	0.79	0.79	0.79	0.77	0.82
MN	0.02	0.02	0.02	0.02	0.02	0.02
MG	1.36	1.36	1.36	1.36	1.37	1.20
CA	0.87	0.87	0.87	0.87	0.87	1.02
NA	0.03	0.03	0.03	0.03	0.03	0.06
K	0.00	0.00	0.00	0.00	0.00	0.00
P	0.01	0.01	0.02	0.01	0.01	0.02
TOTAL	7.98	7.99	7.98	7.99	7.98	7.97

	BZ15	BZ15	BZ15	BZ16	BZ16	BZ16
NA2O	0.87	0.82	0.34	0.88	0.90	0.91
MGO	10.70	10.63	10.50	10.70	10.85	10.97
SIO2	41.10	41.10	40.00	41.40	40.90	41.00
P2O5	0.24	0.22	0.27	0.30	0.25	0.26
AL2O3	18.83	18.72	21.07	19.14	19.23	19.05
K2O	0.00	0.01	0.00	0.00	0.00	0.00
CAO	12.64	12.81	13.27	12.76	12.69	12.62
TIO2	1.37	1.39	1.48	1.34	1.34	1.36
CR2O3	0.11	0.12	0.11	0.13	0.12	0.09
MNO	0.25	0.23	0.26	0.26	0.25	0.26
FEO	12.89	12.89	13.01	12.91	12.93	12.91
TOTAL	99.00	98.95	100.31	99.82	99.44	99.42
SI	3.09	3.10	2.98	3.09	3.07	3.07
TI	0.08	0.08	0.08	0.08	0.08	0.08
AL	1.67	1.66	1.84	1.68	1.70	1.68
CR	0.01	0.01	0.01	0.01	0.01	0.00
FE2	0.81	0.81	0.81	0.80	0.81	0.81
MN	0.02	0.01	0.02	0.02	0.02	0.02
MG	1.20	1.19	1.16	1.19	1.21	1.22
CA	1.02	1.03	1.06	1.02	1.02	1.01
NA	0.06	0.06	0.02	0.06	0.07	0.07
K	0.00	0.00	0.00	0.00	0.00	0.00
P	0.02	0.01	0.02	0.02	0.02	0.02
TOTAL	7.97	7.97	7.99	7.96	7.98	7.98

Group IB Garnets

	BZ16	BZ18	BZ18	BZ18	BZ18	BZ18
NA2O	0.91	1.00	1.03	1.03	1.05	1.04
MGO	10.91	9.89	9.77	10.03	9.90	9.88
SIO2	40.70	40.90	41.20	41.40	41.40	41.60
P2O5	0.27	0.17	0.21	0.23	0.24	0.24
AL2O3	19.01	18.39	18.66	18.53	18.41	18.37
K2O	0.00	0.01	0.00	0.00	0.00	0.00
CAO	12.69	13.67	13.63	13.70	13.84	13.63
TIO2	1.36	2.28	2.28	2.26	2.29	2.28
CR2O3	0.10	0.08	0.10	0.10	0.06	0.07
MNO	0.25	0.28	0.29	0.31	0.28	0.30
FEO	12.91	13.34	13.09	13.27	13.21	13.11
	99.12	100.01	100.27	100.85	100.69	100.53
SI	3.06	3.07	3.08	3.08	3.08	3.10
TI	0.08	0.13	0.13	0.13	0.13	0.13
AL	1.69	1.62	1.64	1.62	1.61	1.61
CR	0.00	0.00	0.01	0.00	0.00	0.00
FE2	0.81	0.84	0.82	0.82	0.82	0.81
MN	0.02	0.02	0.02	0.02	0.02	0.02
MG	1.22	1.10	1.09	1.11	1.10	1.09
CA	1.02	1.10	1.09	1.09	1.10	1.09
NA	0.07	0.07	0.07	0.07	0.08	0.07
K	0.00	0.00	0.00	0.00	0.00	0.00
P	0.02	0.01	0.01	0.01	0.02	0.02
TOTAL	7.99	7.97	7.95	7.96	7.96	7.94
	BZ24	BZ25	BZ25	BZ25	BZ25	BZ25
NA2O	0.25	0.86	1.03	0.85	1.02	1.01
MGO	11.74	9.77	9.82	9.66	9.73	9.76
SIO2	40.80	40.70	41.20	40.70	41.00	41.10
P2O5	0.17	0.22	0.22	0.21	0.19	0.23
AL2O3	21.47	17.99	18.02	17.98	17.84	17.99
K2O	0.00	0.01	0.00	0.00	0.00	0.00
CAO	12.11	13.53	13.71	13.56	13.55	13.80
TIO2	1.28	2.30	2.24	2.27	2.27	2.20
CR2O3	0.14	0.08	0.07	0.05	0.06	0.08
MNO	0.25	0.29	0.29	0.31	0.29	0.30
FEO	12.80	13.81	13.24	13.76	13.62	13.07
	101.01	99.56	99.84	99.35	99.57	99.54
SI	2.99	3.08	3.09	3.08	3.09	3.09
TI	0.07	0.13	0.13	0.13	0.13	0.12
AL	1.85	1.60	1.59	1.60	1.59	1.60
CR	0.01	0.00	0.00	0.00	0.00	0.00
FE2	0.78	0.87	0.83	0.87	0.86	0.82
MN	0.02	0.02	0.02	0.02	0.02	0.02
MG	1.28	1.10	1.10	1.09	1.09	1.09
CA	0.95	1.09	1.10	1.10	1.10	1.11
NA	0.02	0.06	0.07	0.06	0.07	0.07
K	0.00	0.00	0.00	0.00	0.00	0.00
P	0.01	0.01	0.01	0.01	0.01	0.02
TOTAL	7.99	7.97	7.96	7.97	7.96	7.96

Group IB Garnets

	BZ25	BZ32	BZ34	BZ34	BZ34	BZ34
NA2O	1.06	0.32	0.33	0.37	0.35	0.38
MGO	9.54	12.13	10.53	10.45	10.42	10.53
SIO2	41.20	39.40	39.80	40.10	40.20	39.80
P2O5	0.21	0.27	0.26	0.23	0.22	0.25
AL2O3	17.86	19.31	20.78	20.72	20.96	21.04
K2O	0.01	0.02	0.00	0.01	0.00	0.01
CAO	13.50	10.97	13.26	13.27	13.40	13.34
TIO2	2.24	2.59	1.46	1.49	1.52	1.48
CR2O3	0.07	0.10	0.10	0.12	0.13	0.11
MNO	0.29	0.32	0.27	0.25	0.26	0.25
FEO	13.24	13.56	13.01	13.01	13.09	12.97
	99.21	98.98	99.80	100.01	100.56	100.16
SI	3.11	2.97	2.97	2.99	2.99	2.97
TI	0.13	0.15	0.08	0.08	0.08	0.08
AL	1.59	1.71	1.83	1.82	1.83	1.85
CR	0.00	0.00	0.01	0.01	0.01	0.01
FE2	0.83	0.85	0.81	0.81	0.81	0.81
MN	0.02	0.02	0.02	0.02	0.02	0.02
MG	1.07	1.36	1.17	1.16	1.15	1.17
CA	1.10	0.88	1.06	1.06	1.06	1.06
NA	0.08	0.02	0.02	0.03	0.03	0.03
K	0.00	0.00	0.00	0.00	0.00	0.00
P	0.01	0.02	0.02	0.01	0.01	0.02
TOTAL	7.94	7.99	8.00	7.99	7.99	8.00
	BZ35	BZ35	BZ35	BZ37	BZ37	BZ37
NA2O	0.86	0.53	0.34	0.40	0.37	0.35
MGO	13.31	13.32	13.46	13.22	13.42	13.26
SIO2	42.50	41.20	39.70	40.40	40.50	40.30
P2O5	0.20	0.16	0.12	0.17	0.16	0.18
AL2O3	17.54	17.73	18.11	21.65	21.59	21.53
K2O	0.01	0.00	0.00	0.00	0.00	0.00
CAO	10.94	10.71	10.03	8.12	8.09	8.13
TIO2	1.75	1.85	2.71	2.02	0.14	2.03
CR2O3	0.12	0.13	0.17	0.12	0.14	0.13
MNO	0.25	0.28	0.31	0.31	0.31	0.27
FEO	12.24	13.54	14.53	14.38	14.38	14.40
	99.71	99.45	99.48	100.77	99.10	100.58
SI	3.15	3.08	2.99	2.96	3.01	2.96
TI	0.10	0.10	0.15	0.11	0.01	0.11
AL	1.53	1.56	1.60	1.87	1.89	1.86
CR	0.01	0.01	0.01	0.01	0.01	0.01
FE2	0.76	0.85	0.91	0.88	0.89	0.88
MN	0.02	0.02	0.02	0.02	0.02	0.02
MG	1.47	1.48	1.51	1.44	1.49	1.45
CA	0.87	0.86	0.81	0.64	0.65	0.64
NA	0.06	0.04	0.02	0.03	0.03	0.02
K	0.00	0.00	0.00	0.00	0.00	0.00
P	0.01	0.01	0.01	0.01	0.01	0.01
TOTAL	7.96	8.01	8.04	7.97	8.01	7.97

Group IB Garnets

	BZ37	BZ37	BZ37	BZ37	BZ39	BZ39
NA2O	0.38	0.37	0.39	0.23	0.22	0.21
MGO	13.31	13.25	13.15	11.90	11.89	12.02
SIO2	40.10	40.20	40.20	40.10	40.30	40.50
P2O5	0.16	0.13	0.16	0.11	0.11	0.14
AL2O3	21.39	21.36	21.31	22.18	22.30	22.06
K2O	0.00	0.00	0.02	0.02	0.01	0.00
CAO	8.15	8.19	8.13	7.52	7.51	7.50
TIO2	2.06	2.03	2.03	0.31	0.33	0.31
CR2O3	0.13	0.12	0.12	0.06	0.10	0.08
MNO	0.30	0.31	0.30	0.35	0.33	0.37
FEO	14.22	14.37	14.23	16.87	16.93	17.07
	100.20	100.33	100.02	99.66	100.02	100.26
SI	2.96	2.97	2.97	3.00	3.00	3.01
TI	0.11	0.11	0.11	0.02	0.02	0.02
AL	1.86	1.85	1.85	1.95	1.95	1.93
CR	0.01	0.01	0.01	0.00	0.00	0.00
FE2	0.88	0.88	0.88	1.05	1.05	1.06
MN	0.02	0.02	0.02	0.02	0.02	0.02
MG	1.46	1.45	1.45	1.32	1.32	1.33
CA	0.64	0.65	0.64	0.60	0.60	0.60
NA	0.03	0.03	0.03	0.02	0.02	0.02
K	0.00	0.00	0.00	0.00	0.00	0.00
P	0.01	0.01	0.01	0.01	0.01	0.01
TOTAL	7.98	7.98	7.97	7.99	7.99	7.99

	BZ39	BZ39	BZ39	BZ39	BZ39	BZA2
NA2O	0.19	0.20	0.20	0.23	0.21	0.36
MGO	11.93	11.93	11.93	11.93	12.00	10.09
SIO2	40.40	40.70	40.70	40.20	40.40	39.80
P2O5	0.11	0.11	0.11	0.12	0.11	0.24
AL2O3	22.04	22.21	22.21	22.31	22.35	21.10
K2O	0.00	0.00	0.00	0.00	0.01	0.01
CAO	7.48	7.46	7.46	7.51	7.49	11.79
TIO2	0.35	0.34	0.34	0.32	0.34	1.20
CR2O3	0.09	0.09	0.09	0.07	0.07	0.06
MNO	0.39	0.37	0.37	0.38	0.33	0.33
FEO	16.85	16.84	16.84	16.87	16.97	14.95
	99.83	100.26	100.26	99.95	100.29	99.93
SI	3.01	3.02	3.02	3.00	3.00	2.99
TI	0.02	0.02	0.02	0.02	0.02	0.07
AL	1.94	1.94	1.94	1.96	1.95	1.86
CR	0.00	0.00	0.00	0.00	0.00	0.00
FE2	1.05	1.04	1.04	1.05	1.05	0.94
MN	0.02	0.02	0.02	0.02	0.02	0.02
MG	1.32	1.32	1.32	1.32	1.33	1.13
CA	0.60	0.59	0.59	0.60	0.59	0.95
NA	0.01	0.01	0.01	0.02	0.02	0.03
K	0.00	0.00	0.00	0.00	0.00	0.00
P	0.01	0.01	0.01	0.01	0.01	0.02
TOTAL	7.99	7.98	7.98	7.99	7.99	7.99

Group IB Garnets

	BZ42	BZ42	BZ42	BZ42	BZ42
NA2O	0.35	0.34	0.35	0.34	0.35
MGO	10.07	10.04	10.09	10.01	10.18
SIO2	39.90	39.90	39.80	39.80	39.90
P2O5	0.23	0.24	0.25	0.24	0.24
AL2O3	21.23	21.08	20.98	20.92	21.11
K2O	0.00	0.00	0.00	0.00	0.00
CAO	11.70	11.79	11.76	11.74	11.71
TIO2	1.21	1.25	1.19	1.23	1.24
CR2O3	0.07	0.09	0.04	0.06	0.07
MNO	0.31	0.33	0.30	0.29	0.34
FEO	14.99	14.86	14.95	14.91	14.94
	100.06	99.93	99.71	99.54	100.07
SI	2.99	2.99	2.99	2.99	2.99
TI	0.07	0.07	0.07	0.07	0.07
AL	1.87	1.86	1.85	1.85	1.86
CR	0.00	0.00	0.00	0.00	0.00
FE2	0.94	0.93	0.94	0.94	0.93
MN	0.02	0.02	0.02	0.02	0.02
MG	1.12	1.12	1.13	1.12	1.13
CA	0.94	0.95	0.95	0.95	0.94
NA	0.03	0.02	0.03	0.03	0.03
K	0.00	0.00	0.00	0.00	0.00
P	0.01	0.02	0.02	0.02	0.02
TOTAL	7.98	7.98	7.99	7.98	7.99

Group IB Clinopyroxenes.

	BZ1	BZ2	BZ8	BZ2	BZ5	BZ5
NA2O	4.06	3.12	2.96	0.26	5.18	5.22
MGO	12.08	14.32	14.86	15.65	10.03	10.01
SIO2	52.70	54.50	53.80	40.20	54.20	54.50
P2O5	0.23	0.22	0.20	0.11	0.17	0.19
AL2O3	6.91	4.77	6.20	20.84	9.44	9.44
K2O	0.01	0.02	0.03	0.01	0.00	0.00
CAO	16.29	16.05	15.15	6.75	15.01	14.98
TIO2	1.16	0.96	1.06	1.65	0.46	0.45
CR2O3	0.06	0.08	0.08	0.11	0.05	0.09
MNO	0.04	0.07	0.10	0.31	0.06	0.07
FEO	5.45	6.06	6.42	12.84	5.07	4.95
	99.00	100.16	100.87	98.73	99.68	99.90
SI	1.93	1.97	1.93	1.49	1.95	1.96
TI	0.03	0.03	0.03	0.05	0.01	0.01
AL	0.30	0.20	0.26	0.91	0.40	0.40
CR	0.00	0.00	0.00	0.00	0.00	0.00
FE2	0.17	0.18	0.19	0.40	0.15	0.15
MN	0.00	0.00	0.00	0.01	0.00	0.00
MG	0.66	0.77	0.79	0.86	0.54	0.54
CA	0.64	0.62	0.58	0.27	0.58	0.58
NA	0.14	0.11	0.10	0.01	0.18	0.18
K	0.00	0.00	0.00	0.00	0.00	0.00
P	0.01	0.01	0.01	0.00	0.01	0.01
TOTAL	3.88	3.89	3.90	4.00	3.82	3.82

	BZ12	BZ13	BZ14	BZ14	BZ15	BZ18
NA2O	0.41	1.79	4.34	4.23	5.79	6.07
MGO	11.60	15.93	12.06	12.08	9.20	9.23
SIO2	51.70	54.00	53.30	53.30	53.30	54.10
P2O5	0.21	0.18	0.23	0.23	0.22	0.23
AL2O3	7.14	2.54	7.10	7.05	10.26	11.39
K2O	0.00	0.00	0.02	0.01	0.00	0.20
CAO	16.78	15.62	16.18	16.10	12.70	13.10
TIO2	0.91	0.64	1.19	1.21	1.04	1.54
CR2O3	0.04	0.09	0.07	0.09	0.06	0.07
MNO	0.07	0.14	0.06	0.06	0.09	0.07
FEO	5.96	7.89	5.23	5.35	6.82	6.36
	94.82	98.82	99.79	99.70	99.48	102.36
SI	1.96	1.99	1.93	1.93	1.93	1.91
TI	0.03	0.02	0.03	0.03	0.03	0.04
AL	0.32	0.11	0.30	0.30	0.44	0.47
CR	0.00	0.00	0.00	0.00	0.00	0.00
FE2	0.19	0.24	0.16	0.16	0.21	0.19
MN	0.00	0.00	0.00	0.00	0.00	0.00
MG	0.65	0.87	0.65	0.65	0.50	0.48
CA	0.68	0.62	0.63	0.63	0.50	0.50
NA	0.02	0.06	0.15	0.15	0.20	0.21
K	0.00	0.00	0.00	0.00	0.00	0.00
P	0.01	0.01	0.01	0.01	0.01	0.01
TOTAL	3.85	3.93	3.87	3.87	3.81	3.80

Group IB Clinopyroxenes.

	BZ24	BZ24	BZ25	BZ34	BZ34	BZ34
NA2O	3.98	4.00	5.96	4.93	4.87	4.84
MGO	12.51	12.55	9.03	11.03	11.18	11.07
SIO2	54.10	54.10	52.80	53.70	54.10	53.80
P2O5	0.21	0.20	0.19	0.20	0.21	0.20
AL2O3	6.64	6.73	10.89	8.35	8.36	8.09
K2O	0.01	0.00	0.01	0.02	0.00	0.01
CAO	17.10	17.09	13.30	15.90	15.80	15.90
TIO2	0.57	0.55	1.59	0.77	0.80	0.76
CR2O3	0.08	0.07	0.07	0.08	0.05	0.06
MNO	0.08	0.08	0.08	0.05	0.06	0.07
FEO	5.50	5.55	6.55	5.37	5.38	5.72
	100.79	100.93	100.48	100.41	100.81	100.51
SI	1.94	1.94	1.90	1.93	1.94	1.94
TI	0.02	0.01	0.04	0.02	0.02	0.02
AL	0.28	0.28	0.46	0.35	0.35	0.34
CR	0.00	0.00	0.00	0.00	0.00	0.00
FE2	0.17	0.17	0.20	0.16	0.16	0.17
MN	0.00	0.00	0.00	0.00	0.00	0.00
MG	0.67	0.67	0.48	0.59	0.60	0.59
CA	0.66	0.66	0.51	0.61	0.61	0.61
NA	0.14	0.14	0.21	0.17	0.17	0.17
K	0.00	0.00	0.00	0.00	0.00	0.00
P	0.01	0.01	0.01	0.01	0.01	0.01
TOTAL	3.89	3.89	3.81	3.86	3.85	3.86

	BZ35	BZ37	BZ37	BZ39	BZ39	BZ42
NA2O	4.30	4.00	3.93	7.70	7.74	5.79
MGO	12.77	12.52	12.60	7.99	7.94	9.58
SIO2	54.56	52.50	51.50	54.20	54.30	53.80
P2O5	0.22	0.22	0.20	0.16	0.17	0.20
AL2O3	7.09	6.97	7.62	12.96	12.84	9.62
K2O	0.00	0.01	0.02	0.02	0.00	0.00
CAO	15.45	15.09	14.47	10.26	10.46	14.24
TIO2	0.90	1.37	1.41	0.25	0.23	0.72
CR2O3	0.10	0.11	0.08	0.10	0.10	0.05
MNO	0.07	0.08	0.10	0.09	0.07	0.09
FEO	5.36	6.77	7.29	6.00	5.74	6.19
	100.81	99.65	99.21	99.73	99.58	100.30
SI	1.95	1.92	1.89	1.94	1.95	1.94
TI	0.02	0.04	0.04	0.01	0.01	0.02
AL	0.30	0.30	0.33	0.55	0.54	0.41
CR	0.00	0.00	0.00	0.00	0.00	0.00
FE2	0.16	0.21	0.22	0.18	0.17	0.19
MN	0.00	0.00	0.00	0.00	0.00	0.00
MG	0.68	0.68	0.69	0.43	0.42	0.51
CA	0.59	0.59	0.57	0.39	0.40	0.55
NA	0.15	0.14	0.14	0.27	0.27	0.20
K	0.00	0.00	0.00	0.00	0.00	0.00
P	0.01	0.01	0.01	0.00	0.01	0.01
TOTAL	3.86	3.88	3.89	3.77	3.77	3.83

Group IIA Garnets.

	BZ9 1	BZ9 2	BZ9 3	BZ27 1	BZ46 1	BZ46 2
NA2O	1.08	1.04	1.01	0.54	0.98	0.97
MGO	9.52	9.40	9.54	14.32	11.37	11.29
SIO2	41.30	41.80	42.00	43.00	43.30	43.10
P2O5	0.23	0.22	0.23	0.17	0.15	0.14
AL2O3	18.51	18.62	18.54	18.30	18.48	18.31
K2O	0.00	0.00	0.01	0.02	0.02	0.00
CAO	14.54	14.61	14.55	10.95	14.25	14.15
TIO2	1.70	1.68	1.70	1.70	1.44	1.44
CR2O3	0.05	0.03	0.04	0.14	0.11	0.08
MNO	0.24	0.25	0.24	0.24	0.23	0.22
FEO	12.32	12.39	12.15	12.06	10.81	10.88
	99.50	100.02	100.01	101.43	101.12	100.58
SI	3.10	3.12	3.13	3.12	3.16	3.17
TI	0.10	0.09	0.10	0.09	0.08	0.08
AL	1.64	1.64	1.63	1.56	1.59	1.58
CR	0.00	0.00	0.00	0.01	0.00	0.00
FE2	0.77	0.77	0.76	0.73	0.66	0.67
MN	0.02	0.02	0.02	0.01	0.01	0.01
MG	1.06	1.05	1.06	1.55	1.24	1.24
CA	1.17	1.17	1.16	0.85	1.11	1.11
NA	0.08	0.08	0.07	0.04	0.07	0.07
K	0.00	0.00	0.00	0.00	0.00	0.00
P	0.01	0.01	0.01	0.01	0.01	0.01
TOTAL	7.96	7.94	7.93	7.98	7.94	7.94

	BZ46 3	BZ46 4	BZ46 5	BZ46 6
NA2O	1.00	0.96	0.99	0.95
MGO	11.33	11.34	11.36	11.34
SIO2	42.80	42.80	42.60	42.60
P2O5	0.14	0.15	0.14	0.14
AL2O3	18.53	18.53	18.68	18.84
K2O	0.01	0.01	0.01	0.00
CAO	14.28	14.25	14.32	14.24
TIO2	1.43	1.48	1.43	1.43
CR2O3	0.12	0.10	0.13	0.09
MNO	0.19	0.21	0.20	0.22
FEO	10.77	10.82	10.80	10.62
	100.61	100.66	100.66	100.48
SI	3.15	3.15	3.13	3.13
TI	0.08	0.08	0.08	0.08
AL	1.60	1.60	1.62	1.63
CR	0.01	0.01	0.01	0.00
FE2	0.66	0.66	0.66	0.65
MN	0.01	0.01	0.01	0.01
MG	1.24	1.24	1.24	1.24
CA	1.12	1.12	1.13	1.12
NA	0.07	0.07	0.07	0.07
K	0.00	0.00	0.00	0.00
P	0.01	0.01	0.01	0.01
TOTAL	7.95	7.95	7.96	7.95

Group IIB Garnets.

	BZ7	BZ7	BZ7	BZ7	BZ10	BZ10
NA2O	1.09	0.55	0.58	0.52	0.91	1.09
MGO	20.20	21.71	21.91	21.30	9.44	9.62
SIO2	45.60	45.00	45.70	44.60	41.00	41.90
P2O5	0.10	0.08	0.08	0.11	0.20	0.20
AL2O3	14.01	12.77	12.71	13.13	17.73	17.89
K2O	0.00	0.00	0.00	0.01	0.00	0.00
CAO	5.23	4.77	4.77	4.68	14.32	14.80
TIO2	2.19	2.34	2.31	2.39	2.42	2.35
CR2O3	0.30	0.30	0.27	0.27	0.07	0.05
MNO	0.22	0.19	0.21	0.19	0.26	0.21
FEO	11.78	11.70	11.57	12.60	13.96	12.10
	100.70	99.41	100.11	99.81	100.32	100.21
SI	3.28	3.28	3.30	3.25	3.08	3.12
TI	0.12	0.13	0.13	0.13	0.14	0.13
AL	1.19	1.10	1.08	1.13	1.57	1.57
CR	0.02	0.02	0.02	0.02	0.00	0.00
FE2	0.71	0.71	0.70	0.77	0.88	0.75
MN	0.01	0.01	0.01	0.01	0.02	0.01
MG	2.17	2.36	2.36	2.31	1.06	1.07
CA	0.40	0.37	0.37	0.37	1.15	1.18
NA	0.08	0.04	0.04	0.04	0.07	0.08
K	0.00	0.00	0.00	0.00	0.00	0.00
P	0.01	0.01	0.00	0.01	0.01	0.01
TOTAL	7.98	8.02	8.01	8.03	7.97	7.94

	BZ10	BZ10	BZ10	BZ10	BZ19	BZ19
NA2O	0.98	1.09	0.51	1.17	0.94	0.93
MGO	9.27	9.62	8.78	9.82	14.38	14.40
SIO2	40.70	41.70	39.40	41.80	43.70	44.00
P2O5	0.19	0.19	0.20	0.17	0.18	0.15
AL2O3	17.54	17.88	17.76	18.00	16.47	16.66
K2O	0.00	0.01	0.01	0.00	0.00	0.00
CAO	14.24	14.54	13.78	14.60	11.73	11.79
TIO2	2.35	2.31	2.66	2.36	1.52	1.51
CR2O3	0.06	0.08	0.08	0.07	0.13	0.10
MNO	0.30	0.26	0.33	0.26	0.19	0.21
FEO	14.33	12.68	16.66	12.20	11.22	11.21
	99.96	100.35	100.17	100.45	100.47	100.96
SI	3.08	3.11	3.01	3.11	3.20	3.21
TI	0.13	0.13	0.15	0.13	0.08	0.08
AL	1.56	1.57	1.60	1.58	1.42	1.43
CR	0.00	0.00	0.00	0.00	0.01	0.00
FE2	0.90	0.79	1.06	0.76	0.69	0.68
MN	0.02	0.02	0.02	0.02	0.01	0.01
MG	1.04	1.07	1.00	1.09	1.57	1.56
CA	1.15	1.16	1.13	1.17	0.92	0.92
NA	0.07	0.08	0.04	0.08	0.07	0.07
K	0.00	0.00	0.00	0.00	0.00	0.00
P	0.01	0.01	0.01	0.01	0.01	0.01
TOTAL	7.98	7.95	8.02	7.95	7.98	7.98

Group IIB Garnets

	BZ19	BZ19	BZ19	BZ19	BZ19	BZ19
NA2O	0.95	0.85	0.88	0.92	0.62	0.89
MGO	14.38	14.08	14.18	14.33	15.47	14.36
SIO2	44.00	42.90	43.70	43.60	41.50	44.00
P2O5	0.17	0.15	0.16	0.18	0.17	0.17
AL2O3	16.72	16.55	16.66	16.70	17.05	16.94
K2O	0.00	0.00	0.00	0.00	0.00	0.00
CAO	11.71	11.73	11.70	11.70	10.62	11.60
TIO2	1.51	1.50	1.50	1.53	1.64	1.55
CR2O3	0.10	0.12	0.15	0.11	0.14	0.11
MNO	0.23	0.22	0.23	0.23	0.24	0.22
FEO	11.06	11.13	11.06	11.19	12.97	11.45
	100.83	99.23	100.23	100.50	100.42	101.30
SI	3.21	3.19	3.21	3.19	3.07	3.20
TI	0.08	0.08	0.08	0.08	0.09	0.08
AL	1.44	1.45	1.44	1.44	1.48	1.45
CR	0.00	0.01	0.01	0.01	0.01	0.01
FE2	0.67	0.69	0.68	0.68	0.80	0.69
MN	0.01	0.01	0.01	0.01	0.01	0.01
MG	1.56	1.56	1.55	1.56	1.70	1.55
CA	0.91	0.93	0.92	0.92	0.84	0.90
NA	0.07	0.06	0.06	0.07	0.04	0.06
K	0.00	0.00	0.00	0.00	0.00	0.00
P	0.01	0.01	0.01	0.01	0.01	0.01
TOTAL	7.97	7.99	7.97	7.98	8.07	7.97

	BZ19	BZ21	BZ21	BZ21	BZ21	BZ21
NA2O	0.87	0.99	0.96	0.95	0.49	0.49
MGO	14.23	11.74	11.87	13.85	11.42	11.42
SIO2	43.90	42.50	42.50	42.60	42.60	40.80
P2O5	0.17	0.28	0.16	0.25	0.27	0.24
AL2O3	16.58	18.19	18.15	18.34	18.40	18.40
K2O	0.00	0.00	0.00	0.00	0.00	0.00
CAO	11.91	13.77	13.77	13.69	13.78	12.95
TIO2	1.47	1.14	1.09	1.11	1.13	1.23
CR2O3	0.10	0.09	0.10	0.07	0.07	0.09
MNO	0.22	0.21	0.24	0.21	0.23	0.28
FEO	11.12	10.86	10.86	10.84	10.87	13.51
	100.57	99.77	99.69	101.92	99.26	99.41
SI	3.21	3.15	3.15	3.09	3.16	3.07
TI	0.08	0.06	0.06	0.06	0.06	0.07
AL	1.43	1.59	1.59	1.57	1.61	1.63
CR	0.00	0.00	0.00	0.00	0.00	0.00
FE2	0.68	0.67	0.67	0.66	0.67	0.85
MN	0.01	0.01	0.01	0.01	0.01	0.02
MG	1.55	1.29	1.31	1.50	1.26	1.28
CA	0.93	1.09	1.09	1.06	1.10	1.04
NA	0.06	0.07	0.07	0.07	0.04	0.04
K	0.00	0.00	0.00	0.00	0.00	0.00
P	0.01	0.02	0.01	0.02	0.02	0.02
TOTAL	7.97	7.96	7.97	8.04	7.94	8.02

Group IIB Garnets

	BZ21	BZ22	BZ22	BZ22	BZ22	BZ22
NA2O	1.01	1.15	1.23	1.25	0.90	1.21
MGO	11.90	10.33	10.35	10.29	10.22	10.40
SIO2	42.60	42.30	42.20	42.50	41.50	42.40
P2O5	0.25	0.21	0.23	0.24	0.26	0.23
AL2O3	18.21	17.82	17.82	17.91	17.87	17.96
K2O	0.00	0.00	0.00	0.00	0.00	0.00
CAO	13.55	14.08	14.11	14.21	14.10	14.09
TIO2	1.14	1.99	1.94	2.02	2.03	1.92
CR2O3	0.09	0.08	0.05	0.05	0.07	0.06
MNO	0.23	0.24	0.23	0.27	0.26	0.24
FEO	10.60	12.12	11.76	11.85	12.86	12.02
	99.58	100.32	99.93	100.60	100.08	100.53
SI	3.16	3.14	3.14	3.15	3.10	3.14
TI	0.06	0.11	0.11	0.11	0.11	0.11
AL	1.59	1.56	1.56	1.56	1.57	1.57
CR	0.00	0.00	0.00	0.00	0.00	0.00
FE2	0.66	0.75	0.73	0.73	0.80	0.74
MN	0.01	0.01	0.01	0.02	0.02	0.01
MG	1.31	1.14	1.15	1.13	1.14	1.15
CA	1.07	1.12	1.13	1.13	1.13	1.12
NA	0.07	0.08	0.09	0.09	0.07	0.09
K	0.00	0.00	0.00	0.00	0.00	0.00
P	0.02	0.01	0.01	0.02	0.02	0.01
TOTAL	7.96	7.94	7.94	7.93	7.97	7.94

	BZ22	BZ29	BZ29	BZ29	BZ29	BZ29
NA2O	1.23	0.81	1.01	1.01	1.06	0.80
MGO	10.38	15.22	15.24	15.24	15.33	15.40
SIO2	42.60	43.90	44.50	44.50	44.60	44.00
P2O5	0.22	0.14	0.13	0.13	0.13	0.12
AL2O3	17.84	17.60				
K2O	0.01	0.00	0.00	0.00	0.00	0.01
CAO	14.07	8.67	8.92	8.92	8.85	8.95
TIO2	1.99	0.57	0.56	0.58	0.56	0.56
CR2O3	0.05	0.13	0.17	0.17	0.10	0.12
MNO	0.24	0.23	0.26	0.26	0.21	0.24
FEO	11.87	12.32	11.76	11.76	11.73	11.66
	100.51	99.60	99.96	99.98	100.09	99.74
SI	3.15	3.22	3.25	3.25	3.25	3.22
TI	0.11	0.03	0.03	0.03	0.03	0.03
AL	1.56	1.52	1.50	1.50	1.50	1.54
CR	0.00	0.01	0.01	0.01	0.00	0.01
FE2	0.73	0.76	0.72	0.72	0.71	0.71
MN	0.02	0.01	0.02	0.02	0.01	0.02
MG	1.14	1.66	1.66	1.66	1.66	1.68
CA	1.12	0.68	0.70	0.70	0.69	0.70
NA	0.09	0.06	0.07	0.07	0.06	0.06
K	0.00	0.00	0.00	0.00	0.00	0.00
P	0.01	0.01	0.01	0.01	0.01	0.01
TOTAL	7.93	7.97	7.95	7.95	7.95	7.96

Group IIB Garnets

	BZ29	BZ29	BZ43	BZ43	BZ43	BZ43
NA2O	0.96	1.04	0.87	0.88	0.98	0.88
MGO	15.17	15.13	14.55	14.48	14.38	14.30
SIO2	44.20	44.20	44.40	44.40	44.60	43.90
P2O5	0.14	0.16	0.12	0.15	0.14	0.12
AL2O3	17.54	17.34	16.94	16.96	16.98	16.78
K2O	0.01	0.01	0.01	0.02	0.00	0.00
CAO	8.92	8.90	11.72	11.58	11.59	11.62
TIO2	0.57	0.56	1.55	1.51	1.53	1.54
CR2O3	0.12	0.12	0.20	0.09	0.11	0.10
MNO	0.23	0.21	0.19	0.20	0.20	0.23
FEO	11.82	11.83	11.13	11.07	10.91	11.00
	99.68	99.50	101.67	101.36	101.41	100.46
SI	3.24	3.25	3.21	3.21	3.23	3.21
TI	0.03	0.03	0.08	0.08	0.08	0.08
AL	1.51	1.50	1.44	1.45	1.44	1.44
CR	0.01	0.01	0.01	0.00	0.01	0.00
FE2	0.72	0.72	0.67	0.67	0.66	0.67
MN	0.01	0.01	0.01	0.01	0.01	0.01
MG	1.66	1.65	1.57	1.56	1.55	1.56
CA	0.70	0.70	0.91	0.90	0.90	0.91
NA	0.07	0.07	0.06	0.06	0.07	0.06
K	0.00	0.00	0.00	0.00	0.00	0.00
P	0.01	0.01	0.01	0.01	0.01	0.01
TOTAL	7.96	7.95	7.97	7.96	7.95	7.97

	BZ43	BZ45	BZ45	BZ45	BZ45	BZ47
NA2O	0.89	1.14	1.18	1.04	1.15	1.10
MGO	14.68	9.65	9.77	9.81	9.69	14.30
SIO2	44.60	42.60	43.00	42.10	42.60	44.00
P2O5	0.12	0.22	0.23	0.20	0.18	0.18
AL2O3	16.95	18.66	18.63	18.64	16.64	17.15
K2O	0.00	0.00	0.00	0.00	0.00	0.01
CAO	11.51	14.40	14.55	14.48	14.41	10.46
TIO2	1.55	1.78	1.79	1.79	1.79	2.25
CR2O3	0.11	0.05	0.03	0.04	0.04	0.09
MNO	0.23	0.25	0.24	0.25	0.24	0.20
FEO	11.07	12.04	12.06	12.39	12.40	11.72
	101.71	100.79	101.49	100.74	99.14	101.47
SI	3.22	3.14	3.15	3.12	3.21	3.19
TI	0.08	0.10	0.10	0.10	0.10	0.12
AL	1.44	1.62	1.61	1.62	1.48	1.46
CR	0.01	0.00	0.00	0.00	0.00	0.00
FE2	0.67	0.74	0.74	0.77	0.78	0.71
MN	0.01	0.02	0.02	0.02	0.02	0.01
MG	1.58	1.06	1.07	1.08	1.09	1.54
CA	0.89	1.14	1.14	1.15	1.16	0.81
NA	0.06	0.08	0.08	0.07	0.08	0.08
K	0.00	0.00	0.00	0.00	0.00	0.00
P	0.01	0.01	0.01	0.01	0.01	0.01
TOTAL	7.96	7.92	7.92	7.95	7.93	7.94

Group IIB Garnets

	BZ47	BZ47	BZ48	BZ48	BZ48	BZ48
NA2O	1.14	0.46	0.45	0.41	0.46	0.46
MGO	14.23	14.21	14.02	14.02	14.02	14.25
SIO2	44.20	41.20	42.30	42.70	42.80	42.50
P2O5	0.17	0.18	0.17	0.16	0.17	0.17
AL2O3	17.34	19.05	16.42	16.34	16.24	16.43
K2O	0.00	0.00	0.00	0.01	0.01	0.00
CAO	10.38	9.03	12.81	12.84	12.84	12.74
TIO2	2.29	2.88	1.08	1.03	1.04	1.05
CR2O3	0.11	0.12	0.07	0.10	0.08	0.10
MNO	0.21	0.31	0.28	0.26	0.26	0.26
FEO	11.83	13.67	11.61	11.61	11.73	11.60
	101.91	101.11	99.20	99.49	99.66	99.57
SI	3.19	3.02	3.16	3.18	3.18	3.16
TI	0.12	0.16	0.06	0.06	0.06	0.06
AL	1.47	1.64	1.44	1.43	1.42	1.44
CR	0.01	0.01	0.00	0.01	0.00	0.00
FE2	0.71	0.83	0.72	0.72	0.73	0.72
MN	0.01	0.02	0.02	0.02	0.02	0.02
MG	1.53	1.55	1.56	1.55	1.55	1.58
CA	0.80	0.71	1.02	1.02	1.02	1.01
NA	0.08	0.03	0.03	0.03	0.03	0.03
K	0.00	0.00	0.00	0.00	0.00	0.00
P	0.01	0.01	0.01	0.01	0.01	0.01
TOTAL	7.93	7.98	8.04	8.03	8.03	8.04

	BZ48	BZ50	BZ50	BZ50	BZ50	BZ50
NA2O	3.32	0.76	0.80	0.81	0.91	0.52
MGO	13.26	12.31	12.29	12.35	12.49	11.82
SIO2	41.50	43.70	43.40	43.80	43.90	41.60
P2O5	0.18	0.15	0.15	0.17	0.17	0.14
AL2O3	16.22	19.00	18.93	18.97	18.25	21.53
K2O	0.00	0.00	0.00	0.00	0.02	0.01
CAO	12.49	13.73	13.76	13.73	14.09	9.79
TIO2	1.07	0.93	0.95	0.92	0.94	0.93
CR2O3	0.11	0.13	0.11	0.08	0.11	0.10
MNO	0.29	0.22	0.22	0.20	0.23	0.32
FEO	13.45	10.55	10.57	10.58	10.50	14.86
	101.87	101.50	101.17	101.61	101.61	101.62
SI	3.08	3.16	3.16	3.17	3.18	3.04
TI	0.06	0.05	0.05	0.05	0.05	0.05
AL	1.42	1.62	1.62	1.62	1.56	1.85
CR	0.01	0.01	0.01	0.00	0.01	0.00
FE2	0.83	0.64	0.64	0.64	0.64	0.91
MN	0.02	0.01	0.01	0.01	0.01	0.02
MG	1.47	1.33	1.33	1.33	1.35	1.29
CA	0.99	1.07	1.07	1.06	1.09	0.77
NA	0.04	0.05	0.06	0.06	0.06	0.04
K	0.00	0.00	0.00	0.00	0.00	0.00
P	0.01	0.01	0.01	0.01	0.01	0.01
TOTAL	7.93	7.95	7.96	7.95	7.97	7.97

Group IIB Clinopyroxene.

	BZ10	BZ19	BZ21	BZ21	BZ22	BZ22
NA2O	5.98	4.40	6.52	5.90	6.49	6.31
MGO	8.61	12.38	8.82	9.91	9.17	9.02
SIO2	52.60	53.20	52.80	54.00	54.00	53.60
P2O5	0.18	0.23	0.23	0.24	0.23	0.20
AL2O3	10.55	6.99	11.31	11.03	10.69	10.91
K2O	0.01	0.01	0.00	0.01	0.01	0.01
CAO	13.19	15.10	11.44	13.61	12.21	12.72
TIO2	1.70	1.04	0.74	0.59	1.36	1.44
CR2O3	0.05	0.12	0.08	0.07	0.03	0.02
MNO	0.07	0.10	0.08	0.10	0.09	0.12
FEO	7.40	6.20	5.74	5.03	6.44	6.66
	100.35	99.76	97.77	100.48	100.73	101.01
SI	1.90	1.93	1.93	1.93	1.93	1.91
TI	0.05	0.03	0.02	0.02	0.04	0.04
AL	0.45	0.30	0.49	0.46	0.45	0.46
CR	0.00	0.00	0.00	0.00	0.00	0.00
FE2	0.22	0.19	0.18	0.15	0.19	0.20
MN	0.00	0.00	0.00	0.00	0.00	0.00
MG	0.46	0.67	0.48	0.53	0.49	0.48
CA	0.51	0.59	0.45	0.52	0.47	0.49
NA	0.21	0.16	0.23	0.20	0.22	0.22
K	0.00	0.00	0.00	0.00	0.00	0.00
P	0.01	0.01	0.01	0.01	0.01	0.01
TOTAL	3.81	3.88	3.79	3.81	3.80	3.81

	BZ22	BZ29	BZ29	BZ29	BZ43	BZ48
NA2O	5.89	5.68	3.82	5.96	4.33	4.19
MGO	8.97	11.61	13.21	11.91	12.54	12.60
SIO2	52.70	53.80	47.40	55.50	52.40	53.00
P2O5	0.20	0.17	0.14	0.16	0.12	0.14
AL2O3	10.89	9.55	14.57	10.61	6.97	6.79
K2O	0.02	0.01	0.01	0.00	0.10	0.02
CAO	13.24	11.39	9.91	10.92	15.10	15.28
TIO2	1.37	0.31	0.41	0.32	1.06	1.11
CR2O3	0.04	0.05	0.13	0.07	0.07	0.08
MNO	0.08	0.08	0.20	0.11	0.11	0.10
FEO	6.40	5.57	9.16	6.16	6.27	6.36
	99.81	98.23	98.95	101.72	99.08	99.67
SI	1.91	1.96	1.74	1.95	1.92	1.93
TI	0.04	0.01	0.01	0.01	0.03	0.03
AL	0.46	0.41	0.63	0.44	0.30	0.29
CR	0.00	0.00	0.00	0.00	0.00	0.00
FE2	0.19	0.17	0.28	0.18	0.19	0.19
MN	0.00	0.00	0.01	0.00	0.00	0.00
MG	0.48	0.63	0.72	0.62	0.69	0.68
CA	0.51	0.44	0.39	0.41	0.59	0.60
NA	0.21	0.20	0.14	0.20	0.15	0.15
K	0.00	0.00	0.00	0.00	0.00	0.00
P	0.01	0.01	0.00	0.00	0.00	0.00
TOTAL	3.81	3.82	3.92	3.82	3.89	3.88

Group IIB Clinopyroxene

	BZ45	BZ45	BZ45	BZ47	BZ47	BZ48
NA2O	6.32	6.20	6.38	4.82	4.41	3.32
MGO	8.34	8.36	8.38	12.55	12.72	12.95
SIO2	53.80	53.50	54.30	54.40	53.70	51.20
P2O5	0.23	0.21	0.22	0.19	0.19	0.16
AL2O3	11.41	11.33	11.46	7.92	6.99	6.11
K2O	0.03	0.04	0.03	0.03	0.02	0.01
CAO	12.93	12.90	12.52	14.26	14.96	16.38
TIO2	1.23	1.25	1.28	1.48	1.47	0.67
CR2O3	0.05	0.02	0.03	0.08	0.08	0.08
MNO	0.08	0.10	0.09	0.06	0.09	0.11
FEO	6.98	6.99	7.20	5.68	5.77	7.26
	101.40	100.91	101.88	101.47	100.39	98.24
SI	1.92	1.91	1.92	1.93	1.93	1.91
TI	0.03	0.03	0.03	0.04	0.04	0.02
AL	0.48	0.48	0.48	0.33	0.30	0.27
CR	0.00	0.00	0.00	0.00	0.00	0.00
FE2	0.21	0.21	0.21	0.17	0.17	0.23
MN	0.00	0.00	0.00	0.00	0.00	0.00
MG	0.44	0.45	0.44	0.66	0.68	0.72
CA	0.49	0.49	0.48	0.54	0.58	0.65
NA	0.22	0.22	0.22	0.17	0.15	0.12
K	0.00	0.00	0.00	0.00	0.00	0.00
P	0.01	0.01	0.01	0.01	0.01	0.01
TOTAL	3.80	3.80	3.79	3.85	3.87	3.93

Appendix 3.2

Individual tabulated analyses for inclusions recovered from ten diamonds. The diamonds were analysed for their carbon and nitrogen characteristics.

Garnet Analyses

	BZ121	BZ121	BZ121	BZ121	BZ121	BZ122
NA2O	0.38	0.36	0.37	0.37	0.35	0.99
MGO	10.11	10.13	10.29	10.16	10.16	11.27
SIO2	40.41	40.01	40.39	39.88	39.95	42.21
P2O5	0.03	0.04	0.02	0.02	0.00	0.01
AL2O3	21.35	21.55	21.34	21.41	21.28	18.93
K2O	0.01	0.01	0.00	0.00	0.01	0.00
CAO	13.11	13.09	13.11	13.17	13.06	14.82
TIO2	1.68	1.64	1.67	1.68	1.66	0.94
CR2O3	0.05	0.01	0.04	0.03	0.05	0.12
MNO	0.30	0.29	0.27	0.30	0.29	0.21
FEO	13.90	13.65	13.78	13.72	13.69	9.78
	101.33	100.77	101.30	100.74	100.51	99.29
SI	2.98	2.97	2.98	2.96	2.97	3.14
TI	0.09	0.09	0.09	0.09	0.09	0.05
AL	1.86	1.88	1.86	1.87	1.87	1.66
CR	0.00	0.00	0.00	0.00	0.00	0.01
FE2	0.86	0.85	0.85	0.85	0.85	0.61
MN	0.02	0.02	0.02	0.02	0.02	0.01
MG	1.11	1.12	1.13	1.12	1.13	1.25
CA	1.04	1.04	1.04	1.05	1.04	1.18
NA	0.03	0.03	0.03	0.03	0.03	0.07
K	0.00	0.00	0.00	0.00	0.00	0.00
P	0.00	0.00	0.00	0.00	0.00	0.00
	7.99	7.99	7.99	8.00	8.00	7.97

	BZ122	BZ122	BZ122	BZ122	BZ123	BZ123
NA2O	0.90	0.97	0.70	0.96	0.36	0.36
MGO	11.38	11.15	10.97	11.24	8.90	8.82
SIO2	42.26	42.29	41.37	42.47	40.14	40.33
P2O5	0.03	0.07	0.01	0.05	0.01	0.00
AL2O3	19.02	19.00	18.78	19.09	21.12	21.12
K2O	0.00	0.01	0.00	0.01	0.00	0.00
CAO	14.85	14.82	14.63	14.92	15.61	15.60
TIO2	0.94	0.89	0.91	0.94	1.44	1.42
CR2O3	0.12	0.12	0.11	0.14	0.11	0.07
MNO	0.21	0.22	0.21	0.25	0.28	0.28
FEO	9.69	9.73	10.69	9.79	13.25	13.10
	99.39	99.27	98.37	99.86	101.23	101.10
SI	3.13	3.14	3.12	3.14	2.98	2.99
TI	0.05	0.05	0.05	0.05	0.08	0.08
AL	1.66	1.66	1.67	1.66	1.85	1.85
CR	0.01	0.01	0.01	0.01	0.01	0.00
FE2	0.60	0.60	0.67	0.60	0.82	0.81
MN	0.01	0.01	0.01	0.02	0.02	0.02
MG	1.26	1.23	1.23	1.24	0.99	0.98
CA	1.18	1.18	1.18	1.18	1.24	1.24
NA	0.06	0.07	0.05	0.07	0.03	0.03
K	0.00	0.00	0.00	0.00	0.00	0.00
P	0.00	0.00	0.00	0.00	0.00	0.00
TOTAL	7.97	7.97	7.99	7.97	8.01	8.00

Garnet Analyses.

	BZ123	BZ123	BZ123	BZ123	BZ124	BZ124
NA2O	0.36	0.36	0.36	0.40	1.03	1.01
MGO	8.82	8.81	8.80	9.33	11.66	11.55
SIO2	40.47	40.27	40.26	41.85	41.03	40.68
P2O5	0.03	0.04	0.06	0.05	0.11	0.08
AL2O3	21.32	21.10	21.09	22.07	18.90	18.63
K2O	0.00	0.00	0.00	0.00	0.00	0.00
CAO	15.58	15.58	15.63	15.94	13.79	13.72
TIO2	1.46	1.48	1.48	1.46	1.88	1.87
CR2O3	0.10	0.11	0.05	0.10	0.08	0.07
MNO	0.03	0.26	0.29	0.27	0.22	0.19
FEO	13.21	13.11	13.11	12.72	11.30	11.33
	101.38	101.12	101.14	104.20	100.00	99.14
SI	2.99	2.99	2.99	3.00	3.05	3.05
TI	0.08	0.08	0.08	0.08	0.11	0.11
AL	1.86	1.85	1.85	1.86	1.66	1.65
CR	0.00	0.01	0.00	0.00	0.00	0.00
FE2	0.82	0.81	0.81	0.76	0.70	0.71
MN	0.00	0.02	0.02	0.02	0.01	0.01
MG	0.97	0.97	0.97	1.00	1.29	1.29
CA	1.23	1.24	1.24	1.22	1.10	1.10
NA	0.03	0.03	0.03	0.03	0.07	0.07
K	0.00	0.00	0.00	0.00	0.00	0.00
P	0.00	0.00	0.00	0.00	0.01	0.01
TOTAL	7.99	8.00	8.00	7.98	8.00	8.01

	BZ124	BZ125	BZ125	BZ125	BZ125	BZ126
NA2O	1.03	0.97	0.97	0.97	0.99	0.18
MGO	11.64	11.74	8.95	8.92	9.01	10.84
SIO2	40.89	41.01	40.51	40.42	40.42	40.61
P2O5	0.06	0.07	0.00	0.02	0.03	0.06
AL2O3	18.64	18.76	18.81	18.80	18.69	22.70
K2O	0.01	0.01	0.00	0.01	0.00	0.01
CAO	13.75	13.81	13.70	13.74	13.72	17.73
TIO2	1.88	1.87	2.76	2.73	2.70	0.38
CR2O3	0.09	0.08	0.05	0.08	0.05	0.10
MNO	0.20	0.23	0.30	0.32	0.29	0.13
FEO	11.36	11.38	13.97	13.94	14.10	7.38
	99.55	99.92	100.04	99.94	100.00	100.12
SI	3.06	3.05	3.05	3.05	3.05	2.97
TI	0.11	0.10	0.16	0.15	0.15	0.02
AL	1.64	1.65	1.67	1.67	1.66	1.96
CR	0.00	0.00	0.00	0.00	0.00	0.00
FE2	0.71	0.71	0.88	0.88	0.89	0.45
MN	0.01	0.01	0.02	0.02	0.02	0.01
MG	1.30	1.30	1.00	1.00	1.01	1.18
CA	1.10	1.10	1.11	1.11	1.11	1.39
NA	0.07	0.07	0.07	0.07	0.07	0.01
K	0.00	0.00	0.00	0.00	0.00	0.00
P	0.00	0.00	0.00	0.00	0.00	0.00
TOTAL	8.01	8.01	7.96	7.96	7.96	8.01

Garnet Analyses.

	BZ126	BZ127	BZ127	BZ127	Z128	BZ128
NA2O	0.20	0.90	0.85	0.92	0.88	0.16
MGO	10.95	11.91	11.88	11.99	11.85	11.75
SIO2	40.63	43.06	43.20	43.32	43.17	41.13
P2O5	0.05	0.08	0.08	0.07	0.08	0.05
AL2O3	22.83	19.94	19.83	19.95	19.92	23.05
K2O	0.02	0.01	0.01	0.01	0.01	0.01
CAO	17.54	15.90	15.81	15.79	15.88	16.12
TIO2	0.34	0.62	0.62	0.64	0.66	0.63
CR2O3	0.11	0.12	0.08	0.11	0.11	0.10
MNO	0.19	0.15	0.16	0.13	0.15	0.21
FEO	7.30	8.09	8.09	8.12	8.09	8.72
	100.16	100.77	100.61	101.03	100.79	101.90
SI	2.97	3.13	3.14	3.14	3.44	2.96
TI	0.02	0.03	0.03	0.03	0.04	0.03
AL	1.97	1.71	1.70	1.70	1.87	1.96
CR	0.01	0.01	0.00	0.01	0.01	0.00
FE2	0.45	0.49	0.49	0.49	0.54	0.52
MN	0.01	0.01	0.01	0.01	0.01	0.01
MG	1.19	1.29	1.29	1.29	0.22	1.26
CA	1.38	1.24	1.23	1.22	1.36	1.24
NA	0.01	0.06	0.06	0.06	0.07	0.01
K	0.00	0.00	0.00	0.00	0.00	0.00
P	0.00	0.01	0.01	0.00	0.01	0.00
TOTAL	8.01	7.97	7.96	7.97	7.56	8.02

	BZ129	BZ129	BZ130	BZ130	BZ130	BZ130
NA2O	1.00	0.99	0.16	0.15	0.23	0.14
MGO	11.88	11.96	14.60	14.52	14.52	14.81
SIO2	44.01	43.92	40.93	40.99	40.49	41.16
P2O5	0.05	0.11	0.05	0.03	0.06	0.05
AL2O3	21.59	21.66	22.20	22.89	22.72	23.13
K2O	0.01	0.01	0.01	0.00	0.03	0.00
CAO	15.55	15.65	13.32	13.36	13.40	13.42
TIO2	0.51	0.50	0.26	0.25	0.30	0.30
CR2O3	0.11	0.10	0.19	0.16	0.20	0.20
MNO	0.15	0.17	0.19	0.17	0.18	0.16
FEO	8.12	8.13	7.56	7.49	7.49	7.59
	102.97	103.20	99.48	100.03	99.62	100.95
SI	3.12	3.10	2.99	2.97	2.95	2.96
TI	0.03	0.03	0.01	0.01	0.02	0.02
AL	1.80	1.81	1.91	1.95	1.95	1.96
CR	0.00	0.00	0.01	0.01	0.01	0.01
FE2	0.48	0.48	0.46	0.45	0.46	0.45
MN	0.01	0.01	0.01	0.01	0.01	0.01
MG	1.25	1.26	1.59	1.57	1.58	1.59
CA	1.18	1.19	1.04	1.04	1.05	1.03
NA	0.07	0.07	0.01	0.01	0.02	0.01
K	0.00	0.00	0.00	0.00	0.00	0.00
P	0.00	0.01	0.00	0.00	0.00	0.00
TOTAL	7.95	7.95	8.03	8.03	8.04	8.04

Clinopyroxene Analyses.

	BZ121	BZ121	BZ122	BZ122	BZ123	BZ126
NA2O	5.05	5.04	5.86	4.34	5.66	6.33
MGO	11.04	11.05	9.42	9.83	10.42	9.16
SIO2	54.55	54.60	53.07	47.39	55.18	53.53
P2O5	0.01	0.03	0.06	0.06	0.00	0.00
AL2O3	8.44	8.50	11.77	14.45	9.69	13.40
K2O	0.03	0.03	0.03	0.02	0.02	0.00
CAO	16.04	15.90	13.73	14.20	15.97	14.58
TIO2	0.89	0.92	0.62	0.84	0.68	0.15
CR2O3	0.04	0.04	0.07	0.11	0.06	0.10
MNO	0.08	0.04	0.06	0.15	0.05	0.00
FEO	5.49	5.39	4.74	8.52	5.75	2.30
	101.66	101.53	99.43	99.89	103.47	99.55
SI	1.94	1.94	1.91	1.74	1.93	1.91
TI	0.02	0.02	0.02	0.02	0.02	0.00
AL	0.35	0.36	0.50	0.63	0.40	0.56
CR	0.00	0.00	0.00	0.00	0.00	0.00
FE2	0.16	0.16	0.14	0.26	0.17	0.07
MN	0.00	0.00	0.00	0.00	0.00	0.00
MG	0.59	0.59	0.51	0.54	0.54	0.49
CA	0.61	0.61	0.53	0.56	0.60	0.56
NA	0.17	0.17	0.20	0.15	0.19	0.22
K	0.00	0.00	0.00	0.00	0.00	0.00
P	0.00	0.00	0.00	0.00	0.00	0.00
TOTAL	3.86	3.85	3.82	3.92	3.85	3.80

	BZ126	BZ126	BZ126
NA2O	6.42	6.42	6.21
MGO	9.21	9.21	9.20
SIO2	53.47	53.47	53.54
P2O5	0.01	0.01	0.00
AL2O3	13.37	13.37	13.35
K2O	0.05	0.05	0.05
CAO	14.55	14.55	14.64
TIO2	0.15	0.15	0.16
CR2O3	0.11	0.11	0.09
MNO	0.01	0.01	0.01
FEO	2.25	2.25	2.26
	99.60	99.60	99.51
SI	1.90	1.90	1.91
TI	0.00	0.00	0.00
AL	0.56	0.56	0.56
CR	0.00	0.00	0.00
FE2	0.07	0.07	0.07
MN	0.00	0.00	0.00
MG	0.49	0.49	0.49
CA	0.56	0.56	0.56
NA	0.22	0.22	0.21
K	0.00	0.00	0.00
P	0.00	0.00	0.00
TOTAL	3.81	3.81	3.80

Appendix 3.3

Infra red and carbon isotope characteristics for ten garnet-bearing diamonds from Sao Luiz.

Garnet Inclusions.

	A(ppm)	B(ppm)	μ7.3	1282/1180	$\delta^{13}C$
BZ121	27.33	83.61	0.09	0.68	-8.75
BZ122	84.61	142.09	0.13	0.89	-10.98
BZ123	31.86	59.13	0.31	0.84	-8.02
BZ124	39.41	110.92	0.02	0.71	-12.57
BZ125	8.52	68.83	0.46	0.50	-11.75
BZ126	49.13	106.51	0.30	0.78	-6.42
BZ127	31.90	81.00	0.08	0.74	-8.37
BZ128	119.09	72.46	0.25	1.34	-6.70
BZ129	64.25	160.70	0.45	0.75	-6.70
BZ130	124.19	147.51	0.29	1.04	-6.98

Appendix 4

Magnesiowustite and non-garnet silicate-bearing diamonds from Sao Luiz.

Appendix 4.1

Averaged tabulated analyses for magnesiowustite and non-garnet silicate inclusions.

Magnesiowustite Inclusions.

	BZ65	BZ66	BZ67	BZ69	BZ70	BZ72
MGO	54.81	25.16	41.35	77.19	57.14	54.74
SIO2	0.00	0.00	0.00	0.00	0.00	0.00
AL2O3	0.00	0.20	0.00	0.00	0.10	0.00
TIO2	0.03	0.05	0.02	0.02	0.03	0.02
CR2O3	0.30	1.00	0.00	0.50	0.70	0.30
FEO	45.36	71.74	58.42	23.33	40.54	43.26
NIO	0.30	0.15	0.27	1.02	0.38	0.26
	100.80	98.30	100.06	102.06	98.89	98.58
SI	0.00	0.00	0.00	0.00	0.00	0.00
TI	0.00	0.00	0.00	0.00	0.00	0.00
AL	0.00	0.20	0.00	0.00	0.10	0.00
CR	0.01	0.03	0.02	0.02	0.02	0.01
FE2	31.50	60.30	44.00	14.30	28.10	30.50
MG	67.80	37.70	55.50	84.40	70.60	68.80
NI	0.20	0.12	0.20	0.60	0.25	0.18
	99.51	98.35	99.72	99.32	99.08	99.49
F/F+M	0.31	0.61	0.44	0.14	0.28	0.30

	BZ73	BZ78	BZ80	BZ87	BZ88	BZ99
MGO	58.39	66.85	62.41	75.08	54.43	56.55
SIO2	0.00	0.00	0.00	0.00	0.00	0.00
AL2O3	0.00	0.00	0.00	0.00	0.10	0.00
TIO2	0.02	0.02	0.02	0.01	0.02	0.04
CR2O3	0.30	0.80	0.40	0.50	0.00	0.30
FEO	42.01	31.22	35.73	25.20	44.98	42.34
NIO	0.32	0.89	0.74	0.00	0.00	0.00
	101.04	99.78	99.30	100.79	99.53	99.23
SI	0.00	0.00	0.00	0.00	0.00	0.00
TI	0.00	0.00	0.00	0.00	0.00	0.00
AL	0.00	0.00	0.00	0.00	0.10	0.00
CR	0.01	0.01	0.02	0.01	0.03	0.01
FE2	28.50	20.40	24.00	15.70	31.50	29.40
MG	70.70	78.00	74.90	83.60	68.00	70.00
NI	0.21	0.56	0.48	0.00	0.00	0.00
	99.42	98.97	99.40	99.31	99.63	99.41
F/F+M	0.29	0.21	0.24	0.16	0.32	0.30

Colourless Inclusions.

	BZ97	BZ99	BZ103	BZ104	BZ111	BZ115
NA2O	0.01	0.01	0.00	0.04	0.04	0.01
MGO	0.08	0.01	0.02	17.82	49.55	0.14
SIO2	50.97	99.99	99.26	53.86	40.70	51.74
P2O5	0.75	0.01	0.00	0.45	0.01	0.00
AL2O3	0.09	0.00	0.04	0.15	0.02	0.08
K2O	0.00	0.01	0.00	0.00	0.01	0.00
CAO	48.41	0.01	0.01	24.49	0.05	47.56
TIO2	0.02	0.01	0.01	0.05	0.02	0.02
CR2O3	0.02	0.02	0.01	0.02	0.05	0.01
MNO	0.04	0.01	0.01	0.13	0.08	0.02
FEO	0.08	0.01	0.07	1.59	8.82	0.12
	100.47	100.09	99.43	98.60	99.35	99.70
SI	32.71	49.97	49.95	32.98	24.98	33.39
TI	0.01	0.00	0.00	0.02	0.01	0.01
AL	0.07	0.00	0.02	0.11	0.01	0.06
CR	0.01	0.01	0.00	0.01	0.02	0.00
FE2	0.04	0.00	0.03	0.81	4.53	0.06
MN	0.02	0.00	0.00	0.07	0.04	0.01
MG	0.08	0.01	0.02	16.26	45.32	0.13
CA	33.28	0.01	0.01	16.07	0.03	32.89
NA	0.01	0.00	0.00	0.02	0.02	0.01
K	0.00	0.00	0.00	0.00	0.00	0.00
P	0.41	0.00	0.00	0.23	0.01	0.00
TOTAL	66.63	50.01	50.03	66.59	74.98	66.57

	BZ116	BZ117B	BZ119	BZ106
NA2O	0.04	0.03	0.02	0.04
MGO	0.46	47.60	0.06	0.01
SIO2	52.01	40.90	51.03	43.62
P2O5	0.00	0.00	0.00	0.33
AL2O3	0.05	0.05	0.07	35.76
K2O	0.00	0.07	0.00	0.25
CAO	46.94	0.04	45.75	18.99
TIO2	0.05	0.00	0.02	0.01
CR2O3	0.01	0.04	0.01	0.00
MNO	0.00	0.13	0.04	0.01
FEO	0.08	10.65	0.04	0.42
	99.64	99.51	97.04	99.99
SI	33.49	25.25	33.70	25.29
TI	0.02	0.00	0.01	0.01
AL	0.04	0.04	0.05	24.45
CR	0.00	0.02	0.00	0.00
FE2	0.04	5.50	0.02	0.20
MN	0.00	0.07	0.02	0.21
MG	0.44	43.79	0.06	0.01
CA	32.39	0.03	32.37	11.79
NA	0.02	0.02	0.01	0.02
K	0.00	0.03	0.00	0.09
P	0.00	0.00	0.00	0.16
TOTAL	66.46	74.72	66.26	62.23

Appendix 4.2

Nitrogen Characteristics for Diamonds containing Magnesiowustites and non-garnet silicates.

Nitrogen Characteristics for Sao Luiz Diamonds.

Sample	Appm	Bppm	μ7.3	1282/1180	Incl.
BZ65		Type II			MW
BZ66		Type II			MW
BZ67		Type II			MW
BZ69		Type II			MW
BZ70		Type II			MW
BZ71		Type II			MW
BZ72		Type II			MW
BZ73		Type II			MW
BZ74		Type II			MW
BZ75		Type II			MW
BZ76	566.7	268.2	0.67	1.5	MW
BZ77		Type II			MW
BZ78		Type II			MW
BZ79		Type II			MW
BZ80		Type II			MW
BZ81	2369.2	5442.4	121.4	0.8	MW
BZ82	0	954.4	6.85	0.2	MW
BZ83		Type II			MW
BZ84		Type II			MW
BZ88	0	1135.4	0	0.0	MW
BZ89		Type II			MW
BZ90	0	1073.8	0	0.0	CL
BZ91		Type II			CL
BZ92		Type II			CL
BZ93		Type II			CL
BZ94		Type II			CL

Sample	Appm	Bppm	μ7.3	1282/1180	Incl.
BZ95		Type II			CL
BZ96	0	1354.3	12.02	0.0	CL
BZ97		Type II			CL
BZ98		Type II			CL
BZ99	70.61	672.2	0.20	0.48	MULT.
BZ100		Type II			MULT.
BZ101	18.83	170.3	0.56	0.49	MULT.
BZ102		Type II			MULT.
BZ104		Type II			MULT.
BZ105	0	127.15	0.0	0.26	MULT.
BZ106		Type II			MULT.
BZ107		Type II			MULT.
BZ109		Type II			MULT.
BZ111	822.2	143.1	0.0	1.78	MULT.
BZ113		Type II			MULT.
BZ114		Type II			MULT.
BZ115		Type II			MULT.
BZ116	50.7	577.0	11.8	0.47	MULT.
BZ117	1.5	28.8	0.5	0.33	MULT.
BZ118		Type II			MULT.
BZ119		Type II			MULT.
BZ120		Type II			MULT.

MW = Magnesiowustite
CL = Colourless
MULT = Multiple

Appendix 4.3

Nitrogen and Carbon Characteristics for five diamonds containing magnesiowustite and non-garnet silicate inclusions from Sao Luiz

Magnesiowustite Inclusions.

	A(ppm)	B(ppm)	μ7.3	$\delta^{13}C$
BZ65	0.00	0.00	0.00	-4.16
BZ66	0.00	0.00	0.00	-5.02
BZ65	0.00	0.00	0.00	-4.49

Colourless Inclusions.

	A(ppm)	B(ppm)	μ7.3	$\delta^{13}C$
BZ97	0.00	0.00	0.00	-4.89
BZ99	0.00	0.00	0.00	-4.14

Appendix 5

Detection Limits and Precision for Electron Microprobe Analyses.

Formula Used.

$$\text{Detection Limit} = \frac{3}{m}\sqrt{\frac{Rb}{Tb}}$$

$$\text{Precision}(\sigma) = \frac{100}{\sqrt{Tp}} \quad \frac{1}{\sqrt{Rp} - \sqrt{Rb}} \%$$

Where

m is Counts sec^{-1} wt $\%^{-1}$

Rp is peak count rate

Rb is background count rate

Tp is time on peak (secs)

Tb is time on background (secs)

Chromites

Element	Detection limit	Precision
Ti	0.026	0.266
Cr	0.037	0.003
Mg	0.016	0.010
Al	0.015	0.012
Fe	0.045	0.016
Mn	0.048	0.206
Ni	0.051	0.329
Si	0.018	0.198

Chrome Pyrope Garnet.

Element	Detection Limit	Precision
Ca	0.015	0.069
Mg	0.012	0.007
Mn	0.019	0.017
Al	0.011	0.008
Fe	0.021	0.021
Si	0.016	0.002
Ni	0.028	1.478
Cr	0.020	0.025

Olivine

Element	Detection Limit	Precision
Mg	0.018	0.004
Si	0.018	0.005
Fe	0.036	0.022
Ca	0.019	0.073
Al	0.012	4.591
Mn	0.036	0.426
Ti	0.019	1.670
Cr	0.024	0.686
Ni	0.044	0.144

Pyroxene

Element	Detection Limit	Precision
Mg	0.017	0.005
Si	0.018	0.004
Fe	0.038	0.029
Ca	0.019	0.075
Na	0.028	0.726
Al	0.013	0.044
Mn	0.034	0.359
Ti	0.020	0.498
Cr	0.024	0.053
Ni	0.042	0.365

High-Silica Garnets

Element	Detection Limit	Precision
Na	0.025	0.244
Mg	0.016	0.012
Al	0.016	0.008
Si	0.017	0.006
Ca	0.026	0.010
Ti	0.021	0.042
Cr	0.027	0.459
Mn	0.034	0.147
Ni	0.048	
K	0.025	

Pyroxene (High-Jadeite)

Element	Detection Limit	Precision
Na	0.028	0.025
Mg	0.016	0.012
Al	0.013	0.012
Si	0.018	0.046
Ca	0.027	0.009
Ti	0.020	0.069
Cr	0.035	0.770
Mn	0.034	0.025
Fe	0.034	0.025
Ni	0.040	1.199

Magnesiowustite

Element	Detection Limit	Precision
Mg	0.002	0.004
Fe	0.058	0.011
Al	0.011	0.492
Cr	0.042	0.117
Mn	0.040	0.157
Ti	0.022	
Ni	0.043	0.050
Si	0.015	